CHAPTER FIVE

5 Analysis of Serrated Trailing Edge Blades

5.1 Introduction

Fours sets of modified trailing edge GE-Rotor-B blades were investigated in the Virginia Tech linear cascade tunnel to evaluate their effectiveness in increasing both the spreading and decay rate of the blade wakes which is predicted to reduce the pitchwise variation of the mean streamwise velocity. Hence, reduce the tonal noise at the downstream stator vane leading edge. Included in these four sets of modified blades, were two different serration sizes (1.27 cm and 2.54 cm) and for each different serration size a second set of blades with added trailing edge camber. The geometries of these four modified blade sets were described in detail in chapter 4.

In this chapter the blade loading, mean velocity, turbulence and wake characteristics measured by a four sensor hot-wire at the four downstream axial locations $0.61c_a$, $1.18c_a$, $1.82c_a$, and $2.38c_a$ will be presented for each set of modified blades. Also the results of the Pitot-static measurements at x/c_a = 0.84 and 1.88 are shown and described in detail. This data will then be compared to the baseline case, described in detail in chapter 3, to determine to what extent the wakes of the new blades differ from the baseline GE-Rotor-B blades. Also, the spectral data will be analyzed to determine if vortex shedding is present. Cross-sections at the two downstream locations of $0.61c_a$ and $1.82c_a$ will be compared to the baseline to determine if the tip leakage vortex has changed. From this analysis it will be possible to determine the advantages and disadvantages of the modified blades from a fluid dynamics point of view.

5.2 Blade Loading

The blade loading was measured for all for blade sets using the embedded pressure ports located on the surfaces of blade 4 and 5, at the spanwise location of y/c_a = 0.95. A detailed description of the embedded pressure ports as well as their coordinates is given in chapter 4. Figure 5-1(a) through (d) are plots of the blade loading, $C_{p,s}$, calculated by equation 3-1, versus the axial coordinate measured from the leading line, x_1/c_a, for the four trailing edge serration case. The four cases are plotted against the baseline configuration results (with the controlled blade root opening).

The 1.27cm case, figure 5-1(a), matches the baseline configuration blade loading. On the pressure side, the blade loading curves are almost identical with the most variation occurring in the vicinity of the blade trip at approximately x_1/c_a = 0.06. On the suction side the pressure is slightly higher between the x_1/c_a = 0.06 and 0.5, which may be due to the effects of the trailing edge.

The 1.27cm serration with droop produces a noticeably higher pressure on the pressure side of the blade that extends from the leading edge to the trailing edge. From the leading edge to near the trailing edge, the pressure on the pressure side steadily increases until it reaches x_1/c_a = 0.88, where it then drops quickly most likely due to the effects of the droop. The blade loading is fuller especially near the trailing edge then the baseline and the 1.27cm case.

The 2.54cm case has a blade loading that is similar to the baseline blade loading except on the suction side. On the suction side between x_1/c_a = 0.06 and 0.55, the pressure is higher by a maximum of $0.05C_{p,s}$ at x_1/c_a = 0.25 and the difference is twice is large as the difference between the 1.27cm and the baseline. This may be due to the larger serration size and the pressure ports are located near a valley which has a shorter chord length (figure 4-3(b)).

The final serration set, 2.54cm serration with droop matches the baseline from the leading edge to x_1/c_a = 0.35 on the pressure side and x_1/c_a = 0.20 on the suction side. On the pressure side the pressure slowly begins to rise, similar to what was seen in the 1.27cm with droop case, and then droops quickly at x_1/c_a = 0.8. On the suction side, the pressure is only slightly lower then the baseline case by only $0.025C_{p,s}$. In general, the effect of the droop increases the blade loading on the blade over the trailing edge region.

The variations in the blade loading of the various serrated blade configurations compared to the baseline can also be seen in the circulations. Using equation 3-3 the circulations were calculated and they can be found in table 5-1 below. The 1.27cm case is slightly lower than the baseline configuration (with blade root covers) while the 1.27cm drooped case is $0.03c_aU_\infty$ larger. The droop presumably acts like a flap on a wing and increases the circulation, which is proportional to the lift. The larger serration size has a negative effect on the circulation and the circulation for the 2.54cm case is $0.04c_aU_\infty$ less than the baseline but the 2.54cm drooped case is almost the same as the baseline, with the droop to increasing the circulation.

Table 5-1: Normalized circulation for each of the modified trailing edge blade configurations and percent variation from the baseline configuration.

Blade Configuration	Γ/c_aU_∞	***Percent Diff.***
Baseline	0.45	-
1.27 cm	0.44	-2.2%
1.27 cm drooped	0.48	6.7%
2.54 cm	0.41	-8.9%
2.54 cm drooped	0.44	-2.2%

5.3 Pitot-Static Cross-Section Measurements

Pitot-static cross-sections at two downstream locations using a telescoping Pitot-static probe were performed to reveal the overall form of the wakes shed by the serrated blades. This reduced the complexity of using four sensor hot-wires on an unknown flow as well as allows the entire spanwise height of downstream tunnel test section to be mapped out.

Figures 5-2 through 5-5 show the Pitot-static cross-sections for the four cases at $x/c_a = 0.84$. In each of these figures three plots are shown. The first plot, denoted as (a) in the four figures, is the contour plot of the coefficient of total pressure, $C_{p,o}$ against pitchwise distance, z/c_a, and spanwise distance, y/c_a. The second plot, (b), is the contour plot of the local mean streamwise velocity normalized on the reference velocity, U/U_∞. The horizontal and vertical axes are also z/c_a and y/c_a, respectively. The dash-dotted

boxes in the figures represent the four sensor hot-wire measurement locations, which are discussed in the later sections.

In figures 5-2(a) to 5-5(a), the total pressure fields outside of the wake region are identical with a maximum value of 1.0. Also, the leakage vortex appears in the same location for all four cases and, compared to the baseline Pitot-static profile in figure 3-7, the vortex center has not shifted for any of the cases, with the center being roughly located between z/c_a = -2.85 to -2.90 and y/c_a = 0.17 to 0.18. Near the upper endwall, the boundary layer is not symmetric around the blade, with the boundary layer on the pressure side being smaller than the on the suction side. It seems, the boundary layer is being sucked off in the vicinity of the blade root, at z/c_a = -3.2 on the pressure side, most likely due to the 1 mm opening in the blade root cover. On the suction side, the boundary layer is thickest at the edge of the blade wake, with a thickness of approximately $0.18c_a$. It steadily decays toward the center of the passage becoming approximately $0.08c_a$ at the pressure side of the next blade.

The most noticeable differences in figures 5-2(a) through 5-5(a) can be found in the wakes. In figure 5-2(a), which is the plot for the 1.27 cm serrated trailing edge, the individual serrations produce no locally visible effects on the wake. Comparing to the baseline case in figure 3-7(a), the plots look identical, except the 1.27 cm serration has a wider wake. For the 1.27 cm drooped case, figure 5-3(a), the individual serrations can be seen to have a slight effect on the pressure side of the wake but not on the suction side, while the 2.54 cm and 2.54 cm drooped cases shown in figures 5-4(a) and 5-5(a), respectively, the effects of the serrations can be seen on both the pressure and suction sides. For the latter three cases, the effects of the serrations appear to be almost periodic with spanwise distance outside of the boundary layer and vortices. Seven peak-to-peak periods can be seen for the 1.27 cm case, while, only two peak-to-peak periods can be seen for the 2.54 cm and 2.54 cm droop cases.

The local mean streamwise velocity, U/U_∞, plots shown in figures 5-2(b) and 5-5(b) show the same flow characteristics as the coefficients of total pressure plots. In the mean streamwise velocity plots the minimum velocity for the 1.27 cm and the 1.27 cm drooped cases, figures 5-2(b) and 4-3(b), occurs along a continuous valley that forms the center of wake. However, for the 2.54 cm and the 2.54 cm drooped cases, the minimum

velocity occurs at those points on the centerline that are directly downstream of the serration peaks as shown in figure 5-4(b) and 5-5(b).

Figures 5-6 through 5-9 show the same plots as figures 5-2 through 5-5 but at the downstream location of x/c_a = 1.88. The same flow characteristics at both the lower and upper endwalls can be seen in these figures as at x/c_a = 0.84. Near the lower endwall, the vortex center locations for the four cases have the same spanwise location of y/c_a = 0.20. The pitchwise location of the vortex center is between z/c_a = -4.4 and -4.5. The baseline case's vortex center is also located at y/c_a = 0.20 with a corresponding pitchwise location between z/c_a = -4.4 and -4.5. The boundary layer is also not symmetric at this downstream location, which can be seen in figures 5-6(a) through 5-9(a). On the pressure side, the removal of the boundary layer near the blade wake can be seen and on the suction side, the thickest portion of the boundary layer is on the wake side. Between, the two stations a growth in the boundary layer thickness can be seen, with a maximum value of $0.23c_a$ and it decreases toward the center of the passage reaching a value of approximately $0.13c_a$.

Between the two downstream stations, it can be seen in figures 5-6(a) through 5-9(a) that wakes have grown. For the smaller serration size, the peaks are not even visible, as they appear to have been 'smudged' out by the growth of the wake. The peaks and valleys are still noticeable for the larger serrations, but they have become more blended with wake. The blending of the peaks and valleys for the 2.54 cm serrations is the most noticeable in the local mean streamwise velocity plots in figures 5-8(b) and 5-9(b).The minimum velocity point is not located at the center of the peak wake as was the case for further upstream, but now in the center of the entire wake.

5.4 Rotation of Three-Component Hot-Wire Results

3-component hotwire data was rotated using the scheme described in the Appendix. The Euler angles that were determined using this method are found in table 5-2 below. Do note that data was not rolled around the *x*-axis.

Table 5-2: Euler angles used to rotate four sensor hot-wire data.

Location (x/c_a)	***Serration Type***	***Measurement***	θ_x	θ_y	θ_z
0.61	1.27 cm	Mid-Span	0	-0.70	-3.7
0.61	1.27 cm	Cross-Section	0	-0.91	-4.0
1.18	1.27 cm	Mid-Span	0	-1.4	-2.4
1.82	1.27 cm	Mid-Span	0	-1.2	-3.8
1.82	1.27 cm	Cross-Section	0	-0.83	-3.7
2.38	1.27 cm	Mid-Span	0	-2.0	-1.6
0.61	1.27 cm droop	Mid-Span	0	3.3	-3.3
0.61	1.27 cm droop	Cross-Section	0	0.17	-3.8
1.18	1.27 cm droop	Mid-Span	0	-0.46	-3.8
1.82	1.27 cm droop	Mid-Span	0	-0.52	-3.5
1.82	1.27 cm droop	Cross-Section	0	-0.41	-3.8
2.38	1.27 cm droop	Mid-Span	0	-1.6	-3.4
0.61	2.54 cm	Mid-Span	0	1.5	-3.5
0.61	2.54 cm	Cross-Section	0	0.10	-3.9
1.18	2.54 cm	Mid-Span	0	0.70	-2.6
1.82	2.54 cm	Mid-Span	0	0.0066	-2.8
1.82	2.54 cm	Cross-Section	0	-0.19	-3.4
2.38	2.54 cm	Mid-Span	0	1.6	-2.0
0.61	2.54 cm droop	Mid-Span (Run 1)	0	5.8	-3.2
0.61	2.54 cm droop	Mid-Span (Run 2)	0	5.4	-3.2
0.61	2.54 cm droop	Cross-Section	0	0.39	-3.8
1.18	2.54 cm droop	Mid-Span	0	2.1	-1.5
1.82	2.54 cm droop	Mid-Span	0	-0.77	-3.9
1.82	2.54 cm droop	Cross-Section	0	-1.8	-4.0
2.38	2.54 cm droop	Mid-Span	0	-0.13	-2.7

5.5 Cross-Sectional Measurements

Cross-sectional measurements were performed with four-sensor hot-wires at two downstream axial locations of $0.61c_a$ and $1.82c_a$ for all four serrated blade sets. The cross-sections were measured over a spanwise distance of $0.028c_a$ to $0.92c_a$ from the lower endwall. The details of the grids used at these axial locations are described in detail in section 4.4 of chapter 4.

5.5.1 Mean Velocity Contours and Vector Plots at $x/c_a = 0.61$

Figure 5-10 shows the contour plots of streamwise velocity, U/U_∞, for all four blade sets as a function of the spanwise, y/c_a, and the pitchwise, z/c_a, coordinates. In all four cases the wakes of blades 4 and 5 as well the tip leakage vortex are seen. The wakes of blades 4 and 5 are represented by the narrow spanwise bands of lower velocity, centered around z/c_a = -1.55 and -3.25, respectively, which match the wake centerline of the baseline configuration shown in figure 3-9(a). For the 1.27 cm serrations, the wake deficit is almost constant with spanwise position, while for the 2.54 cm serrations the lowest velocities are found downstream of the serrations tips. These minima are located at y/c_a = 0.4 and 0.75, for both drooped and non-drooped cases. The minimum velocity in the wake ranges between $0.52U_\infty$ for the 2.54 cm serrations to $0.54U_\infty$ for the 1.27 cm serrations. The 2.54 cm serration valleys, located at the spanwise locations of $0.25c_a$ and $0.55c_a$, also have local velocity minima, but these minima are on the order of $0.54U_\infty$. The width of the wake region also varies for each of the cases, with smallest wake width of $0.32c_a$ found on both 1.27 cm serrations and the largest wake width of $0.46c_a$ found on the 2.54 cm drooped serration, where the wake width is defined as distance between the regions of vertical streamwise velocity gradients. The wakes of both 1.27 cm serrations are uniform in shape and do not vary much with spanwise direction, while the wakes of both 2.54 cm serrations do. As was discussed in the Pitot-static cross-sections above, the wake structures of the 2.54 cm serrations appear ridged.

The tip leakage vortex region, shed by blade 4, is represented by the circular region near the lower endwall in figures 5-10(a) through 5-10(d). This region extends in the pitchwise direction from suction (right) side of the blade 4 wake to the pressure (left) side of the blade 5 wake and is almost identical for all four cases. The vortex region is centered pitchwise between $-2.5c_a$ and $-2.6c_a$, and a spanwise at $0.18c_a$. At this point the minimum streamwise velocity is $0.3U_\infty$ in all cases. The maximum height of the vortex region is $0.4c_a$ and it is located pitchwise at approximately $-2.6c_a$ for all four cases.

The rotating flow in the vortex region can be seen in figures 5-11(a) through 5-11(d). These figures show the normalized cross flow velocity vectors, V/U_∞ and W/U_∞, as a function of the spanwise, y/c_a and pitchwise, z/c_a, coordinates. In all of the cases, a large counter-clockwise rotating tip leakage vortex centered pitchwise and spanwise at $-2.55c_a$ and $0.2c_a$ dominates the flow field near the lower endwall. Smaller much weaker

clockwise rotating secondary vortices can be seen adjacent to the main vortex. Near the mid-span of the blades, the velocity is much less than in the tip leakage vortex. For the 1.27 cm serrations the small clockwise rotating secondary vortex is centered pitchwise and spanwise at -3.0c_a and 0.055c_a while for the 2.54 cm serrations, one large secondary vortex is centered pitchwise and spanwise at -3.67c_a and 0.1c_a. (A second vortex seen at -1.6c_a and 0.1c_a is the same secondary vortex except separated by one period). The secondary vortex created by 2.54 cm serrations are approximately half the size of the main vortex. The one secondary vortex is likely created by the separation of boundary layer fluid off the end wall as it passes out from under the main vortex. Additionally, two more counter-clockwise rotating secondary vortices are found pitchwise and spanwise at-1.7c_a and 0.33c_a, and at -3.3c_a and 0.33c_a for the 2.54 cm serrations, which coincidentally is near the serration peaks of blades 4 and 5. In all four cases, the interaction of the larger main vortex and secondary vortex creates a plane near -2.9c_a where the velocity direction is acting primarly in the spanwise direction.

Figures 5-12(a) through 5-12(d) show the plots of streamwise mean vorticity, $\Omega_x/U_\infty c_a$, contours calculated by equation 3-7, as a function of the spanwise, y/c_a, and pitchwise, z/c_a, coordinates. The main tip leakage vortex is indicated by large region of positive vorticity and it is centered pitchwise and spanwise at -2.55c_a and 0.15c_a. Table 5-3 lists the values for the maximum streamwise vorticities for each case as well as its corresponding pitchwise and spanwise coordinates. In all of the cases the vorticity distributions of the main vortex are similar and the serrations have little effect on the tip leakage vortex. The 2.54 cm serration has a slightly larger streamwise vorticity compared to 1.27 cm serration. Also, the non-drooped blades have a slightly higher streamwise vorticity compared to their drooped counterparts. All cases were higher than the baseline value, which was 2.29$U_\infty c_a$. Adjacent to the large region of positive vorticity is a region of negative vorticity centered pitchwise and spanwise at -2.8c_a and 0.1c_a. This region represents the secondary vortex which was seen in figure 5-10. The most negative streamwise vorticity and their corresponding coordinates are given in table 5-3. These secondary voriticities are approximately three times weaker in magnitude compared to the main vortex. In figures 5-3(c) and 5.3(d), two more negative vorticity regions can

found pitchwise and spanwise at -1.5c_a and 0.1c_a, and at -3.3c_a and 0.1c_a. These negative regions are located downstream of the valley of the serrations.

Table 5-3: Maximum and minimum vorticity, $\Omega_x/U_\infty c_a$, in the cross-sections at x/c_a = 0.61 for the four serrated trailing edge designs.

Serration Type	***Maximum Vorticity***			***Minimum Vorticity***		
	z/c_a	y/c_a	$\Omega_x/U_\infty c_a$	z/c_a	y/c_a	$\Omega_x/U_\infty c_a$
Baseline	-2.57	0.12	1.85	-3.00	0.12	-0.66
1.27 cm	-2.51	0.16	2.34	-2.82	0.072	-0.70
1.27 cm Droop	-2.40	0.16	2.30	-2.82	0.072	-0.76
2.54 cm	-2.40	0.16	2.46	-2.82	0.072	-0.75
2.54 cm Droop	-2.40	0.16	2.43	-2.72	0.028	-0.87

5.5.2 Turbulence Cross-Sectional Contours at x/c_a = 0.61

Figures 5-13 through figure 5-15 are contour plots of normalized Reynolds stresses $\overline{u'^2}/U_\infty^2$, $\overline{v'^2}/U_\infty^2$ and $\overline{w'^2}/U_\infty^2$ as a function of the pitchwise, z/c_a, and spanwise, y/c_a, coordinates for all four serration types. In figure 5-13, the highest streamwise Reynolds stress, $\overline{u'^2}$, for all serration types is found in the crescent region in the tip leakage vortex with a value of 0.0085U_∞^2. In all of the cases the crescent shape of the streamwise turbulence stress region is similar in the tip leakage region, which is also similar to the baseline case in figure 3-12(a). The horizontal arm of the crescent form is centered spanwise at 0.30c_a and extends pitchwise from -2.25c_a to -3.1c_a, while the vertical arm is centered pitchwise at -3.0c_a and extends spanwise from 0.1c_a to 0.35c_a. For the 1.27 cm and 1.27 cm droop serrations, figures 5-13(a) and 5-13(b), the maximum streamwise turbulence stress region in the wake is centered pitchwise around -3.25c_a which is the centerline of the blade 5 wake as was shown in figure 5-10. The maximum turbulence stress for the droop case is slightly higher. For the 2.54 cm and 2.54 cm droop serrations, figures 5-13(c) and 5-13(d), the maximum streamwise turbulence stress in the wake are found spanwise at 0.35c_a and 0.75c_a, which are the serrations tips. The streamwise turbulence stress for drooped case is once again slightly higher.

In figure 5-14, the region of maximum spanwise turbulence stress, $\overline{v'^2}$, is centered pitchwise and spanwise at -2.75c_a and 0.3c_a which is where the velocity is pointing almost vertically. This region of high spanwise stress may be due to the interaction of the main and secondary vortices. The spanwise turbulence stress in this region is $0.0074U_\infty^2$. In the tip leakage vortex region, the distribution and levels of the spanwise turbulence stress is similar for all four cases, which also matches the baseline distribution in figure 3-12(b). In the wake of the 1.27 cm serrations, figures 5-14(a) and (b), the maxims are much lower than those in the vortex region and are found on pressure side of the wakes. The turbulence intensity is slightly higher for the drooped case. For the 2.54 cm serrations, figures 5-14(c) and (d), the maxima are found downstream of the serration peaks and the values are slightly higher for the drooped case.

In figure 5-15, the maximum level of the cross-wake turbulence stress, $\overline{w'^2}$, is found in the vortex for three of the four cases. In the vortex region, the maximum of $0.0072U_\infty^2$ is found in the region centered pitchwise and spanwise on -2.4c_a and 0.2c_a which is near the center of the main vortex. Once again, the trailing edge serrations do little in changing the distribution and levels of the cross-wake turbulence stress in the vortex region. The tip leakage region is very similar for the four cases, which also matches the baseline in figure 3-12(c). In the wake regions of 1.27 cm serration, figure 5-15(a), the maximum is centered along the wake centerline. Oddly, the maximum for the drooped case, figure 5-15(b) is along the pressure side of the wake and is less than the non-drooped. For both 2.54 cm serrations, the maxima are once again found at the serration tips. The maximum intensity in the wake for the drooped case matches those found in the vortex region.

Figures 5-16 through 5-18 are the contour plots of the Reynolds shear stresses, $\overline{u'v'}/U_\infty^2$, $\overline{u'w'}/U_\infty^2$ and $\overline{v'w'}/U_\infty^2$ as a function of the pitchwise, z/c_a, and spanwise, y/c_a, coordinates. In all of the figures, the shear stress levels of $\overline{u'v'}$ are largest in magnitude in the vortex region, most likely due to the vortex rotation. In figure 5-16, a positive shear stress appears in all cases at $y/c_a = 0.35$ in the wake regions of blades 4 and 5. With droop and increased serration size this point increases in magnitude. For the larger serration sizes, a region of negative $\overline{u'v'}$ is found spanwise at 0.65c_a in the wakes of blades 4 and 5.

This spanwise location coincides with the valley of the 2.54 cm serration. Droop increases the magnitude of this negative shear stress. Outside of these maximum shear points, the shear stress is less than $5\text{x}10^{-4}U_\infty^2$ in magnitude.

For the 1.27 mm serrations, figures 5-17(a) and (b), the shear stress $\overline{v'w'}$ is negative along the wake centerlines of blades 4 and 5, while for the 2.54 cm serrations, figures 5-17(c) and (d), negative peaks of $\overline{v'w'}$ are seen at the serration tips. In the valleys of the larger serration, the shear stress $\overline{v'w'}$ is almost 0. The magnitude of the shear stress levels in the larger serrations is larger in magnitude than for the smaller serrations.

In figure 5-18, the same type of shear structure, $\overline{u'w'}$, as was seen in the baseline case is present in these wakes. This includes the negative shear on the wake pressure side and positive shear on the wake suction side. The shape of the shear stress regions in the wake of 2.54 cm serrations look like the mean velocity profiles. The shear stresses in these wakes are greatest in magnitude at the serration tip locations, and lowest in magnitude in the valleys. The droop increases the magnitude of these shear stresses.

Figure 5-19, is the contour plots of the turbulence kinetic energy, k/U_∞^2, as a function of the spanwise, y/c_a, and pitchwise, z/c_a, coordinates. The same crescent shape seen in the vortex region of the streamwise Reynolds stress plots is seen in these plots in the vortex region. Once again the shape of and turbulence kinetic energy levels in the tip leakage vortex region for the four serrated cases and the baseline case (figure 3-14(a)) are similar. The serrations have a minimal effect on the tip leakage vortex. The maximum TKE in the vortex region occurs pitchwise and spanwise at $-2.9c_a$ and $0.2c_a$ which is where the main and secondary vortices interact. Comparing to the baseline, the TKE levels are lower for the serrated blades than for the baseline. Lower levels of TKE are seen in the wake regions of all four cases. The highest levels of TKE in the 1.27 cm serrations are found near the centerline of the wake, while for the 2.54 cm serrations they occur near the tips. The TKE levels for the larger serrations are locally higher in magnitude than the smaller serrations, and the drooped cases show slightly higher TKE levels. This is especially noticeable for the 2.54 cm drooped serration.

Figures 5-20 is a plot of turbulence kinetic energy production contours, $P/U_\infty^3 c_a$, as a function the pitchwise, z/c_a, and spanwise, y/c_a, coordinates. Similar to the TKE plots

in figure 5-19, the tip leakage vortex is only minimally affected by the trailing edge shape, and as a result the tip leakage vortex is similar for all four cases and the baseline (figure 3-15(a)). Not surprisingly, the highest levels of TKE production occur in the vortex regions. TKE production is positive everywhere and largest in magnitude pitchwise and spanwise at -2.7c_a and 0.29c_a with a maximum value of approximately 7.5x10$^{-3}U_\infty^3 c_a$, In the wake, lower levels of TKE production are found. TKE production is highest on the small serrations wake pressure side, while for the largest serrations, TKE production is largest in magnitude at the serration tips. Highest levels of TKE production n the wake are produced by the 2.54 cm drooped case, which has maximum levels around 2.7x10$^{-3}U_\infty^3 c_a$.

5.5.3 Mean Velocity Contours and Vector Plots at x/c_a =1.82

In figure 5-21, the mean streamwise velocity, U/U_∞, contours are plotted as a function of pitchwise, z/c_a, and spanwise, y/c_a, coordinates. Near the lower endwall, between the two wake regions of blade 4 and 5 which are defined by the spanwise running bands of normalized velocity, a circular shaped region represents the tip leakage vortex of blade 4, which dominates the velocity field in this area. For all serrated cases, the vortex region is centered pitchwise and spanwise at -4.3c_a and 0.19c_a. At this point the minimum velocity is approximately 0.48U_∞ which is higher than at x/c_a = 0.61. Also, the outer edge of the vortex region has expanded spanwise to 0.55c_a which is a 0.15c_a increase over x/c_a = 0.61.

The wakes for all four cases are centered at approximately the same pitchwise location. The blade 5 wake is centered on the pitchwise location of -4.75c_a. For the 1.27 cm serrations, the wake is uniform in the spanwise direction, with an approximate wake width of 0.54c_a. The minimum velocity is still located at the wake center and is approximately 0.62U_∞. The oscillatory shape of the wake in the 2.54 cm serration case is still visible, but the regions of minimum velocity points downstream of the serration tips are not. The minimum velocity of 0.62U_∞ is located near center of wake. The effects of the serration tips and valleys can still seen in the flow field spanwise at 0.75c_a and 0.55c_a, respectively.

The rotation of the vortex region is seen in the V/U_∞ and W/U_∞ velocity vector plots shown in figure 5-22 and the streamwise vorticity, $\Omega_x/U_\infty c_a$, contour plots in figure 5-23 as functions of the pitchwise, z/c_a, and spanwise, y/c_a, coordinates. The vectors plots shown in figure 5-22, are almost identical for all four cases and near the mid-span of the blades, the velocity is much less than in the tip leakage vortex. The counter-clockwise rotating tip leakage vortex, centered pitchwise and spanwise at $-4.25c_a$ and $0.2c_a$, is identical for all four cases. Clockwise rotating secondary vortices seen near the lower endwall in the vicinity of the suctions side of blade 4 and blade 5 can be seen in all four cases. These secondary vortices are centered pitchwise and spanwise at $-3.25c_a$ and $0.09c_a$, and at $-5.0c_a$ and $0.09c_a$, respectively. In all four cases, the secondary vortex located near the suction side of blade 5 interacts with the tip leakage vortex of blade 4, creating a plane of nearly vertical flow pitchwise at $-4.7c_a$, which is the approximate location of the wake centerline. Near the midspan, $y/c_a = 0.92$, some residual spanwise velocity can be seen.

The vorticity contours shown in figure 5-23, shows the region of maximum vorticity of the tip leakage vortex to be centered pitchwise and spanwise at $-4.0c_a$ and $0.12c_a$ for the non-drooped cases and $-4.c_a$ and $0.12c_a$ for the drooped cases. In all of the cases and the baseline (figure 3-11(b)), the vorticity distributions of the main vortex are similar and the serrations have little effect on the tip leakage vortex. The maximum values of vorticity in the tip leakage vortex are indicated by the white cross and the magnitudes as well as their corresponding coordinates are given in table 5-4 below. For comparison purposes the minimum vorticity point was also investigated. In all of the cases, the minimum point is located at the same identical point, but this may be due to the grid used for the interpolation. But it is interesting, that the minimum vorticity increases in magnitude as the serration size is increased and droop is added.

Table 5-4: Maximum and minimum vorticity, $\Omega_x/U_\infty c_a$, in the cross-sections at $x/c_a = 1.82$ for the four serrated trailing edge designs.

Serration Type	***Maximum Vorticity***			***Minimum Vorticity***		
	z/c_a	y/c_a	$\Omega_x/U_\infty c_a$	z/c_a	y/c_a	$\Omega_x/U_\infty c_a$
Baseline	-4.28	0.12	0.77	-4.28	0.12	-0.29
1.27 cm	-4.36	0.12	1.00	-5.28	0.028	-0.29

1.27 cm Droop	-4.25	0.12	0.96	-5.28	0.028	-0.36
2.54 cm	-4.36	0.12	1.10	-5.28	0.028	-0.36
2.54 cm Droop	-4.25	0.12	1.00	-5.28	0.028	-0.40

5.5.4 Turbulence Cross-Sectional Contours at $x/c_a = 1.82$

Figures 5-24 through 5-26 are contour plots of the Reynolds stresses, $\overline{u'^2}/U_\infty^2$, $\overline{v^2}/U_\infty^2$ and $\overline{w^2}/U_\infty^2$, as a function of the pitchwise, z/c_a, and spanwise, y/c_a, coordinates. In all of these figures, the Reynolds stresses are dominant in the tip leakage vortex region near the lower endwall, while the magntidue of these stresses in the wake are much lower. Also, the tip leakage vortex region shape and turbulence levels in this region are similar for all four cases and the baseline (figures 3-12(a) through (c)), showing that the trailing edge shape has only a minimal affect on the tip leakage vortex. In figure 5-24, the maximum streamwise turbulence stress, $\overline{u'^2}$, region does not have the crescent shape seen at x/c_a = 0.61 but instead looks more like a lima bean. This region is centered pitchwise and spanwise at $-4c_a$ and $0.3c_a$ which corresponds to the outer edge of tip leakage vortex. The maximum streamwise turbulence stress level decreased in magnitude compare to x/c_a = 0.61. In figure 5-25, the maximum spanwise turbulence stress, $\overline{v'^2}$, region is located in the central region of the tip leakage vortex, with the maximum value located in the vicinity of z/c_a = -4 and y/c_a = 0.15. Similar to the spanwise turbulence stress, the maximum cross-wake turbulence intensity, $\overline{w'^2}$, region, figure 5-26, is found in the internal region of the tip leakage vortex near the maximum value of $\overline{v'^2}$ with a location of z/c_a = -4 and y/c_a = 0.15. In the wakes of blades 4 and 5, the maximum values of the Reynolds stresses are found near the wake centerline. The distinct wake pattern and maximum Reynolds stresses at the serration tips seen at x/c_a = 0.61 have all but disappeared in these three figures. The maximum value for all Reynolds stresses in the wake is approximately $0.002U_\infty^2$.

In figures 5-27 through 5-29, contours of the Reynolds shear stresses, $\overline{u'v'}/U_\infty^2$, $\overline{u'w'}/U_\infty^2$ and $\overline{v'w'}/U_\infty^2$, are plotted as a function of the pitchwise, z/c_a, and spanwise, y/c_a, coordinates. The regions of maximum magnitude of all of the Reynolds shear stresses occur in the vortex region. In figure 5-19, regions of maximum and minimum $\overline{u'v'}$ are located above and below the center point of the vortex. The maximum region is centered at z/c_a = -4.25 and y/c_a = 0.05, while the minimum region is centered at z/c_a = -4.25 and y/c_a = 0.4. The maximum region is smaller in size than the minimum region, which may be due to lower endwall. In the wake, $\overline{u'v'}$ is almost 0, but in the 2.54 cm serrations, maxim and minima can be still seen in the wakes near the serration tips and valleys, respectively.

Similarly to $\overline{u'v'}$, the $\overline{v'w'}$ contour plot has maximum and minimum regions located in the vortex region. The minimum region is located near the lower endwall and is centered at z/c_a = -4 and y/c_a = 0.15 while the maximum region is centered at z/c_a = -4 and y/c_a = 0.45. The minimum region is stronger in magnitude than the maximum region, most likely because the mean velocity vectors of V and W in this area is much higher than in the maximum region. The $\overline{v'w'}$ in the wake is almost 0, except for a small region of negative $\overline{v'w'}$ near the lower endwall on the pressure side of the wake centered at z/c_a = -4.6 and y/c_a = 0.2, which is in the vicinity of the interaction point between the tip leakage vortex and secondary vortex.

In the shear stress plot of $\overline{u'w'}$, two vertical regions are distributed vertically around the tip leakage center point. To the right of this center point is a region of positive $\overline{u'w'}$ shear, which has a maximum point located near the wake centerline of blade 5. This maximum point is at approximately z/c_a = -4.7 and y/c_a = 0.1. The negative $\overline{u'w'}$ region is located to the left of the vortex center point, and the maximum of this region is centered near z/c_a = -4 and y/c_a = 0.2. In the wakes of blade 4 and 5, the pressure side of the wake is still entirely negative $\overline{u'w'}$ and the suction side is of the wake is positive $\overline{u'w'}$. In the

2.54 cm serrations, the wavy pattern is still visible. Also, for some of the serration tips, peak values of $\overline{u'w'}$ are still visible.

Contours of turbulence kinetic energy, k/U_∞^2, are plotted in figure 5-30 as a function of the pitchwise, z/c_a, and spanwise, y/c_a, coordinates. Once again the shape of and turbulence kinetic energy levels in the tip leakage vortex region for the four serrated cases and the baseline case (figure 3-14(b)) are similar. The highest levels of TKE are found in the vortex region and are located in a circular region that is centered on the vortex center at z/c_a = -4.25 and y/c_a = 0.2. The region has a radius of approximately $0.2c_a$. In this region, the maximum TKE levels are found in the half nearer to the suction side of blade 4, where the maximums of all three Reynolds stresses were found. The TKE distribution at this location is much different than that found at x/c_a = 0.61, where the maximum values were in the vicinity of the pressure side of blade 5.

Figure 5-31 shows contours of turbulence kinetic energy production, $P/U_\infty^3 c_a$, as a function of the pitchwise, z/c_a, and spanwise, y/c_a coordinates. TKE production can be seen in the outer rings of the vortex region. Similar to the TKE plots in figure 5-29, the tip leakage vortex is only minimally affected by the trailing edge shape, and as a result the tip leakage vortex is similar for all four cases and the baseline (figure 3-15(b)).The maximum production level for all four cases is found at approximately z/c_a = -4.0 and y/c_a = 0.35. The magnitude of TKE production at this location varies with serration type and it ranges between $0.0018U_\infty^3 c_a$ to $0.0020U_\infty^3 c_a$. The highest levels or TKE production are found in the drooped trailing edge cases. At the center of the tip leakage vortex, the TKE production is almost 0. This is true for all four sets of serrations. In the wakes of the four sets of serrations TKE production is also 0.

5.6 Mid-span Measurements

Cross-sectional measurements were performed in the vicinity of the mid-span (y/c_a = 0.92) for all four serrated trailing edge cases to qualitatively and quantitatively evaluate the effects on the wake at the four downstream locations of $0.61c_a$, $1.18c_a$, $1.82c_a$ and $2.38c_a$. These cross-sections were measured from tip-to-tip across one

serration length as was described in detail in chapter 4, and they were performed on the wake of blade 5.

5.6.1 Contour Plots

5.6.1.1 1.27 cm Serration

Figure 5-32 shows the streamwise velocity, U/U_∞, contour plots as a function of the pitchwise, z/c_a, and spanwise, y/c_a coordinates at the four downstream locations. In each of these plots, the vertical dashed line represents the approximate wake centerline (line intersecting a locus of minimum streamwise velocities), while the horizontal dashed line is the serration centerline, which in this case would be serration valley. These two lines create quadrants and each quadrant will be referred to as I through IV beginning with the upper right hand corner and going counter clockwise. At x/c_a = 0.61, 1.18, 1.82 and 2.38 the wake centerlines are located at approximately z/c_a = -3.2, -3.95, -4.7 and -5.45, respectively. The wake region is defined as the region where velocity gradients in the pitchwise (z) direction are located. In the wake region at x/c_a = 0.61 a slight bend in the wake centerline towards the suction (right) side of the wake near the serration valley similar to that seen for 2.54 cm serrations in the cross-sections, a is present. As the wake develops downstream this slight bend disappears as can be seen in figures 5-32(b) through (d). The minimum velocity downstream of the two serration peaks is almost the same as the minimum velocity at the serration valley, with a value between $0.54U_\infty$ to $0.56U_\infty$ and as the wake propagates downstream the minimum velocity across the serration becomes more and more uniform. The minimum velocity at the tips in the wake at 1.18, 1.82 and 2.38 is $0.64U_\infty$, $0.66U_\infty$ and $0.67U_\infty$, respectively. The wakes widths, measured between the outer edges of the wake region, increase as the wake travels downstream and they vary between the valley and tip. The wake widths at x/c_a = 0.61 are $0.38c_a$ at the valley, and $0.39c_a$ at the tip, while at x/c_a = 2.38, they are $0.76c_a$ and $0.82c_a$, respectively.

Turbulence kinetic energy, k/U_∞^2, is plotted as a function of the pitchwise, z/c_a, and spanwise, y/c_a, coordinates at the four downstream locations in figures 5-33(a)

through 5-33(d). At all four downstream stations, the TKE is greatest in the wake on the pressure side and largest in magnitude at $x/c_a = 0.61$ with a maximum value of $0.007U_\infty^2$. The TKE decays quickly as the wake propagates downstream, with a maximum value of $0.002U_\infty^2$ in the wake at $x/c_a = 2.38$.

Figures 5-34(a) through 5-34(d) show the TKE production, $P/U_\infty^3 c_a$, in the wake at the four downstream locations as a function of the pitchwise, z/c_a, and spanwise, y/c_a, coordinates. The TKE production is greatest at $x/c_a = 0.62$ and the least at $x/c_a = 2.38$. At $x/c_a = 0.62$, TKE production is greatest on the pressure side of the wake and also half-way between the outer edge on the wake suction side and centerline. That on the pressure side is stronger than that on the suction side with maximum close to $0.004U_\infty^2$ compared to $0.003U_\infty^2$. Along, the wake centerline, TKE production is lower than at these two locations with a maximum value of $0.002U_\infty^2$. This can also be seen at $x/c_a = 1.18$. At $x/c_a = 1.82$ and $x/c_a = 2.38$, TKE production has decayed below $0.0005U_\infty^2$ and is not visible in these plots.

5.6.1.2 1.27 cm Serration with Droop

In figure 5-35, the mean streamwise velocity, U/U_∞^2 , contours are plotted as a function of the pitchwise, z/c_a, and spanwise, y/c_a coordinates. In these plots, the approximate wake centerlines at the tips for $x/c_a = 0.61$, 1.18, 1.82 and 2.38 are located at $z/c_a = -3.25$, -3.9, -4.7 and -3.35, respectively. At $x/c_a = 0.61$, wake bending at the serration valley can be seen and this bending appears to be more drastic than for the 1.27 cm serration. As the wake propagates downstream, the wake bending becomes less and less visible. At $x/c_a = 2.28$, the wake appears to be similar to that seen for the baseline. The minimum velocity points at $x/c_a = 0.61$ in the wake are found downstream of the serration tips with a value of $0.54U_\infty$, and the minimum velocity downstream of the serration valley is $0.57U_\infty$. At $x/c_a = 0.61$, the wake width downstream of the tip and valley are both $0.40c_a$ while at $x/c_a = 2.38$ the wake widths are $0.68c_a$ and $0.65c_a$, respectively.

Figure 5-36 shows contour plots of TKE, k/U_∞^2, as a function of the pitchwise, z/c_a, and spanwise, y/c_a, coordinates at the four downstream stations. At all downstream

stations, the shape of the TKE contours reflect the shape of the mean velocity contours in figure 5-35. The highest levels of TKE in the wake are found on the pressure side of the wake. The difference between the pressure side and the suction side TKE levels are most extreme in the x/c_a = 0.61 case. On the pressure side, the TKE has a value of approximately $0.007U_\infty^2$ while on the suction side it is $0.0057U_\infty^2$. This variation between the pressure and suction side almost disappears and the maximum TKE level in the wake decays by the time the wake reaches x/c_a = 2.38, where the pressure and suction sides of the wake have TKE values of $0.002U_\infty$.

The maximum TKE production, $P/U_\infty^3 c_a$, is found downstream of the serration tips and along the outer edges of the wake on the pressure and suction sides, as shown in figures 5-37(a) through 5-37(d). In the wake center, it is much lower than at the wake edges. At x/c_a = 0.61, the maximum TKE production levels on the pressure and suction sides of the wake are $0.004U_\infty^3 c_a$ and $0.0035U_\infty^3 c_a$, respectively, while in the wake center it is only $0.002U_\infty^3 c_a$. This trend can also be seen at x/c_a = 1.18, figure 5-37(b), and also holds true at x/c_a = 1.82 and 2.38 (figures 5-37c) and (d)), but the TKE production level is less than $0.0005U_\infty^3 c_a$.

5.6.1.3 2.54 cm Serration

Figure 5-38(a) through (d) the mean streamwise velocity, U/U_∞^2, contours are plotted as a function of the pitchwise, z/c_a, and spanwise, y/c_a coordinates. Vertical and horizontal dashed lines on the figure represent the mean wake centerline and the serration valley (upper and lower bounds of y-coordinate are serration tips). For the four locations, the wake centerlines downstream of the tips are located at y/c_a = -3.15, -3.9, -4.72 and -5.48. At x/c_a = 0.61, the bending of the wake region is much more drastic for the 2.54 cm cases than for the 1.27 cm cases. Here the difference between the minimum velocity point at the tip and the serration valley is approximately, $-0.1c_a$. The difference between the minimum velocity point downstream of the serration valley and the tip decreases as the wake propagates downstream. For x/c_a = 1.18 through 2.28, figures 5-38(b) through (d), they are $-0.1c_a$, $-0.08c_a$, and $-0.07c_a$. The minimum streamwise velocity points in the wake at x/c_a = 0.61 are along the mean wake centerline downstream of the serration tips.

At these points, the mean velocity is $0.53U_\infty$. At the valley center, the mean streamwise velocity is between $0.60U_\infty$ and $0.62U_\infty$. As the wake propagates downstream, the variation of the mean streamwise velocity across the wake decreases. At x/c_a = 2.38, this variation is only $0.01c_a$, where U/U_∞ = 0.65 downstream of the valley and 0.64 downstream of the tip. Finally, as the wake travels downstream the wake widths grow. At x/c_a = 0.61 the wake widths downstream of the serration tip and valley are $0.40c_a$ and $0.41c_a$, respectively, while at x/c_a = 2.38, these widths are $0.65c_a$ and $0.64c_a$, respectively, with the wake at the serration valley growing a sligtly faster than at the tip.

Contours of turbulence kinetic energy, k/U_∞^2, as a function of the pitchwise, z/c_a, and spanwise, y/c_a, coordinates at the four downstream stations are presented in figures 5-39. At x/c_a = 0.61, the maximum levels of turbulence kinetic energy are found downstream of serration tips on the pressure side of the wake. At this location they reach a maximum of $0.0075U_\infty^2$. Downstream of the valley, TKE is much lower reaching a maximum value of $0.0055U_\infty^2$, which is also found on the pressure side of the wake. As the wake propagates downstream, the region of high and low levels of TKE begin to balance each other out to where the difference between them at x/c_a = 2.38 is minimal. At this location the maximum level of TKE is found at the valley and it is $0.0019U_\infty^2$ (at the tip it is $0.0018U_\infty^2$). Also, as can be seen the TKE levels decay rapidly. At x/c_a = 1.18 the max level is $0.004U_\infty^2$ and at x/c_a = 1.82 it is $0.0025U_\infty^2$.

Figure 5-40 shows the contours of TKE production, $P/U_\infty^3 c_a$, across the serration as a function of the pitchwise, z/c_a, and spanwise, y/c_a, coordinates. At x/c_a = 0.61, TKE production is highest in the near the tips, which is where TKE itself is the highest. At the tip TKE production is approximately $0.006U_\infty^3 c_a$. Near the valley, TKE production levels are below $0.002U_\infty^3 c_a$. Half between the lower serration tip and the valley, a region of negative production is found near the wake minimum velocity line and this is not present between the upper serration tip and valley. At x/c_a = 1.18, TKE production peaks are now located between the tips and the valley and on the pressure side of the wake. This is consistent with the highest levels of TKE at this location. At x/c_a = 1.82 and 2.38, the highest levels of TKE production are now found downstream of the valley, but they are much less than at x/c_a = 0.61.

5.6.1.4 2.54 cm Serration with Droop

In figure 5-41, the mean streamwise velocity, U/U_∞^2, contours are plotted as a function of the pitchwise, z/c_a, and spanwise, y/c_a coordinates. The distinctive bending of the wake is also seen here. The wake centerline downstream of the tips for the four locations are at z/c_a = -3.1, -3.9, -4.7 and -5.5. The difference between the minimum velocity location downstream of the valley and tip for the four locations are -0.14c_a, -0.17c_a, -0.11c_a and -0.10c_a. Thee minimum velocity locations are downstream of the serration tips while the streamwise velocity downstream of the valley is slightly higher. At x/c_a = 0.61, the minimum velocity at the tip is 0.52U_∞ while in the valley it is 0.55U_∞. As the wake propagates downstream, the difference between these points reduces. At x/c_a = 2.38, the minimum mean velocities in the wake downstream of the tip is 0.66U_∞ while in the downstream of the valley it is 0.67U_∞. The width of the wake also varies between the tip and valley. At x/c_a = 0.61, downstream of the tip the wake width is 0.44c_a while at the valley it is 0.39c_a. These wakes widths increase in size as the wake travels downstream, but the difference in width is still present. At x/c_a = 2.38, the wake width at the tip is 0.83c_a while at the valley it is 0.71c_a.

Contours of turbulence kinetic energy, k/U_∞^2, as a function of the pitchwise, z/c_a, and spanwise, y/c_a, coordinates at the four downstream stations are plotted in figure 5-42. Similar to the three cases described in the above sections, TKE levels downstream of the tips are the greatest in the wake, while those downstream of the valley are the least. Also, the highest levels of TKE are found along the pressure side of the wake. Downstream of the serration tip, maximum TKE levels are almost 0.008U_∞^2 while those downstream of the serration valley are 0.0055U_∞^2. The TKE levels decay and the variation between the maximum values downstream of the serration tip and valley also reduce at the further downstream stations. At x/c_a = 2.38, the TKE levels downstream of the serration tip are 0.0018U_∞^2 and downstream of the valley they are 0.0020U_∞^2.

Contour plots of turbulence kinetic energy production, $P/U_\infty^3 c_a$, across the serration as a function of the pitchwise, z/c_a, and spanwise, y/c_a, coordinates.are shown in figure 5-43. At x/c_a = 0.61, TKE production is greatest downstream of the serration tips on the pressure side of the wake and the lowest along the minimum mean streamwise velocity line. At y/c_a = 0.83, there is a region of negative TKE production which does not

occur periodically in the spanwise direction. As the wake propagates downstream, the maximum TKE production levels propagate towards the serration valley region of the wake. Also, TKE production is equal on both the suction and pressure side of the wakes, and approximately 0 along the minimum mean streamwise velocity line.

5.6.2 Wake Characteristics of Serrated Trailing Edged Blades

In the next sections the wake characteristics for the four blade sets will be introduced. These include the wake mean velocity deficit, the half-wake width, the edge velocity and the momentum thickness, which were defined in section 3.7.1. Also, the mean velocity and turbulence profiles will be presented normalized on the wake properties to show how these wakes differ from those of the baseline. Finally, the maximum values for both the mean velocity and turbulence will be plotted and compared to the baseline configuration.

The wake characteristics, in particular the wake spreading and the mean streamwise velocity deficit decay rates, are of interest because it is predicted by increasing these two rates a more uniform mean streamwise velocity profile in the pitchwise direction will be present, which is predicted to decrease the tonal noise at downstream stator vane leading edge due to the reduction of the periodic fluctuations in the mean velocity of the rotor blade wake.

5.6.2.1 1.27 cm Serration

5.6.2.1.1 Wake Characteristics

The wake characteristics for the 1.27 cm serration were calculated at the five spanwise measurement locations of $0.83c_a$, $0.87c_a$, $0.91c_a$, $0.95c_a$, and $0.99c_a$ at the four downstream locations of $0.61c_a$, $1.18c_a$, $1.82c_a$, and $2.38c_a$, using the definitions and technique described in section 3.7.1. These values are listed in table 5.5 below. Figure 5-44 is a plot of the wake half-width normalized on the momentum thickness, L_w/θ, as a function of the streamwise coordinate normalized on the momentum thickness, X/θ. In this plot, the quad-wire data for baseline blades are plotted along with the five spanwise

locations for this serration size. Curve fits were plotted on the y/c_a = 0.91, 0.95 and 0.99 data sets (assuming periodic behavior in spanwise direction, and furthest locations from lower endwall effects) as well as on the baseline. From these curve fits, it was determined that the spreading rates for these three spanwise locations are proportional to $(X/\theta)^{0.40}$, $(X/\theta)^{0.46}$ and $(X/\theta)^{0.47}$, respectively. The spreading rates downstream of the serration tip and the half-way point are greater than the baseline rate of $(X/\theta)^{0.45}$. The spreading rate of the wake downstream of the serration valley is slower than the baseline and the other two spanwise locations.

Table 5-5: Wake parameters downstream of the 1.27cm serrated trailing edge.

x/c_a	y/c_a	U_e/U_∞	U_w/U_∞	L_w/c_a	θ/c_a
0.61	0.833	0.766	0.214	0.0584	0.0268
0.61	0.871	0.764	0.199	0.0603	0.0261
0.61	0.909	0.763	0.194	0.0608	0.0252
0.61	0.948	0.762	0.201	0.0570	0.0248
0.61	0.986	0.761	0.205	0.0547	0.0244
1.18	0.833	0.770	0.140	0.0773	0.0256
1.18	0.871	0.770	0.136	0.0793	0.0255
1.18	0.909	0.771	0.133	0.0791	0.0248
1.18	0.948	0.771	0.136	0.0773	0.0247
1.18	0.986	0.771	0.134	0.0768	0.0241
1.82	0.833	0.770	0.112	0.102	0.0254
1.82	0.871	0.769	0.113	0.0947	0.0256
1.82	0.909	0.769	0.110	0.0944	0.0250
1.82	0.948	0.769	0.109	0.0930	0.0245
1.82	0.986	0.768	0.107	0.0906	0.0234
2.38	0.833	0.758	0.0963	0.106	0.0254
2.38	0.871	0.758	0.0966	0.106	0.0252
2.38	0.909	0.758	0.0941	0.103	0.0245
2.38	0.948	0.758	0.0922	0.105	0.0239
2.38	0.986	0.758	0.0927	0.103	0.0243

The centerline velocity deficit normalized on the edge velocity, U_w/U_e, as a function of the streamwise downstream distance normalized on the momentum thickness, X/θ, is plotted in figure 5-45. The data from the five spanwise locations are plotted in comparison to the baseline data. Curve fits were applied to the data at y/c_a = 0.91, 0.95 and 0.99 to determine the centerline velocity deficit decay rate, and they were determined to be $(X/\theta)^{-0.51}$, $(X/\theta)^{-0.55}$ and $(X/\theta)^{-0.57}$, respectively. Comparing to the baseline data, the

decay rate downstream of the serration tip is larger, while the half-way location is the same as the baseline. The decay rate downstream of the serration valley is the slowest.

The normalized momentum thickness, θ/c_a, at each spanwise location was calculated using equation 3-10 and plotted in figure 5-46 versus the downstream streamwise coordinate normalized on the axial chord, X/c_a. For each spanwise location the momentum thickness remains almost constant in the streamwise direction. However, the momentum thickness varies across the span. The largest momentum thickness at all downstream locations is found at the lower serration tip, y/c_a = 0.83, while the smallest momentum thickness is found at the upper serration tip, y/c_a = 0.99. The average percent variation across all four downstream locations is approximately 7.1%. This variation may be due to the slight non two-dimensionality of the flow field at these locations.

The momentum thickness for each spansiwe location, calculated above, were normalized on the half-wake width, θ/L_w, and plotted versus the normalized centerline velocity deficit, U_w/U_e, in figure 5-47 to determine if the momentum thickness follows the same unique relationship as those for the baseline blades. This unique relationship is the second order polynomial, equation 3-11, developed by Wyganski *et al.(*1986). In section 3.7.2, the coefficients of this polynomial, Ψ_1 and Ψ_2, for the baseline case were determined to be 2.138 and 1.758, respectively. In figure 5-43, the five spanwise locations of 0.83c_a, 0.87c_a, 0.91c_a, 0.95c_a, and 0.99c_a as well as the baseline case are plotted. Curve fits were applied to the data at y/c_a = 0.91, 0.95 and 0.99, to determine the coefficients (table 5-6). For the serration tip and the half-way point, the coefficients are similar to those determined for the baseline blades. If more data points were available, the polynomial coefficients may be identical for all three cases. However, at serration valley, the polynomial deviates from the other three cases.

Table 5-6: Coefficients of the momentum thickness curve fit for 1.27 cm serration

Measurement	Ψ_1	Ψ_2
Baseline Blades (Quad-Wire)	2.138	1.758
$y/c_a = 0.91$	2.176	2.147
$y/c_a = 0.95$	2.087	1.639
$y/c_a = 0.99$	2.101	1.674

5.6.2.1.2 Mean Velocity Profiles

Figure 5-4(a) through (e) are the normalized mean velocities, (U-U_e/U_w), versus the normalized cross-wake distance, Z/L_w, at y/c$_a$ = 0.83c_a, 0.87c_a, 0.91c_a, 0.95c_a, and 0.99c_a. It can be seen that at all of the spanwise locations, the plots have all almost collapsed on each other, meaning they have almost reached self-similarity which was the same trend seen in the baseline case described in section 3.7.3. At y/c_a = 0.99, figure 5-47(e), x/c_a = 1.82 does not fit the trend, but this is most likely because the maximum velocity deficit was not at the wake centerline.

The curve fit developed by Wygnanski *et al.* (1986), which accurately describes the profile shape of the mean velocity curve of the plane wakes, was plotted on the mean velocity plots in figure 5-48(a) through (e). Both, the curve the parameter values determined to fit the baseline blades and those determined by Devenport *et al* (1998) were plotted. Devenport *et al.*'s curve fit fits the data points at y/c_a = 0.83, 0.91, and 0.99better than that determine for the baseline. None of the curves fit the profiles at y/c_a = 0.87c_a and 0.95c_a, which are the points located between the serration tip and valley.

Figure 5-49(a) through (e) are the plots of the normalized spanwise velocity, V/Uw, at the five spanwise locations and four downstream locations. The spanwise velocity variation ranges between 8%U_w and 13%U_w, which is almost double the variation seen for the baseline. The plots at the four downstream locations collapse or are close to collapsing on each other at all spanwise locations. Similar to the baseline, the larger positive spanwise variations occur at the furthest downstream locations, which may be due to the effects of the tip leakage vortex as it grows in area as it travels downstream.

Finally, figures 5-50(a) through (e) show the plots of the normalized cross-wake velocity distribution, W/U_w, at the five spanwise locations and four downstream locations. All spanwise locations have the same saw-tooth profile of the cross-wake velocity, where the difference between the minimum and maximum values decays with downstream location. At x/c_a = 0.61 difference between minimum and maximum is approximately 0.1U_w while at x/c_a = 1.82 this difference is approximately 0.04U_w. The first three axial locations follow the same pattern of oscillating around the horizontal axis of plots, but at x/c_a = 2.38 the entire plot is shifted in the positive direction and does not oscillate around

the *y*-axis. Also, at all downsteam locations the profiles are becomimg more and more positive with increasing spanwise location.

5.6.2.1.3 Turbulence Profiles

Figures 5-51 through 5-53 are the plots of the normalized normal stress $\overline{u'^2/U_w^2}$ $\overline{v'^2/U_w^2}$, and $\overline{w'^2/U_w^2}$ while figures 5-54 through 5-56 are the normalized shear stresses $\overline{u'v'/U_w^2}$, $\overline{u'w'/U_w^2}$, and $\overline{v'w'/U_w^2}$. All of the plots are a function of the normalized local cross-wake coordinate, Z/L_w. It can be seen that the Reynolds stresses in figures 5-51, 5-52 and 5-55 are all approaching self-similarity, similar to was seen in the baseline cases. The Reynolds stress, $\overline{u'^2}$, is approaching a maximum value between $0.15U_w^2$ and $0.17U_w^2$, $\overline{v'^2}$ is approaching a value between $0.13U_w^2$ and $0.15U_w^2$ and $\overline{u'w'}$ is approaching a maximum and minimum value of $0.4U_w^2$ and $-0.5U_w^2$. However, $\overline{w'^2}$ seems to following a different trend than what was seen with the baseline cases. Instead of progressing towards a maximum value, it is reaches its maximum at x/c_a = 1.18 and then begins to drop in magnitude with each downstream station there after.

For this trailing edge serration $\overline{u'v'}$ is still less than ¼ of the shear stress $\overline{u'w'}$ (similar to baseline), but $\overline{v'w'}$ is now larger in magnitude with the peak value being ½ the smallest peak value of $\overline{u'w'}$. Also, the profile shapes of both shear stresses are quite unique. The shear stress $\overline{u'v'}$ has between 3 to 4 minimum and maximum peaks, compared to the 2 seen for the baseline, which was also anti-symmetric. The shear stress $\overline{v'w'}$ has only one minimum peak which seems to be progressing towards 0, as the wake propagates downstream.

Turbulence kinetic energy, k/U_w^2, profiles are plotted in figure 5-57. It can be seen that in all of the plots in figure 5-53, the TKE is progressing toward self-similarity which is located between $0.20U_w^2$ and $0.24U_w^2$. The same increase of the maximum value with increasing spanwise direction that was seen with the Reynolds stresses can also be seen here.

The final plots, figures 5-58 and 5-59, are plots of the maximum values of Reynolds stresses $\overline{u'^2}/U_e^2$ $\overline{v'^2}/U_e^2$ $\overline{w'^2}/U_e^2$ $\overline{u'v'}/U_e^2$ $\overline{u'w'}/U_e^2$ and $\overline{v'w'}/U_e^2$ and turbulence kinetic energy, k/U_e^2, as a function of the downstream locations, x/c_a. The Reynolds stresses, $\overline{u'^2}$, $\overline{v'^2}$ and $\overline{u'w'}$, have the same magnitude as the baseline at all four downstream locations. The Reynolds stresses $\overline{u'v'}$ and $\overline{v'w'}$ are slightly lower at all spanwise and downstream locations, while $\overline{w'^2}$ is at least $0.05U_e^2$ lower than the baseline at all downstream locations. As a result the TKE is lower than the baseline at all downstream locations and all spanwise locations. In all of the plots, the larger values are found at the higher spanwise locations, which is what was seen in the turbulence profile plots.

On a final note, figure 5-60, shows a plot of the wake centerline location for each of the spanwise locations. The wake centerline at the first three downstream locations is at the same approximate coordinates and follows the same path as the baseline case. However, when it reaches the last axial location, it seems the wake have leaned spanwise, resulting in the lowest spanwise location being more positive than the other spanwise locations.

5.6.2.2 1.27 cm Serration with Droop

5.6.2.2.1 Wake Characteristics

The wake characteristics for the 1.27 cm drooped trailing edge serration were calculated at the five spanwise locations across the serration height at each downstream location. Table 5-7 below lists these values for these characteristics. Figure 5-61 is a plot of the wake half-width normalized on the momentum thickness, L_w/θ, as a function of the streamwise coordinate normalized on the momentum thickness, X/θ. In this plot, the quad-wire data for baseline blades are plotted along with the five spanwise locations for this serration size. Curve fits were plotted on the y/c_a = 0.91, 0.95 and 0.99 data sets as well as on the baseline data set. From these curve fits, it was determined that the spreading rates at these three locations are proportional to $(X/\theta)^{0.43}$, $(X/\theta)^{0.45}$ and $(X/\theta)^{0.43}$, respectively. The spreading rates at the serration tip and the serration valley are equal,

while for the 1.27 cm case the spreading rate of the serration tip was larger than at the serration valley. The location half-way between the serration tip and valley experienced a slightly larger spreading rate, than the other two locations. All three spanwise locations are comparable to the baseline spreading rate of $(X/\theta)^{0.45}$.

Table 5-7: Wake parameters downstream of the 1.27cm serrated trailing edge.

x/c_a	y/c_a	U_e/U_∞	U_w/U_∞	L_w/c_a	θ/c_a
0.608	0.833	0.759	0.227	0.0591	0.0305
0.608	0.871	0.761	0.214	0.0630	0.0289
0.608	0.909	0.762	0.204	0.0589	0.0263
0.608	0.948	0.762	0.208	0.0576	0.0261
0.608	0.986	0.762	0.221	0.0611	0.0277
1.178	0.833	0.754	0.144	0.0797	0.0269
1.178	0.871	0.755	0.101	0.0811	0.0271
1.178	0.909	0.756	0.143	0.0793	0.0264
1.178	0.948	0.757	0.143	0.0819	0.0269
1.178	0.986	0.757	0.143	0.0777	0.0261
1.819	0.833	0.770	0.142	0.0951	0.0269
1.819	0.871	0.771	0.118	0.0964	0.0269
1.819	0.909	0.770	0.118	0.0954	0.0265
1.819	0.948	0.769	0.116	0.0954	0.0261
1.819	0.986	0.769	0.115	0.0937	0.0258
2.382	0.833	0.768	0.115	0.109	0.0267
2.382	0.871	0.768	0.101	0.107	0.0265
2.382	0.909	0.769	0.102	0.105	0.0259
2.382	0.948	0.769	0.101	0.105	0.0257
2.382	0.986	0.770	0.100	0.107	0.0264

Figure 5-62 is a plot of the centerline velocity deficit normalized on the edge velocity, U_w/U_e, as a function of the streamwise downstream distance normalized on the momentum thickness, X/θ. The data from the five spanwise locations are plotted in comparison to the baseline data. Curve fits were applied to the data at y/c_a = 0.91, 0.95 and 0.99 to determine the centerline velocity deficit decay rate, and they were determine to be $(X/\theta)^{-0.52}$, $(X/\theta)^{-0.53}$ and $(X/\theta)^{-0.56}$, respectively. Comparing to 1.27 cm serration, the spreading rates are comparable to those at the same location. The spreading rate of the serration valley is only slightly higher, while those at the mid-point and the serration tip are slightly lower.

The normalized momentum thickness, θ/c_a, at each spanwise location is plotted in figure 5-63 versus the streamwise coordinate normalized on the axial chord, X/c_a. For each spanwise location the momentum thickness remains almost constant in the streamwise direction, except for y/c_a = 0.87 and 0.99 at x/c_a = 0.61. After this axial location, the momentum thickness at these spanwise locations become thinner and remains constant. Also, the spanwise variation of 7.1% seen in the 1.27cm case is now only an average of 3.5%. The momentum thickness at all spanwise locations are approximately $0.001c_a$ thicker than the baseline case.

In figure 5-64, the momentum thickness for each spanwise location were normalized on the half-wake width, θ/L_w, and plotted versus the normalized centerline velocity deficit, U_w/U_e. From this plot the coefficients of this polynomial curve fit, Ψ_1 and Ψ_2, were determined. These curve fits were applied to the data at y/c_a = 0.91, 0.95 and 0.99, to determine the coefficients (table 5-8). The serration valley and the half-way point match the baseline case the best, but they do deviate from this case after U_w/U_e = 0.3. However, the polynomial fit to the serration tip data deviates the most from the other three cases after U_w/U_e = 0.2 which is reverse of 1.27 cm case.

Table 5-8: Coefficients of the momentum thickness curve fit for 1.27 cm serration with droop

Measurement	Ψ_1	Ψ_2
Baseline Blades (Quad-Wire)	2.138	1.758
$y/c_a = 0.909$	2.028	1.373
$y/c_a = 0.948$	2.055	1.459
$y/c_a = 0.986$	2.166	2.071

5.6.2.2.2 Mean Velocity Profiles

Figure 5-65(a) through (e) are the normalized mean velocities, $(U-U_e/U_w)$, versus the normalized cross-wake distance, Z/L_w across the serration. It can be seen that at all of the spanwise locations, the plots have all collapsed on each other, meaning they have almost reached self-similarity which was the same trend seen in 1.27 cm serration and the baseline cases. The profile shape of these velocity curves, defined by equation 3-13 and

using the parameters for the baseline blades and those determined by Devenport *et al*., were plotted. Devenport *et al*.'s curve fit fits the data points best all spanwise locations.

Figure 5-66(a) through (e) are the plots of the normalized spanwise velocity profile, V/U_w, at the five spanwise locations and four downstream locations. The spanwise velocity variation ranges between 9%U_w and 14%U_w, which is the similar to the 1.27 cm serration. The plots at the four downstream locations collapse or are close to collapsing on each other at all spanwise locations. Similar to the baseline and 1.27 cm serration case, the larger positive spanwise variations occur at the furthest downstream locations, which may be the result of due to the effects of the tip leakage vortex as it grows in area as it travels downstream.

Finally, figures 5-67(a) through (e) show the plots of the normalized cross-wake velocity profile, W/U_w, at the five spanwise locations and four downstream locations. All spanwise locations have the same profile which is different from the saw-tooth profile seen for the 1.27 cm serration case. At x/c_a = 0.61 the cross-flow velocity is positive at all locations inside and outside of the wake and the magnitude is much larger, with a value of 0.225U_w, than what was seen for the baseline and the 1.27 cm serration. The difference between the maximum and minimum values at this location of 0.15U_w is comparable to what was seen in the baseline case. As the wake propagates downstream, the plot shifts down toward the negative origin, and the difference between the maximum and minimum values fall below 0.05U_w. Also, at all downstream locations the profile become more and more positive with decreasing spanwise location, opposite of what was seen for the 1.27 cm serration.

5.6.2.2.3 Turbulence Profiles

Figures 5-68 through 5-70 are the plots of the normalized normal stress $\overline{u'^2/U_w^2}$ $\overline{v'^2/U_w^2}$, and $\overline{w'^2/U_w^2}$ versus the normalized cross-wake coordinate, while figures 5-71 through 5-73 are the normalized shear stresses $\overline{u'v'/U_w^2}$, $\overline{u'w'/U_w^2}$, and $\overline{v'w'/U_w^2}$ as a function of the normalized local cross-wake coordinate, Z/L_w. It can be seen that the Reynolds stresses in figures 5-68 through 5-70 and 5-72 are all approaching self-similarity, similar

to was seen in the baseline cases. The stress term, $\overline{u'^2}$, is lower than that of the 1.27 cm serrated droop, reaching a maximum value between $0.13U_w$ and $0.14U_w$, while the same is true is for $\overline{v'^2}$ which has a maximum value between $0.11U_w$ and $0.12U_w$. The stress term $\overline{w'^2}$ is tending toward the maximum value between $0.13U_w$ and $0.14U_w$ which is the similar trend seen in the baseline. All of these maximum values are less than that seen in the baseline. The shear stress $\overline{u'w'}$ has the same minimum and maximums as the baseline and the 1.27 cm case.

The same Reynolds shear stresses $\overline{u'v'}$ and $\overline{v'w'}$ shear stress profiles that were seen for the 1.27 cm case, is seen here. The shear stress $\overline{u'v'}$ is still less than ¼ of the shear stress $\overline{u'w'}$ and $\overline{v'w'}$ has a single peak that is ½ the smallest peak value of $\overline{u'w'}$. The major difference between this case and the 1.27 cm is the profile shape of $\overline{u'v'}$. As the wake propagates downstream the shear stress $\overline{u'v'}$ tends toward an anti-symmetric profile shape centered on the wake centerline with minimum and maximum values of $\pm 0.1U_w^2$. The same shape was seen in the baseline case. The shear stress $\overline{v'w'}$ still only one minimum peak which seems to be progressing towards 0, as the wake propagates downstream.

Turbulence kinetic energy profiles, k/U_w^2, are plotted in figure 5-74. It can be seen that in all of the plots in figure 5-80, TKE is progressing toward self-similarity which is located between $0.18U_w^2$and $0.19U_w^2$. These values are between $0.02U_w^2$ and $0.04U_w^2$ smaller than the 1.27 cm and the baseline cases. Increase of the maximum value with increasing spanwise direction can also be seen here.

The plots of the maximum values of Reynolds stress $\overline{u'^2}/U_e^2$ $\overline{v'^2}/U_e^2$ $\overline{w'^2}/U_e^2$ $\overline{u'v'}/U_e^2$ $\overline{u'w'}/U_e^2$ and $\overline{v'w'}/U_e^2$ and turbulence kinetic energy, k/U_e^2, as a function of the downstream locations, x/c_a, are shown in figures 5-75 and 5-76. The Reynolds stresses $\overline{u'^2}$ and $\overline{v'^2}$, are lower in magnitude than the baseline at x/c_a = 1.82 and 2.38. For the stresses $\overline{u'^2}$ and $\overline{v'^2}$, the baseline maximum values were $0.02U_e^2$ lower than for this case, but by x/c_a = 2.38, the baseline is $0.003U_e^2$ higher. The cross-wake Reynolds stress, $\overline{w'^2}$, is lower than the baseline at every station. At x/c_a = 0.61, the baseline is $0.04U_e^2$ higher, but by x/c_a = 2.38, the baseline is less than $0.003U_e^2$ higher than this case. The

shear stresses, $\overline{u'v'}$, $\overline{u'w'}$, and $\overline{v'w'}$, have the same magnitude as the baseline or are slightly lower at all downstream locations. Also, TKE is lower than the baseline at all downstream locations except for $x/c_a = 0.61$. At the three other downstream locations, the TKE levels of the 1.27 cm serrated trailing edge with droop are at least $0.0005U_e^2$ lower than the baseline.

Figure 5-77 is a plot of the wake centerline as a function of the spanwise location as it propagates downstream. The wake at all five spanwise locations propagate parallel to the baseline wake and the variation of the wake center locations is barely visible at $x/c_a = 0.61$, and follows almost the same propagation line at $x/c_a = 2.38$ as the baseline.

5.6.2.3 2.54 cm Serration

5.6.2.3.1 Wake Characteristics

The values of the wake characteristics for the 2.54 cm serration are listed in table 5-9 below. Figure 5-78 is a plot of the wake half-width normalized on the momentum thickness, L_w/θ, as a function of the streamwise coordinate normalized on the momentum thickness, X/θ. In this plot, the quad-wire data for baseline blades are plotted along with the five spanwise locations for this serration size. Curve fits were plotted on the y/c_a = 0.87, 0.95 and 1.02 data sets as well as on the baseline data set. The spreading rates for these three locations were determined from the curve fits and they were determined to be proportional to $(X/\theta)^{0.38}$, $(X/\theta)^{0.47}$ and $(X/\theta)^{0.54}$, respectively. The spreading rates downstream of the serration tip and valley are larger than the baseline case, $(X/\theta)^{0.45}$, while the serration valley is slower. Comparing to the 1.27 cm and the 1.27 cm serration with droop, the spreading rate downstream of the serration tip is also much larger, while the mid-point spreading rate is only slightly higher. The serration valley for this case has a spreading rate that is slower than the 1.27 cm and the 1.27 cm with droop, which both had spreading rates of $(X/\theta)^{0.40}$ and $(X/\theta)^{0.43}$, respectively.

Table 5-9: Wake parameters downstream of the 2.54cm serrated trailing edge.

x/c_a	y/c_a	U_e/U_∞	U_w/U_∞	L_w/c_a	θ/c_a
0.608	0.715	0.768	0.228	0.057	0.027

0.608	0.792	0.768	0.208	0.079	0.031
0.608	0.868	0.768	0.170	0.065	0.024
0.608	0.945	0.767	0.203	0.063	0.028
0.608	1.021	0.767	0.224	0.057	0.027
1.178	0.715	0.763	0.135	0.086	0.027
1.178	0.792	0.766	0.134	0.095	0.030
1.178	0.868	0.766	0.128	0.085	0.025
1.178	0.945	0.766	0.126	0.088	0.026
1.178	1.021	0.766	0.134	0.083	0.026
1.819	0.715	0.774	0.108	0.111	0.028
1.819	0.792	0.773	0.108	0.109	0.028
1.819	0.868	0.773	0.108	0.104	0.027
1.819	0.945	0.771	0.104	0.105	0.026
1.819	1.021	0.770	0.110	0.107	0.028
2.382	0.715	0.738	0.089	0.124	0.027
2.382	0.792	0.745	0.094	0.121	0.029
2.382	0.868	0.746	0.092	0.116	0.026
2.382	0.945	0.749	0.090	0.117	0.027
2.382	1.021	0.748	0.092	0.121	0.027

Figure 5-79 is a plot of the centerline velocity deficit normalized on the edge velocity, U_w/U_e, as a function of the streamwise downstream distance normalized on the momentum thickness, X/θ. The data from the five spanwise locations are plotted in comparison to the baseline data. Curve fits were applied to the data at y/c_a = 0.87, 0.95 and 1.02 to determine the centerline velocity deficit decay rate, and they were determined to be $(X/\theta)^{-0.46}$, $(X/\theta)^{-0.57}$ and $(X/\theta)^{-0.65}$, respectively. The decay rates downstream of the serration tip and the serration mid-height are higher than the baseline and the two 1.27 cm serration cases. On the other hand, the serration valley is quite a bit lower than the baseline and the two 1.27cm serration cases.

The normalized momentum thickness, θ/c_a, at each spanwise location is plotted in figure 5-80 versus the downstream streamwise coordinate normalized on the axial chord, X/c_a. For this serration case, the momentum thickness does not seem to remain constant for all streamwise locations. They oscillate up and down with streamwise location. Also, the momentum thickness is not constant with spanwise location either. The thickest momentum thickness of $0.029c_a$ is found at y/c_a = 0.79, while the thinnest of $0.026c_a$ is found at y/c_a = 0.87. It would seem the thickest momentum thickness should be found downstream of the serration tips because that is where the largest amount of surface area

is found. The thickest momentum thickness is 5.5% thicker than the 1.27cm with droop, 12.3% thicker than the 1.27 cm and 13.8% thicker than the baseline.

In figure 5-81, the momentum thickness was normalized on the half-wake width, θ/L_w, and plotted versus the normalized centerline velocity, U_w/U_e. From this plot the coefficients of this polynomial curve fit, Ψ_1 and Ψ_2, were determined. These curve fits were applied to the data at y/c_a = 0.87, 0.95 and 1.02, to determine these coefficients (table 5-10). Similar to the 1.27 cm serration, the curve fit for the serration tip and the serration mid-point match the baseline curve fit the closest. Once again, if more points were taken, the values of Ψ_1 and Ψ_2 may be almost identical. The serration valley on the other hand deviates from the baseline curve after $0.2U_w/U_e$, which was also seen in the 1.27 cm case.

Table 5-10: Coefficients of the momentum thickness curve fit for 2.54 cm serration

Measurement	Ψ_1	Ψ_2
Baseline Blades (Quad-Wire)	2.138	1.758
$y/c_a = 0.868$	2.117	1.924
$y/c_a = 0.945$	2.084	1.659
$y/c_a = 1.021$	2.072	1.670

5.6.2.3.2 Mean Velocity Profiles

Figure 5-82(a) through (e) are the normalized mean velocities, $(U-U_e/U_w)$, versus the normalized cross-wake distance, Z/L_w at y/c_a = $0.72c_a$, $0.79c_a$, $0.87c_a$, $0.95c_a$, and $1.02c_a$. It can be seen that at all of the spanwise locations, the plots have all collapsed on each other, meaning they have almost reached self-similarity which was the same trend seen in both 1.27 cm serration and the baseline cases. The curve fit from Devenport *et al.*. matches the data better than the baseline curve fit. The only exception occurs at $0.72c_a$ were neither curve fit matches the data. Also, at this same spanwise location, the profile at x/c_a = 2.38 does not overlap the other three axial locations, which may be due to the minimum velocity point not being located at the wake center. At the inner spanswise locations of $0.79c_a$, $0.87c_a$, and $0.95c_a$, and at the axial location of 0.61, the positive side

half of the velocity profile seems to still be developing. This is similar to what was seen at $x/c_a = 0.002$ for the baseline. This effect is most noticeable at $y/c_a = 0.79$.

Figure 5-83(a) through (e) are the plots of the normalized spanwise velocity distribution, V/U_w, versus the normalized cross-wake coordinate, Z/L_w. The spanwise velocity varies much more than the 1.27 cm serration cases with the peak spanwise velocity being 20%U_w. Unlike the 1.27 cm cases and the baseline, these velocity plots do not seem to be collapsing on each other and vary greatly with axial downstream location as well as with the spanwise location.

Figures 5-84(a) through (e) show the plots of the normalized cross-wake velocity distribution W/U_w, versus the normalized cross-wake coordinate, Z/L_w. Similar to the spanwise velocity, these plots are far from collapsing on each other. The variation between the velocity profiles at each axial downstream location is great. The major difference between this case and the 1.27 cm cases in that the velocity profiles become more and more positive with increasing axial downstream location. This also occurs with increasing spanwise location, which is similar to what was seen in the 1.27 cm serration.

5.6.2.3.3 Turbulence Profiles

Figures 5-85 through 5-87 are the plots of the normalized normal stress $\overline{u'^2/U_w^2}$ $\overline{v'^2/U_w^2}$, and $\overline{w'^2/U_w^2}$ versus the, while figures 5-88 through 5-90 are the normalized shear stresses $\overline{u'v'/U_w^2}$, $\overline{u'w'/U_w^2}$, and $\overline{v'w'/U_w^2}$. All of the plots are a function of the normalized cross-wake coordinate, Z/L_w. It can be seen that the Reynolds stresses in figures 5-86 and 5-90 are approaching self-similarity, similar to was seen in the baseline cases, while the stresses plotted in 5-85 and 5-87 reach their maximum peak value at $x/c_a = 1.18$ and then begin to decrease. The Reynolds stress term, $\overline{u'^2}$, reaches a maximum value of $0.16U_w^2$, the $\overline{v'^2}$ term reaches a maximum value of $0.14U_w^2$ ($y/c_a = 0.95$ is higher with a value of $0.16U_w^2$) and the stress term $\overline{w'^2}$ reaches a maximum between $0.17U_w^2$ and $0.18U_w^2$ ($y/c_a = 0.95$ is higher with a value of $0.20U_w^2$). All of these maximum values are approximately the same as the baseline, except for some of the stresses, which decay after

reaching their maximum value. The shear stress $\overline{u'w'}$ has minimum and maximum of -$0.05U_w^2$ and $0.04U_w^2$ which is similar to those seen in the baseline and the 1.27 cm cases.

The Reynolds shear stress profile of $\overline{u'v'}$ for this case, figure 5-88, is different than was seen in the other two cases and the baseline. The maximum value of this shear stress has increased, with a maximum value of approximately ½ the smallest peak value of. $\overline{u'w'}$. Also, the profile shape varies with spanwise location. The two serration tip profiles do not match, with the shear stress profile at y/c_a = 0.75 most likely being affected by the tip leakage vortex. At y/c_a = 1.02, the first two axial locations the profiles have two positive and two negative peaks. As the wake propagates downstream, it seems the profile is changing to a positive peak on the negative side of the wake centerline and negative peak on the positive side of the wake centerline. At central serration locations of $0.79c_a$, $0.87c_a$, and $0.95c_a$ the profiles have a distinct positive and negative peak. In all three cases, the peaks are decaying with downstream location. The peaks are largest in magnitude at $0.79c_a$ and $0.95c_a$ with maximum values of almost $0.03U_w^2$. Also, at these locations the profiles are mirror images (inverted) of each other.

The $\overline{v'w'}$ shear stress profile, figure 5-90, is similar to the 1.27 cm cases. For the serration tips and valley, $\overline{v'w'}$ has a single peak that is ½ the smallest peak value of $\overline{u'w'}$. This peak seems to be progressing towards 0 as the wake propagates downstream. At the spanwise locations of $0.79c_a$ and $0.95c_a$ the profiles are different. At $0.79c_a$, the profile is oscillating around the *x*-axis of the plot, while at $0.95c_a$ the magnitude of the maximum shear stress value is over twice as large as the other spanwise locations, which also seems to be progressing towards 0.

Turbulence kinetic energy profiles, k/U_w^2, are plotted in figure 5-91. At y/c_a = 0.87, the plot is tending towards self-similarity, while at the other four spanwise locations the maximum value of TKE is reached at x/c_a = 1.18 and then decays thereafter. The maximum TKE levels are found at $0.79c_a$, $0.87c_a$, and $0.95c_a$, with values ranging between $0.23U_w^2$ through $0.25U_w^2$. These maximum values are larger than the 1.27 cm serration cases. The lowest maximum values of TKE are found at the serration tips with values ranging between $0.20U_w^2$ and $0.22U_w^2$.

The plots of the maximum values of Reynolds stress $\overline{u'^2}/U_e^2$ $\overline{v'^2}/U_e^2$ $\overline{w'^2}/U_e^2$ $\overline{u'v'}/U_e^2$ $\overline{u'w'}/U_e^2$ and $\overline{v'w'}/U_e^2$ and turbulence kinetic energy, k/U_e^2, as a function of the downstream locations, x/c_a, are shown in figures 5-92 and 5-93. The Reynolds stresses $\overline{u'^2}$ and $\overline{v'^2}$ for the serration valley is lower in magnitude than the baseline at $x/c_a = 0.61$, while the serration tips and mid-heights are larger. As the wake propagates downstream, the turbulence intensities decay more rapidly for serration tips and the mid-heights until all of the maximum intensities in the serration are of approximately the same magnitude. They are also less than the baseline with a value of $0.003U_e^2$. The cross-wake Reynolds stress $\overline{w'^2}$ is lower than the baseline at every station. At $x/c_a = 0.61$, the highest values are found at the serration tips and the mid-heights while the valley is the lowest. As the wake propagates downstream, all of them have the same $\overline{w'^2}$ level of approximately $0.002U_e^2$. For the shear stress $\overline{u'v'}$ at $x/c_a = 0.61$ the serration mid-heights are higher in magnitude than the baseline, the serration tips are approximately the same as the baseline, and the serration valley is lower. As the wake travels downstream, the shear stress at all of the spanwise locations become the same as the baseline. For the shear stress $\overline{u'w'}$, all of the spanwise locations have the same magnitude as the baseline or are slightly lower at all downstream locations. The same is true for the shear stress $\overline{v'w'}$ with the exception of $y/c_a = 0.79$, which is higher at the first two axial locations than the other locations but then decays to the same level. The TKE levels for the serration mid-heights and the tips are almost the same as or higher than the baseline and the valley is less than the baseline at $x/c_a = 0.61$. At $x/c_a = 2.382$ they all are less than the baseline with a value of $0.003U_e^2$.

Figure 5-94 is a plot of the wake centerline in the *x-z* plane as it propagates downstream. The wake at all five spanwise locations propagates parallel to the baseline wake and the variation of the wake center locations is visible at $x/c_a = 0.61$. The serration valley is further to the left of the baseline, and the serration tip to the right of the baseline. The serration mid-heights are located at the same location as the baseline point. As the wake propagates downstream, the pitchwise difference between the wake centerline locations are less, and they are located to the left of the baseline, with the exception of $y/c_a = 0.72$, which may be affected by the tip leakage vortex.

5.6.2.4 2.54 cm Serration with Droop

5.6.2.4.1 Wake Characteristics

The wake characteristics were calculated for the 2.54cm serration were calculated and can be found in table 5-11 below. Figure 5-95 is a plot of the wake half-width normalized on the momentum thickness, L_w/θ, as a function of the streamwise coordinate normalized on the momentum thickness, X/θ. In this plot, the quad-wire data for baseline blades are plotted along with the nine spanwise locations for this serration size. Curve fits were plotted on the y/c_a = 0.87, 0.95 and 1.03 data sets as well as on the baseline data set. The spreading rates at these there locations were determined from the curve fits and they were found to be proportional to $(X/\theta)^{0.44}$, $(X/\theta)^{0.33}$ and $(X/\theta)^{0.57}$, respectively. The spreading rates at the tips are larger than the baseline case, $(X/\theta)^{0.45}$, while the serration mid-height is the slowest. Downstream of the serration valley the decay rate is only slightly lower than the baseline. Comparing to the 2.54 cm, 1.27 cm and the 1.27 cm drooped cases, the spreading rate downstream of the serration tip is also larger than those cases, while the mid-point spreading rate is much lower than the other cases. The serration valley for this case has a spreading rate that is slower than the other three cases.

Table 5-11: Wake parameters downstream of the 2.54 cm serrated trailing edge with droop.

x/c_a	y/c_a	U_e/U_∞	U_w/U_∞	L_w/c_a	θ/c_a
0.608	0.720	0.714	0.209	0.065	0.031
0.608	0.751	0.713	0.200	0.067	0.031
0.608	0.812	0.713	0.162	0.077	0.030
0.608	0.874	0.713	0.145	0.061	0.021
0.608	0.935	0.712	0.150	0.072	0.026
0.608	0.996	0.710	0.202	0.066	0.029
0.608	1.027	0.715	0.212	0.064	0.030
1.178	0.720	0.761	0.128	0.097	0.029
1.178	0.792	0.759	0.114	0.114	0.030
1.178	0.874	0.757	0.109	0.089	0.023
1.178	0.950	0.756	0.111	0.103	0.027
1.178	1.027	0.754	0.127	0.096	0.030
1.819	0.720	0.770	0.101	0.125	0.030
1.819	0.792	0.772	0.099	0.132	0.030

1.819	0.874	0.775	0.098	0.111	0.026
1.819	0.950	0.778	0.094	0.120	0.027
1.819	1.027	0.782	0.104	0.120	0.030
2.382	0.720	0.755	0.085	0.137	0.029
2.382	0.792	0.759	0.087	0.138	0.029
2.382	0.874	0.763	0.086	0.127	0.027
2.382	0.950	0.767	0.083	0.125	0.026
2.382	1.027	0.768	0.083	0.130	0.025

Figure 5-96 a plot of the centerline velocity deficit normalized on the edge velocity, U_w/U_e, as a function of the streamwise downstream distance normalized on the momentum thickness, X/θ. The data from this serration case is compared to the baseline data. Curve fits were applied to the data at y/c_a = 0.87, 0.95 and 1.03 to determine the centerline velocity deficit decay rates, and they were determine to be $(X/\theta)^{-0.52}$, $(X/\theta)^{-0.40}$ and $(X/\theta)^{-0.66}$, respectively. The decay rates downstream of the serration tip higher than the baseline and the two 1.27 cm serration cases and approximately the same as the 2.54 cm serration. On the other hand, the serration mid-height is quite a bit lower than the baseline, the 2.54 cm serration and the two 1.27 cm serration cases. The serration valley is approximately the same as the 1.27 cm and 1.27 cm droop cases.

The normalized momentum thickness, θ/c_a, at each spanwise location is plotted in figure 5-97 versus the downstream streamwise coordinate normalized on the axial chord, X/c_a. For this case, the momentum thickness does not seem to remain constant for all streamwise locations and at some spanwise locations oscillations in the thickness can be seen. At y/c_a = 0.87 the momentum thickness is still growing as the wake is propagating downstream.. The thickest momentum thickness of $0.03c_a$ is found at y/c_a = 0.72 which is the lower serration tip and is approximately the same as the 2.54 cm case.

In figure 5-98, the momentum thickness was normalized on the half-wake width, θ/L_w, and plotted versus the normalized centerline velocity, U_w/U_e. From this plot the coefficients of this polynomial curve fit, Ψ_1 and Ψ_2, were determined. These curve fits were applied to the data at y/c_a = 0.87, 0.95 and 1.03, to determine the coefficients (table 5-12). The curve fit for the serration tip and the serration valley match the baseline curve fit the closest, while the serration mid-height does not match the baseline. The serration valley deviates from the baseline curve after U_w/U_e = 0.2, which was also seen in the 1.27

cm and the 1.27 cm droop cases, while the mid-height deviates from the baseline after $U_w/U_e = 0.15$.

Table 5-12: Coefficients of the momentum thickness curve fit for 2.54 cm droop serration

Measurement	Ψ_1	Ψ_2
Baseline Blades (Quad-Wire)	2.138	1.758
$y/c_a = 0.87$	2.084	1.802
$y/c_a = 0.95$	2.148	2.345
$y/c_a = 1.03$	2.039	1.443

5.6.2.4.2 Mean Velocity Profiles

Figure 5-99(a) through (e) are the normalize mean velocities, $(U-U_e/U_w)$, versus the normalized cross-wake distance, Z/L_w It can be seen that at $y/c_a = 0.72c_a$, $0.87c_a$ and $1.03c_a$ the plots have all collapsed on each other, while at $0.79c_a$ and $0.95c_a$ the plots are close to collapsing on each other. These plots do not quite collapse on either the positive or negative side of the wake centerline. Curve fits matching the profile shape were also plotted, and Devenport *et al.* (1998) fit once again matches the data better than the baseline curve fit for $y/c_a = 0.72c_a$, $0.87c_a$ and $1.03c_a$ while neither curve matches the profiles at $0.79c_a$ and $0.95c_a$.

Figure 5-100(a) through (e) are the plots of the normalized spanwise velocity distribution, V/U_w, versus the normalized cross-wake coordinate, Z/L_w. Unlike 2.54 cm serration, the spanwise velocity distribution once again collapses on each other. The velocity plot tends toward having peak values of $\pm 0.1U_w$, except for the two mid-height locations, which have peak values of $-0.15U_w$ and $0.1U_w$. These maxim and minima are still lower than the 2.54 cm case and are comparable to the 1.27 cm cases. .

Finally, figures 5-101(a) through (e) are the plots of the normalized spanwise velocity distribution, W/U_w, versus the normalized cross-wake coordinate, Z/L_w.. Similar to 2.54 cm case, these plots are far from collapsing on each other. The variation between the velocity profiles at each axial downstream location is large. As the wake propagates downstream, the velocity profile tends to become more and more positive in magnitude.

Also, the velocity magnitude increases with increasing spanwise location, ranging from $0.1U_w$ near the lower serration tip to $0.25U_w$ at the upper serration tip.

5.6.2.4.3 Turbulence Profiles

Figures 5-102 through 5-104 are the plots of the normalized normal stress $\overline{u'^2/U_w^2}$ $\overline{v'^2/U_w^2}$, and $\overline{w'^2/U_w^2}$ while figures 5-105 through 5-107 are the normalized shear stresses $\overline{u'v'/U_w^2}$, $\overline{u'w'/U_w^2}$, and $\overline{v'w'/U_w^2}$. All of the plots are plotted versus the normalized cross-wake coordinate, Z/L_w. It can be seen that the Reynolds stress $\overline{v'^2}$, figure 5-103 is the only one that follows the trends seen in the baseline case and as the wake travels downstream it is approaching self-similarity. The other stresses, $\overline{u'^2}$ and $\overline{w'^2}$ in figures 5-102 and 5-104 do not follow this trend and peak at x/c_a = 1.18 before decaying. The stress $\overline{u'^2}$ reaches a maximum of $0.24U_w^2$, $\overline{v'^2}$ has a maximum of $0.21U_w^2$ and $\overline{w'^2}$ has a maximum of $0.25U_w^2$. For all of the Reynolds stresses the maximum values were found downstream of the serration mid-heights. The shear stress $\overline{u'w'}$ was initially higher in magnitude but the minimum and maximum peaks still tend to $-0.05U_w^2$ and $0.04U_w^2$ which is what was the baseline and the other serration cases.

The Reynolds shear stresses $\overline{u'v'}$, figure 5-105, seen here is different than in any of the other cases. The maximum value of this shear stress has increased, with the maximum magnitude being approximately the same magnitude as the smallest peak value of $\overline{u'w'}$. Also, the profile shape varies with spanwise location. The two serraton tip profiles are similar to each other with a minimum and maximum peak at x/c_a = 0.61 which then changes to one strong positive peak with a value between $0.01U_w^2$ and $0.015U_w^2$. At mid-heights of the serration at the spanwise locations of $y/c_a = 0.79c_a$ and $0.95c_a$ the profiles have distinct positive and negative peaks, and they are mirror images of each other. In both cases, the peak on the positive side of the wake has the largest magnitude, For $y/c_a = 0.792c_a$ the peak value is $-0.05U_w^2$ and $y/c_a = 0.95c_a$ it is $0.05U_w^2$. In both cases, the peaks are decaying with downstream location. Downstream of the serration valley, the profile is a mirror image of that at the serration tips.

The $\overline{v'w'}$ Reynolds shear stress profile, figure 5-107, is similar to the 2.54 cm case. For the serration tips and valley, $\overline{v'w'}$ has a single peak that is ½ the smallest peak value of $\overline{u'w'}$, This peak seems to be progressing towards 0 as the wake propagates downstream. At the spanwise locations of $0.79c_a$ and $0.95c_a$ the profiles are similar to what was seen in the 2.54 cm case.

Turbulence kinetic energy profiles, k/U_w^2, are plotted in figure 5-108 as a function of the cross-wake coordination, Z/L_w. Downstream of the serration tips at, $y/c_a = 0.79$ and 0.95, the plot is tending toward self-similarity with a maximum value of approximately $0.25U_w^2$. The other three spanwise locations reach maxims between $0.34U_w^2$ and $0.35U_w^2$ at $x/c_a = 1.18$ after which they decay. These are the highest levels of TKE seen in any of the other three cases and the baseline.

The plots of the maximum values of Reynolds stress $\overline{u'^2}/U_e^2$ $\overline{v'^2}/U_e^2$ $\overline{w'^2}/U_e^2$ $\overline{u'v'}/U_e^2$ $\overline{u'w'}/U_e^2$ and $\overline{v'w'}/U_e^2$ and turbulence kinetic energy, k/U_e^2, as a function of the downstream locations, x/c_a, are shown in figures 5-109 and 5-110. The Reynolds stress $\overline{u'^2}$ for the serration valley is lower in magnitude than the baseline at $x/c_a = 0.61$, while the serration tips and mid-heights are larger. This is similar to what was seen for the 2.54 cm case. Once again the maximum values decay more rapidly for serration tips and the mid-heights, and they are the same or less than the baseline beyond $x/c_a = 1.82$. The spanwise stress $\overline{v'^2}$ is greater than the baseline at all spanwise locations at $x/c_a = 0.61$, but decays below the baseline level by the time the wake reaches $x/c_a = 2.38$. The cross-wake stress $\overline{w'^2}$ is lower than the baseline at every station. Once again, at $x/c_a = 0.61$, the highest values of the five spanwise locations are found at the serration tips and the mid-heights while the valley is the lowest. As the wake propagates downstream, all of them have the same maximum $\overline{w'^2}$ level of approximately $0.002U_e^2$ For the shear stresses $\overline{u'v'}$ at $x/c_a = 0.61$ the levels are higher than the baseline everywhere except for the serration valley but as the wake travels downstream, the shear stress at all of the spanwise locations reduce in magnitude and are almost the same as the baseline. For the shear stress $\overline{u'w'}$ the serration tips and the mid-heights have levels that are higher than the baseline, while the serration valley is lower. As the wake propagates downstream, they all

decay below the baseline. The shear stress $\overline{v'w'}$ at the mid-heights of the serration are higher than the baseline, but they decay to the same level as the other spanwise locations. The TKE for the mid-height and the serration tips are higher than the baseline and the valley is less than the baseline at x/c_a = 0.61. They all decay and they are less than the baseline at x/c_a = 2.38 with a magnitude of $0.003U_e^2$.

Figure 5-111 is a plot of the wake centerline in the *x-z* plane as it propagates downstream. Similar to the 2.54 cm serration the wake at all five spanwise locations propagate parallel to the baseline wake and the difference between the wake center locations is visible at x/c_a = 0.608 with the serration valley further to the left of the baseline, and the serration tip to the right of the baseline. The serration mid-heights are located near the baseline point. As the wake propagates downstream, the pitchwise difference between spanwise locations becomes less. At x/c_a = 2.38 the serration mid-heights and valley are to the left of the baseline, while the serration tips are to the right. This is different from the 2.54 cm case.

5.6.3 Spectra at Wake Center at Mid-span of Serrated Blades

Spectral measurements were made at every point in the mid-span cross-section and at all downstream locations for all sets of trailing edge serrations. The spectral measurements were made to determine if these trailing edge modifications introduce any periodic behavior that is present in the turbulence and determine the amount of energy in this periodic behavior. The wake center spectral plots are analyzed and compared to the baseline in this section.

For the 1.27 cm case, figures 5-112 through 5-114 are plots of normalized spectra at the wake center for each measurement row in the mid-span cross-section. The spectral functions G_{uu}, G_{vv} and G_{ww} on the vertical axis are normalized by and the frequency, *f*, on the horizontal axis is normalized by $(L_{w,p}/U_e)$. In figure 5-112(a) through (e), the normalized spectral function G_{uu} is plotted for all five spanwise locations. It can be seen that for all of the spanwise locations, the spectral plots are progressing toward self similarity similar to what was seen in the baseline configuration. At the serration mid-heights, peaks in the spectral plots are seen at the normalized frequency of 0.2 at x/c_a =

0.608, but quickly disappears as the wake propagates downstream. Peaks are also seen at the mid-heights of the serrations in the spectral function plots of G_{vv} in figures 5-113(b) and (d) at the normalized frequency of 0.3 at $x/c_a = 0.61$. For both spectral function these peaks disappear by $x/c_a = 1.18$. Similar to the baseline the spectral function peaks at $1(U_e/L_{w,p})/(1/U_w^2)$ for G_{ww} in figure 5-114 at all spanwise locations but decays to $0.5(U_e/L_{w,p})/(1/U_w^2)$ and shifts to the normalized frequency of 0.5 by $x/c_a = 2.38$.

For the 1.27 cm serration case with droop, peaking is seen in the G_{uu} in figure 5-115 at the mid-height of the serration. These peaks are small and on the order of what was seen in the 1.27 cm case. As the wake propagates downstream the peaks disappear and the spectral plot tends toward self-similarity. In figure 5-116, a small peak is seen in the spectral plot of G_{vv} at the mid-height locations at the normalized frequency of 0.4 at $x/c_a = 0.61$, but this also disappears by $x/c_a = 1.18$. For the spectral plot G_{ww}, in figure 5-117, peaking is seen at all spanwise locations but is only $0.4(U_e/L_{w,p})/(1/U_w^2)$ compared to $1(U_e/L_{w,p})/(1/U_w^2)$ seen in the 1.27 cm case.. Interestingly, it increases slightly as it the wake propagates downstream to $0.5(U_e/L_{w,p})/(1/U_w^2)$, and it shifts to the higher normalized frequency of 0.4 to 0.3.

The spectral function of G_{uu} in figure 5-118 for the 2.54 cm case only has peaking at serration valley occurring only at the downstream location of $x/c_a = 0.61$. At the mid-height of the serration, the energy level is lowest at $x/c_a = 0.61$ and it increases as the wake travels downstream. At $x/c_a = 0.61$, the value is $0.2(U_e/L_{w,p})/(1/U_w^2)$ but at $x/c_a = 2.38$ it is $0.4(U_e/L_{w,p})/(1/U_w^2)$. Also, it can be seen that the plot is tending to towards self-similarity. In the G_{vv} spectral plot in figure 5-119, small peaks can be seen at all of the spanwise locations, but at the serration valley, this peak is the largest with a spectral level of $0.4(U_e/L_{w,p})/(1/U_w^2)$ at the normalized frequency of 0.3 at the downstream location of $x/c_a = 0.61$. This peak, like the others, decays as the wake progresses downstream. In figure 5-120, peaks of $1(U_e/L_{w,p})/(1/U_w^2)$ in the spectral function of G_{ww} can be seen at all spanwise locations, which is what was seen in the baseline case. Similarly, it decays and shifts to the higher frequencies as the wake propagates downstream.

Finally, the 2.54cm serration with droop, has spectral peaking at all spanwise locations at $x/c_a = 0.61$ in the spectral fuction of G_{uu} shown in figure 5-121. The peaking is not greater than for the other cases seen prior. In the G_{vv} spectral function, shown in

figure 5-122, the largest peak is seen at the serration valley, with a peak spectral level of $0.5(U_e/L_{w,p})/(1/U_w^2)$ at the normalized frequency of 0.3. Finally, the G_{ww} spectral function shown in figure 5-123, has spectral peaks of almost $1(U_e/L_{w,p})/(1/U_w^2)$ at all of the spanwise locations. As the wake travels downstream, the peak values decay and the wake tends toward self-similarity.

5.7 Summary

In this chapter measurements were performed on the four types of serrated trailing edged GE-Rotor-B blades in the Virginia Tech linear cascade tunnel to investigate their effect on the downstream turbulent wake. The four sets of serrated blades, defined in detail in chapter 4, included two different serration sizes (1.27 cm and 2.54 cm) and for each different serration size a second set of blades with added trailing edge camber. The measurements that were performed were blade loading, Pitot-static cross-sections and four sensor hot-wire cross sections at two axial downstream locations of $0.84c_a$ and $1.88c_a$ as well as at mid-span at four downstream axial locations $0.61c_a$, $1.18c_a$, $1.82c_a$, and $2.38c_a$

Blade loading measurements showed that the blade loading and the circulation were slightly dependent on the trailing edge shape. The blade loadings of the serrated blades compared to the baseline were identical on both the pressure and suction sides over the first 10% of the axial chord but after encountering the trip, deviations in the blade loading could be seen, especially on the pressure side for the drooped cases. The circulation for the 1.27 cm serration and the 2.54 cm serration with droop nearly matched the baseline (2.2% lower), while the circulation for the 1.27 cm serration with droop was 6.7% larger and for the 2.54 cm it was 8.9% less.

The Pitot-static cross-sections of the four serrated blades showed that flow-fields near the upper and lower endwalls were similar to the baseline at both downstream locations. The largest variation occurred in the wake shed by blades. The 1.27 cm wake was similar to the baseline, while in the plot of the 1.27 cm drooped serration the individual serration peaks could be seen. For both sets of the 2.54 cm wake, the serration peaks and valleys could clearly be seen and the wake had an oscillatory shape in the

spanwise direction. But as the wakes propagated downstream the tips and valleys of the serrations were not as well defined for all four cases

Three-component velocity measurements were performed between the lower endwall and the mid-height of the tunnel to reveal in detail the tip leakage vortex. The mean velocity and turbulence properties of the tip leakage vortex were qualitatively and quantitatively nearly the same as the baseline. The largest differences were seen in the streamwise vorticity of the tip leakage. The maximum streamwise vorticity increased with serration size, and compared to the baseline they were between 24% to 33% stronger at x/c_a = 0.61 and at x/c_a = 1.82, they were 23% stronger. The shape of the secondary vortex also appeared to have changed for each of the serrations, but the strength of this vortex for the 1.27 cm cases was nearly the same as the baseline, while the 2.54 cm cases were slightly stronger.

The four-sensor hot-wire measurements at the blade mid-spans revealed in detail the wakes of serrated blades away from the influence of the tip-leakage vortex. Qualitatively, the magnification of the bending of the wake with increased serration size and droop was seen. At the furthest upstream location, the mean velocity deficits, turbulence kinetic energies, and turbulence kinetic energy production were greatest on the pressure side of wake downstream of the serration tips. Downstream of the serration valleys these properties were least. As the wake traveled downstream, the streamwise velocity, TKE and TKE production became more uniform through-out the entire wake region. At x/c_a = 2.38, TKE production was almost 0.

From the mid-span measurements the wake properties at the four downstream locations for the four serrated blades were calculated. The wake properties showed that the wake spread faster downstream of the serration tips for the 1.27 cm and the 2.54 cm cases. Increasing the serration size increases the spreading rate, but adding droop did not show any apparent improvement. In most cases, as the spreading rates downstream of the serration tips were accelerated, the spreading rate downstream of the serration valley decreased as was seen in the 2.54 cm cases. The decay of the centerline velocity deficit also showed the same trends. With the increase of these rates, this will be beneficial in the reduction of tonal noise at the leading edge of the downstream stator vane due to the

reduction of the periodic fluctuations in the pitchwse direction of the mean streamwsie velocity of the rotor blade wake.

Comparing the normalized velocity profiles at the four downstream locations at each spanwise location showed that the smaller serration size, 1.27 cm, had the best agreement with turbulent plane wake theory investigated by Wygnanski *et al.* (1986). As the serration size was increased and droop was added, the less the profiles collapsed and the agreement with theory decayed. Plots of maximum Reynolds stresses and kinetic energy for the serrated blades showed that they were usually higher (except for $\overline{w'^2}$ which was less) at $x/c_a = 0.61$ compared to the baseline but decayed to levels that were below or equal to those found in the baseline by $x/c_a = 2.38$.

Finally, wake centerline spectral plots in the three velocity directions were plotted. Compared to the baseline spectral plots, the same similarity can be seen in the four serrated trailing edge cases. Peaking was once again seen in both the *V* and *W* directions. Also peaking was seen in the *U* direction in the spectral plots, but these peaks become more dominant as the serration size is increased and droop is added. The peaking in the spectral plots was assumed to be due to the coherent vortex shedding.

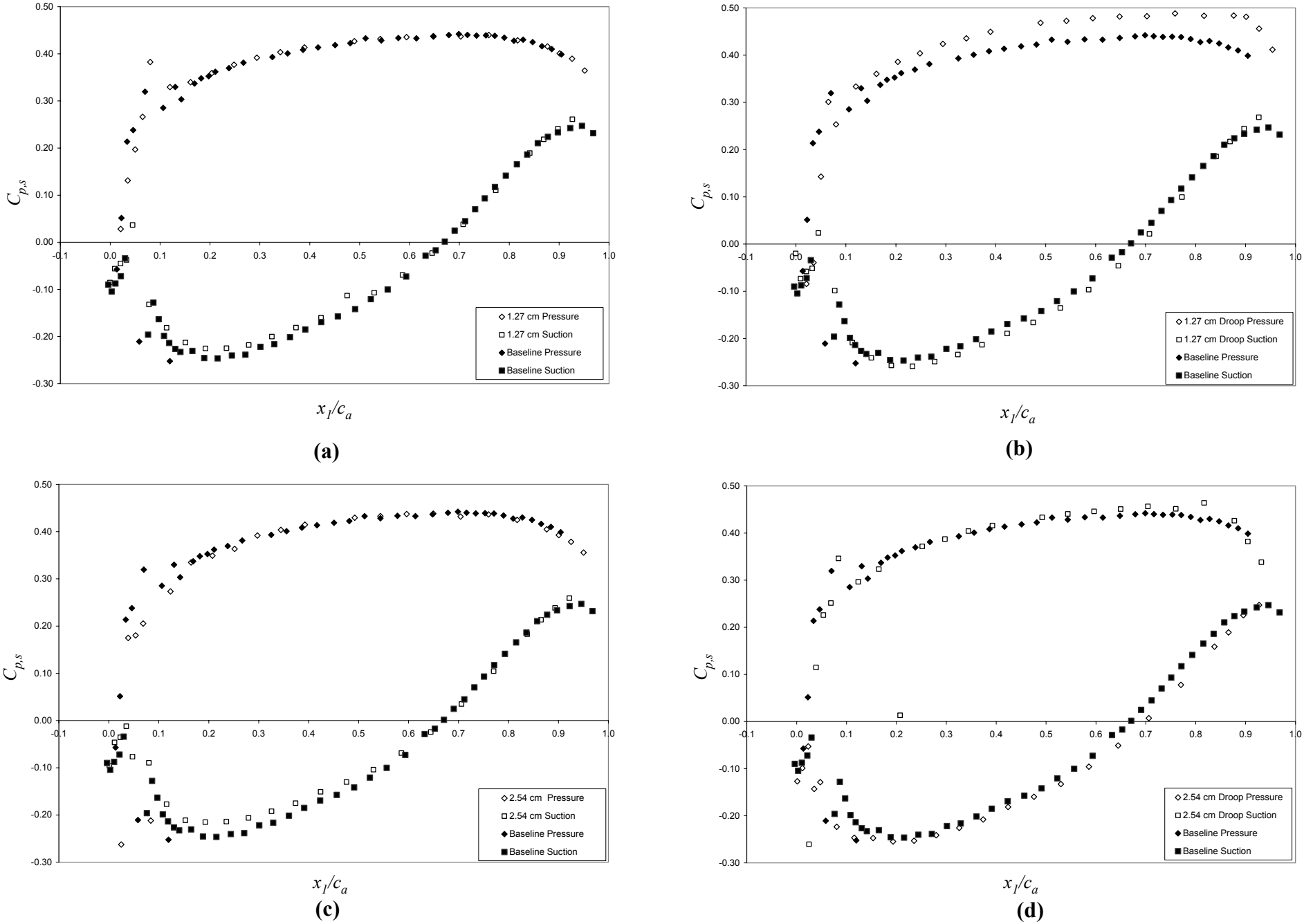

Figure 5-1: Blade loading, $C_{p,s}$, for the four serrated trailing edges compared to the baseline: **(a)** 1.27 cm, **(b)** 1.27 cm droop, **(c)** 2.54 cm, **(d)** 2.54 cm droop.

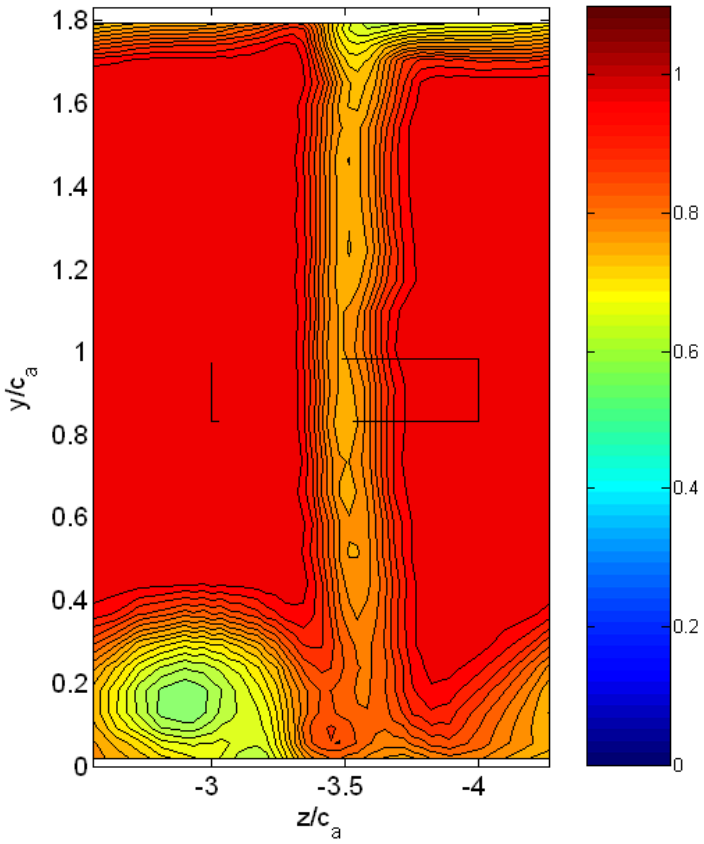

(a) Total pressure coefficient, $C_{p,o}$

(b) Local mean streamwise velocity normalized on the reference velocity, U/U_∞

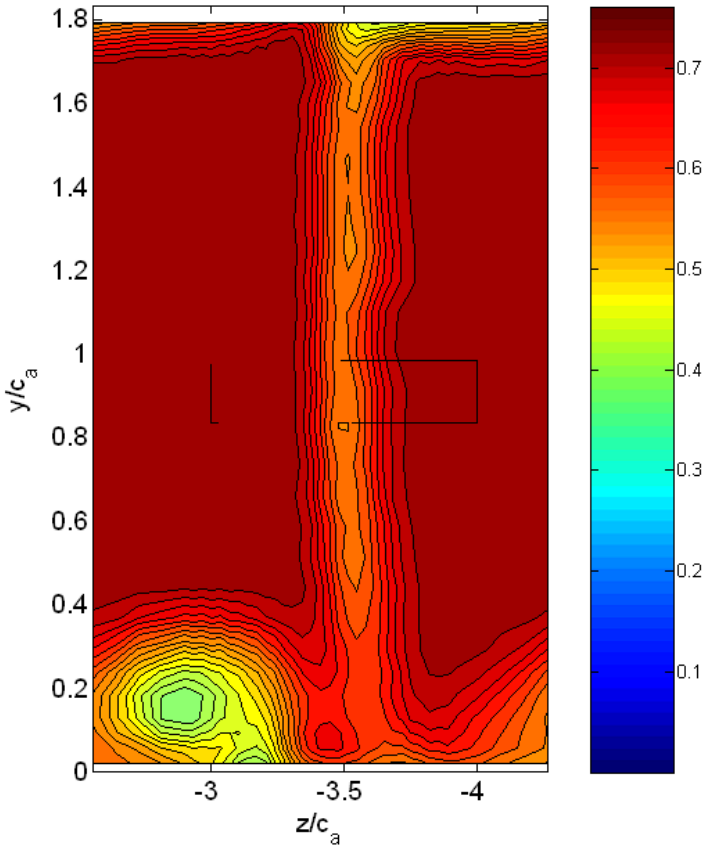

Figure 5-2: Pitot-static cross-sectional measurements for the 1.27 cm serrated blade at $x/c_a = 0.84$

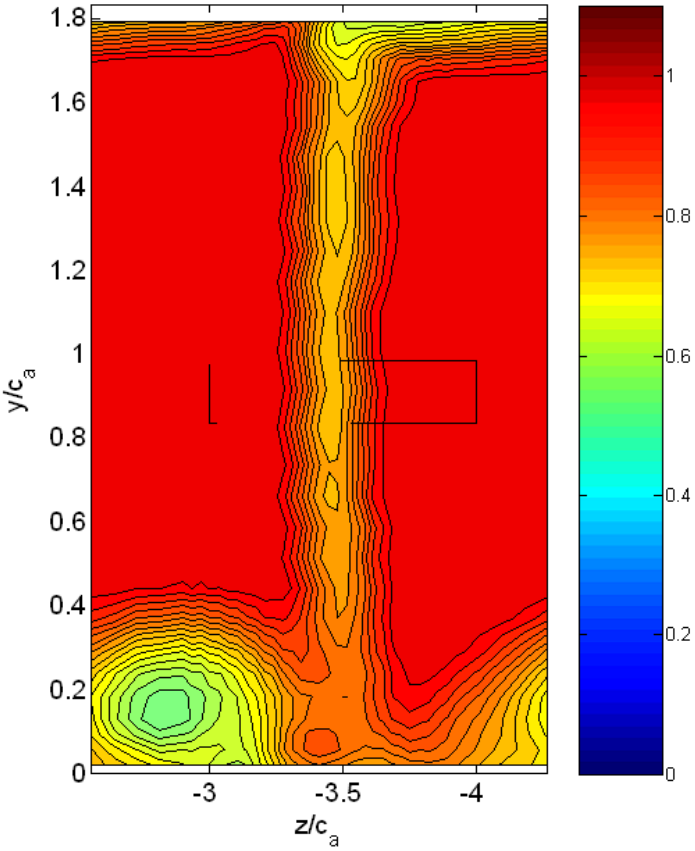

(a) Total pressure coefficient, $C_{p,o}$

(b) Local mean streamwise velocity normalized on the reference velocity, U/U_∞

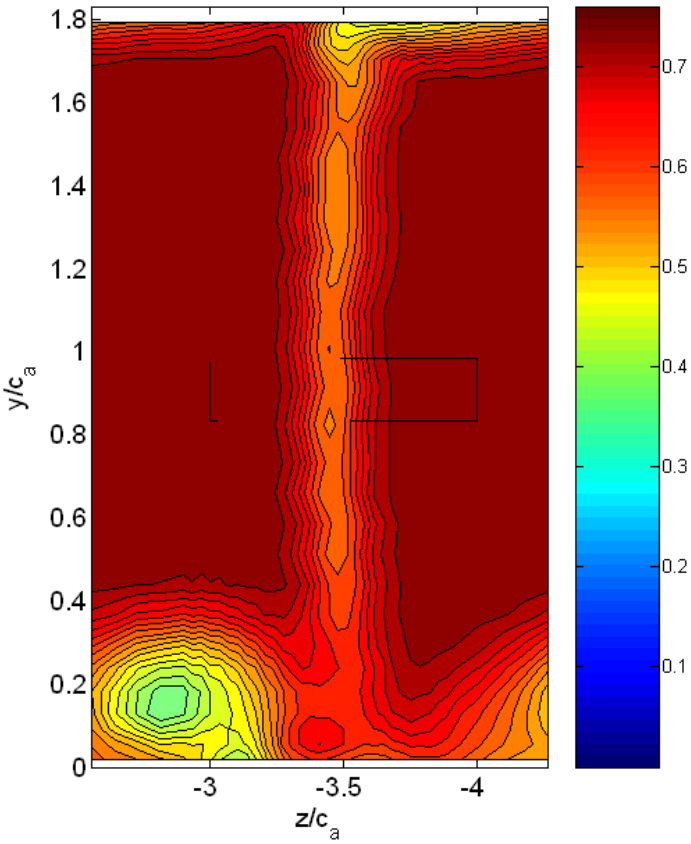

Figure 5-3: Pitot-static cross-sectional measurements for the 1.27 cm drooped serrated blade at $x/c_a = 0.84$

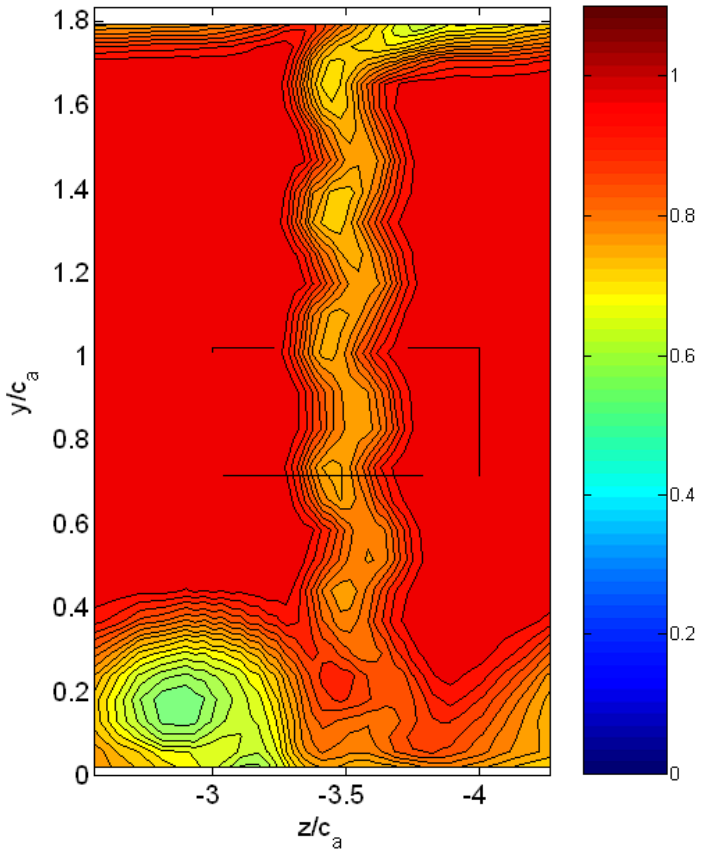

(a) Total pressure coefficient, $C_{p,o}$

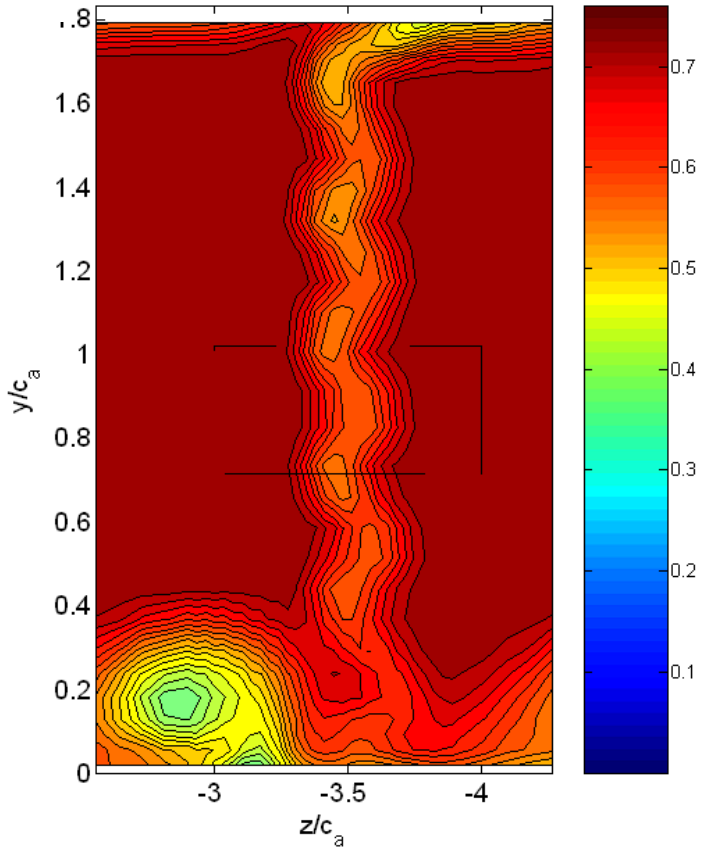

(b) Local mean streamwise velocity normalized on the reference velocity, U/U_∞

Figure 5-4: Pitot-static cross-sectional measurements for the 2.54 cm serrated blade at $x/c_a = 0.84$.

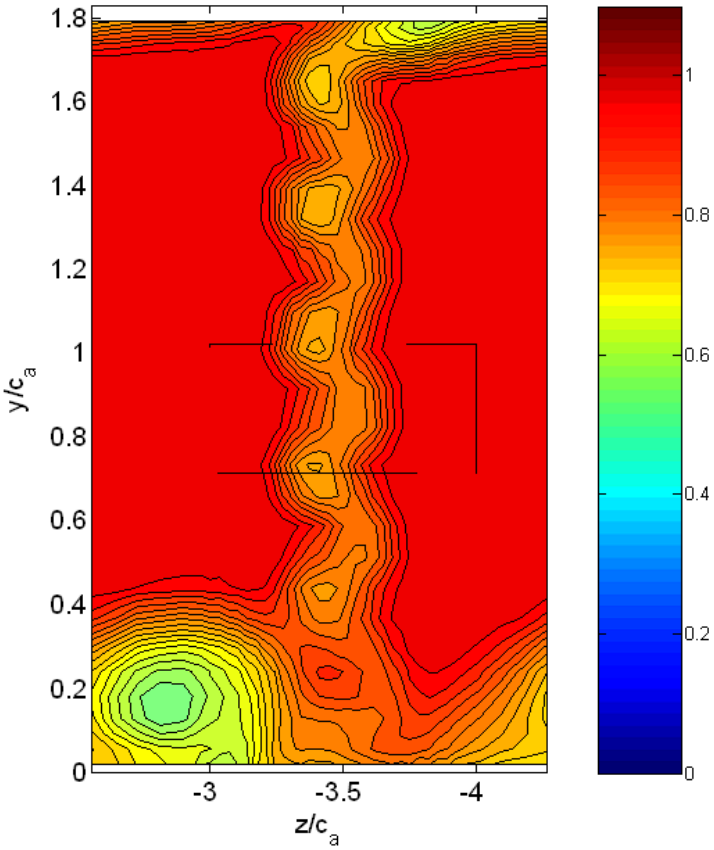

(a) Total pressure coefficient, $C_{p,o}$

(b) Local mean streamwise velocity normalized on the reference velocity, U/U_∞

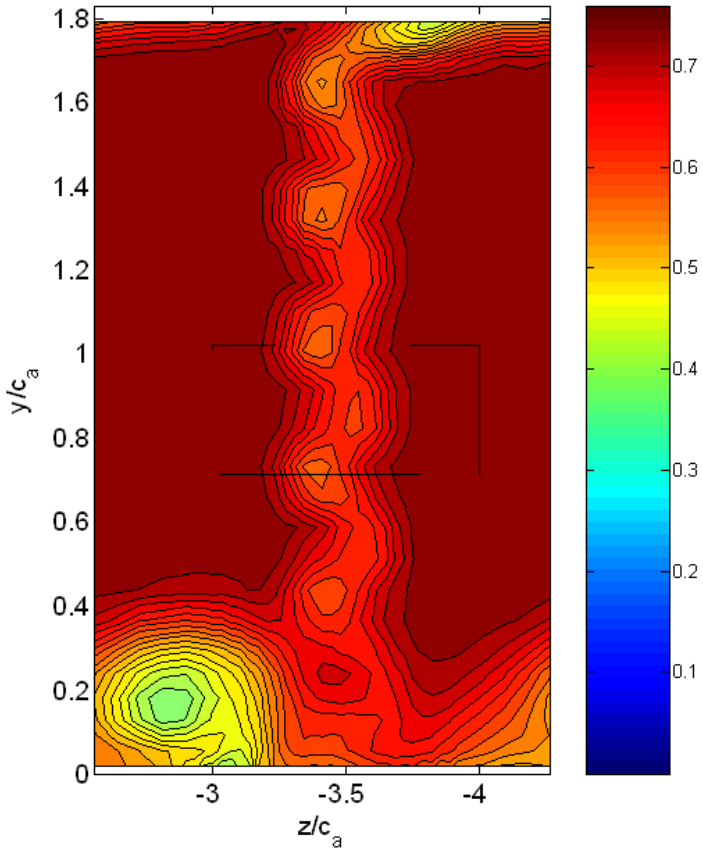

Figure 5-5: Pitot-static cross-sectional measurements for the 2.54 cm drooped serrated blade at $x/c_a = 0.84$

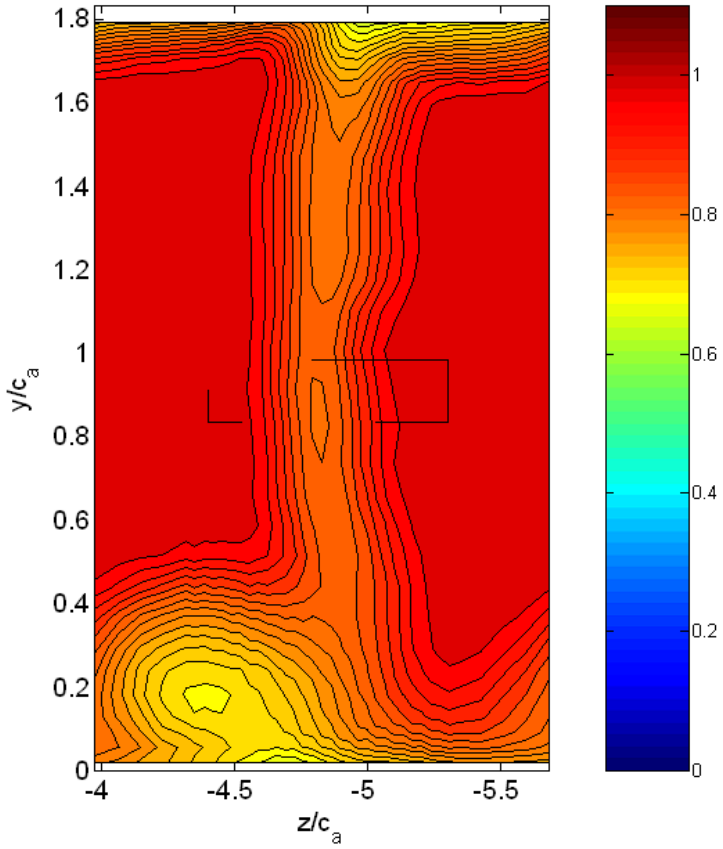

(a) Total pressure coefficient, $C_{p,o}$

(b) Local mean streamwise velocity normalized on the reference velocity, U/U_∞

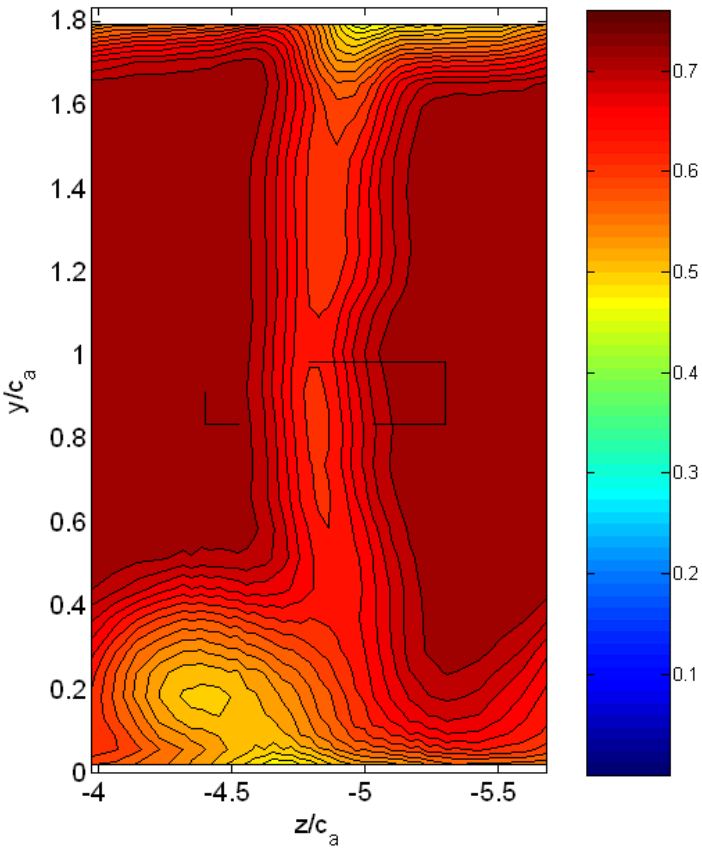

Figure 5-6: Pitot-static cross-sectional measurements for the 1.27 cm serrated blade at x/c_a=1.88

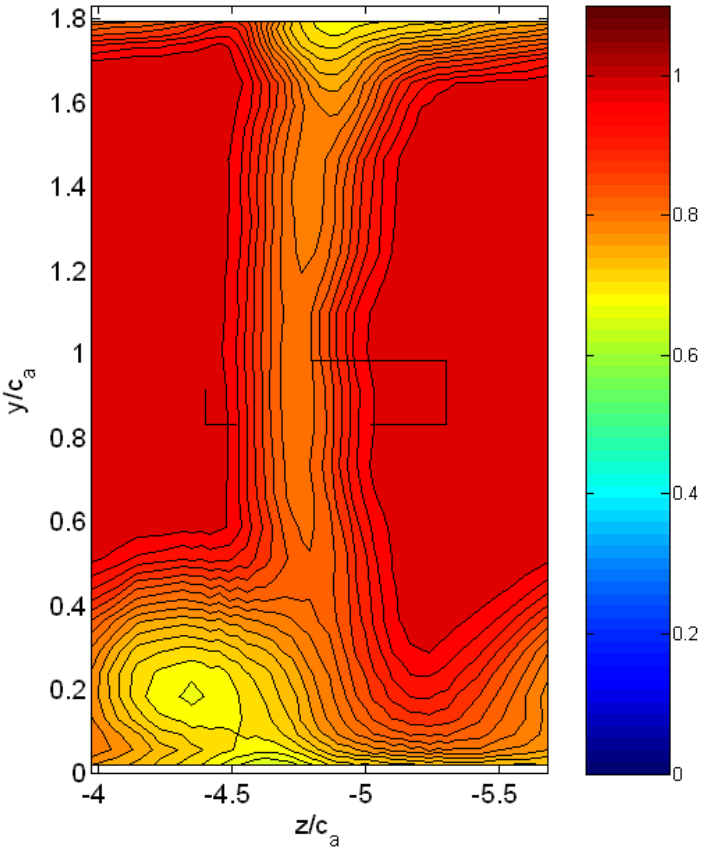

(a) Total pressure coefficient, $C_{p,o}$

(b) Local mean streamwise velocity normalized on the reference velocity, U/U_∞

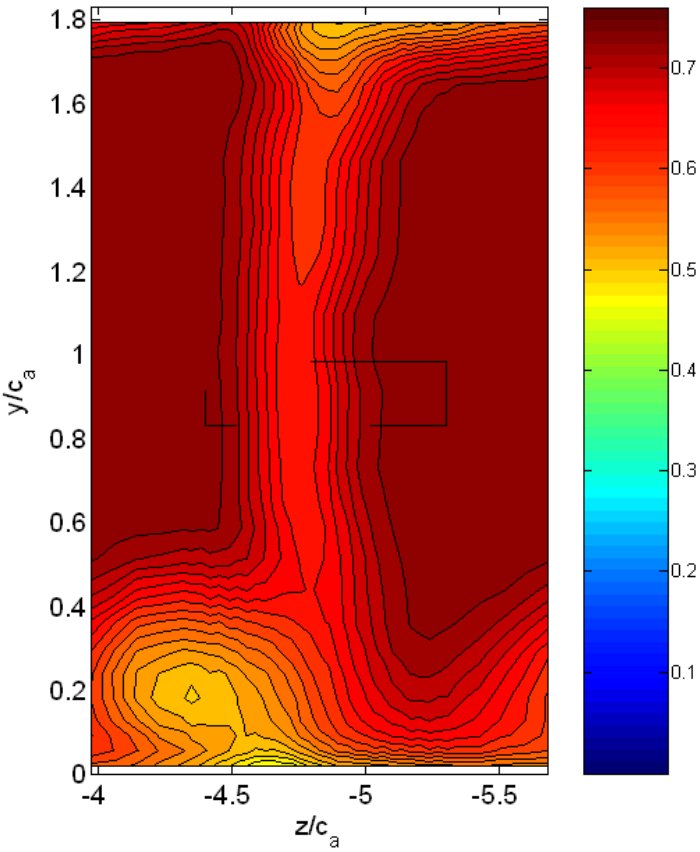

Figure 5-7: Pitot-static cross-sectional measurements for the 1.27 cm serrated blade at $x/c_a = 1.88$

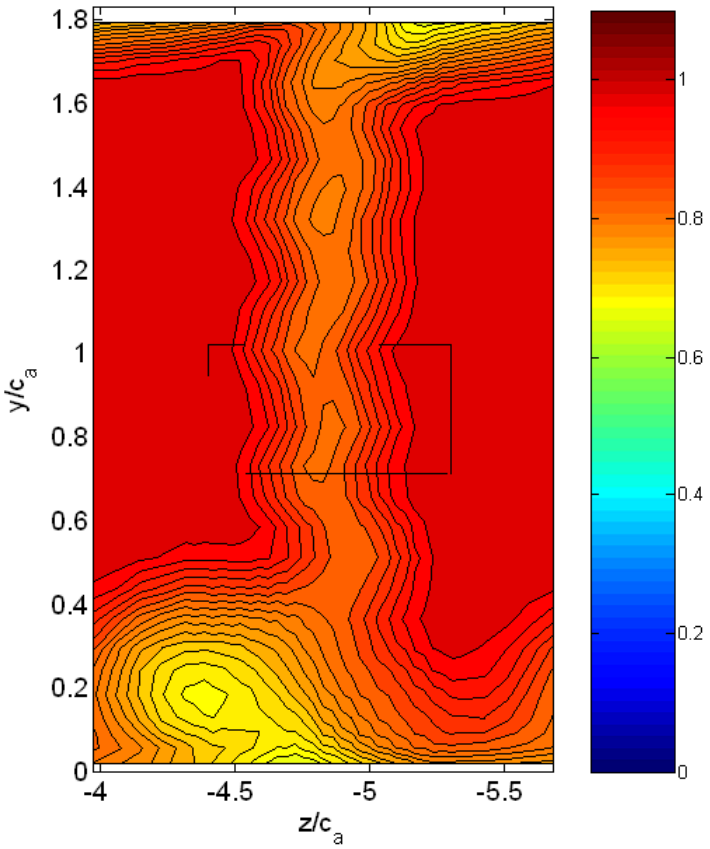

(a) Total pressure coefficient, $C_{p,o}$

(b) Local mean streamwise velocity normalized on the reference velocity, U/U_∞

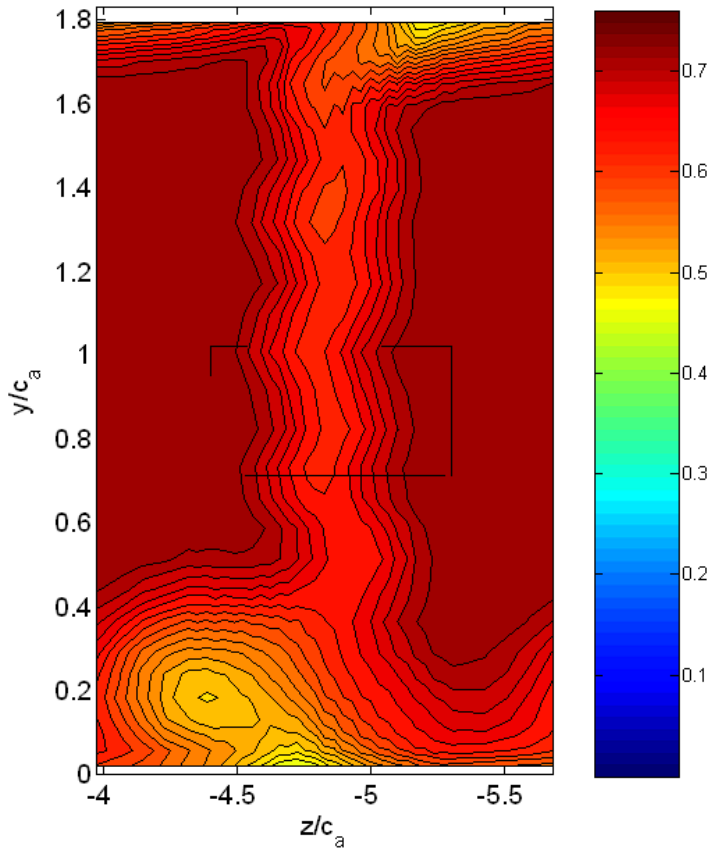

Figure 5-8: Pitot-static cross-sectional measurements for the 2.54 cm serrated blade at $x/c_a = 1.88$

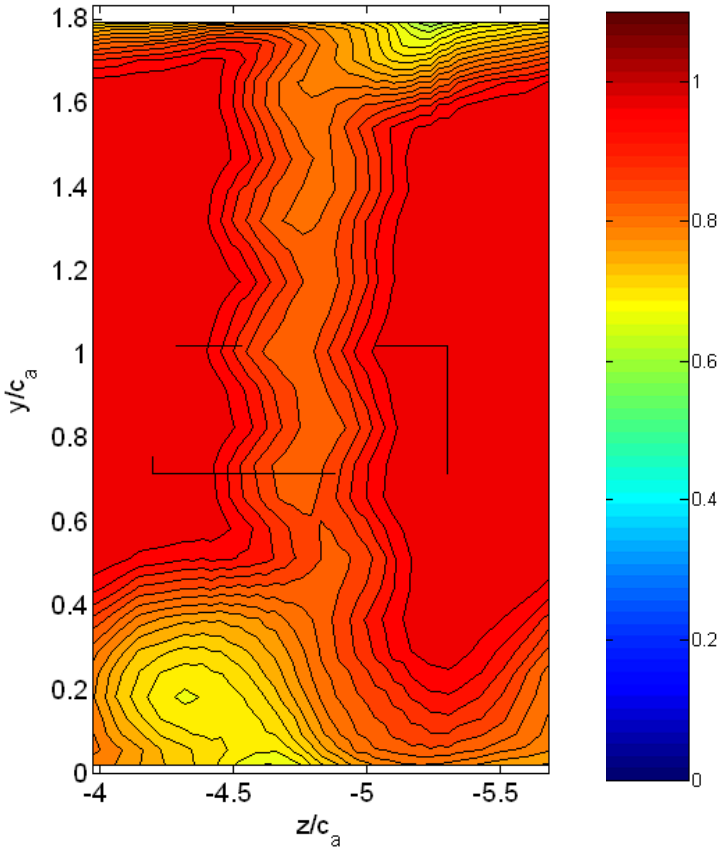

(a) Total pressure coefficient, $C_{p,o}$

(b) Local mean streamwise velocity normalized on the reference velocity, U/U_∞

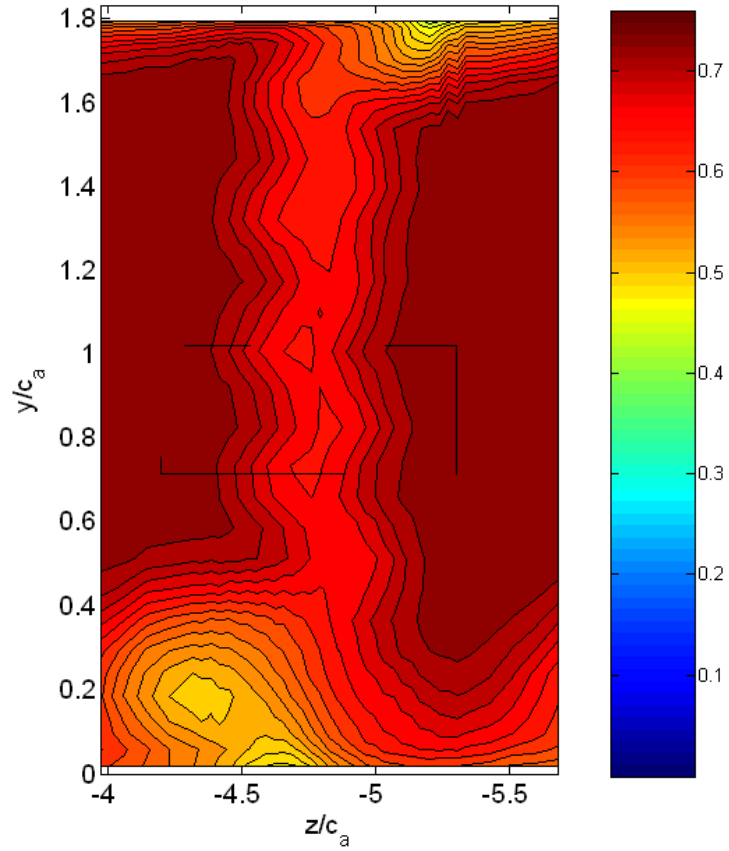

Figure 5-9: Pitot-static cross-sectional measurements for the 2.54 cm drooped serrated blade at $x/c_a = 1.88$

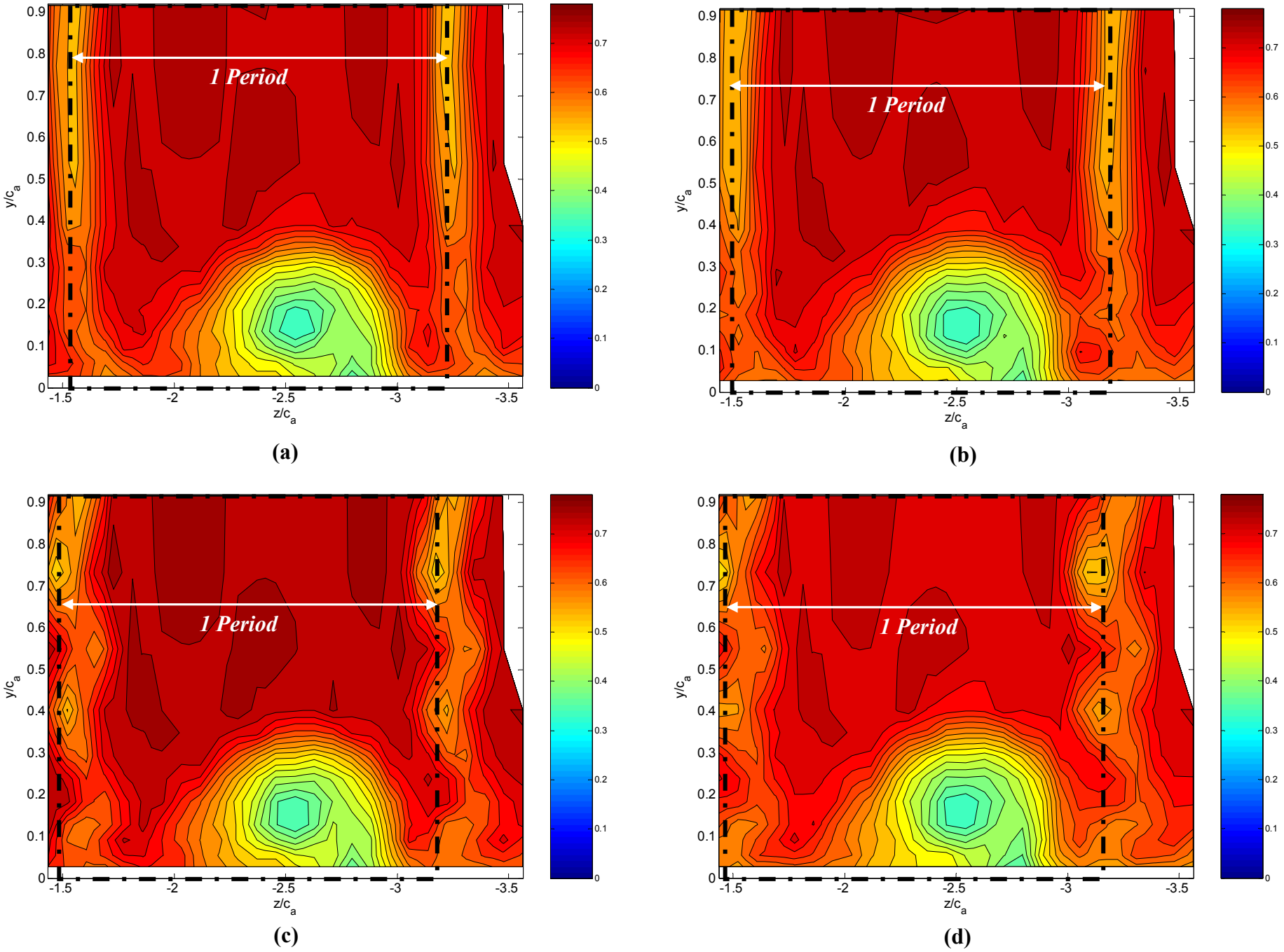

Figure 5-10: Mean streamwise velocity, U/U_∞, cross-sections at $x/c_a = 0.61$: **(a)** 1.27 cm, **(b)** 1.27 cm droop, **(c)** 2.54 cm, **(d)** 2.54 cm droop.

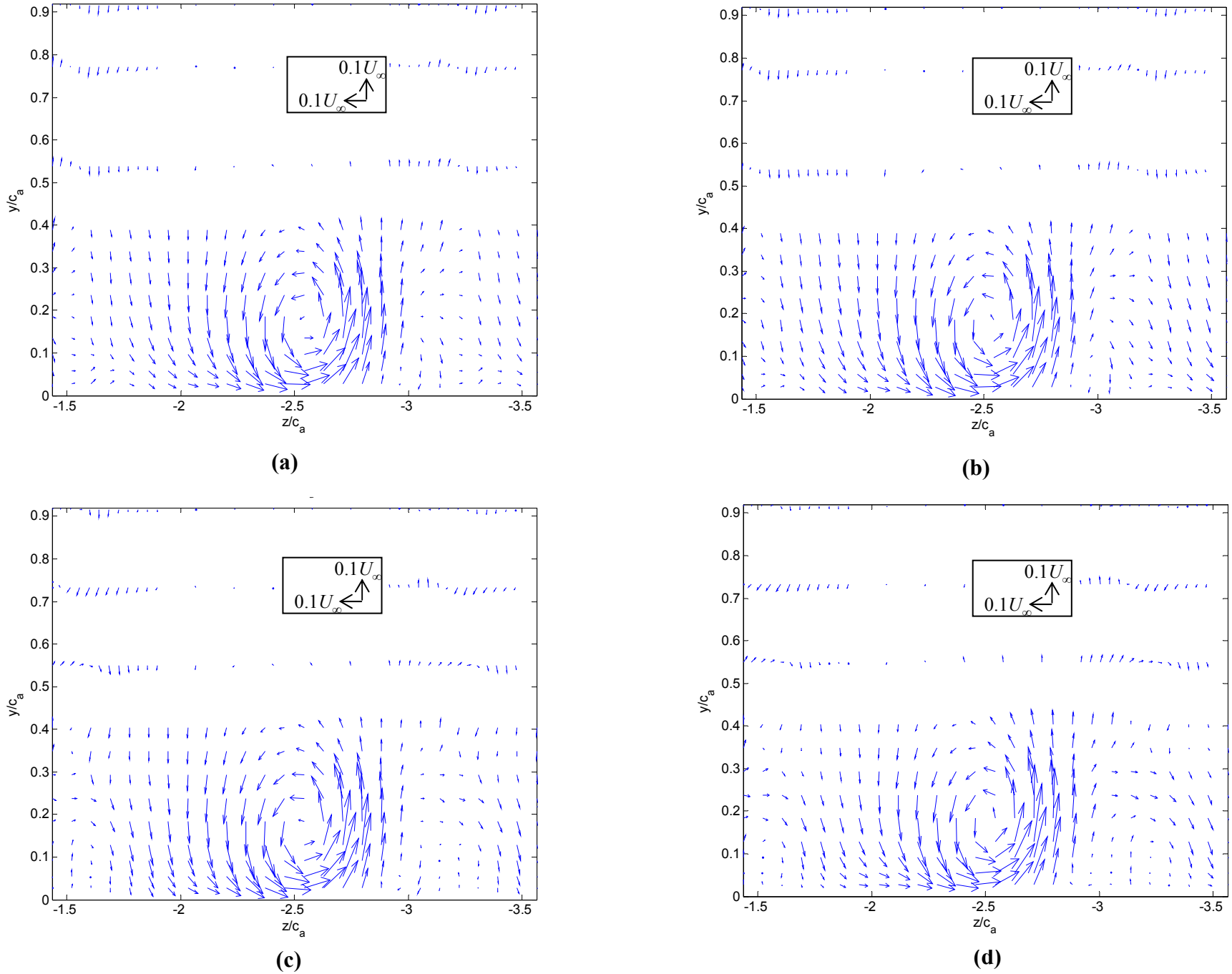

Figure 5-11: Vector plots of V/U_∞ and W/U_∞ at x/c_a = 0.61: **(a)** 1.27 cm, **(b)** 1.27 cm droop, **(c)** 2.54 cm, **(d)** 2.54 cm droop

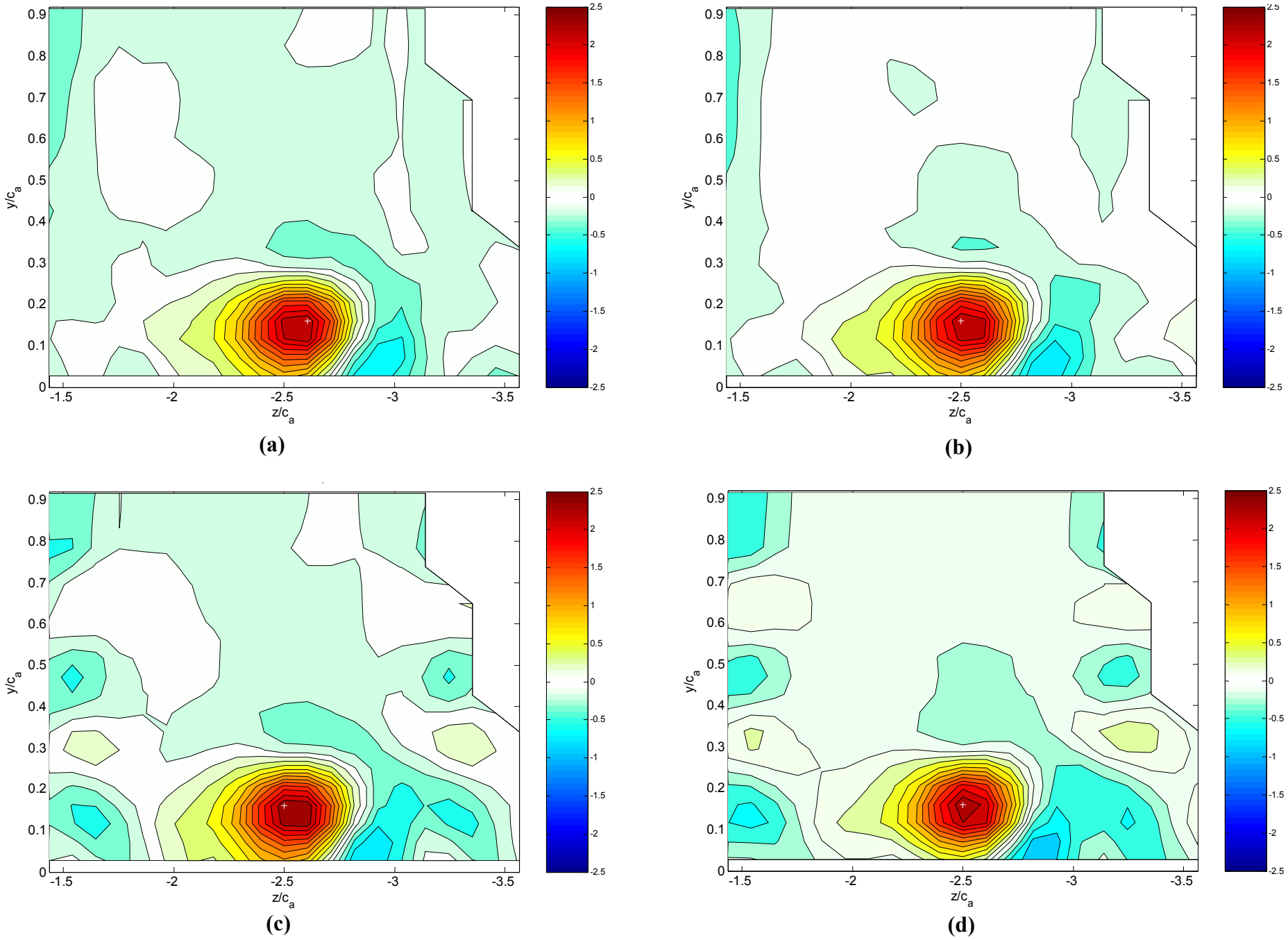

Figure 5-12: Contours of mean streamwise vorticity, $\Omega_x/U_\infty c_a$, at $x/c_a = 0.61$: **(a)** 1.27 cm, **(b)** 1.27 cm droop, **(c)** 2.54 cm, **(d)** 2.54 cm droop

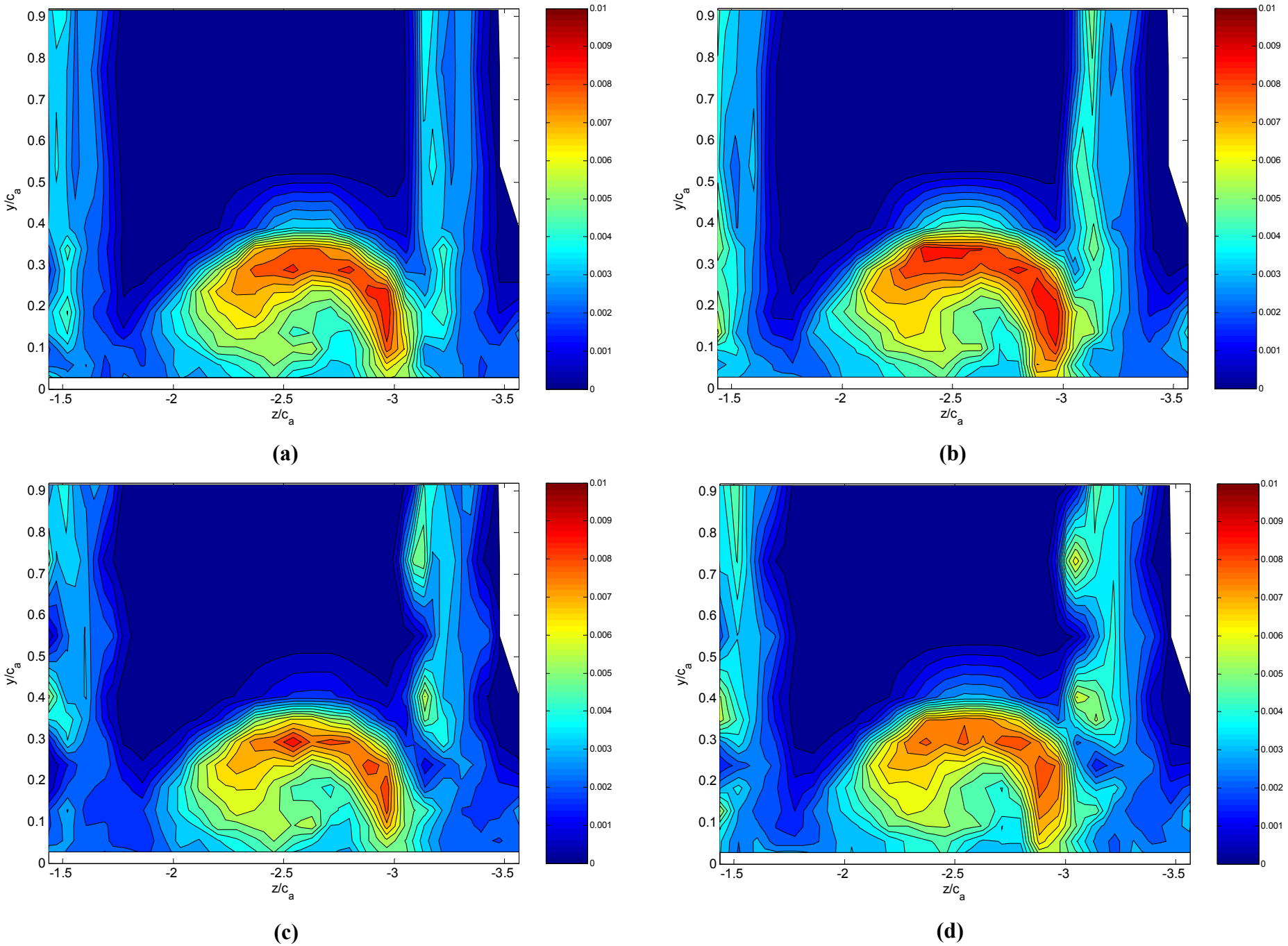

Figure 5-13: Contours of streamwise turbulence stress, $\overline{u'^2/U_\infty^2}$, at x/c_a = 0.61: **(a)** 1.27 cm, **(b)** 1.27 cm droop, **(c)** 2.54 cm, **(d)** 2.54 cm droop

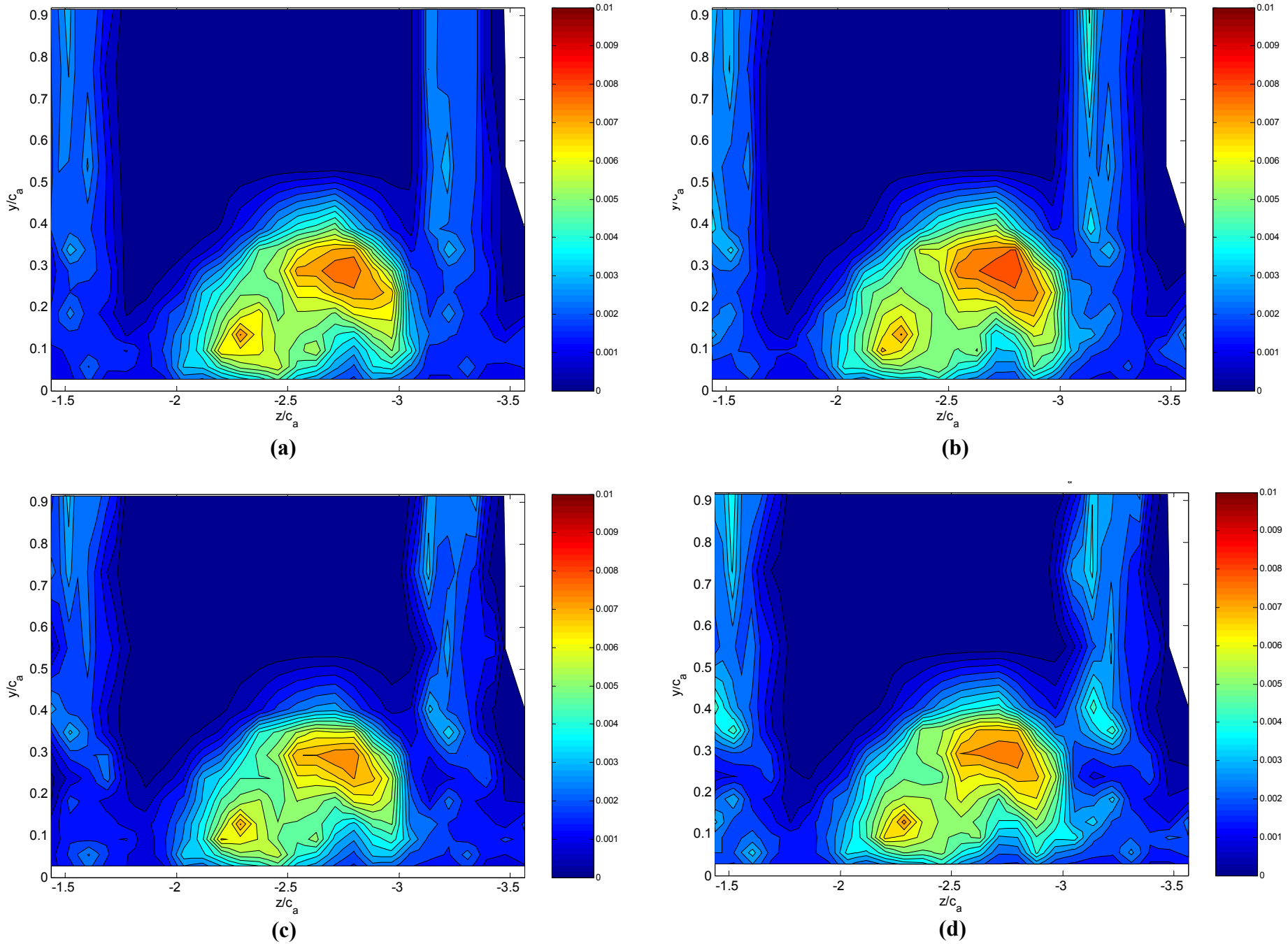

Figure 5-14: Contours of spanwise turbulence stress, $\overline{v'^2/U_\infty^2}$, at $x/c_a = 0.61$: **(a)** 1.27 cm, **(b)** 1.27 cm droop, **(c)** 2.54 cm, **(d)** 2.54 cm droop

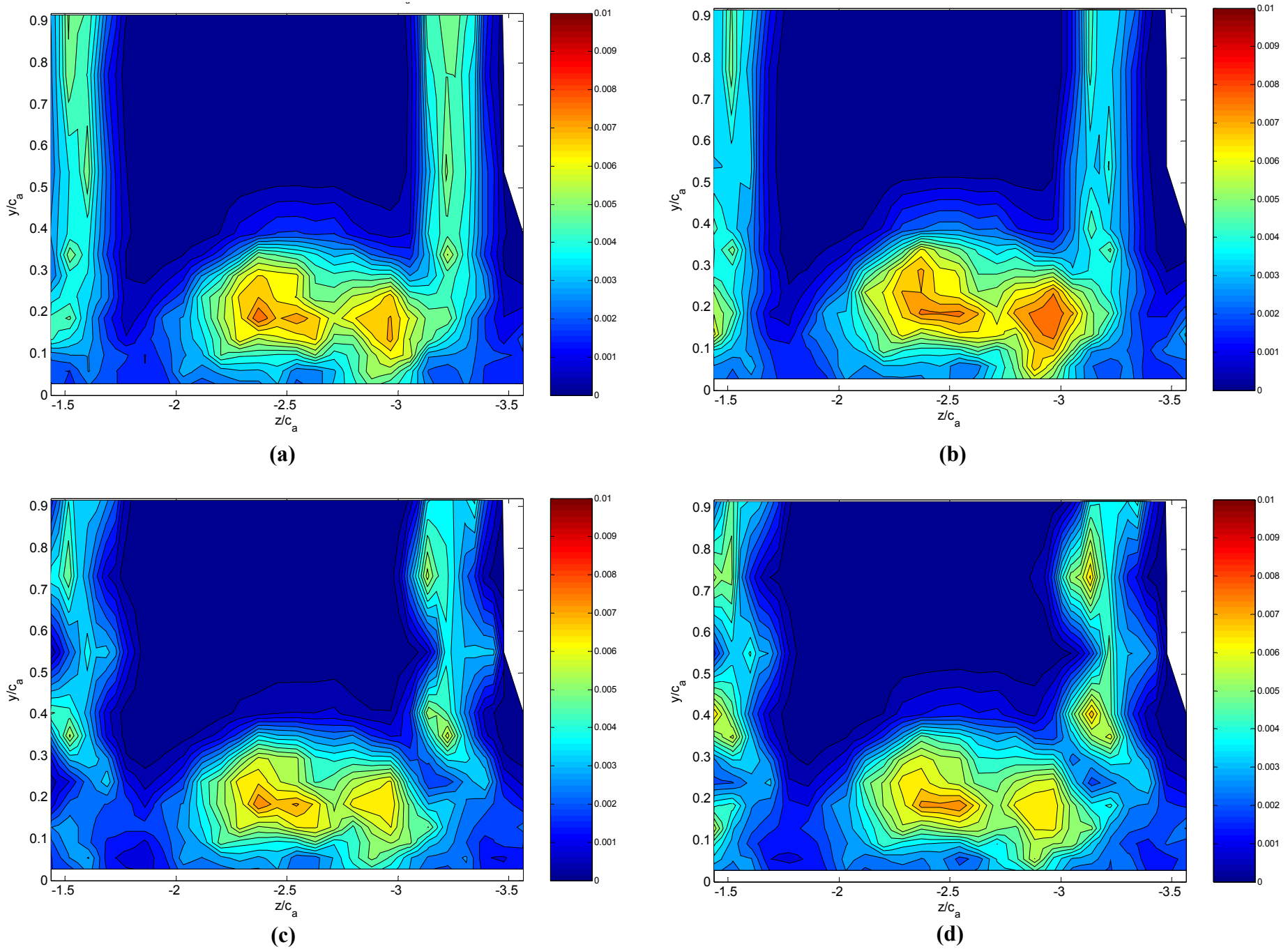

Figure 5-15: Contours of cross-wake turbulence stress, $\overline{w'^2}/U_\infty^2$, at $x/c_a = 0.61$: **(a)** 1.27 cm, **(b)** 1.27 cm droop, **(c)** 2.54 cm, **(d)** 2.54 cm droop

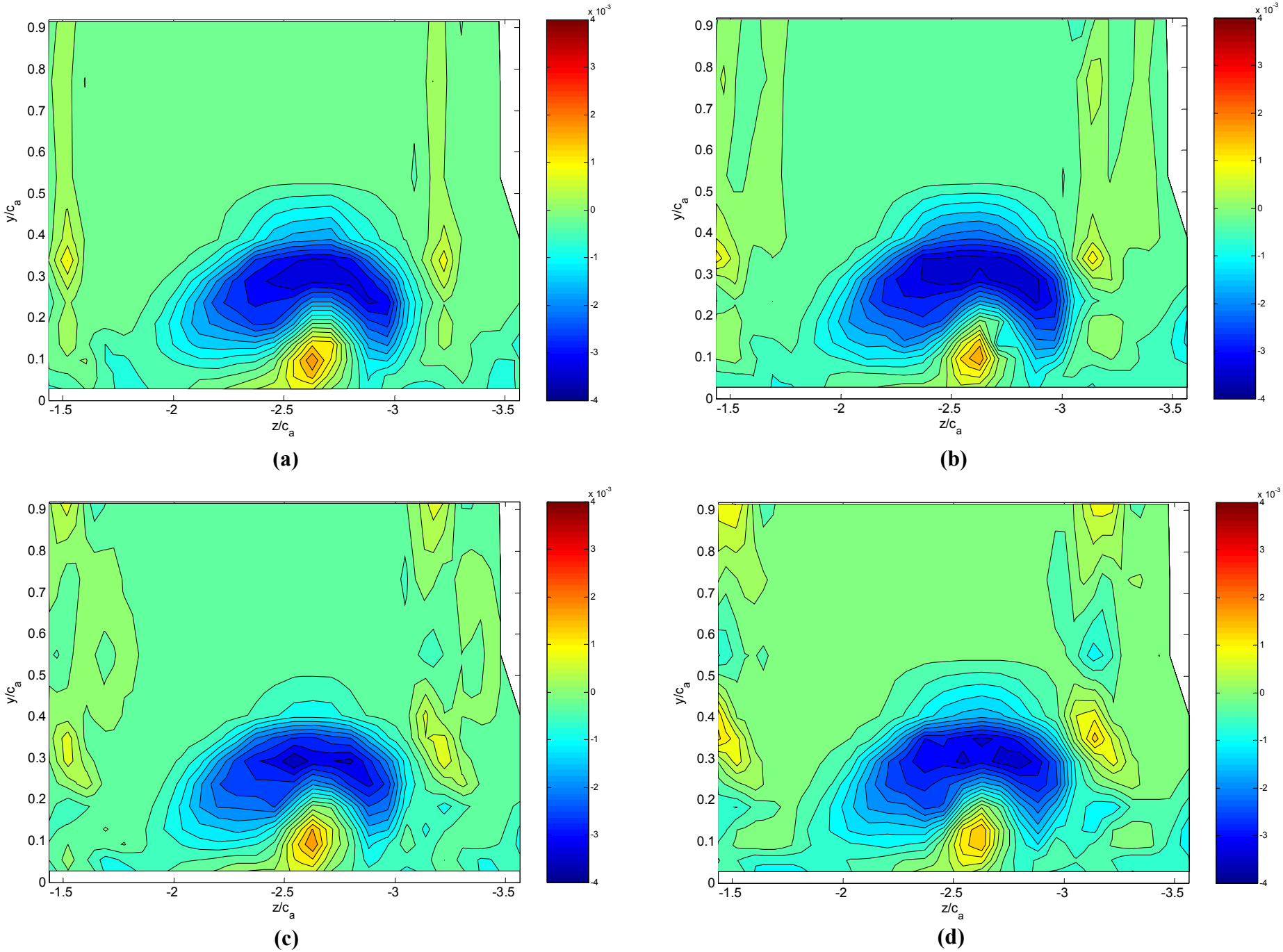

Figure 5-16: Contours of Reynolds shear stress, $\overline{u'v'}/U_\infty^2$, at $x/c_a = 0.61$: **(a)** 1.27 cm, **(b)** 1.27 cm droop, **(c)** 2.54 cm, **(d)** 2.54 cm droop

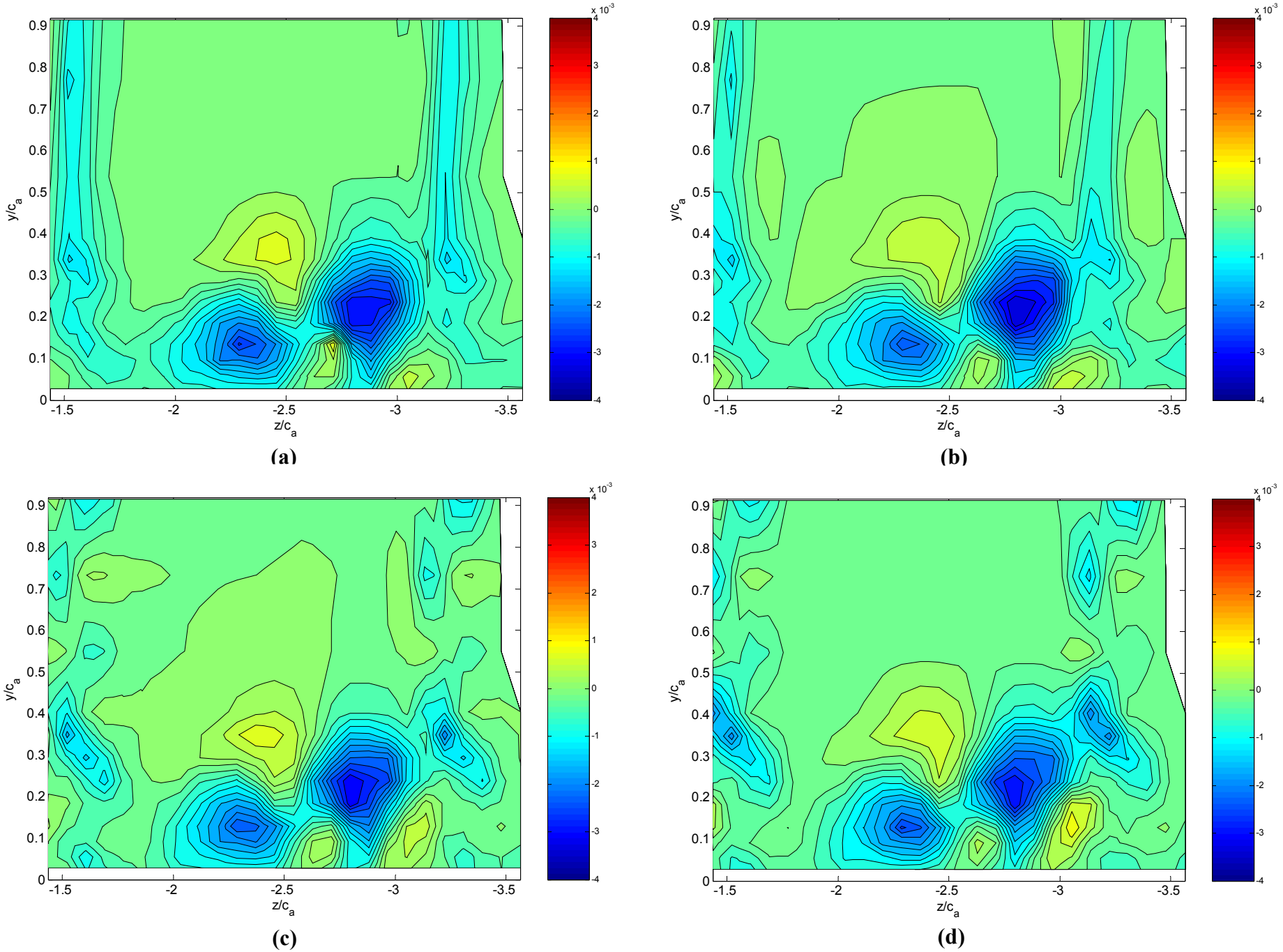

Figure 5-17: Contours of Reynolds shear stress, $\overline{v'w'}/U_\infty^2$, at $x/c_a = 0.61$: **(a)** 1.27 cm, **(b)** 1.27 cm droop, **(c)** 2.54 cm, **(d)** 2.54 cm droop

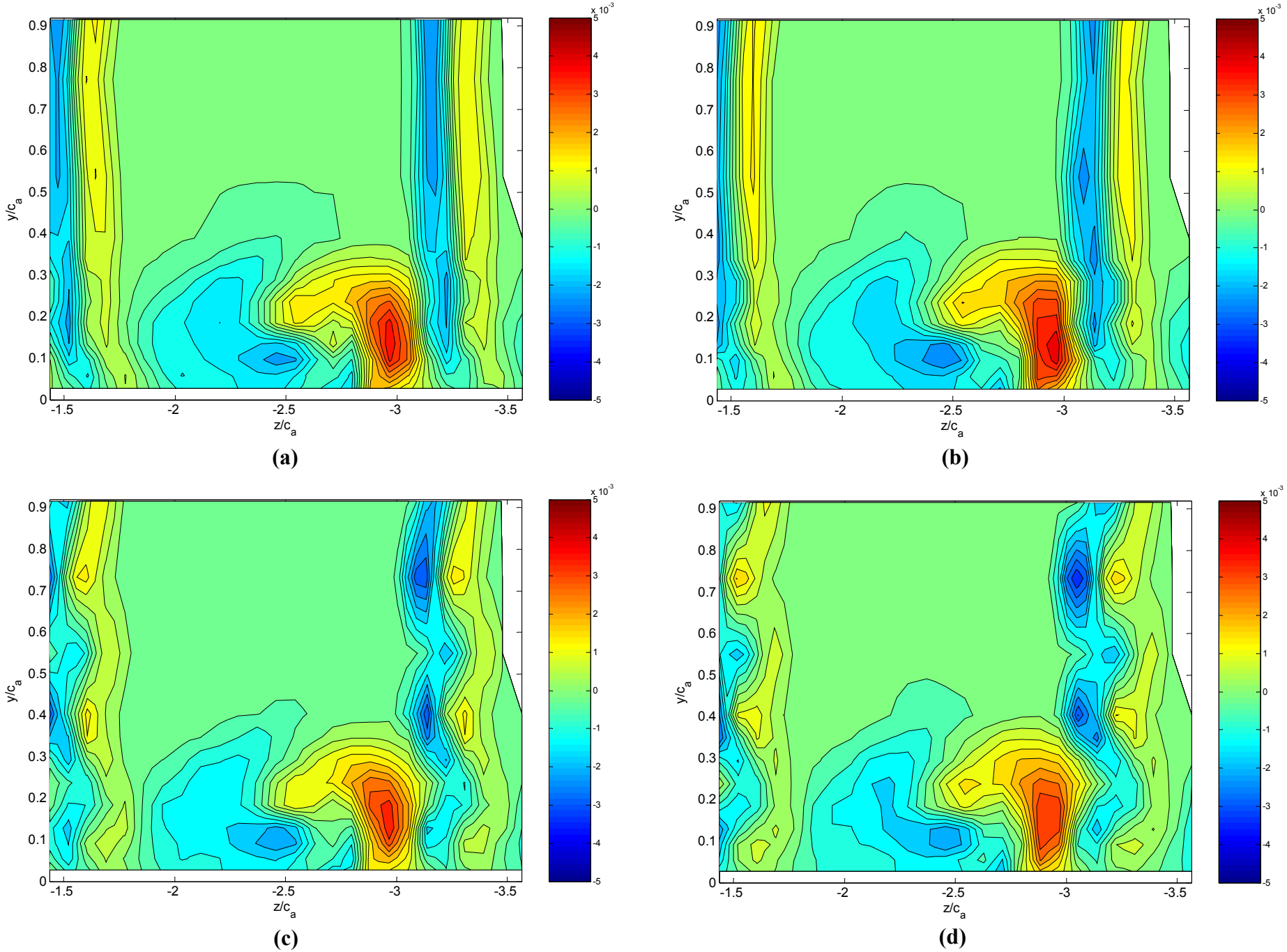

Figure 5-18: Contours of Reynolds shear stress, $\overline{u'w'}/U_\infty^2$, at $x/c_a = 0.61$: **(a)** 1.27 cm, **(b)** 1.27 cm droop, **(c)** 2.54 cm, **(d)** 2.54 cm droop

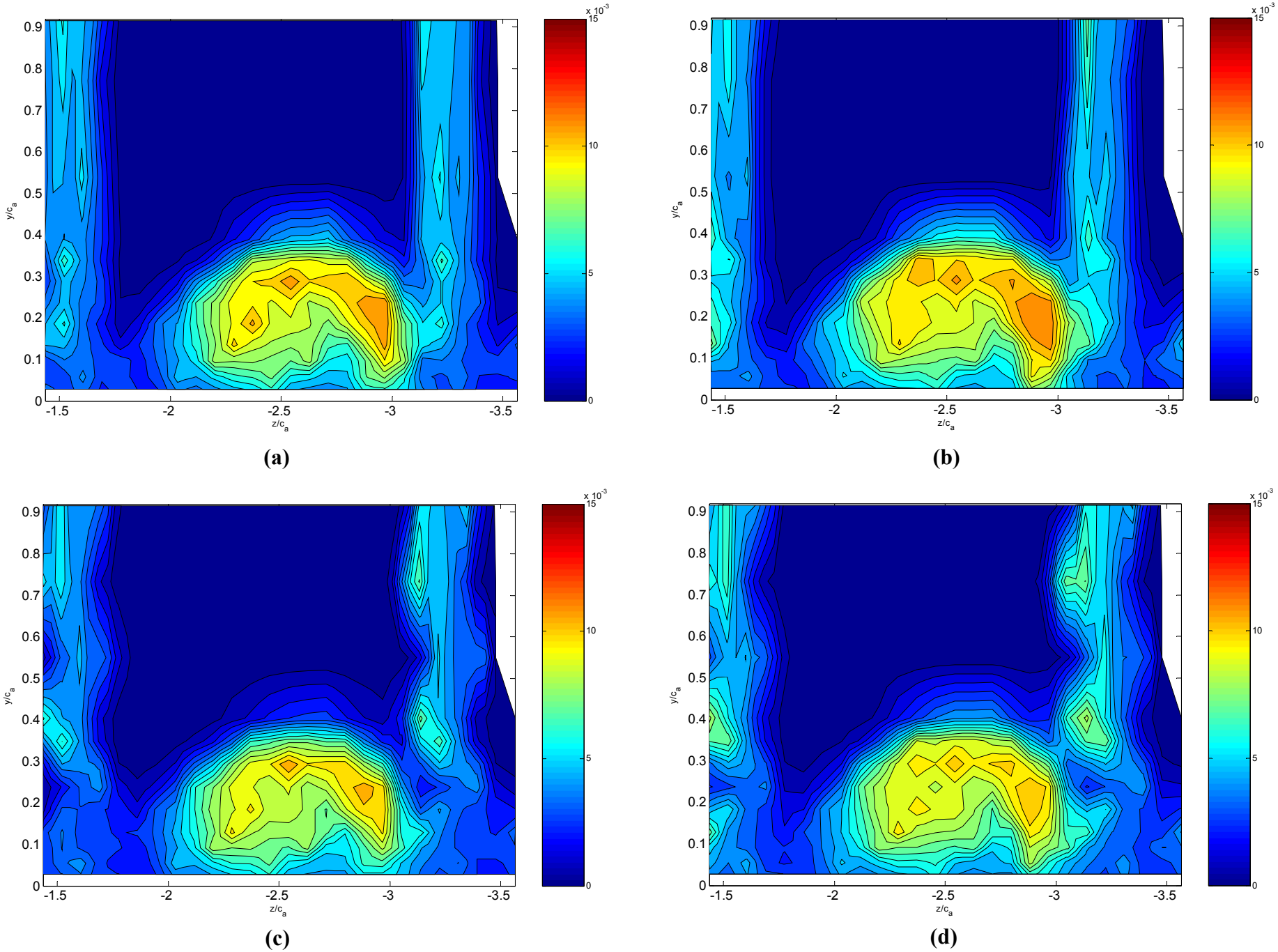

Figure 5-19: Contours of turbulence kinetic energy, $k/U_{\infty}^{2,}$ at x/c_a = 0.61: **(a)** 1.27 cm, **(b)** 1.27 cm droop, **(c)** 2.54 cm, **(d)** 2.54 cm droop

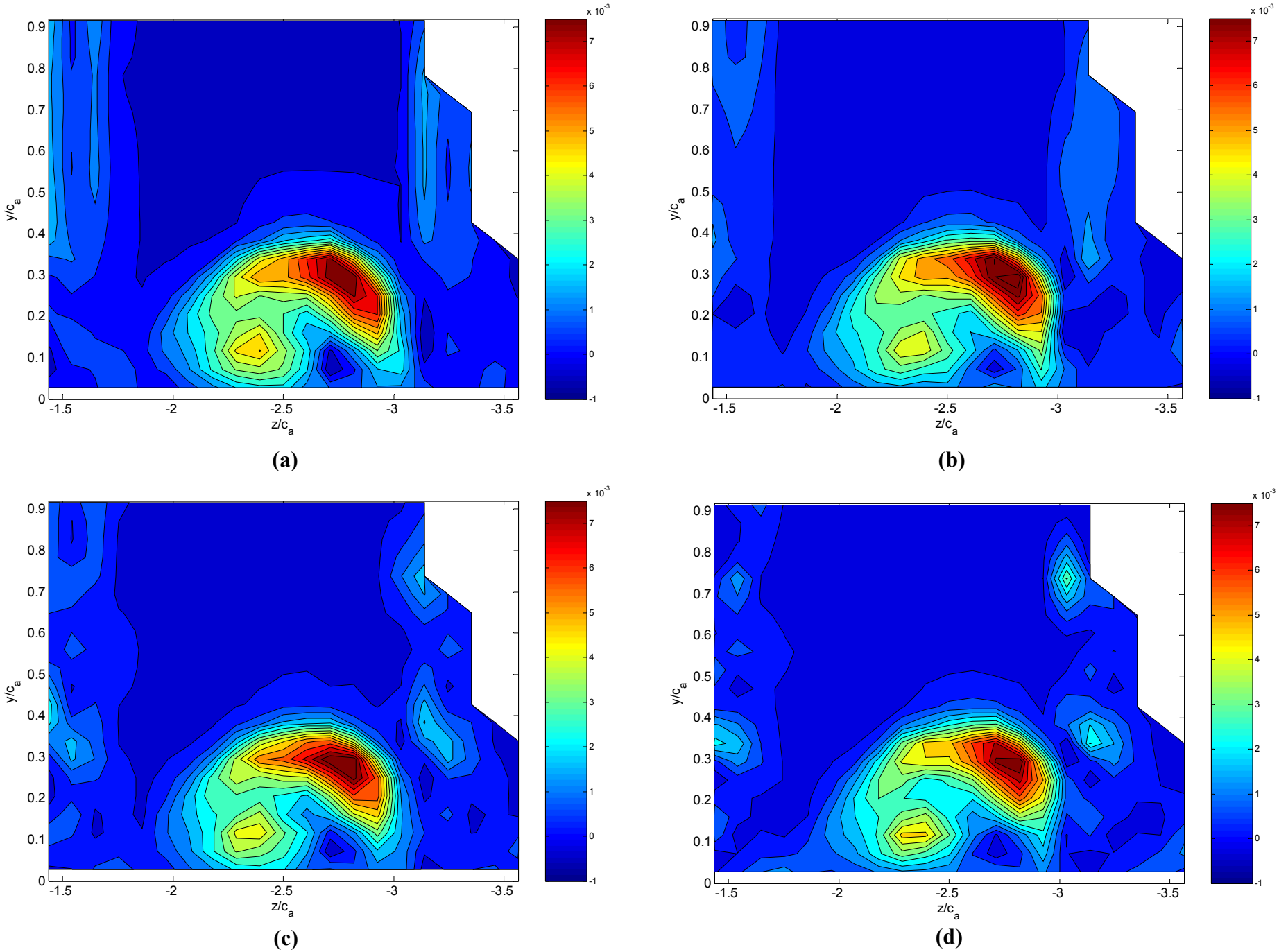

Figure 5-20: Contours of turbulence kinetic energy production, $P_k/c_aU_\infty^{3,}$ at $x/c_a = 0.61$: **(a)** 1.27 cm, **(b)** 1.27 cm droop, **(c)** 2.54 cm, **(d)** 2.54 cm droop

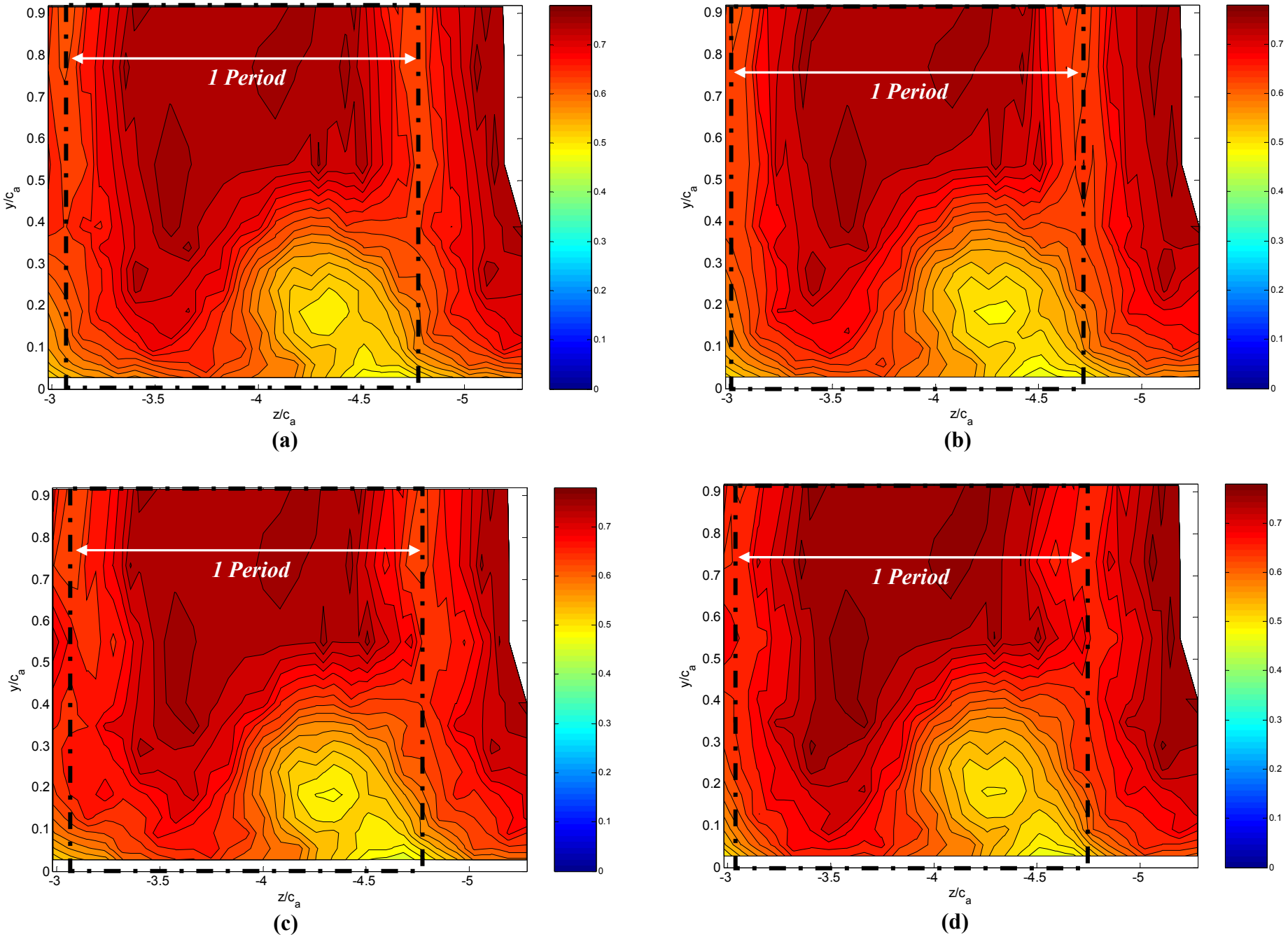

Figure 5-21: Mean streamwise velocity, U/U_∞, cross-sections at x/c_a = 1.82: **(a)** 1.27 cm, **(b)** 1.27 cm droop, **(c)** 2.54 cm, **(d)** 2.54 cm droop.

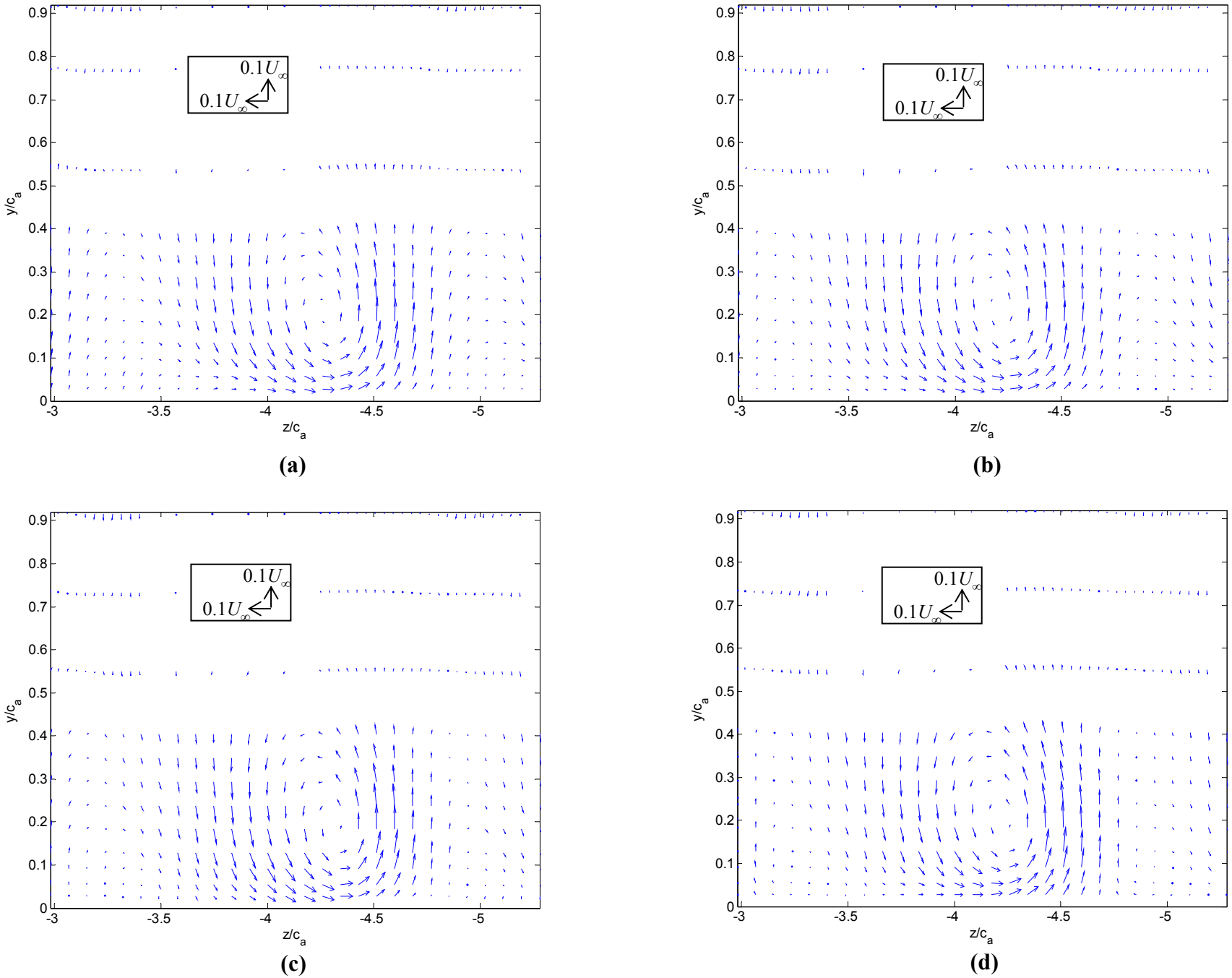

Figure 5-22: Vector plots of V/U_∞ and W/U_∞ at x/c_a = 1.82: **(a)** 1.27 cm, **(b)** 1.27 cm droop, **(c)** 2.54 cm, **(d)** 2.54 cm droop

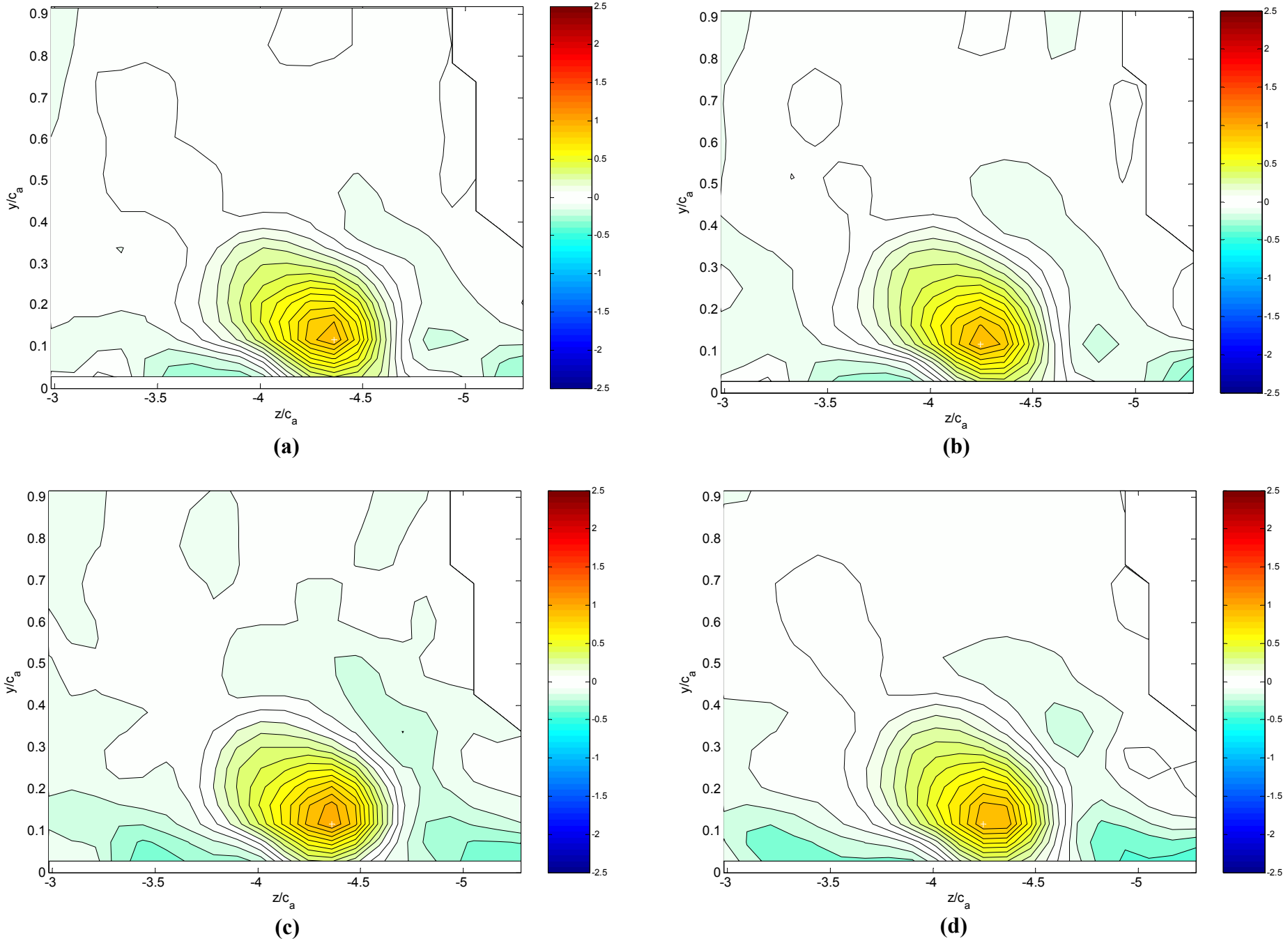

Figure 5-23: Contours of mean streamwise vorticity, $\Omega_x/U_\infty c_a$, at x/c_a = 1.82: **(a)** 1.27 cm, **(b)** 1.27 cm droop, **(c)** 2.54 cm, **(d)** 2.54 cm droop

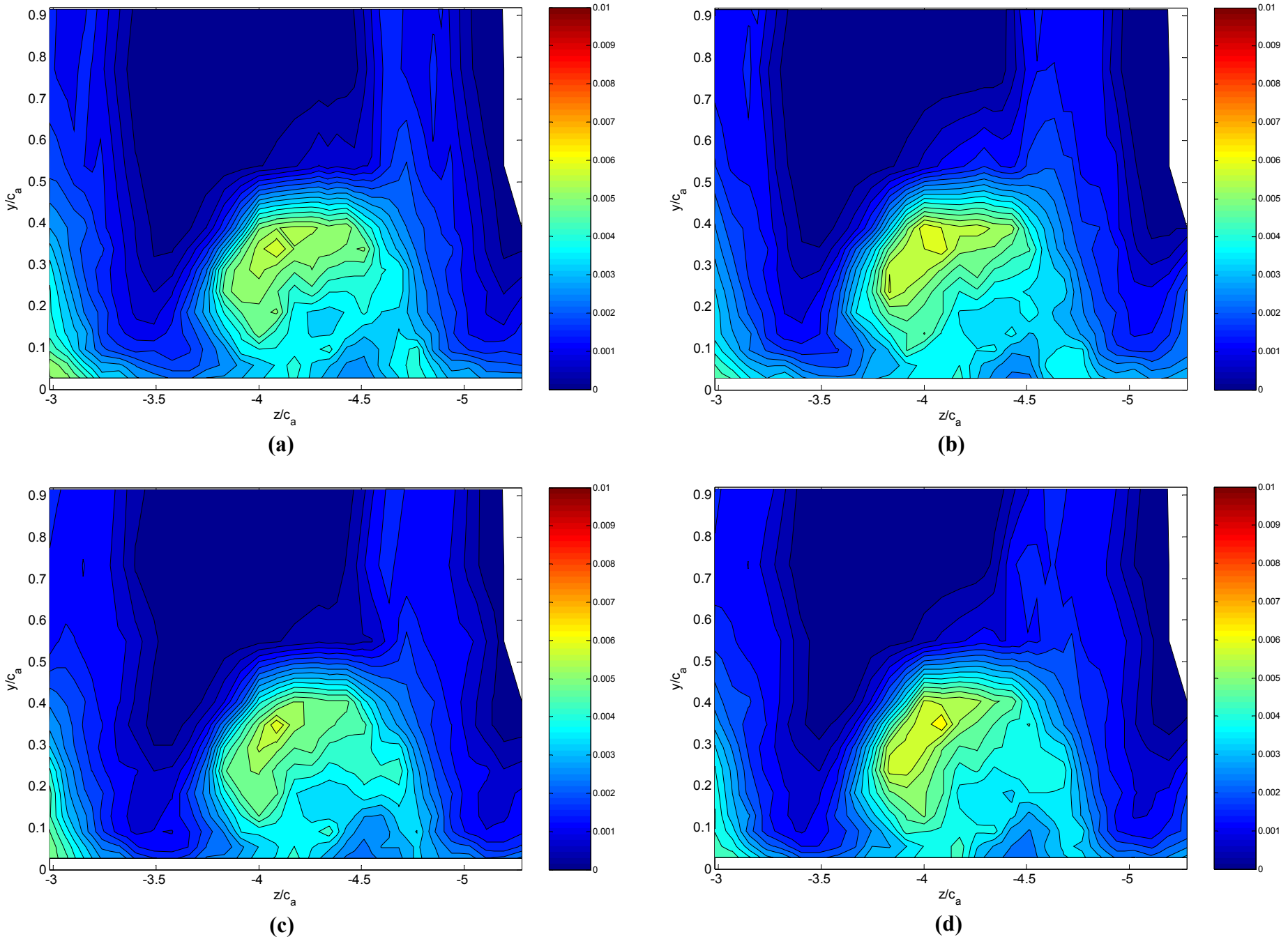

Figure 5-24: Contours of streamwise turbulence stress, $\overline{u'^2/U_\infty^2}$, at x/c_a = 1.82: **(a)** 1.27 cm, **(b)** 1.27 cm droop, **(c)** 2.54 cm, **(d)** 2.54 cm droop

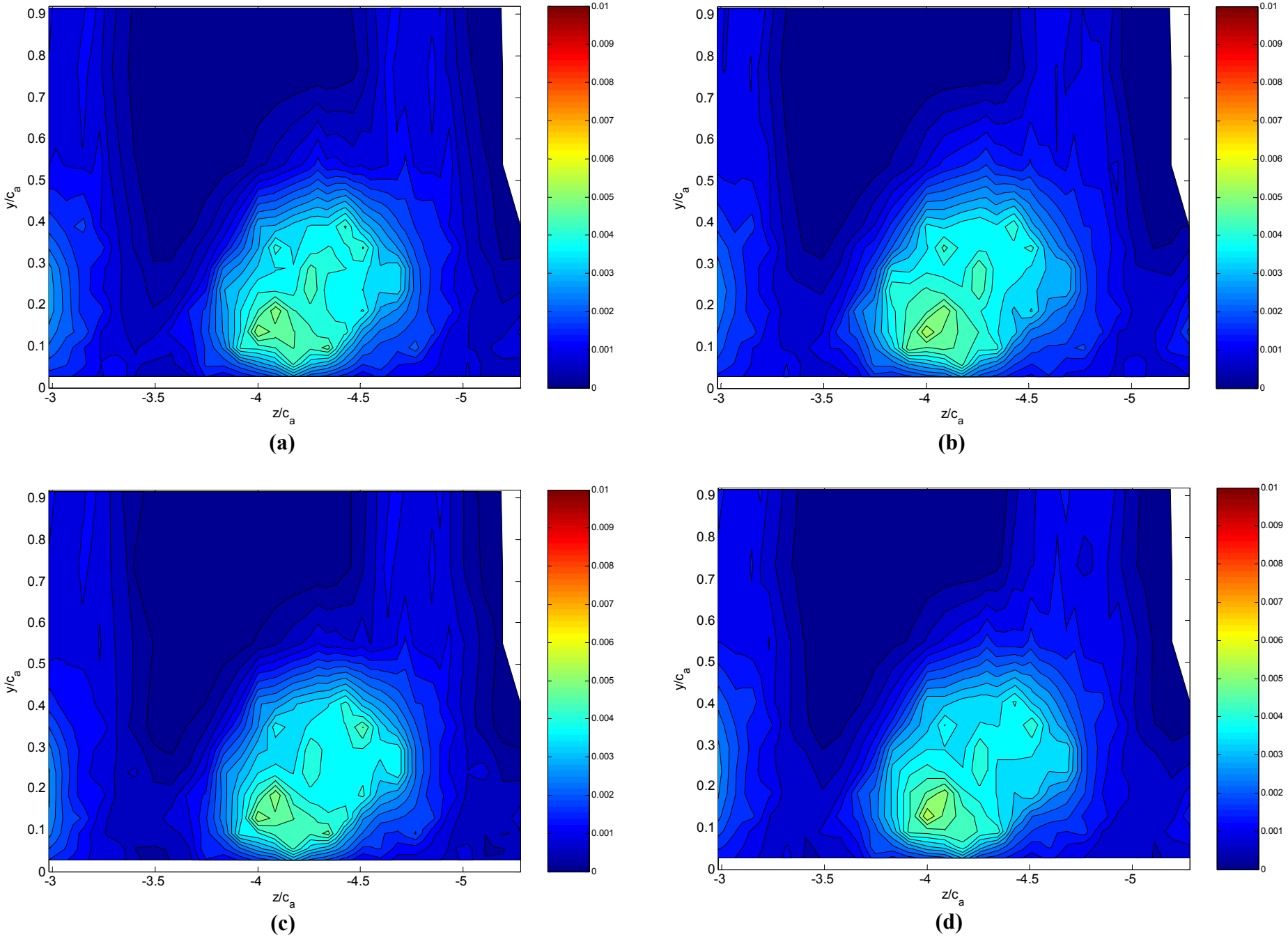

Figure 5-25: Contours of spanwise turbulence stress, $\overline{v'^2/U_\infty^2}$, at $x/c_a = 1.82$: **(a)** 1.27 cm, **(b)** 1.27 cm droop, **(c)** 2.54 cm, **(d)** 2.54 cm droop

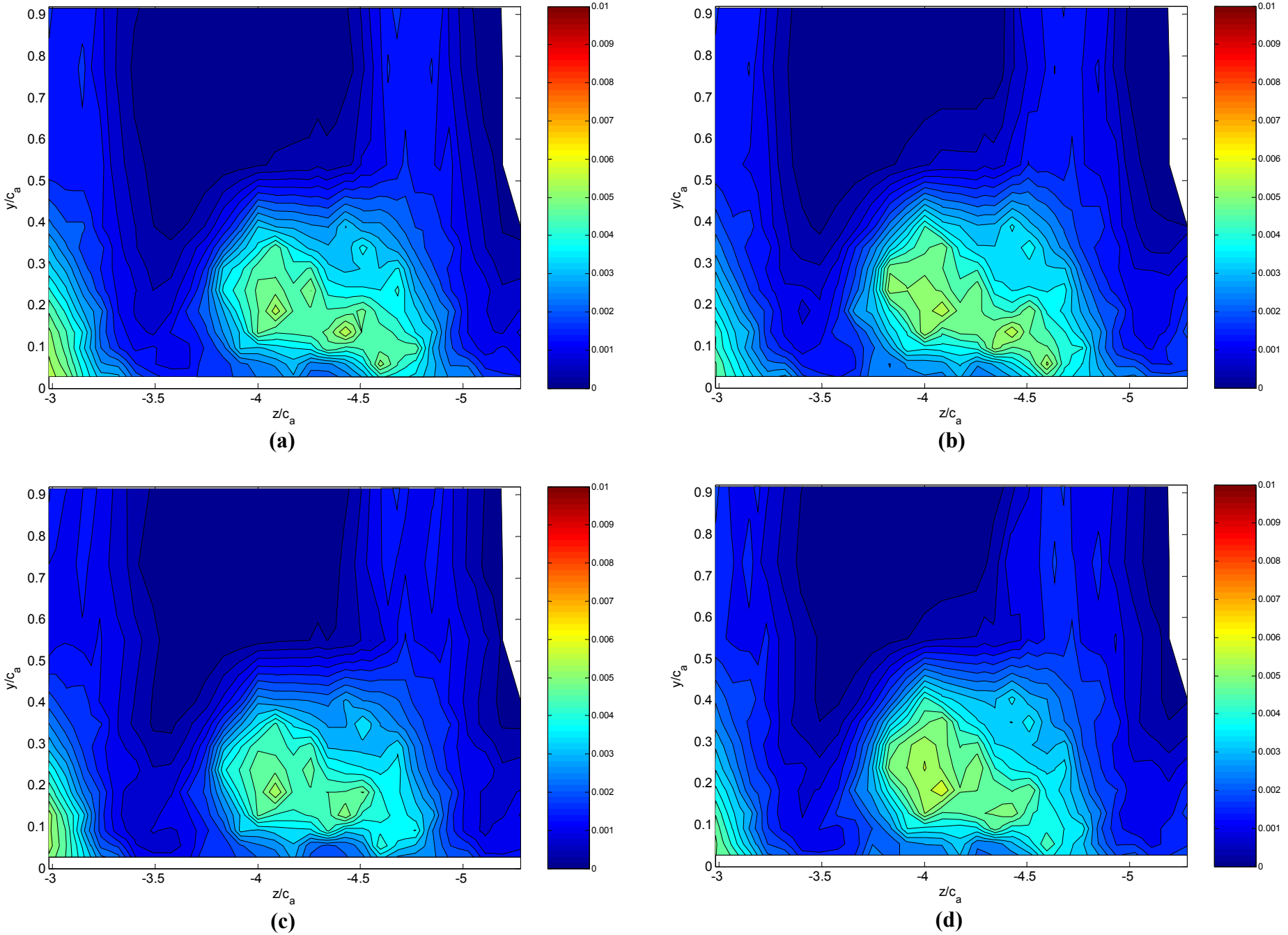

Figure 5-26: Contours of cross-wake turbulence stress, $\overline{w'^2/U_\infty^2}$, at x/c_a = 1.82: **(a)** 1.27 cm, **(b)** 1.27 cm droop, **(c)** 2.54 cm, **(d)** 2.54 cm droop

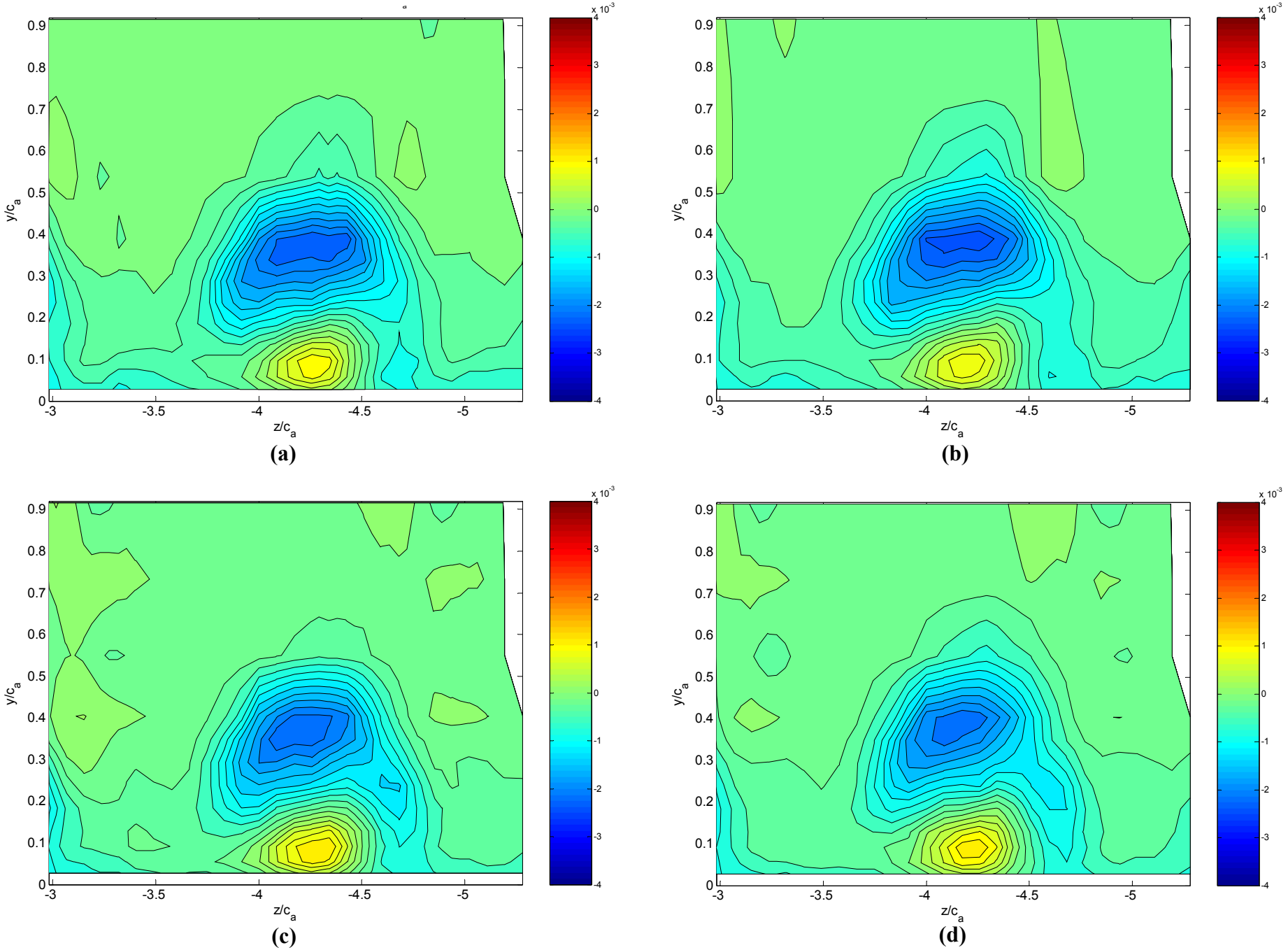

Figure 5-27: Contours of Reynolds shear stress, $\overline{u'v'}/U_\infty^2$, at x/c_a = 1.82: **(a)** 1.27 cm, **(b)** 1.27 cm droop, **(c)** 2.54 cm, **(d)** 2.54 cm droop

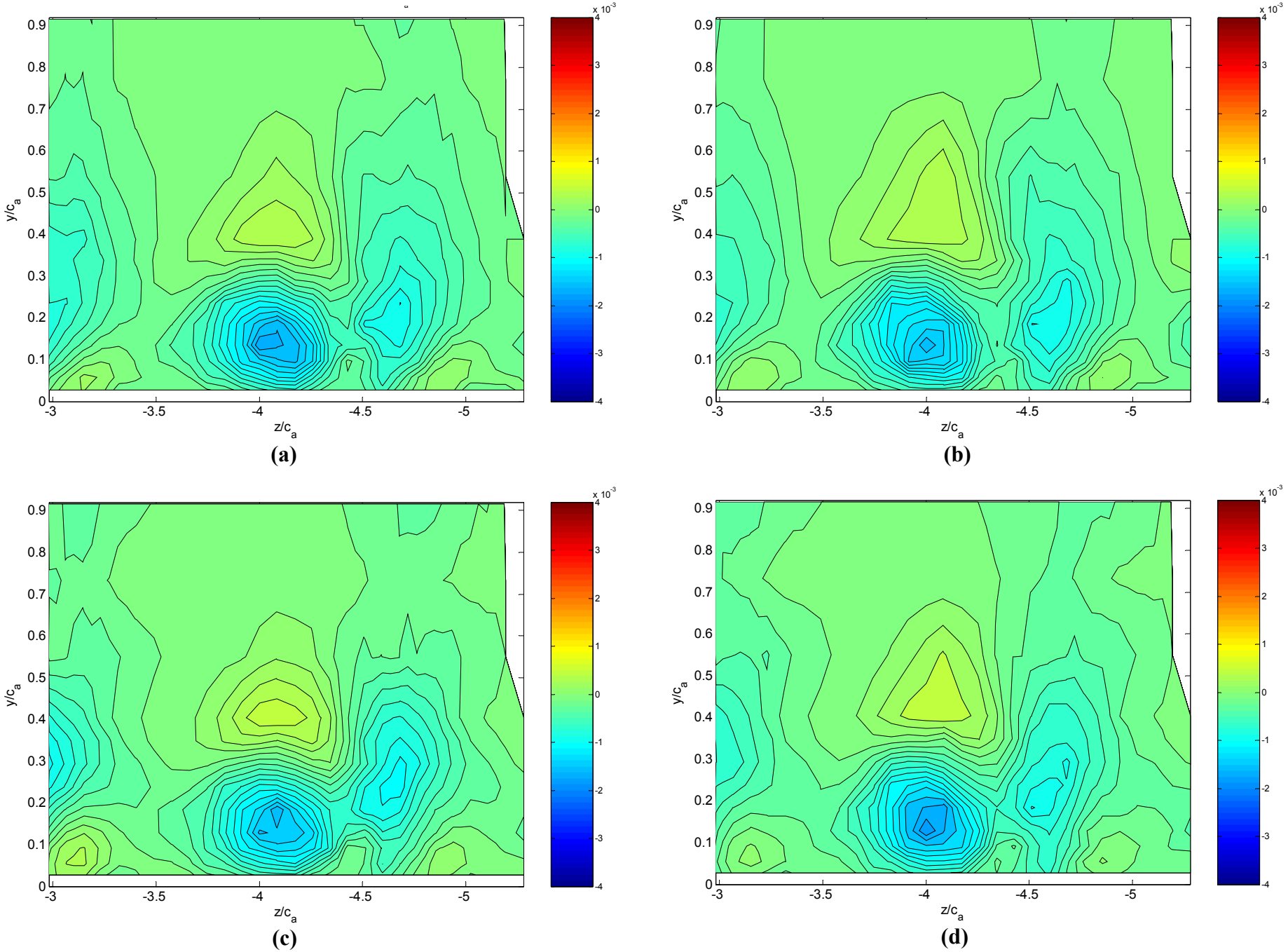

Figure 5-28: Contours of Reynolds shear stress, $\overline{v'w'/U_\infty^2}$, at x/c_a = 1.82: **(a)** 1.27 cm, **(b)** 1.27 cm droop, **(c)** 2.54 cm, **(d)** 2.54 cm droop

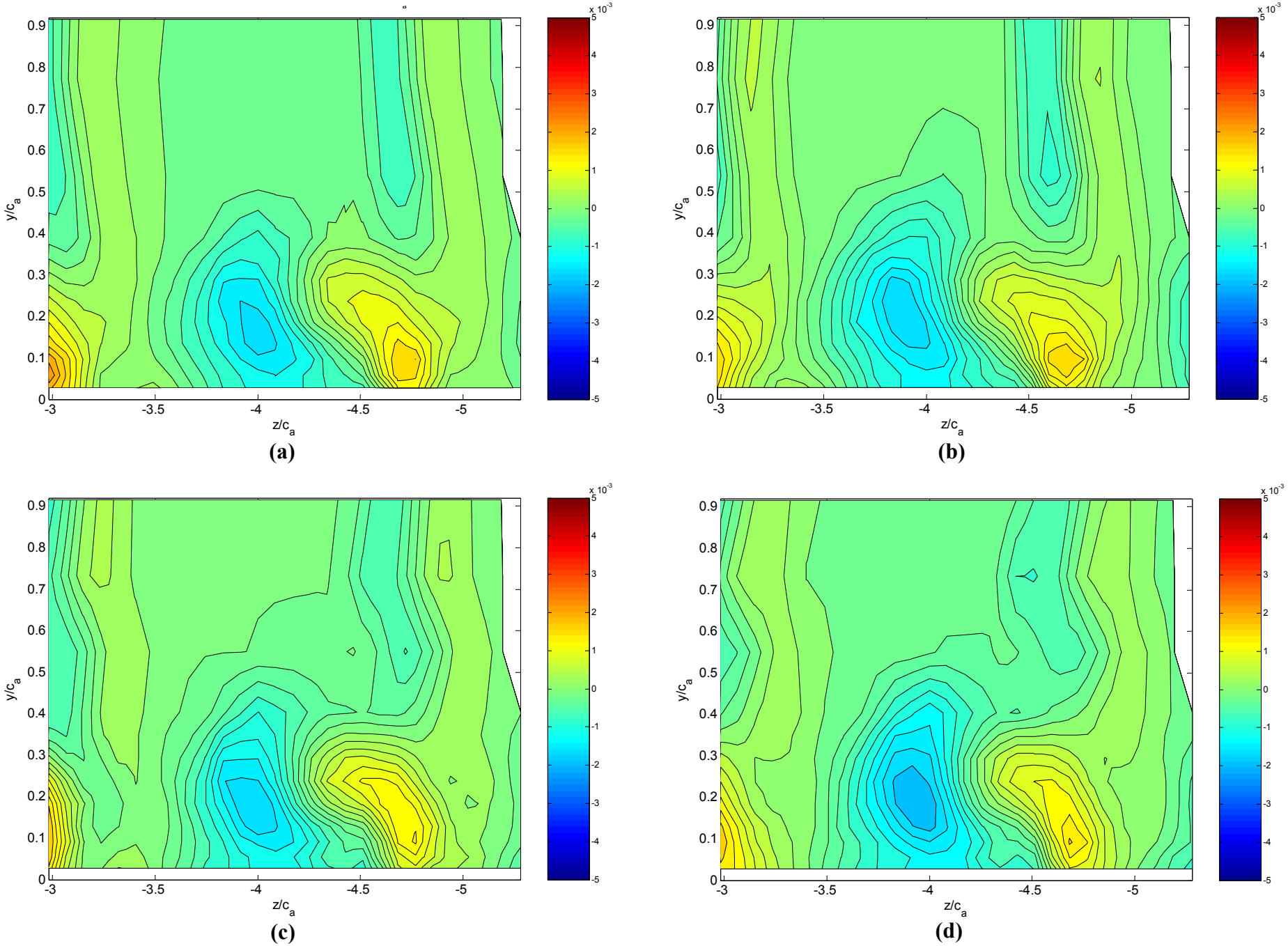

Figure 5-29: Contours of Reynolds shear stress, $\overline{u'w'}/U_\infty^2$, at x/c_a = 1.82: **(a)** 1.27 cm, **(b)** 1.27 cm droop, **(c)** 2.54 cm, **(d)** 2.54 cm droop

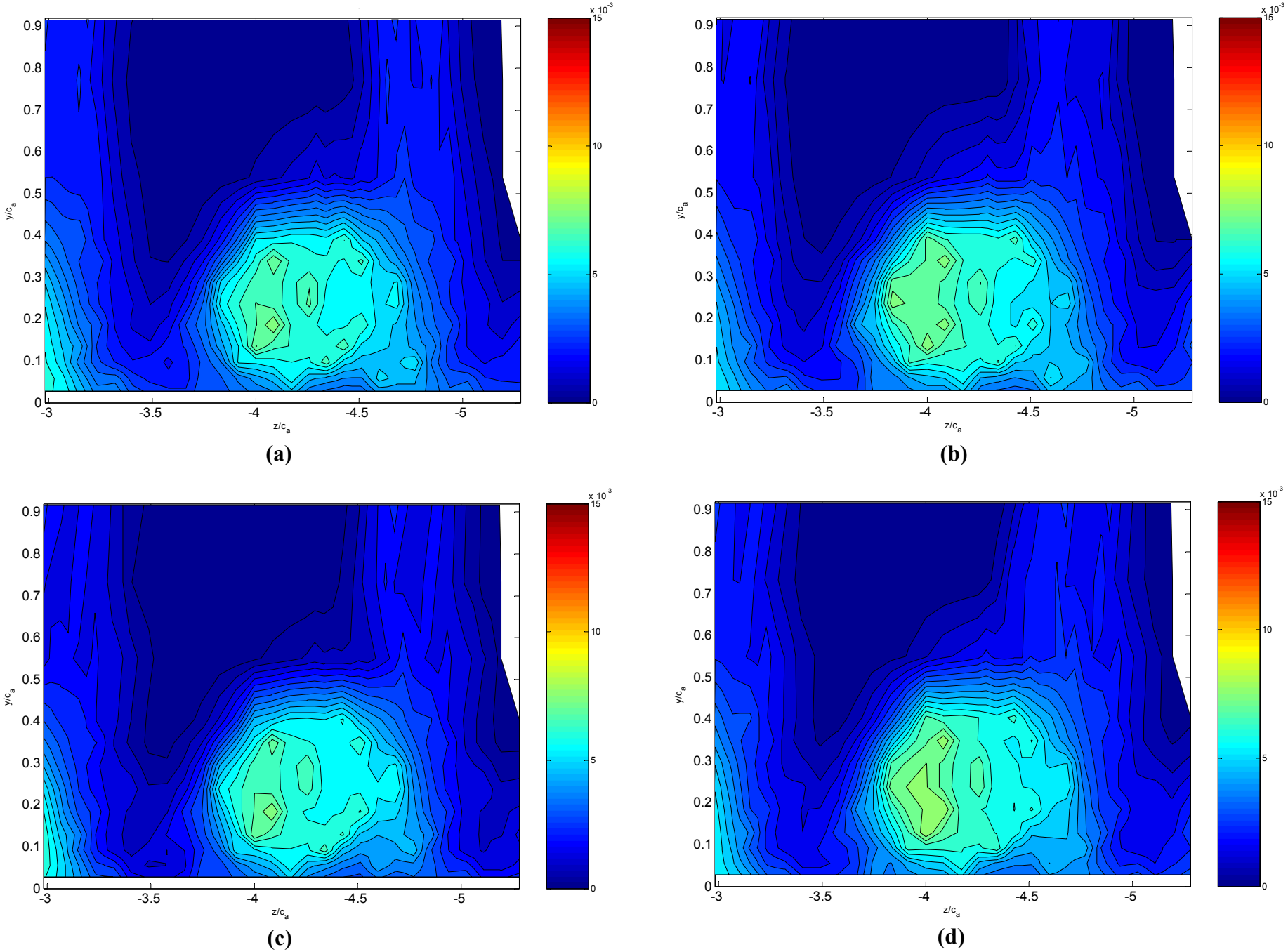

Figure 5-30: Contours of turbulence kinetic energy, $k/U_{\infty}^{2,}$ at x/c_a = 1.82: **(a)** 1.27 cm, **(b)** 1.27 cm droop, **(c)** 2.54 cm, **(d)** 2.54 cm droop

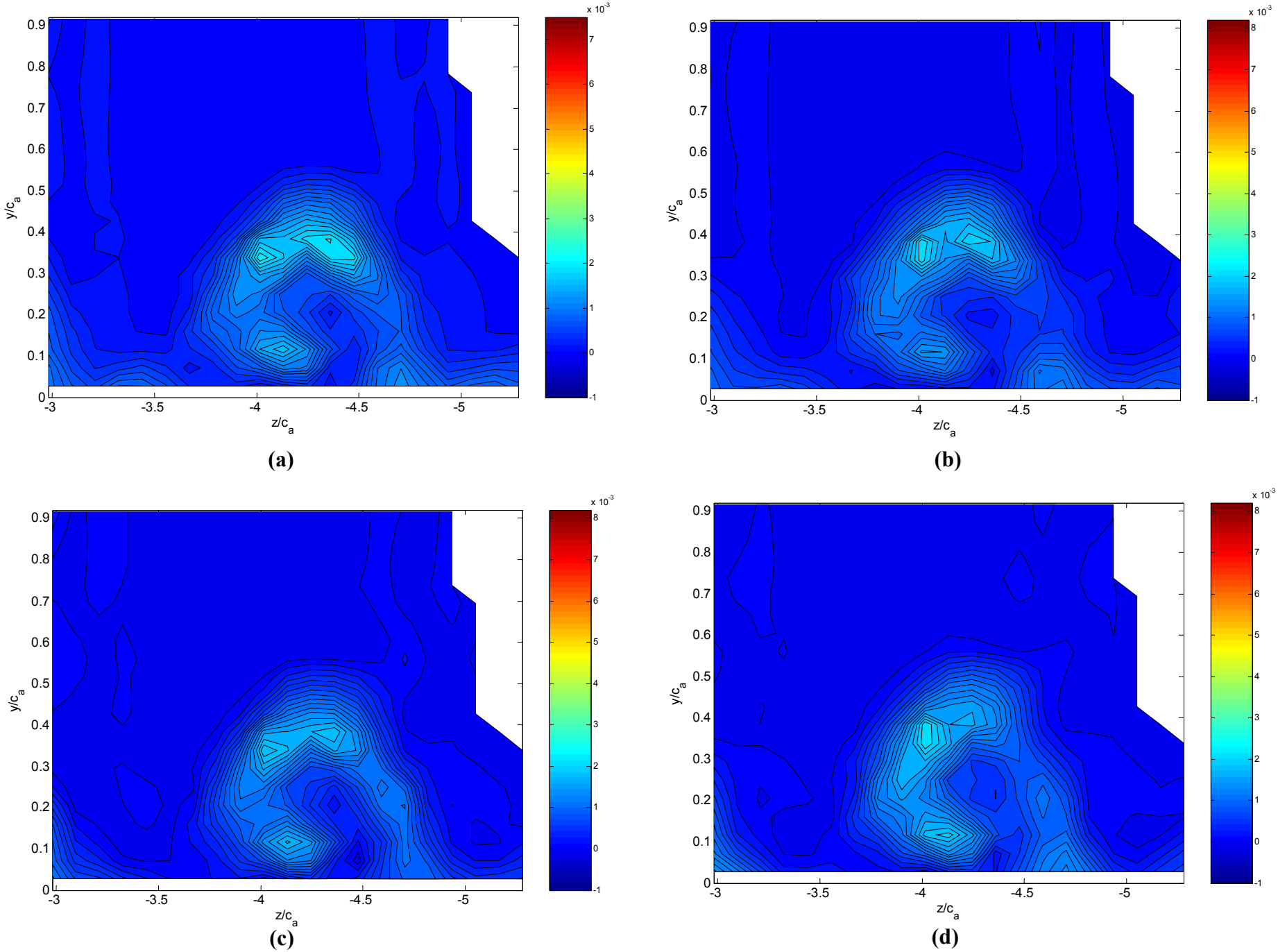

Figure 5-31: Contours of turbulence kinetic energy production, $P_k/c_a U_\infty^{3,}$ at x/c_a = 1.82: **(a)** 1.27 cm, **(b)** 1.27 cm droop, **(c)** 2.54 cm, **(d)** 2.54 cm droop

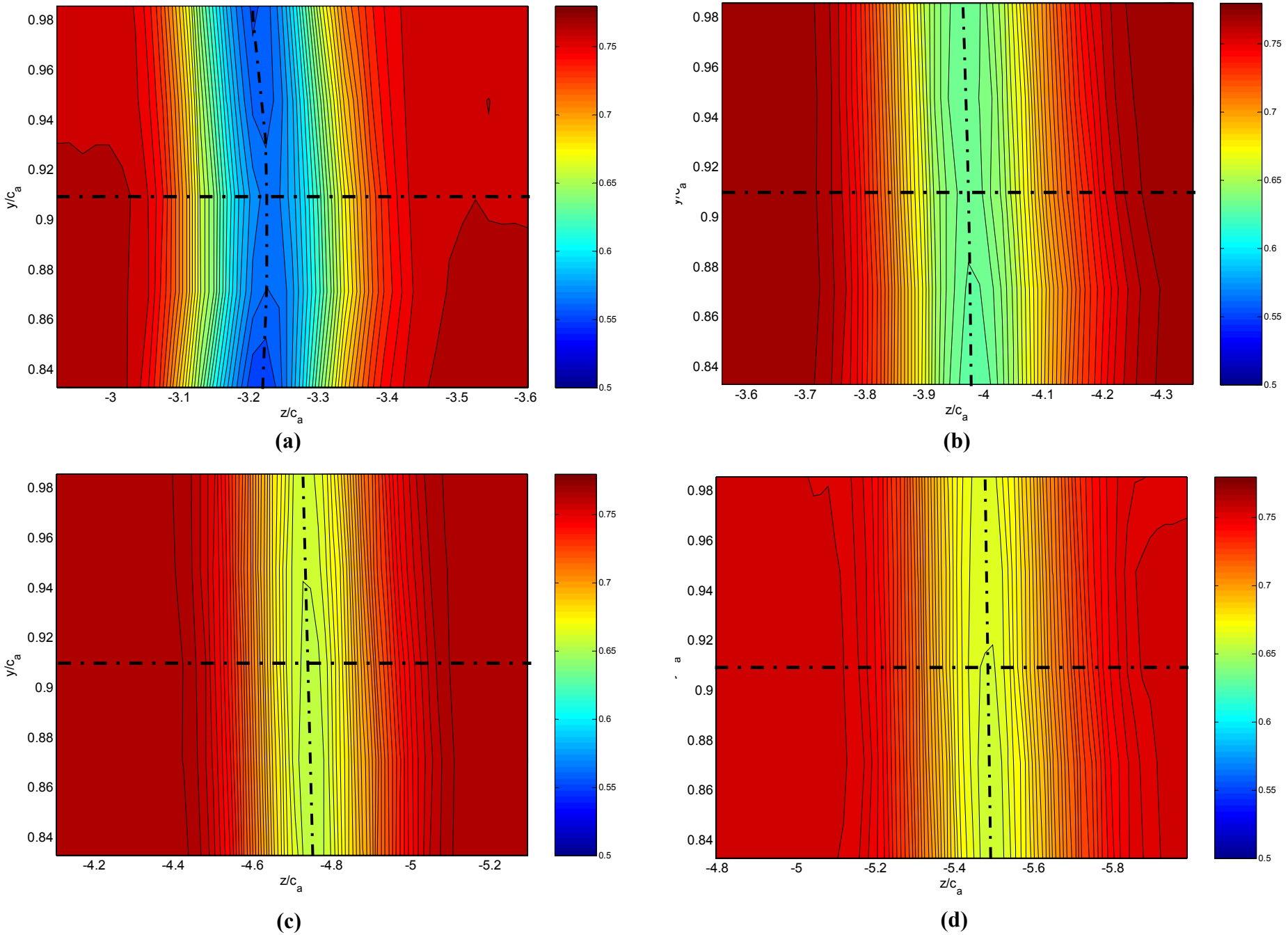

Figure 5-32: Contours of mean streamwise velocity , $U/U_{\infty,}$ measured across one serration for the 1.27 cm serration: **(a)** $x/c_a = 0.61$, **(b)** $x/c_a = 1.18$, **(c)** $x/c_a = 1.82$, **(d)** $x/c_a = 2.38$.

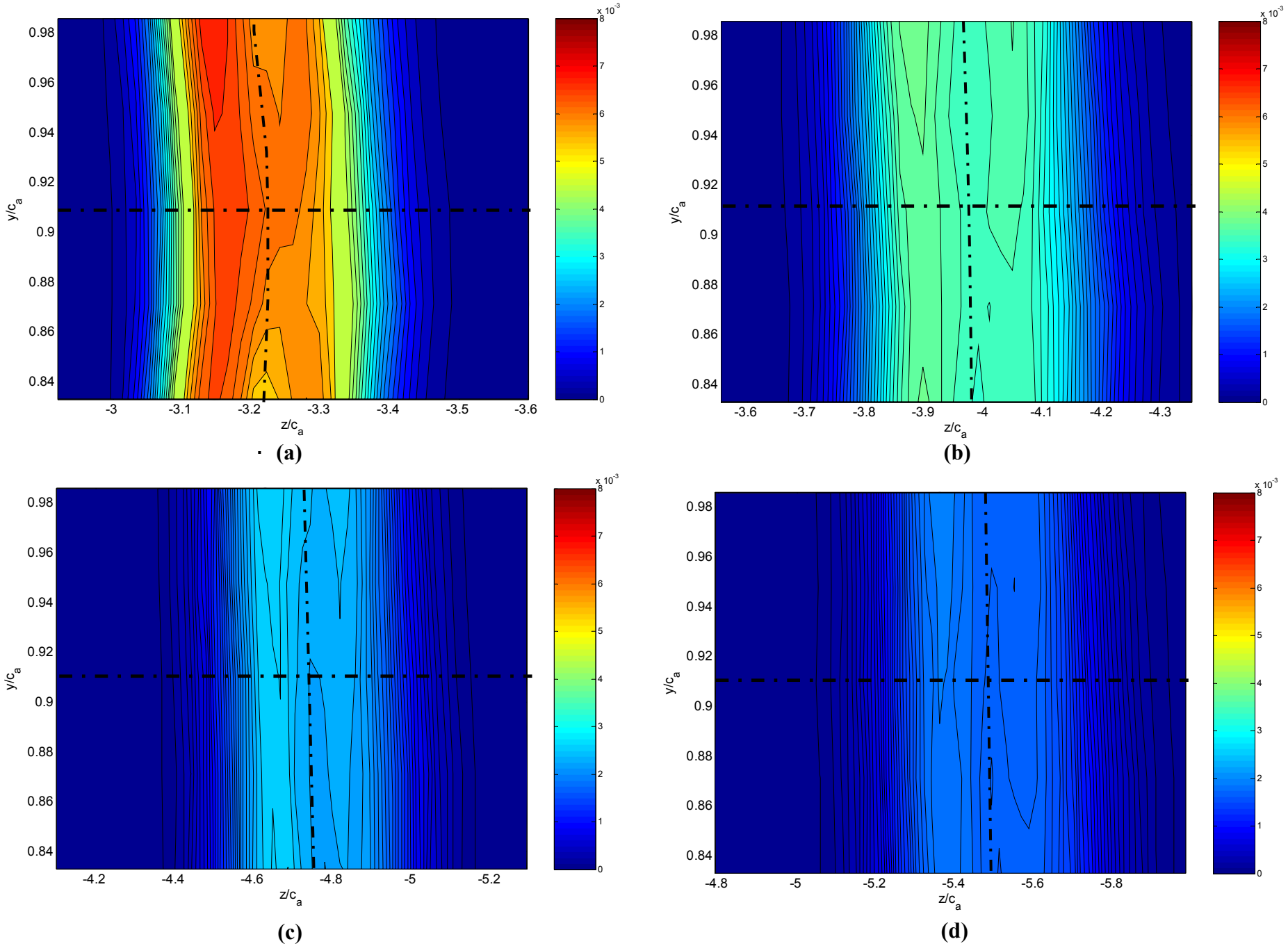

Figure 5-33: Contours of turbulence kinetic energy, k/U_∞^2, measured across one serration for the 1.27 cm serration: **(a)** $x/c_a = 0.61$, **(b)** $x/c_a = 1.18$, **(c)** $x/c_a = 1.82$, **(d)** $x/c_a = 2.38$.

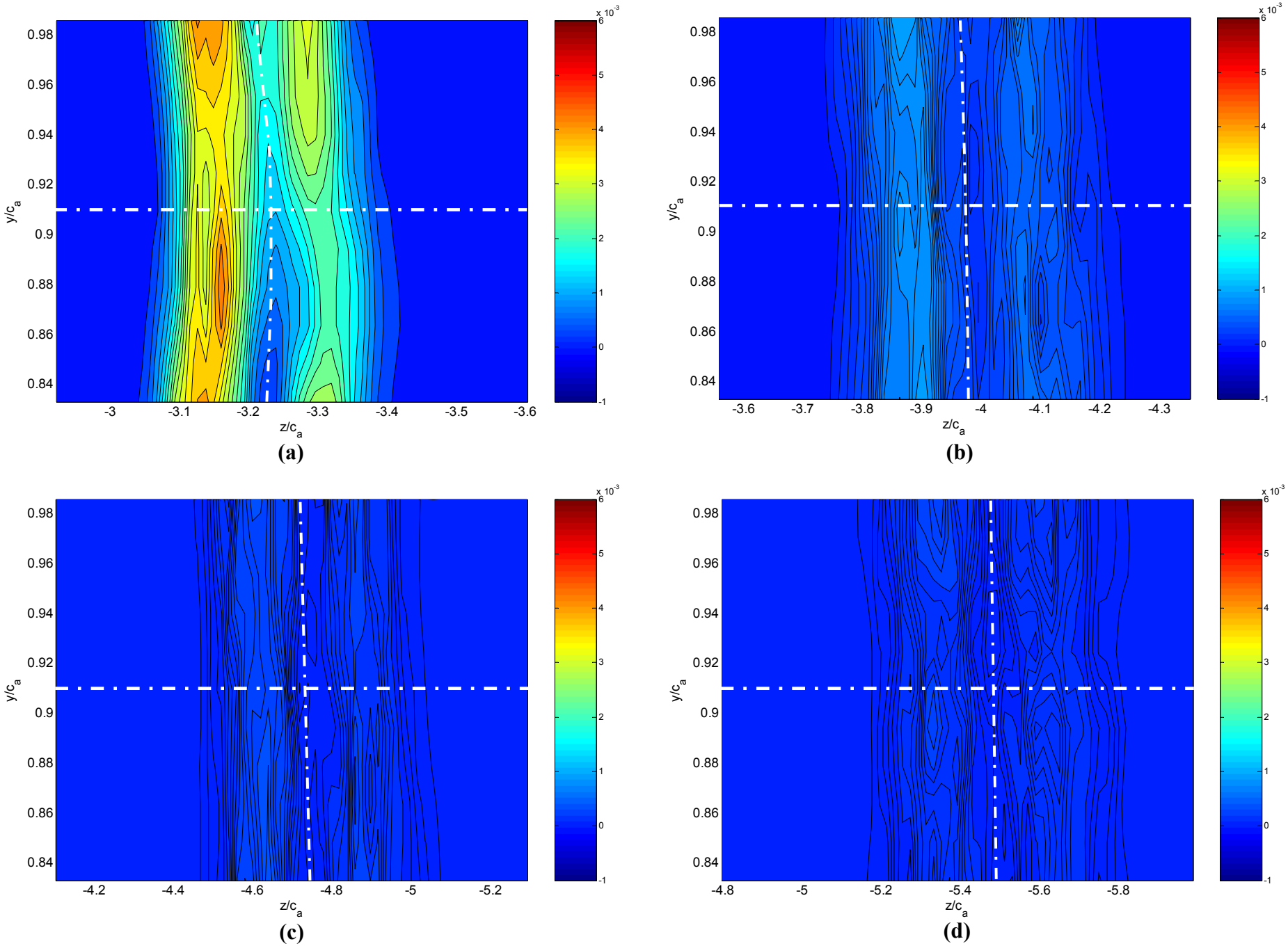

Figure 5-34: Contours of turbulence kinetic energy production, $P_k/c_aU_\infty^3$, across one serration for the 1.27 cm serration: **(a)** x/c_a = 0.61, **(b)** x/c_a = 1.18, **(c)** x/c_a = 1.82, **(d)** x/c_a = 2.38.

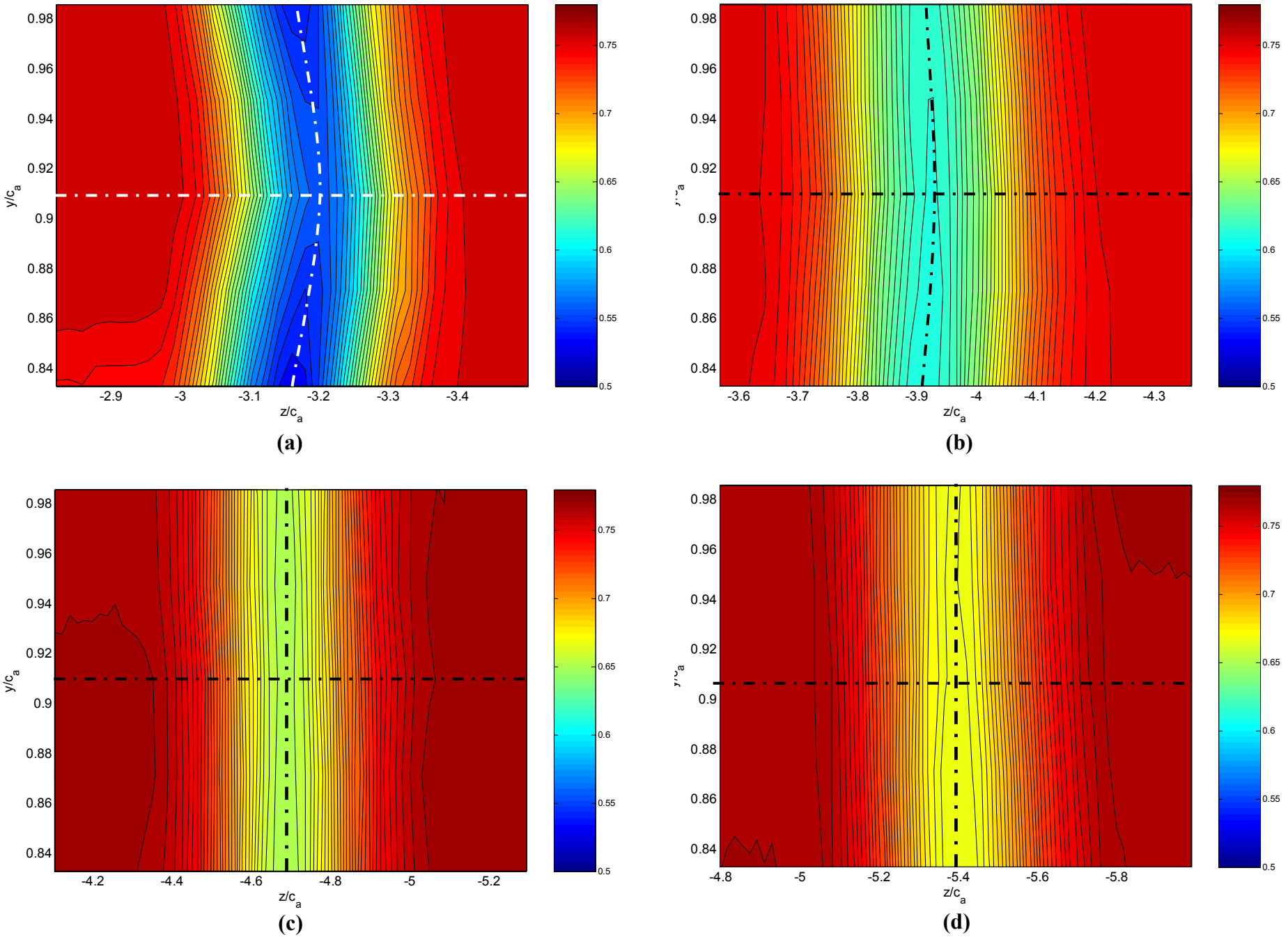

Figure 5-35: Contours of mean streamwise velocity , $U/U_{\infty,}$ measured across one serration for the 1.27 cm droop serration: **(a)** x/c_a = 0.61, **(b)** x/c_a = 1.18, **(c)** x/c_a = 1.82, **(d)** x/c_a = 2.38.

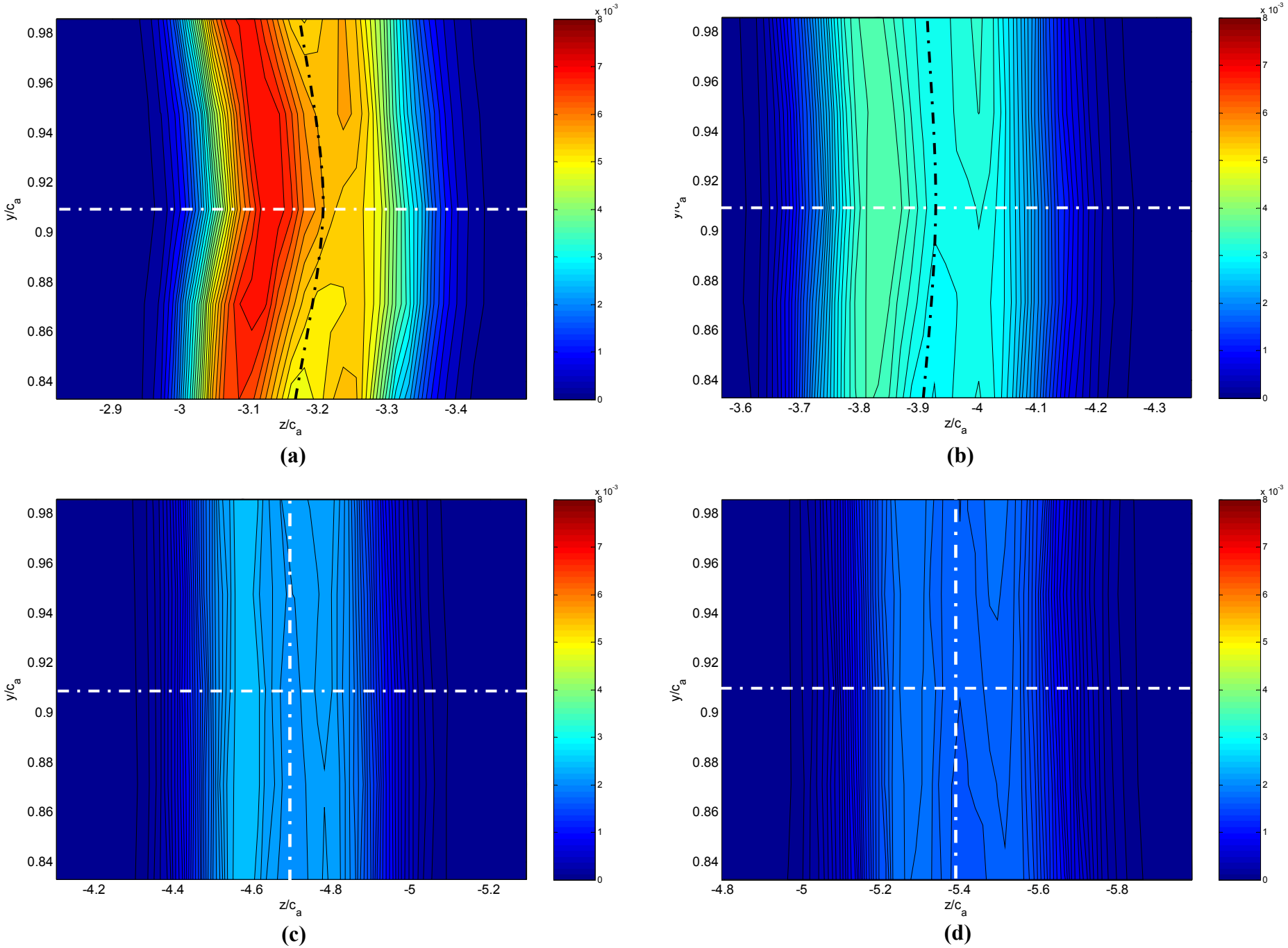

Figure 5-36: Contours of turbulence kinetic energy, k/U_∞^2, measured across one serration for the 1.27 cm droop serration: **(a)** x/c_a = 0.61, **(b)** x/c_a = 1.18, **(c)** x/c_a = 1.82, **(d)** x/c_a = 2.38.

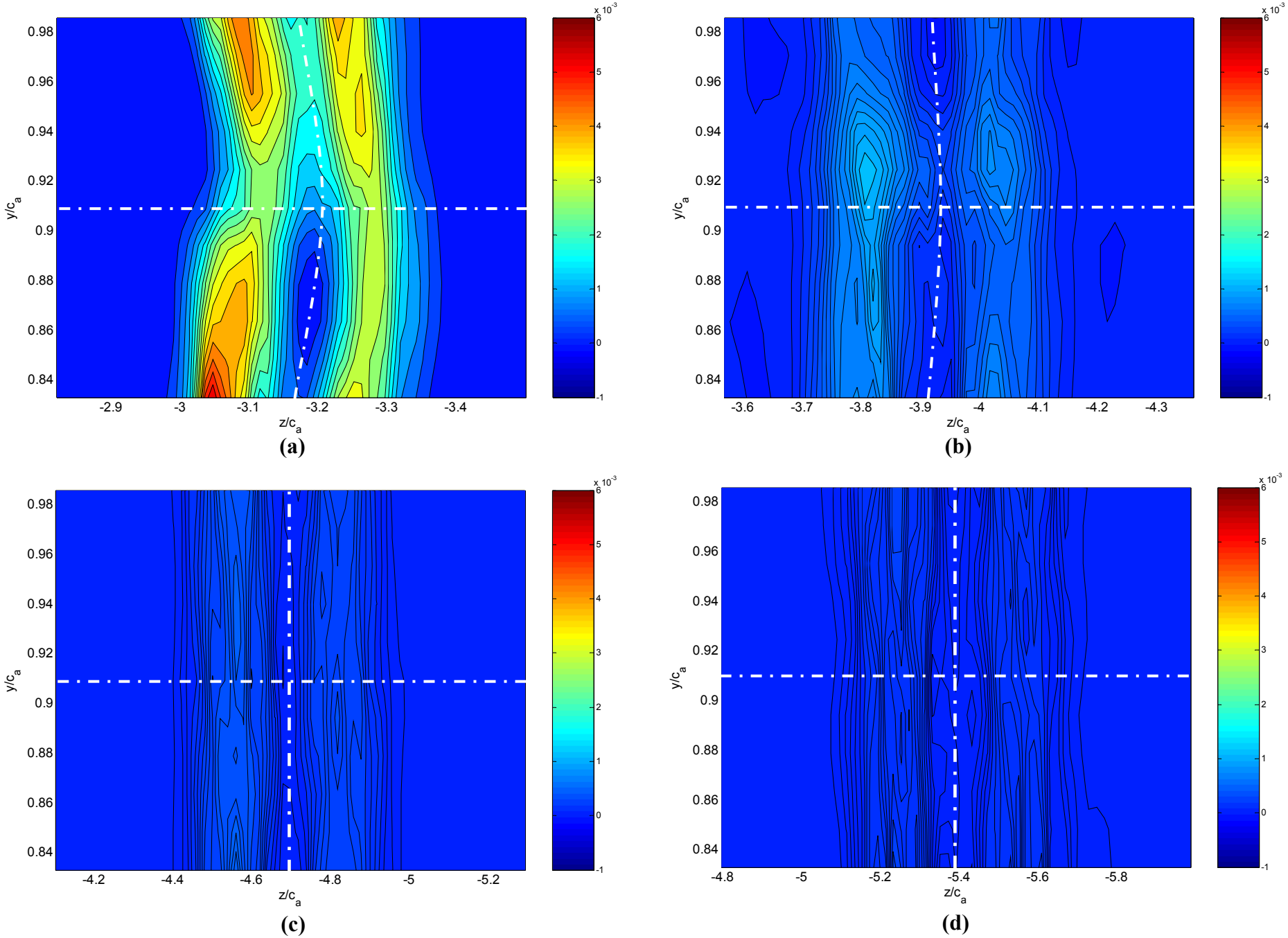

Figure 5-37: Contours of turbulence kinetic energy production, $P_k/c_aU_\infty^3$, across one serration for the 1.27 cm droop serration: **(a)** $x/c_a = 0.61$, **(b)** $x/c_a = 1.18$, **(c)** $x/c_a = 1.82$, **(d)** $x/c_a = 2.38$

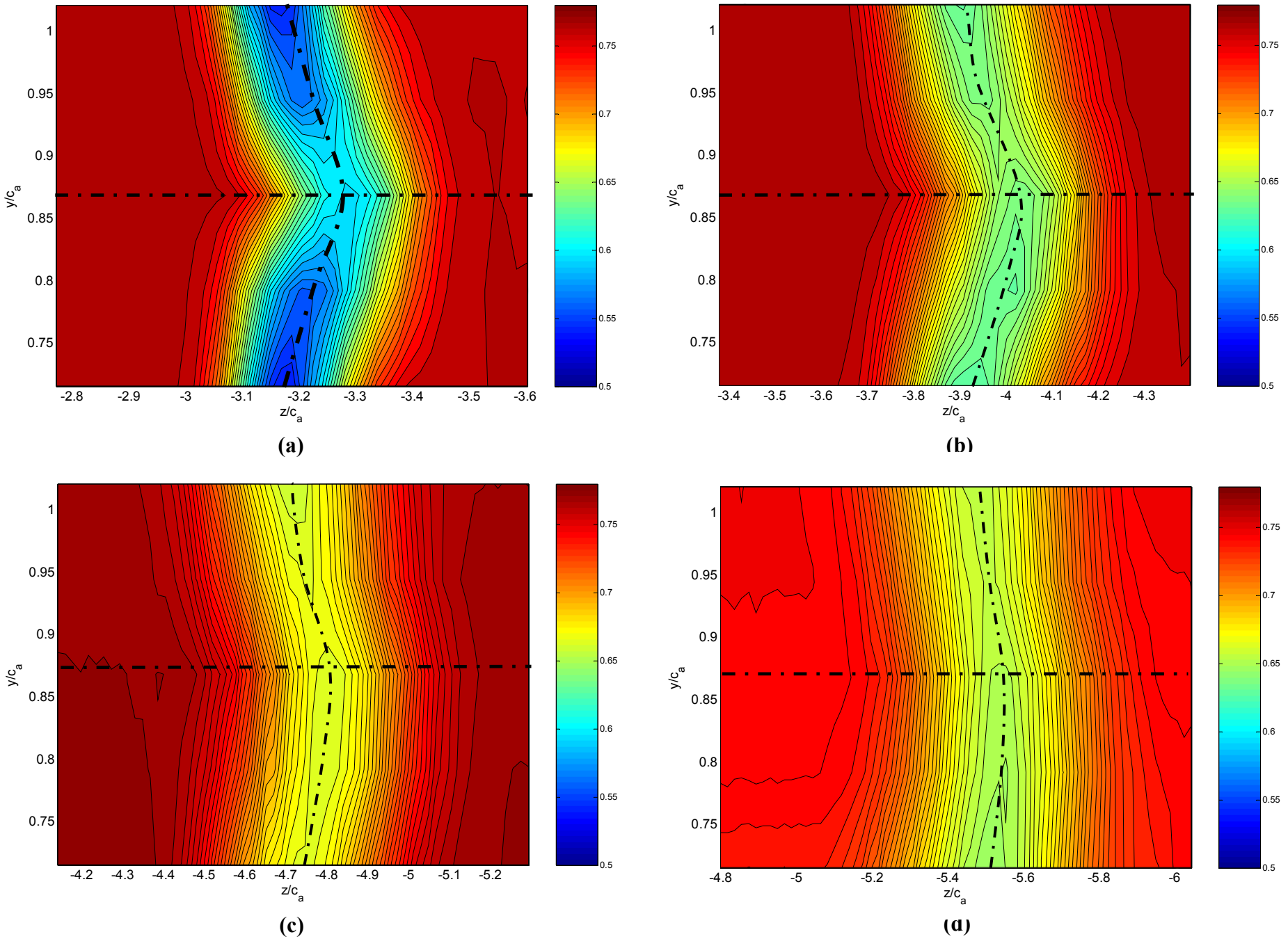

Figure 5-38: Contours of mean streamwise velocity , $U/U_{\infty,}$ measured across one serration for the 2.54 cm serration: **(a)** $x/c_a = 0.61$, **(b)** $x/c_a = 1.18$, **(c)** $x/c_a = 1.82$, **(d)** $x/c_a = 2.38$.

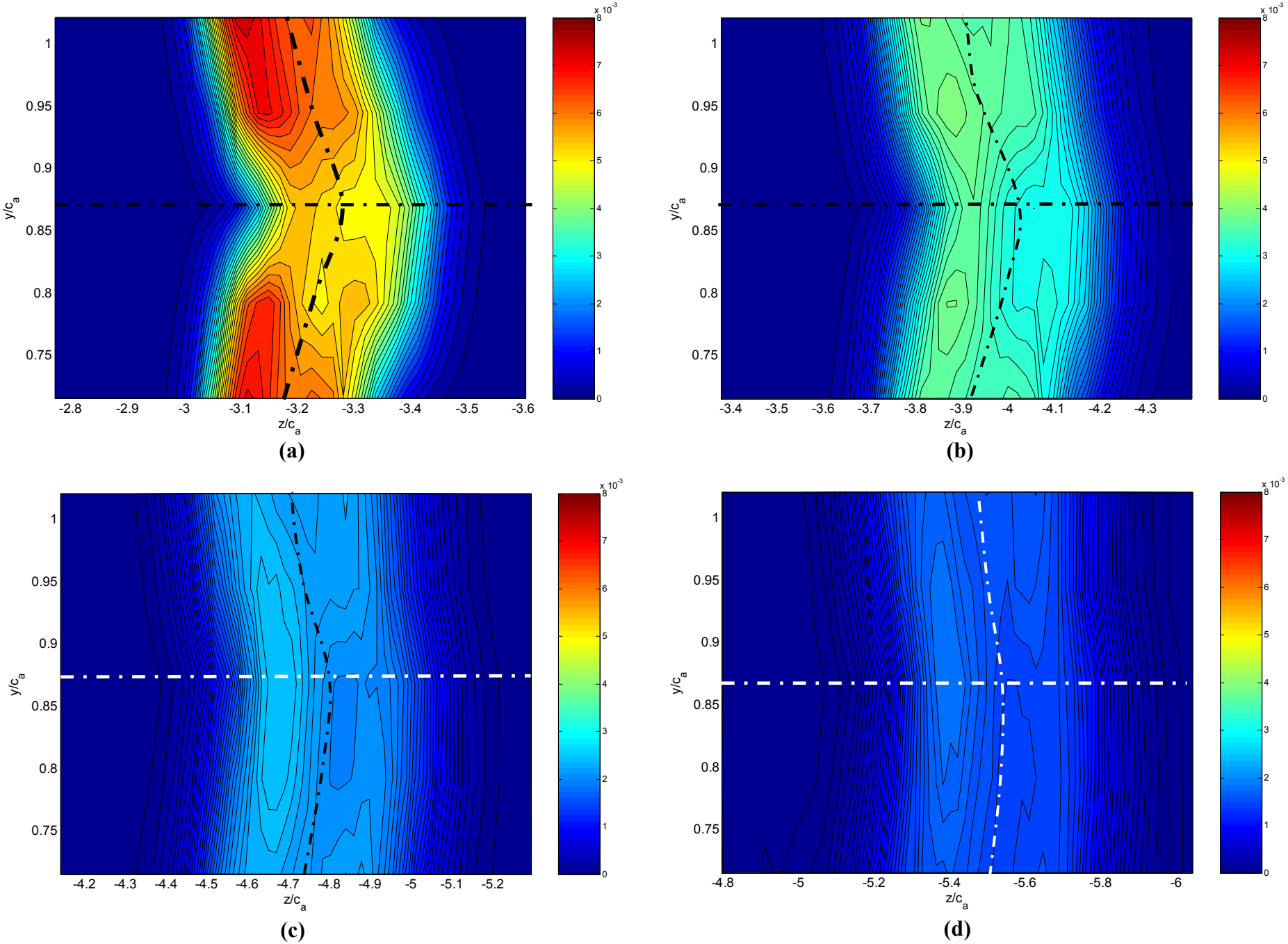

Figure 5-39: Contours of turbulence kinetic energy, k/U_∞^2, measured across one serration for the 2.54 cm serration: **(a)** $x/c_a = 0.61$, **(b)** $x/c_a = 1.18$, **(c)** $x/c_a = 1.82$, **(d)** $x/c_a = 2.38$.

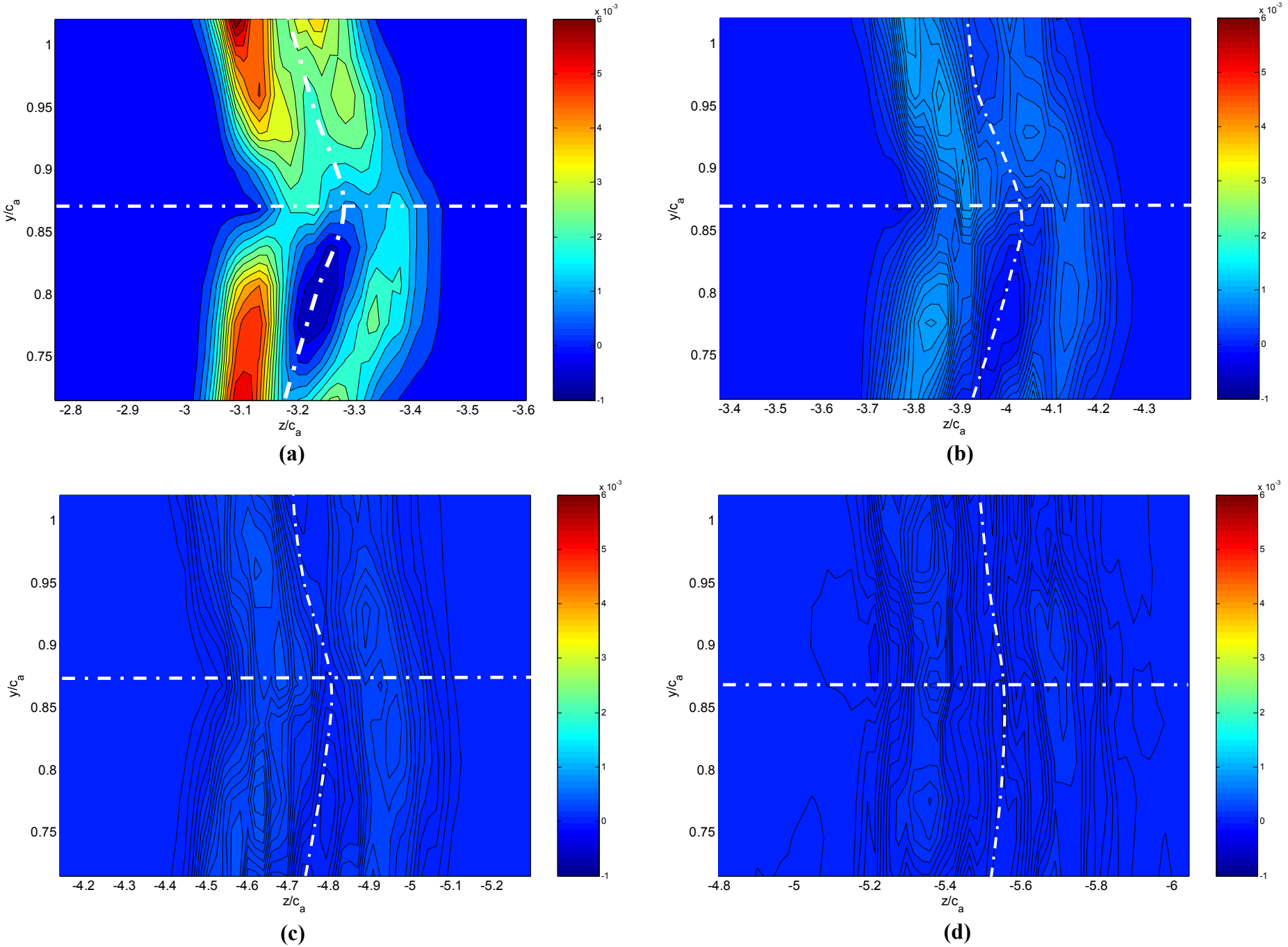

Figure 5-40: Contours of turbulence kinetic energy production, $P_k/c_a U_\infty^3$, across one serration for the 2.54 cm serration: **(a)** x/c_a = 0.61, **(b)** x/c_a = 1.18, **(c)** x/c_a = 1.82, **(d)** x/c_a = 2.38.

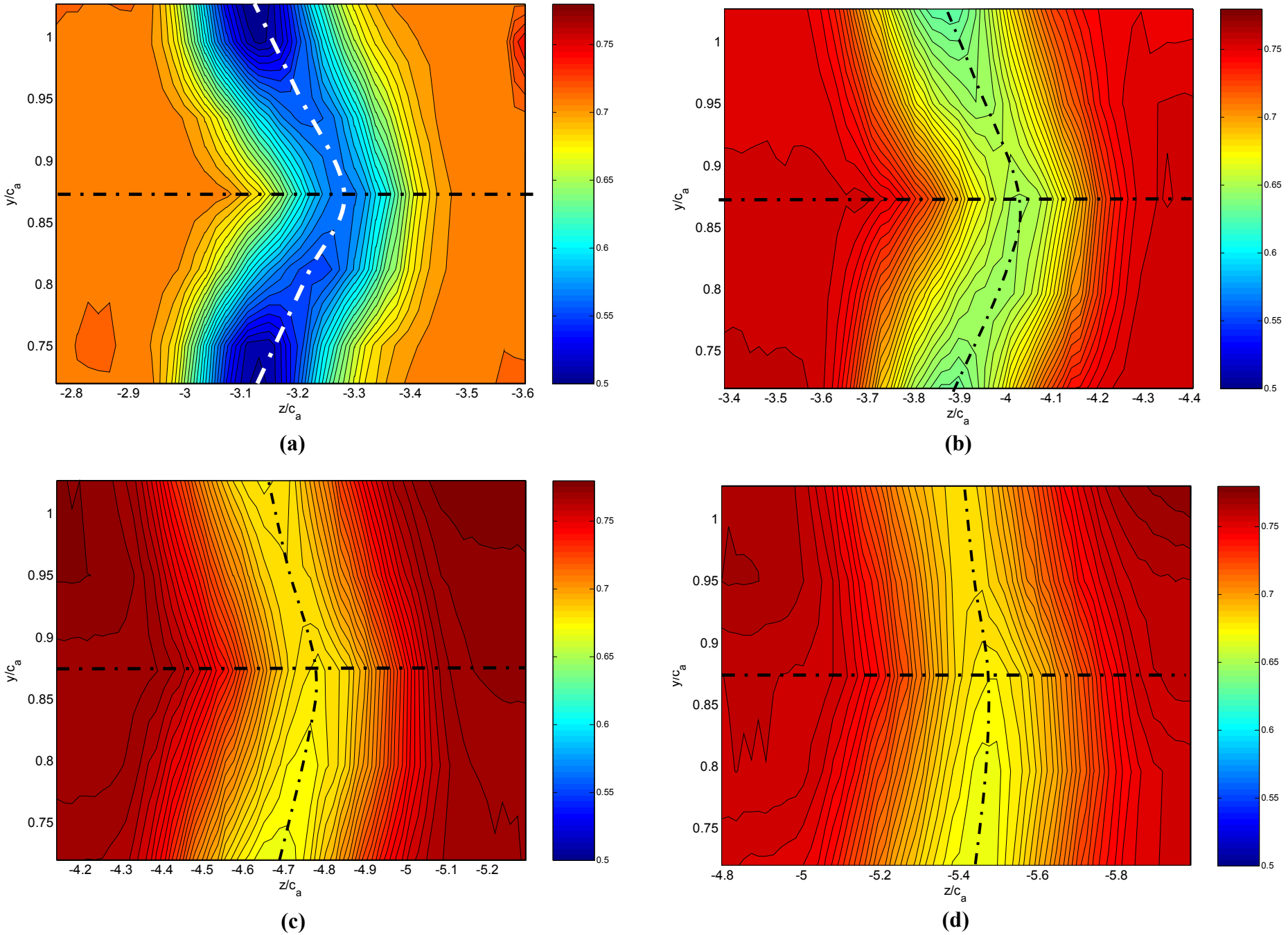

Figure 5-41: Contours of mean streamwise velocity , $U/U_{\infty,}$ measured across one serration for the 2.54 cm droop serration: **(a)** x/c_a = 0.61, **(b)** x/c_a = 1.18, **(c)** x/c_a = 1.82, **(d)** x/c_a = 2.38.

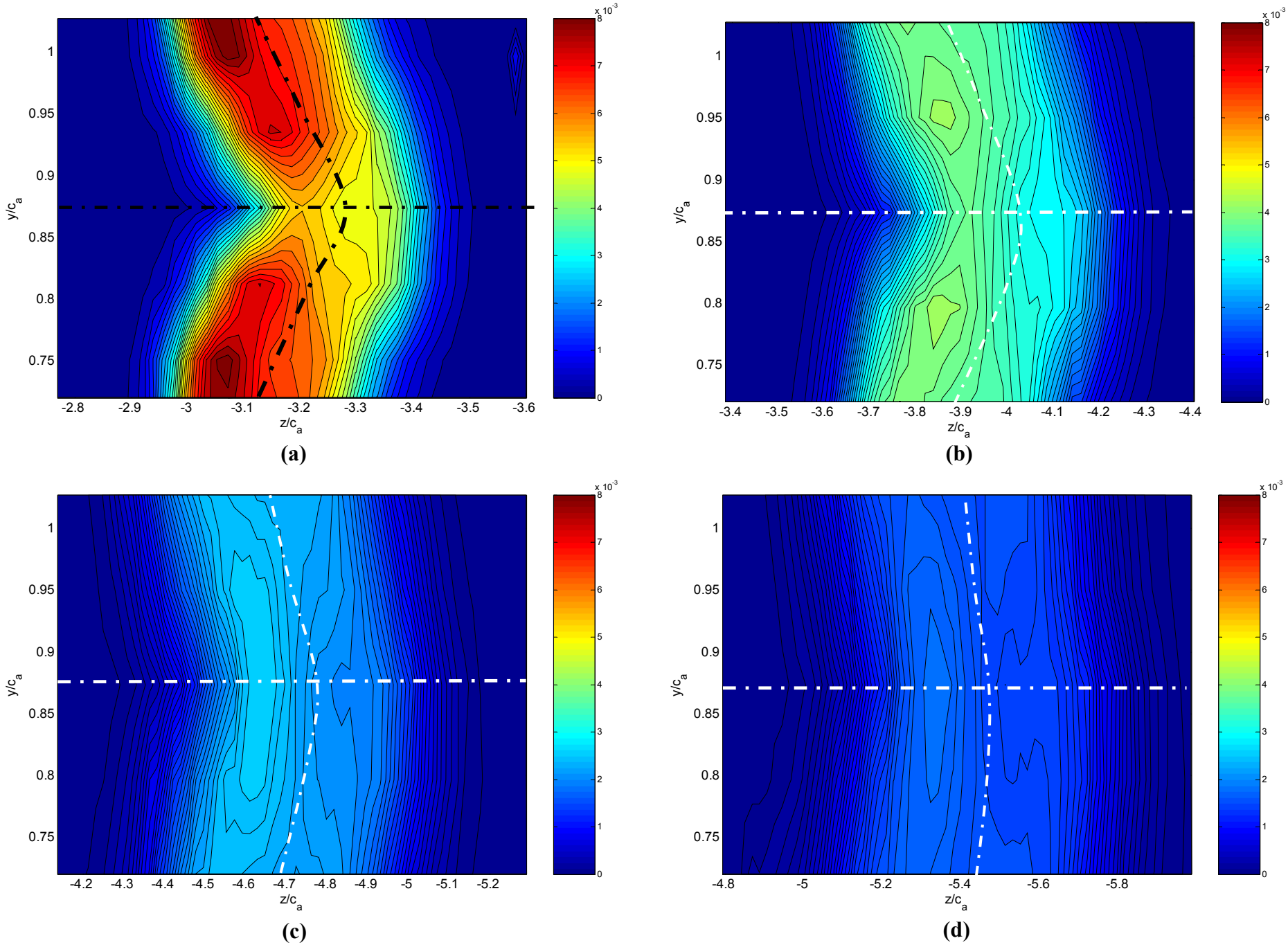

Figure 5-42: Contours of turbulence kinetic energy, k/U_∞^2, measured across one serration for the 2.54 cm droop serration: **(a)** x/c_a = 0.61, **(b)** x/c_a = 1.18, **(c)** x/c_a = 1.82, **(d)** x/c_a = 2.38.

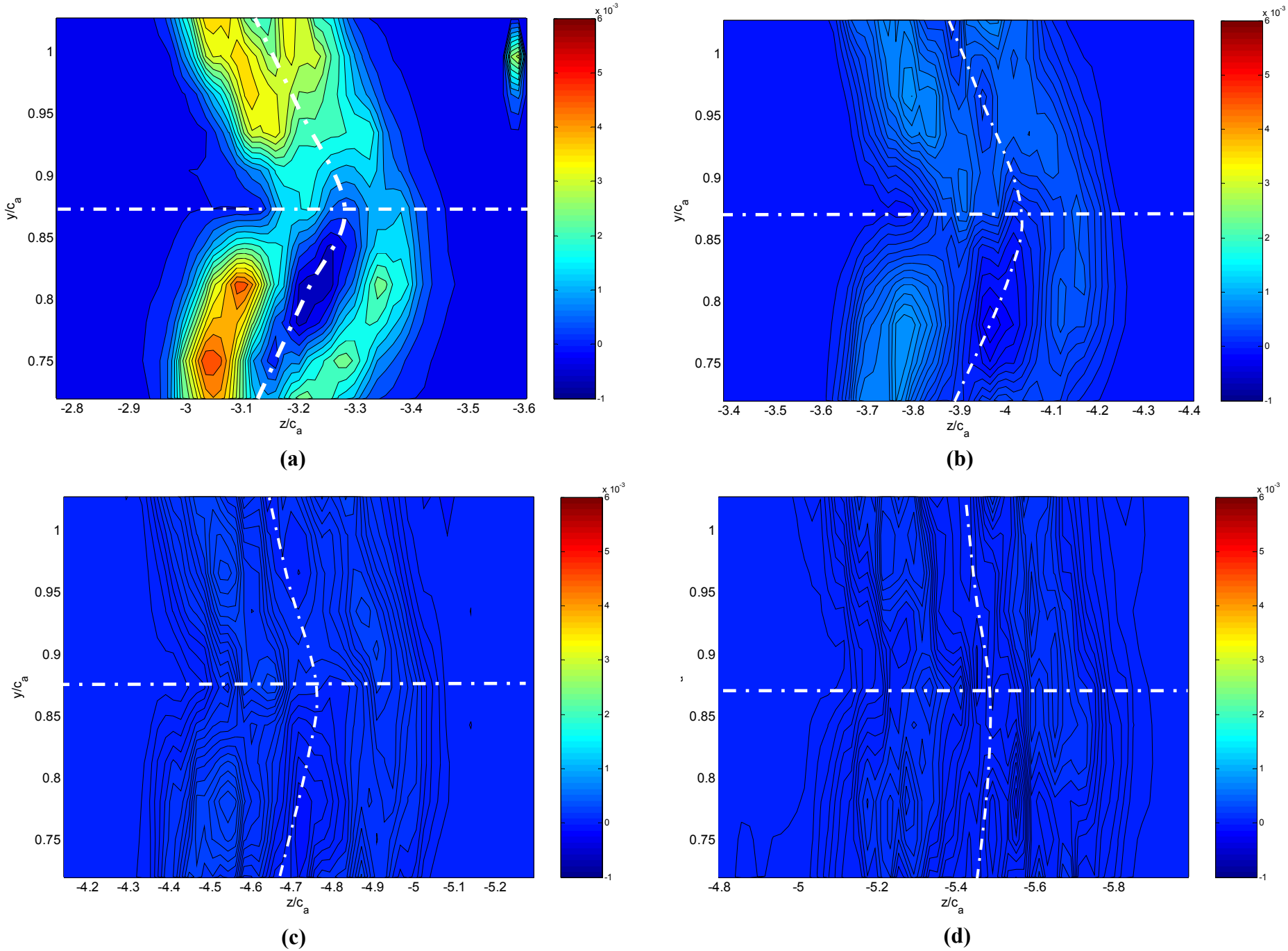

Figure 5-43: Contours of turbulence kinetic energy production, $P_k/c_aU_\infty^3$, across one serration for the 2.54 cm droop serration: **(a)** $x/c_a = 0.61$, **(b)** $x/c_a = 1.18$, **(c)** $x/c_a = 1.82$, **(d)** $x/c_a = 2.38$.

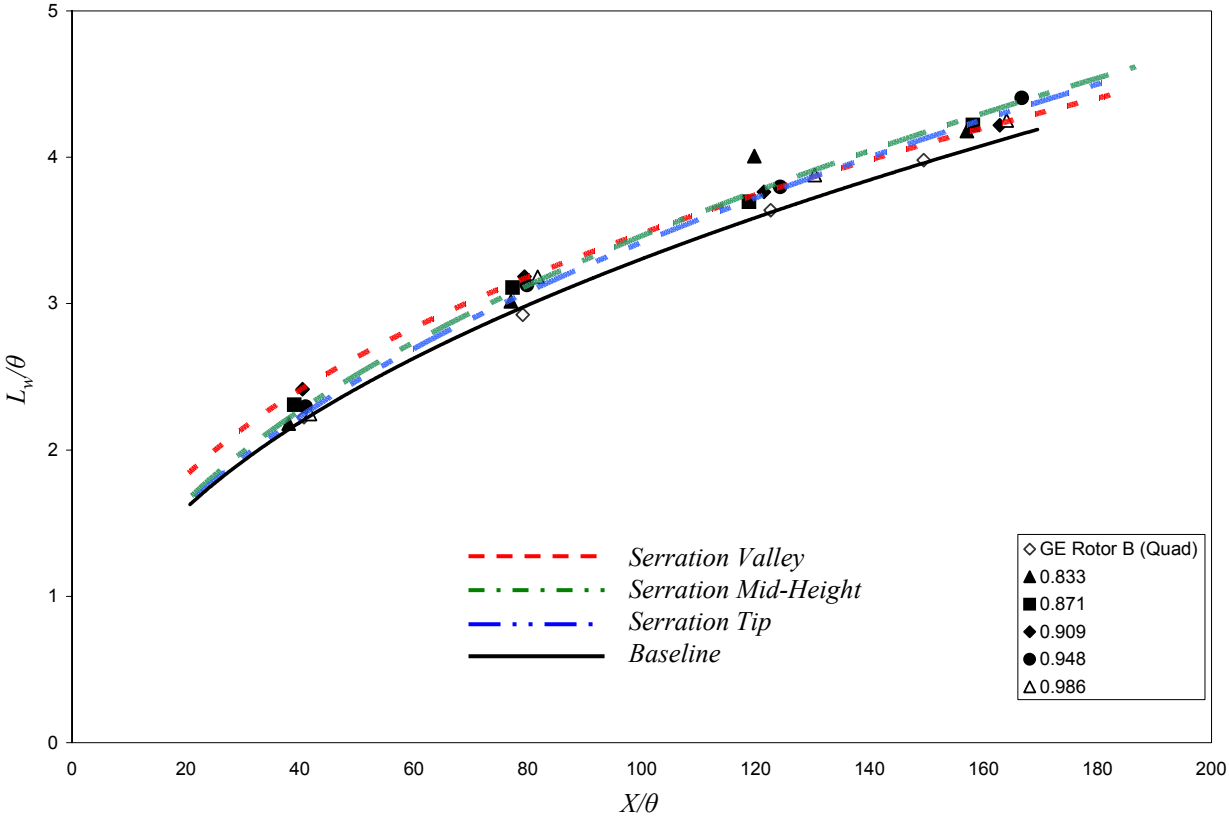

Figure 5-44: Normalized wake half-width of the wake, L_w/θ, as a function of normalized downstream distance, X/θ, for the 1.27 cm serration.

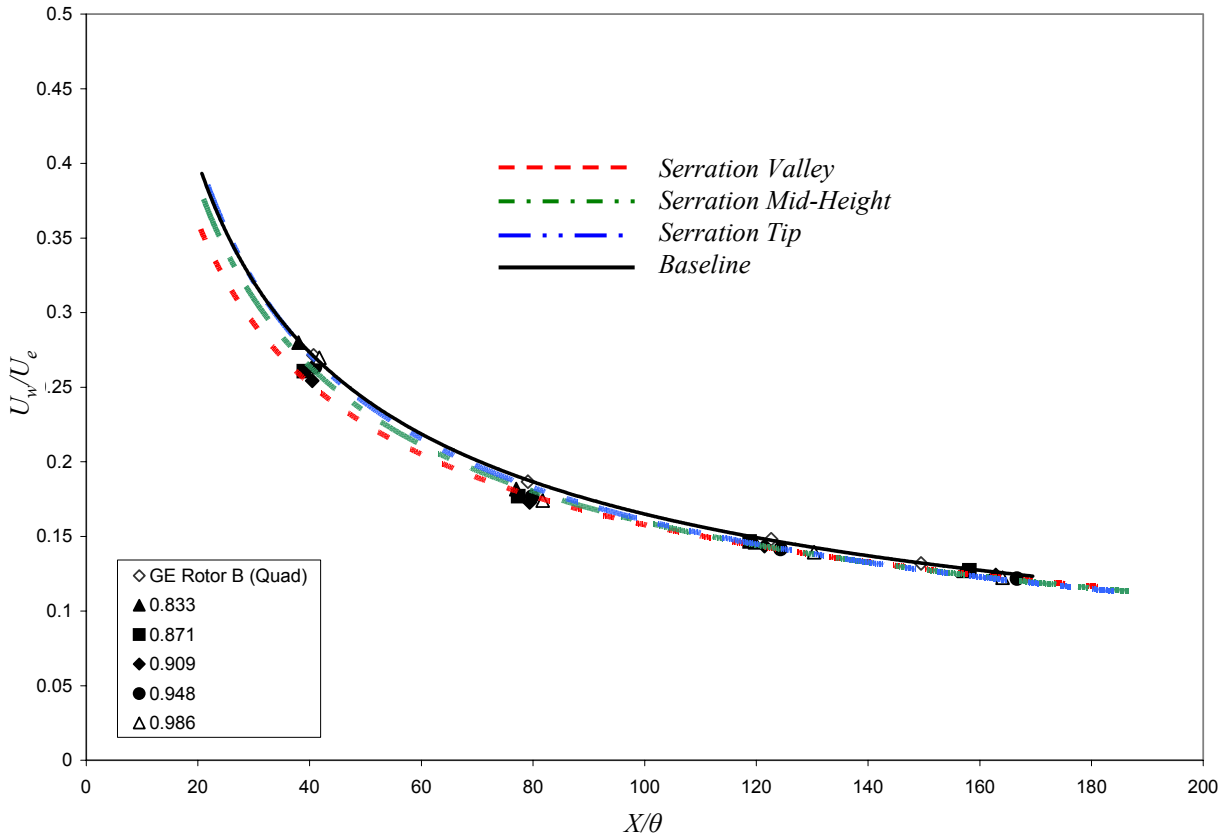

Figure 5-45: Normalized maximum velocity deficit in the wake, U_w/U_e, function of the normalized downstream distance, X/θ, for the 1.27 cm serration.

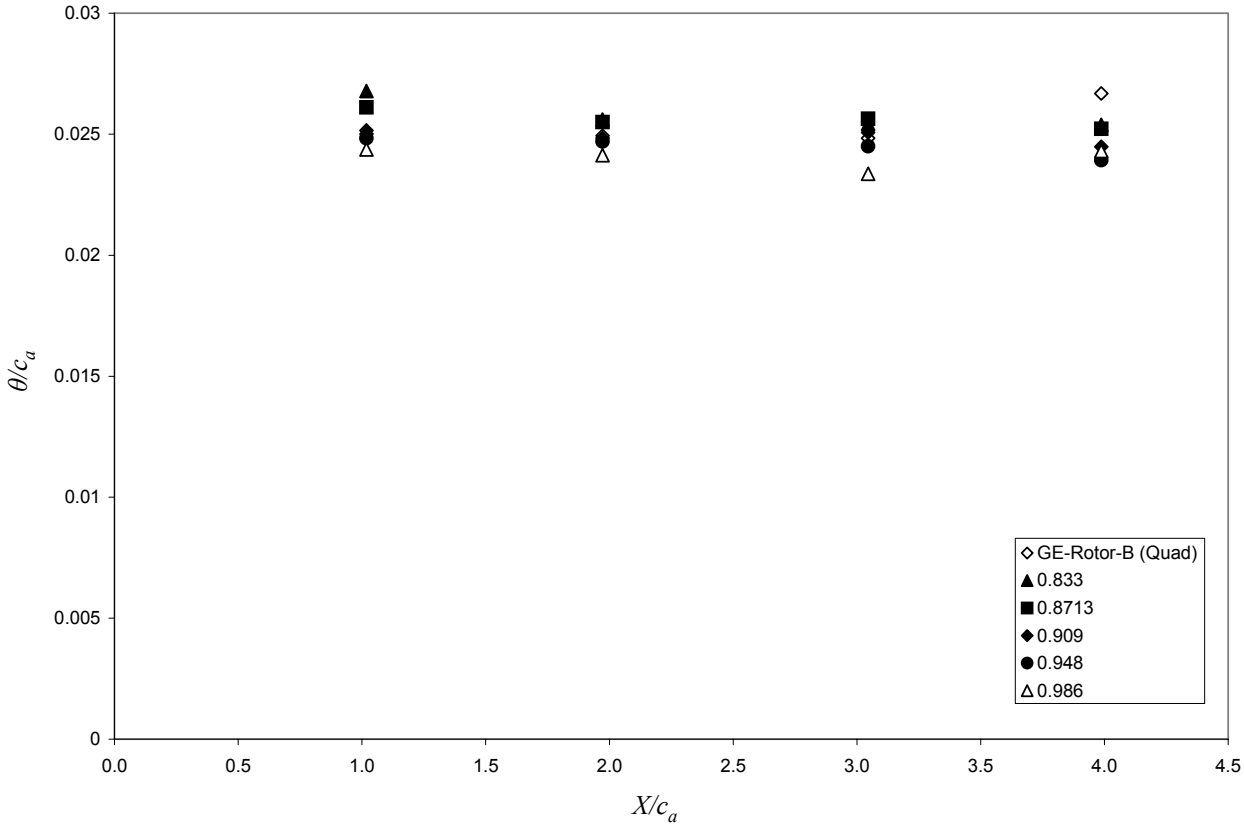

Figure 5-46: Normalized momentum thickness, θ/c_a, as a function of normalized distance downstream, X/c_a, for the 1.27 cm serration.

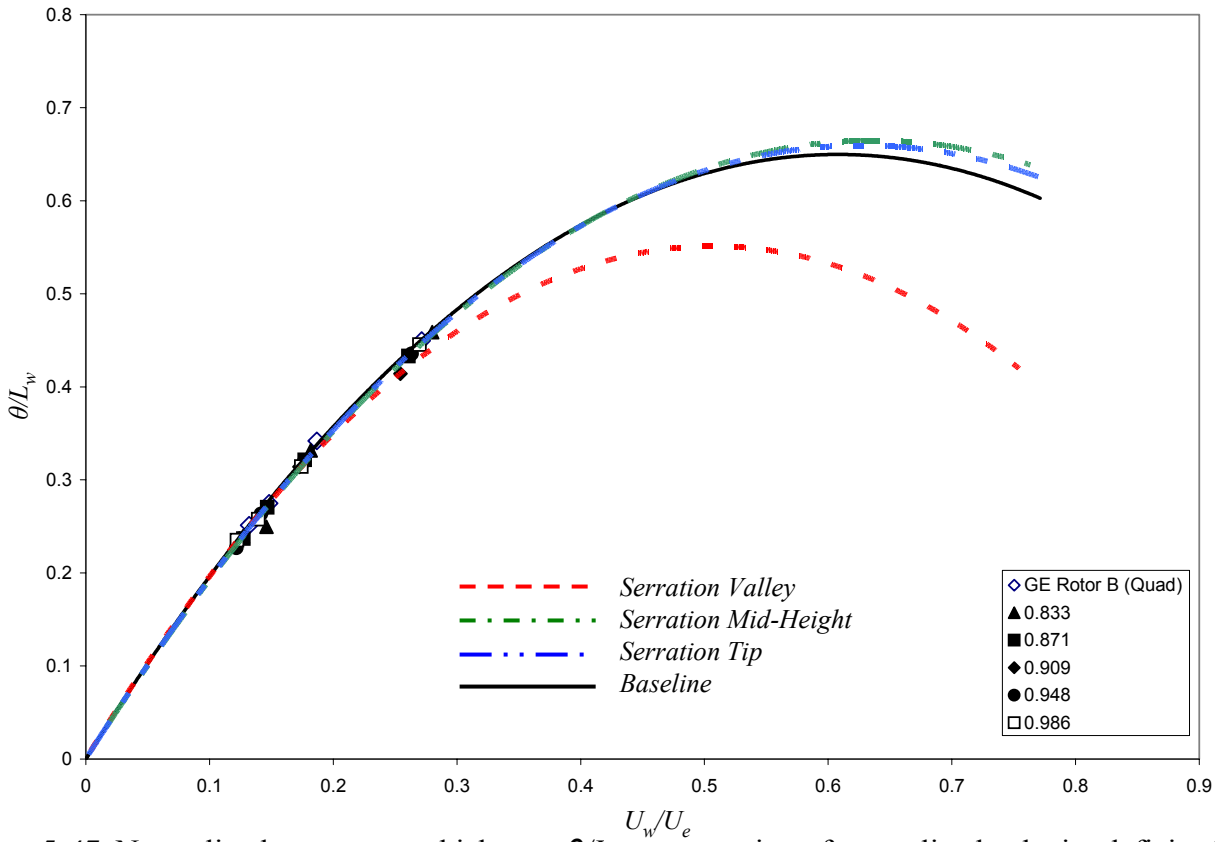

Figure 5-47: Normalized momentum thickness, θ/L_w as a function of normalized velocity deficit of wake, $U_w/U_{e,}$ for the 1.27 cm serration.

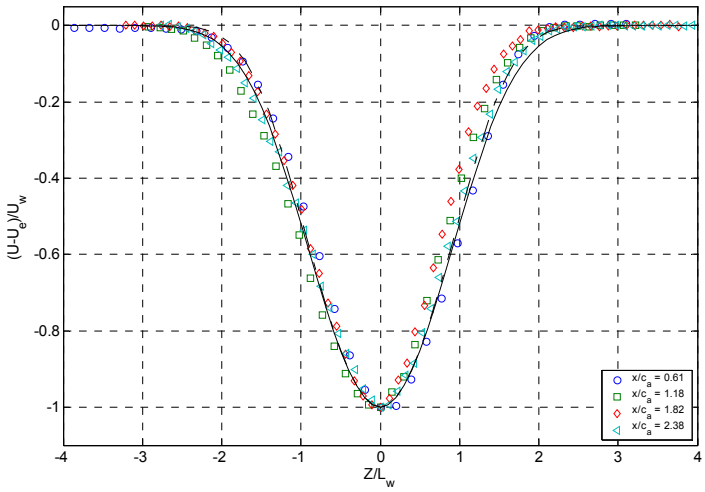

(a)

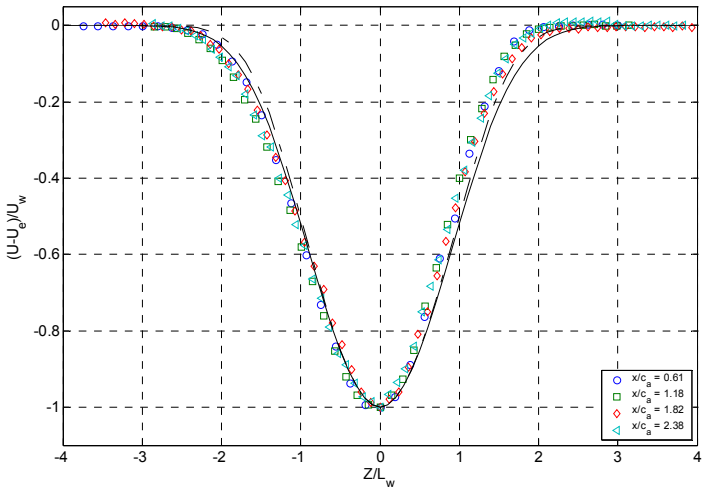

(b)

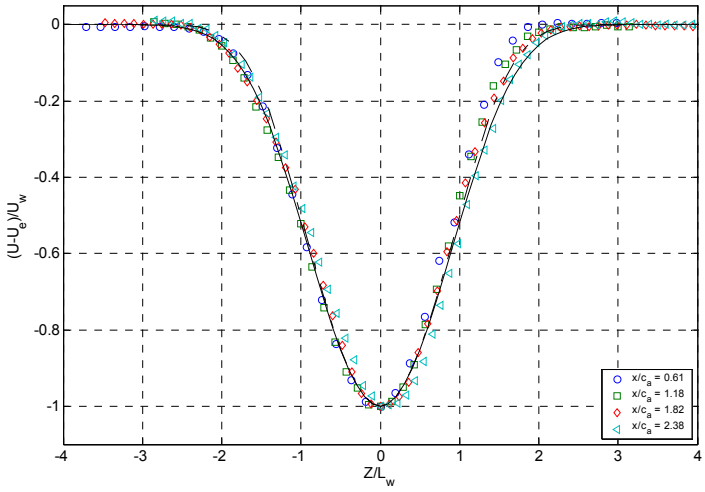

(c)

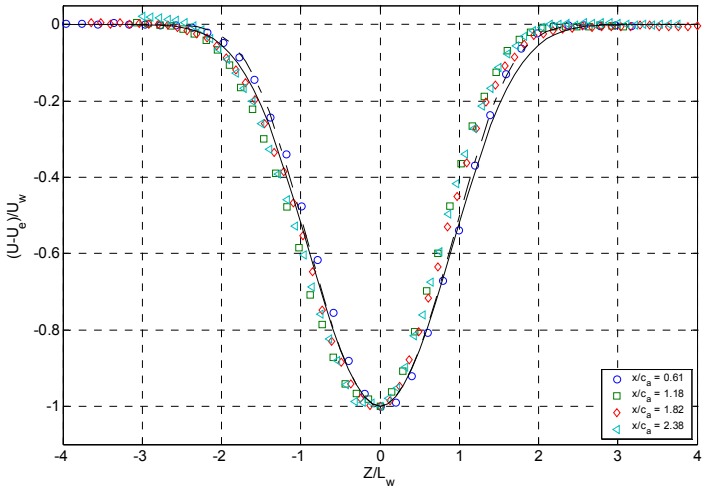

(d)

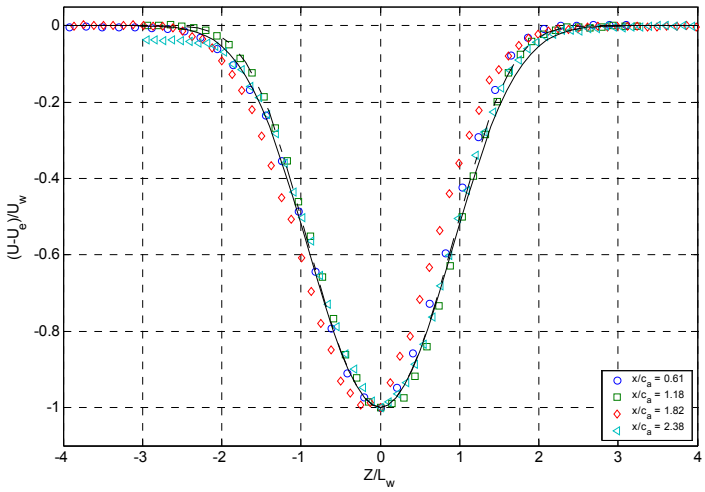

(e)

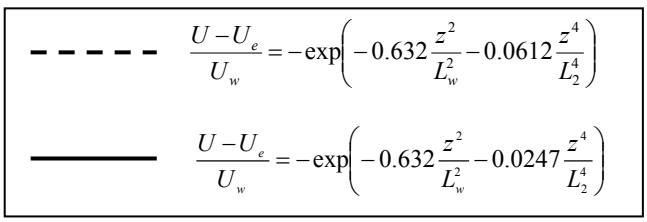

Figure 5-48: Streamwise mean velocity profile, $(U\text{-}U_e)/U_w$ at five spanwise locations across one serration for the 1.27 cm serration: **(a)** $y/c_a = 0.83$, **(b)** $y/c_a = 0.87$, **(c)** $y/c_a = 0.91$, **(d)** $y/c_a = 0.95$, **(e)** $y/c_a = 0.97$

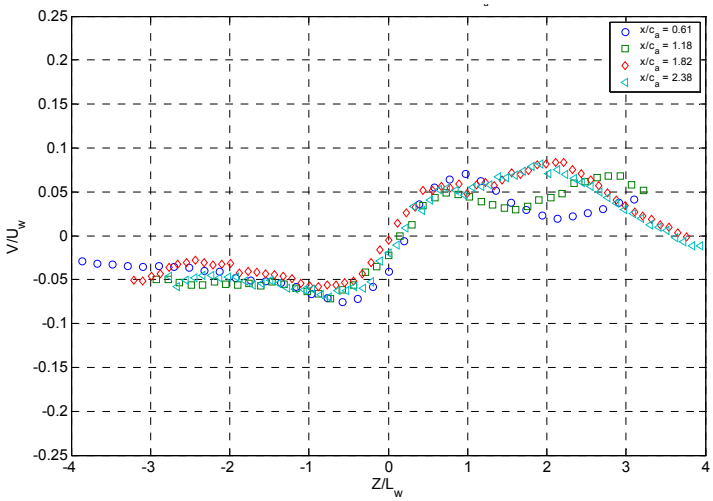

(a)

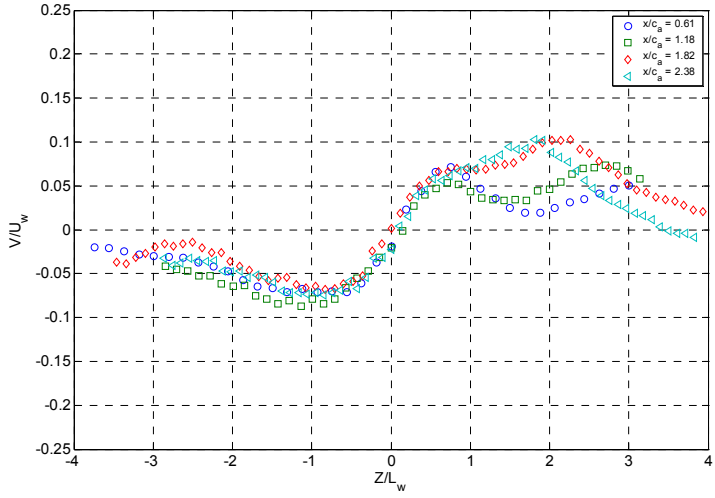

(b)

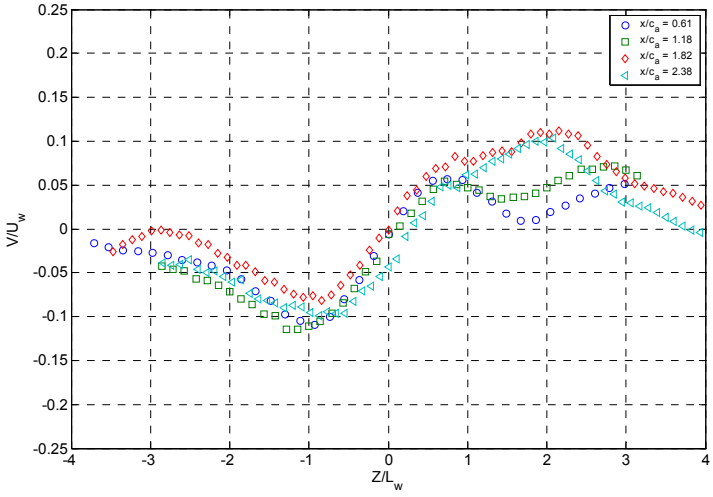

(c)

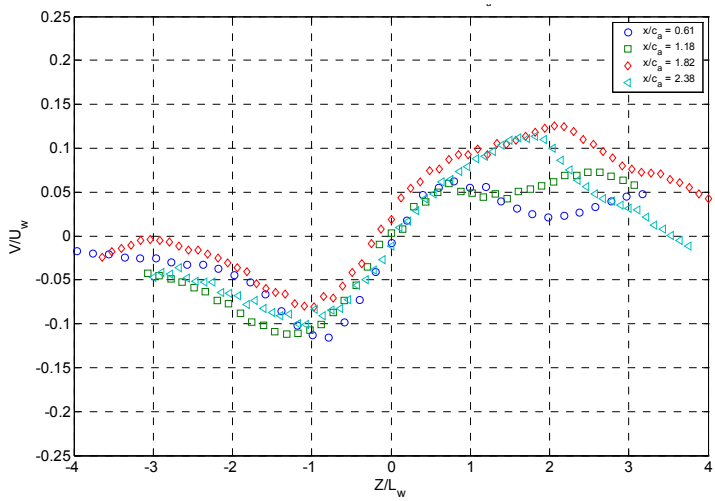

(d)

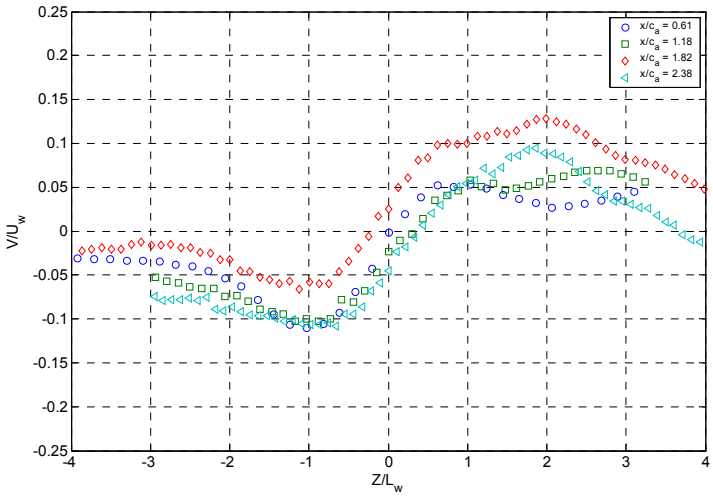

(e)

Figure 5-49: Spanwise mean velocity profiles, $V/U_{w.}$ at five spanwise locations across one serration for the 1.27 cm serration: **(a)** $y/c_a = 0.83$, **(b)** $y/c_a = 0.87$, **(c)** $y/c_a = 0.91$, **(d)** $y/c_a = 0.95$, **(e)** $y/c_a = 0.97$

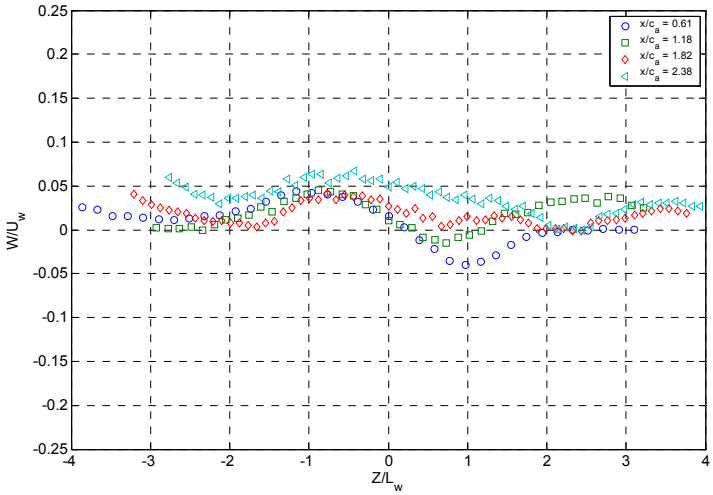

(a)

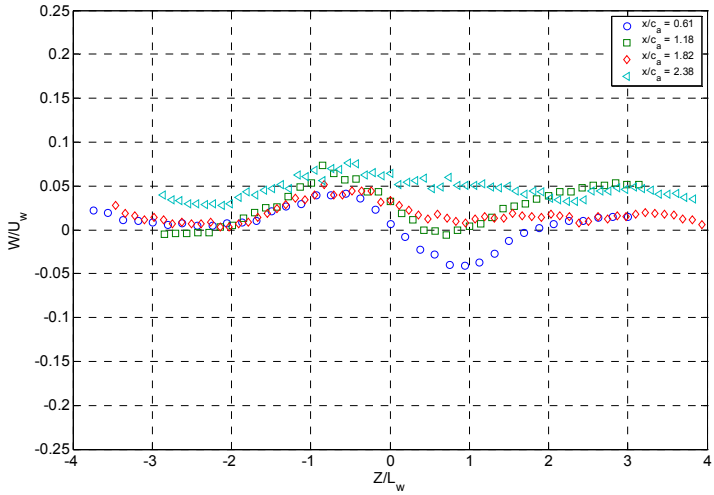

(b)

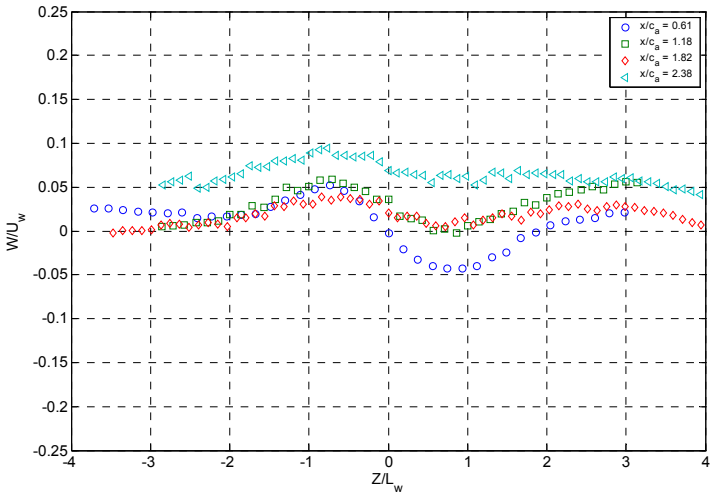

(c)

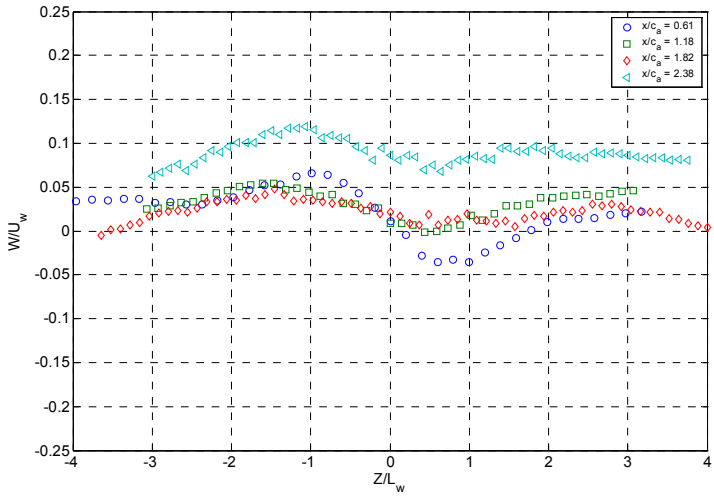

(d)

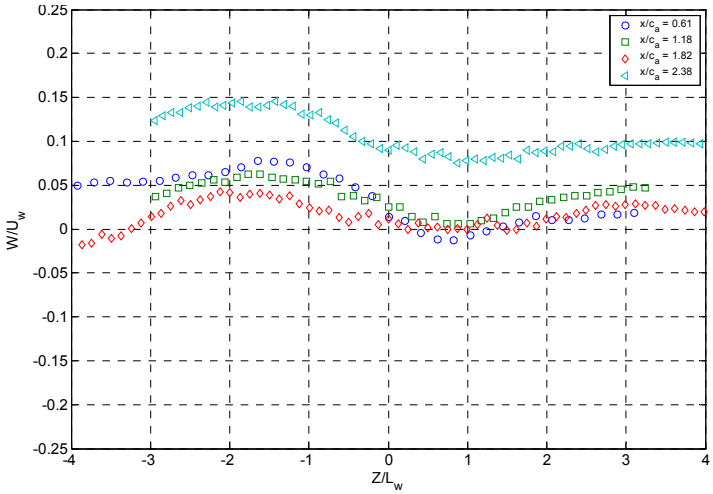

(e)

Figure 5-50: Cross-wake mean velocity profiles, $W/U_{w.}$ at five spanwise locations across one serration for the 1.27 cm serration: **(a)** $y/c_a = 0.83$, **(b)** $y/c_a = 0.87$, **(c)** $y/c_a = 0.91$, **(d)** $y/c_a = 0.95$, **(e)** $y/c_a = 0.97$

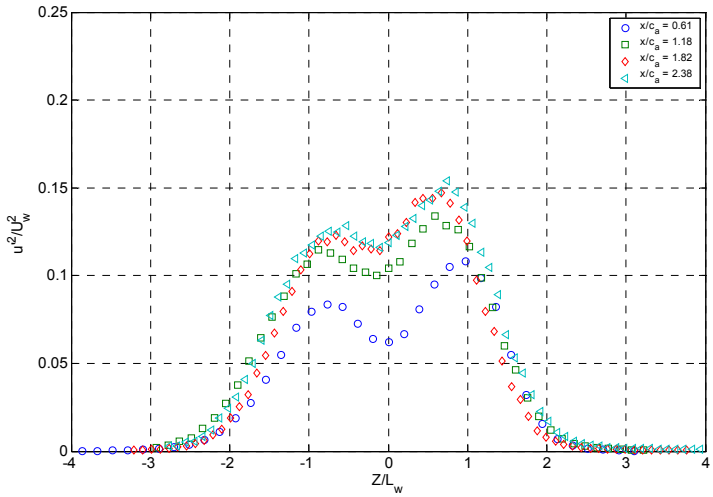

(a)

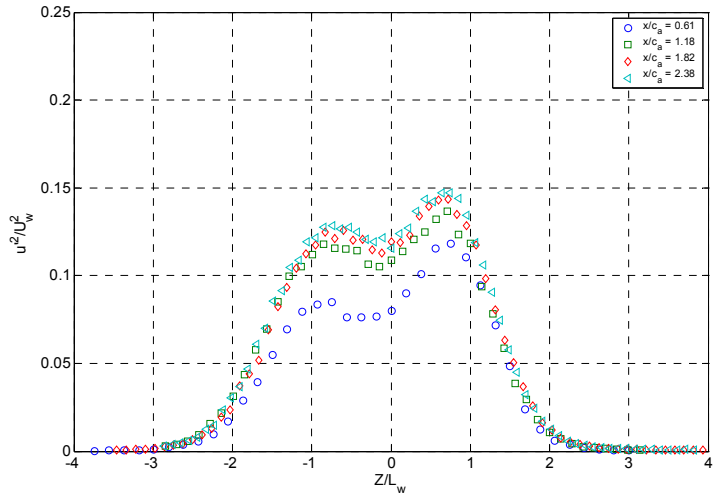

(b)

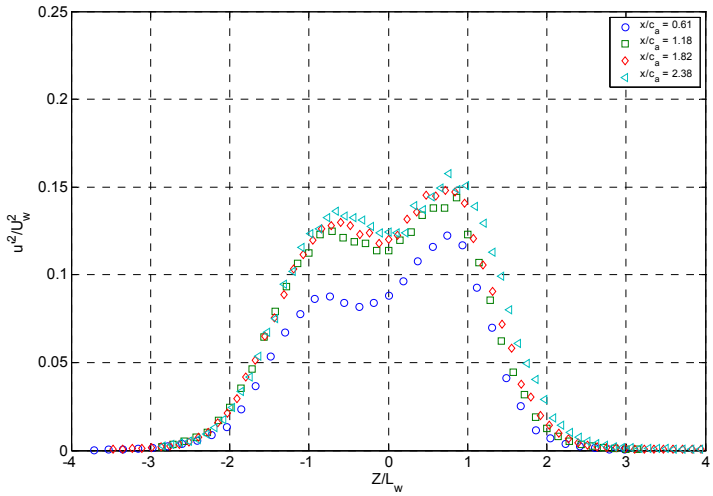

(c)

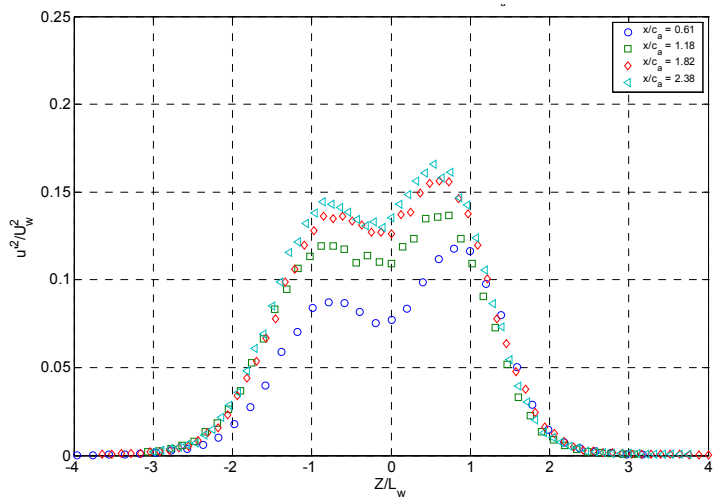

(d)

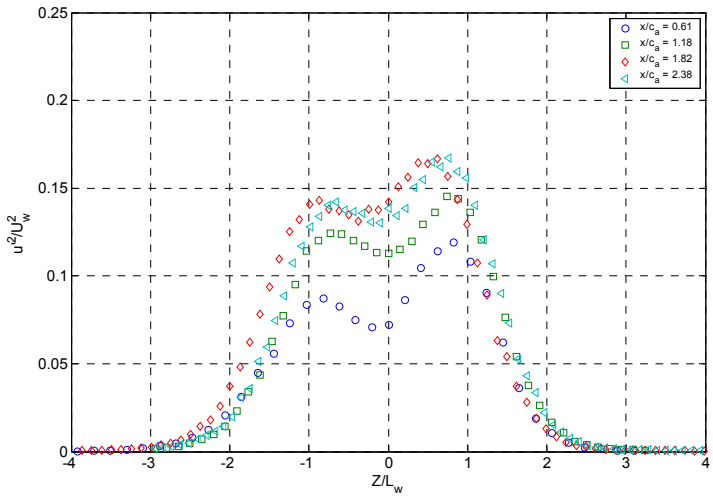

(e)

Figure 5-51: Streamwise Reynolds stress profiles, $\overline{u'^2/U_w^2}$ at five spanwise locations across one serration for the 1.27 cm serration: **(a)** $y/c_a = 0.83$, **(b)** $y/c_a = 0.87$, **(c)** $y/c_a = 0.91$, **(d)** $y/c_a = 0.95$, **(e)** $y/c_a = 0.97$

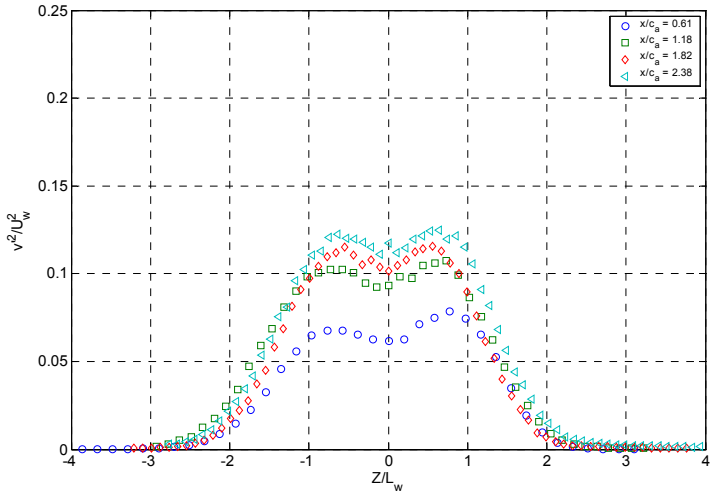

(a)

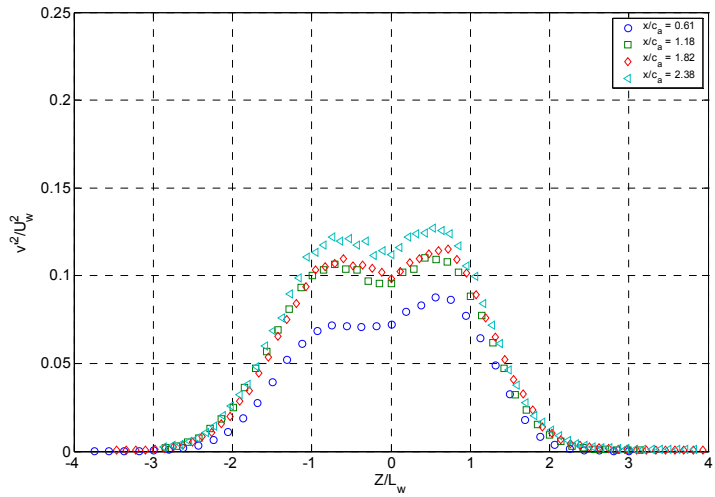

(b)

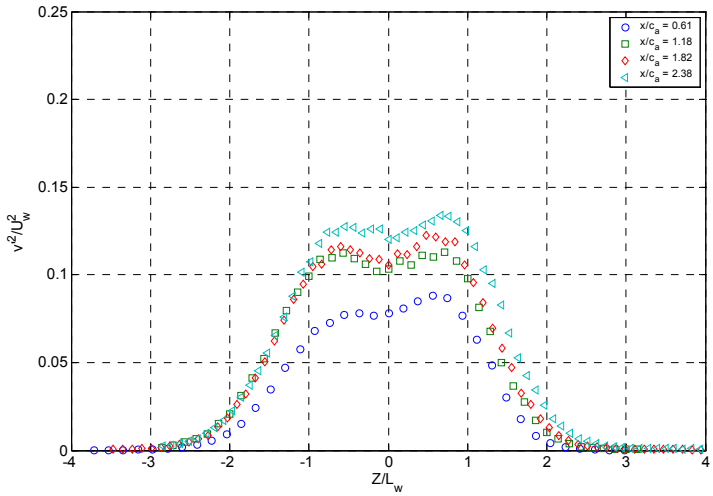

(c)

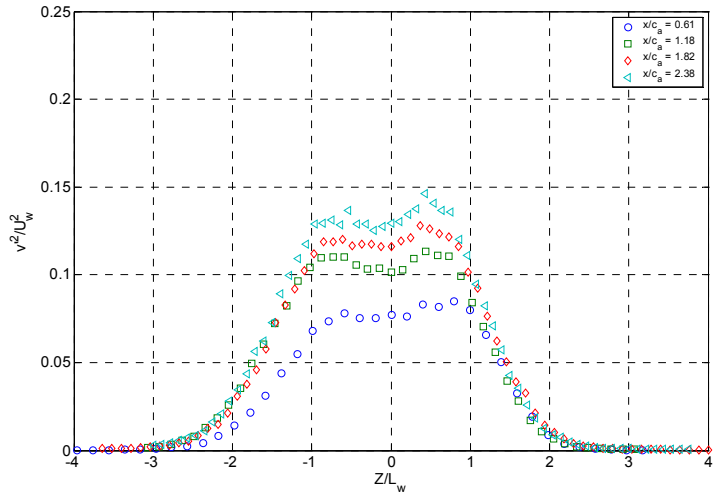

(d)

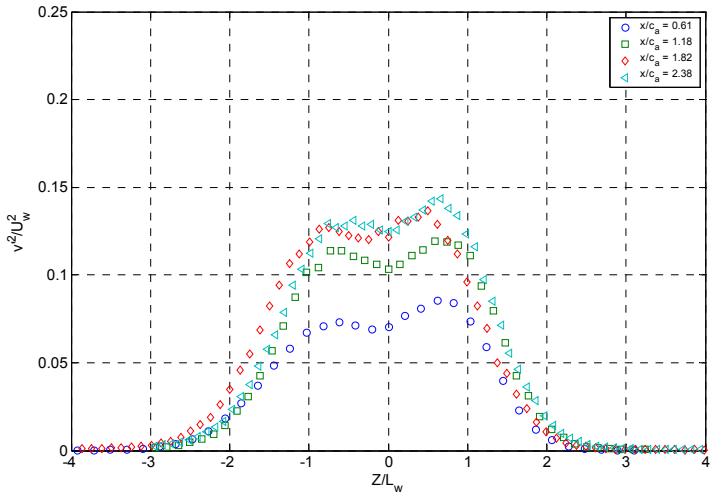

(e)

Figure 5-52: Spanwise Reynolds stress profiles, $\overline{v'^2/U_w^2}$ at five spanwise locations across one serration for the 1.27 cm serration: **(a)** $y/c_a = 0.83$, **(b)** $y/c_a = 0.87$, **(c)** $y/c_a = 0.91$, **(d)** $y/c_a = 0.95$, **(e)** $y/c_a = 0.97$

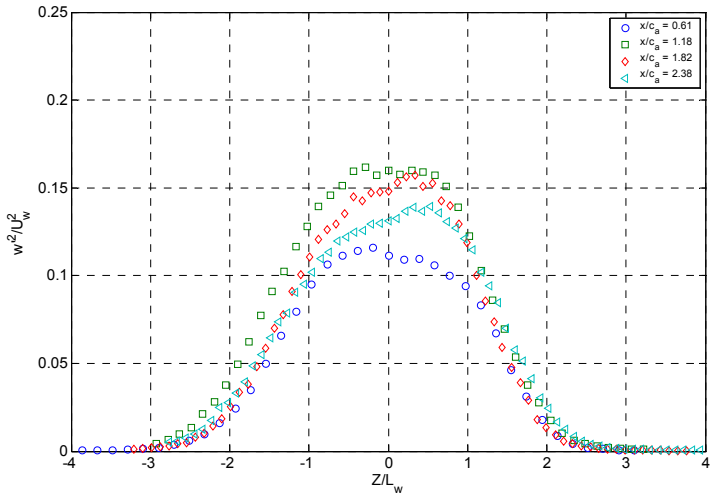

(a)

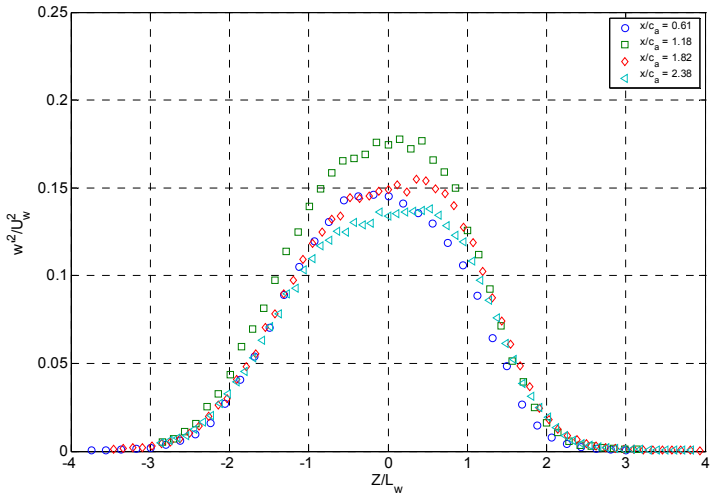

(b)

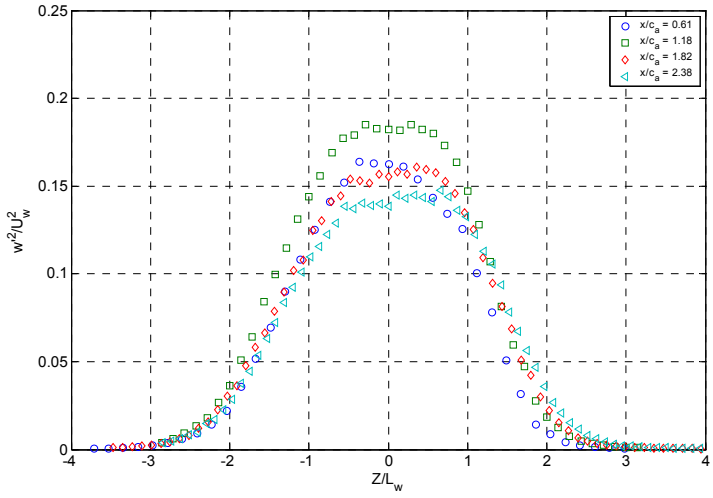

(c)

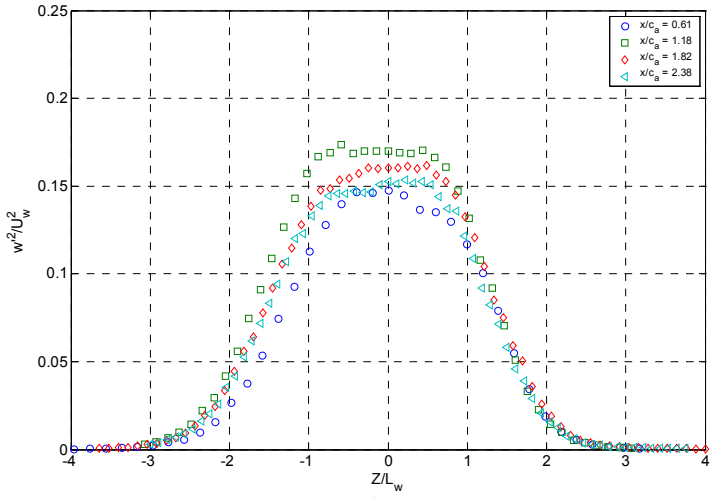

(d)

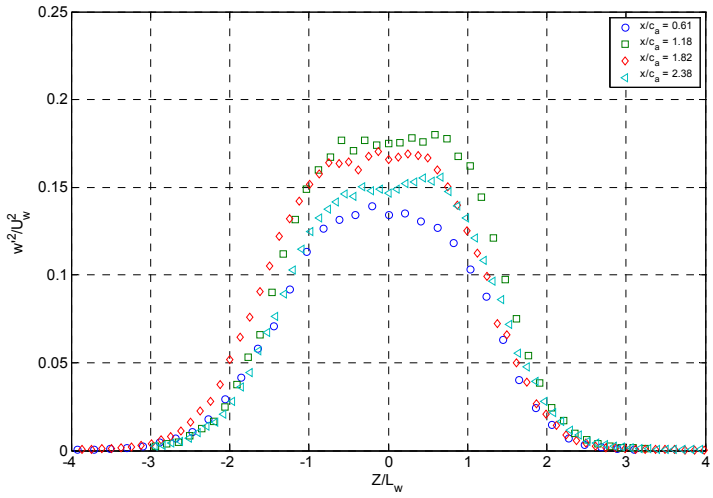

(e)

Figure 5-53: Cross-wake Reynolds stress profiles, $\overline{w'^2/U_w^2}$ at five spanwise locations across one serration for the 1.27 cm serration: **(a)** $y/c_a = 0.83$, **(b)** $y/c_a = 0.87$, **(c)** $y/c_a = 0.91$, **(d)** $y/c_a = 0.95$, **(e)** $y/c_a = 0.97$

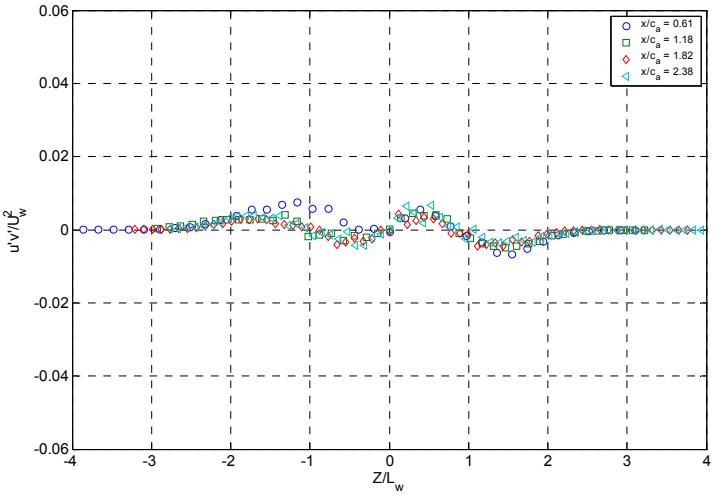

(a)

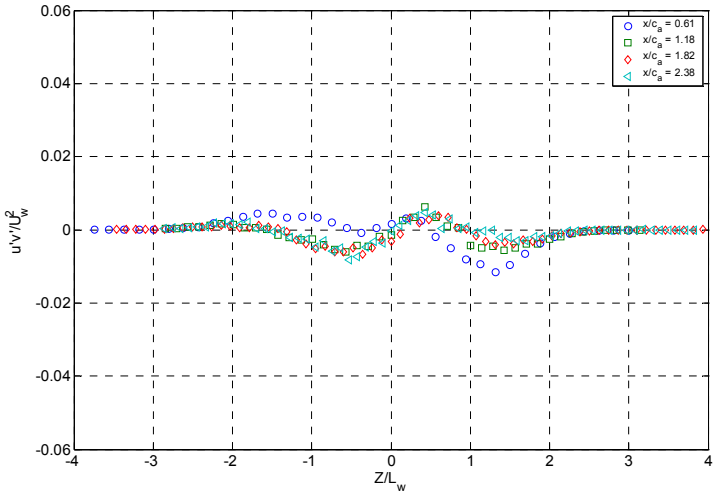

(b)

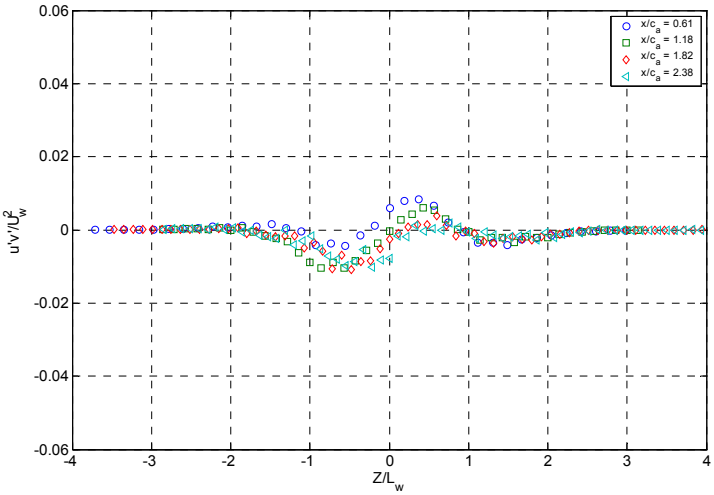

(c)

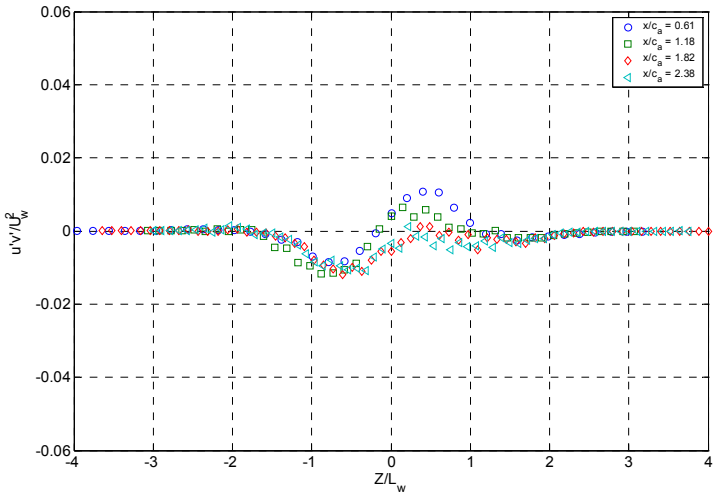

(d)

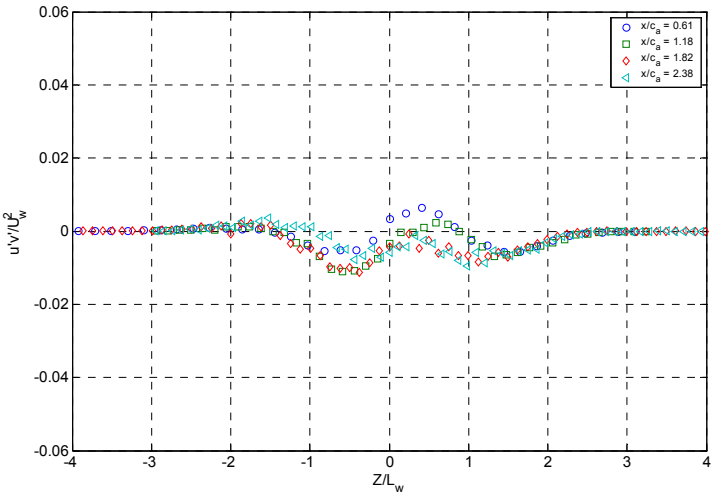

(e)

Figure 5-54: Reynolds shear stress profiles, $\overline{u'v'/U_w^2}$ at five spanwise locations across one serration for the 1.27 cm serration: **(a)** $y/c_a = 0.83$, **(b)** $y/c_a = 0.87$, **(c)** $y/c_a = 0.91$, **(d)** $y/c_a = 0.95$, **(e)** $y/c_a = 0.97$

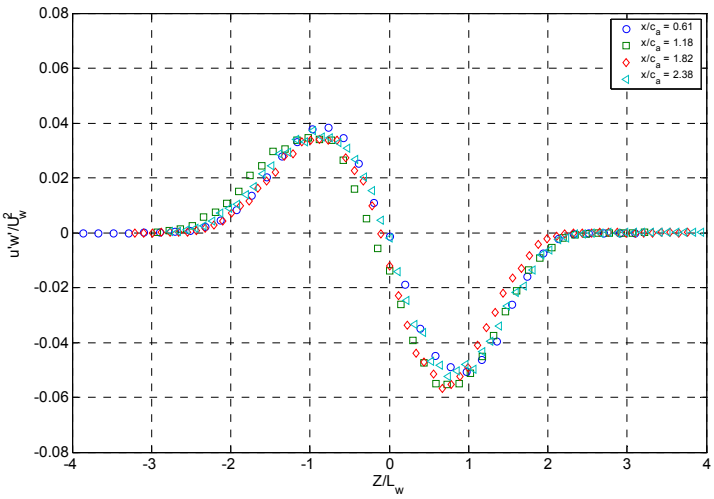

(a)

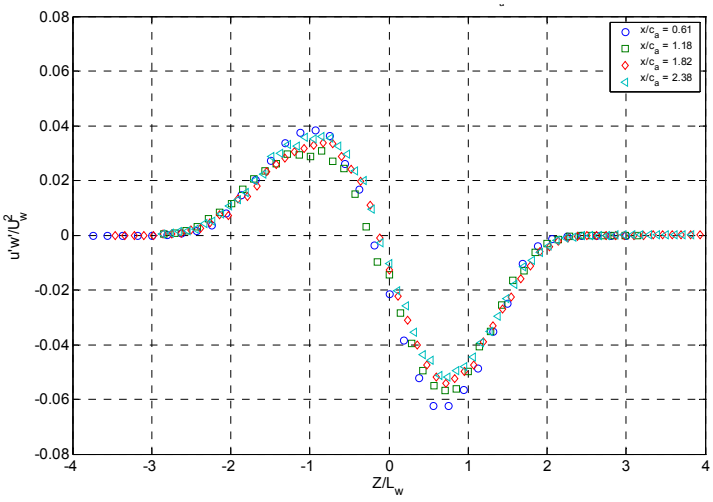

(b)

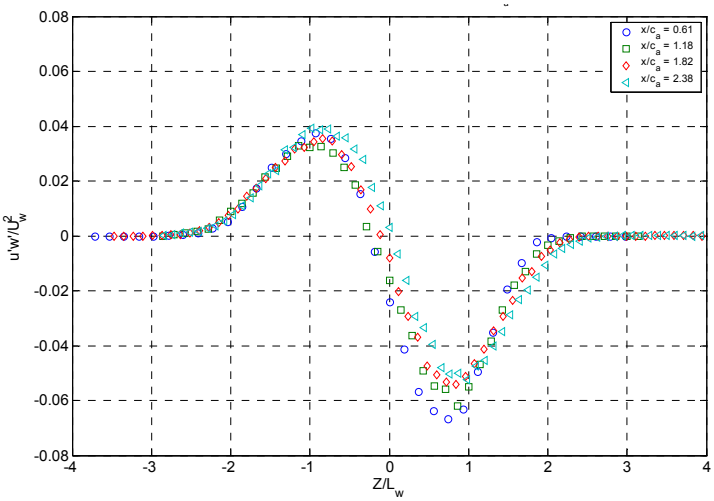

(c)

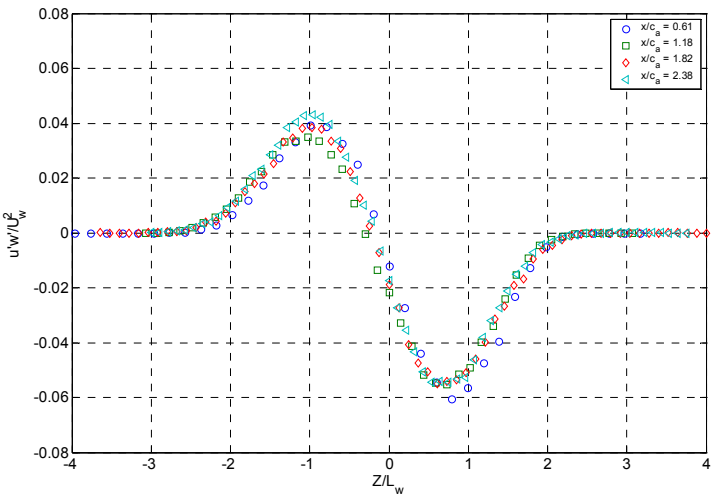

(d)

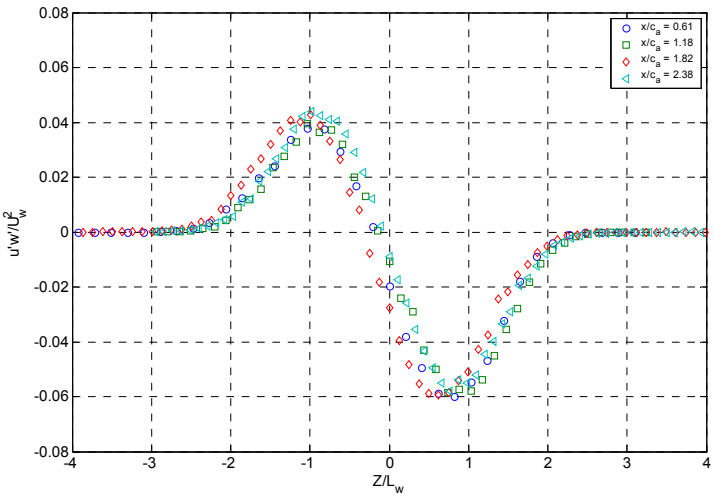

(e)

Figure 5-55: Reynolds shear stress profiles, $\overline{u'w'/U_w^2}$ at five spanwise locations across one serration for the 1.27 cm serration: **(a)** $y/c_a = 0.83$, **(b)** $y/c_a = 0.87$, **(c)** $y/c_a = 0.91$, **(d)** $y/c_a = 0.95$, **(e)** $y/c_a = 0.97$

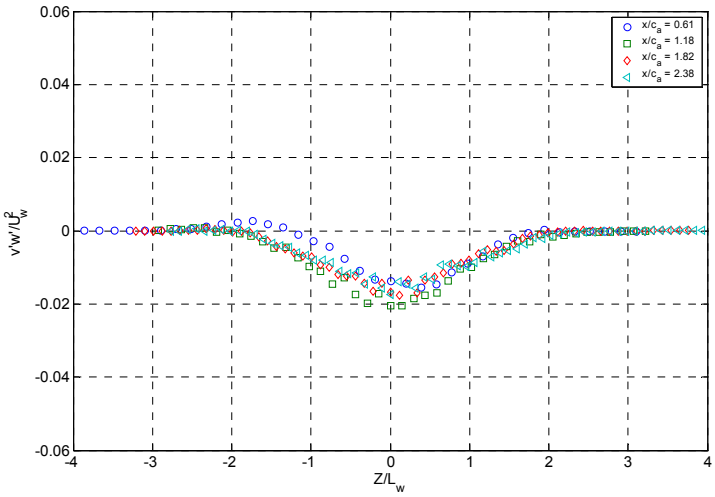

(a)

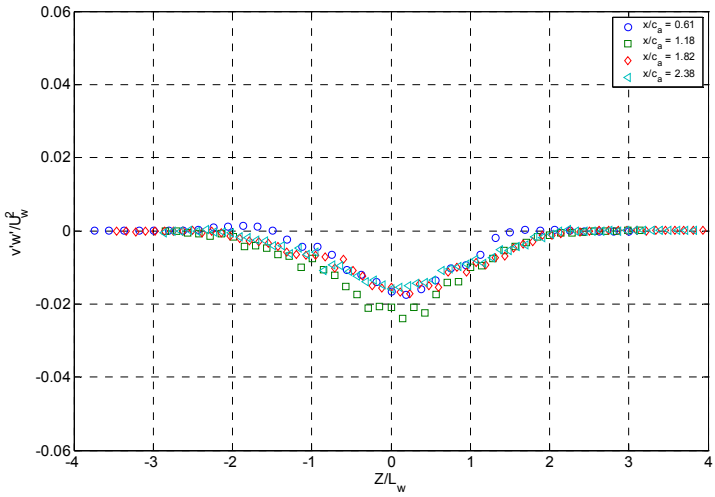

(b)

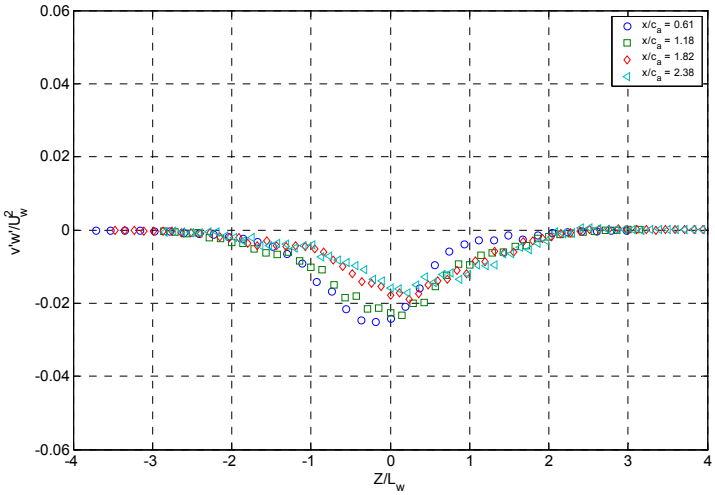

(c)

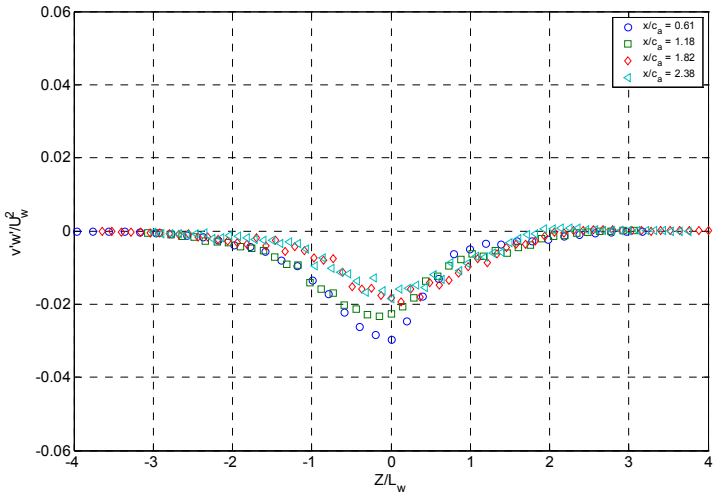

(d)

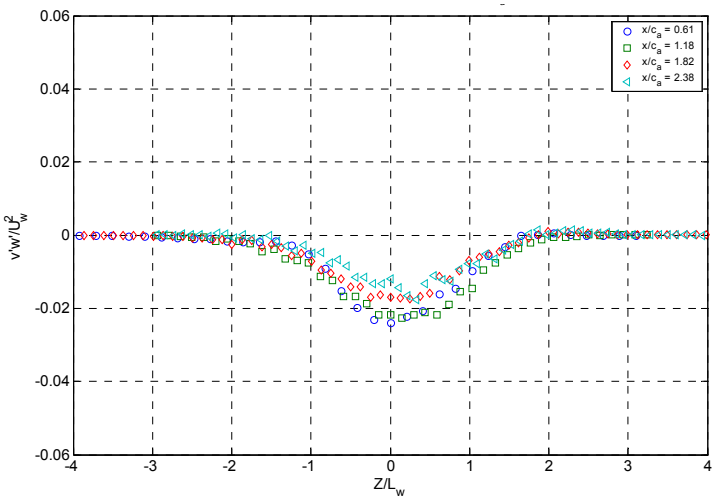

(e)

Figure 5-56: Reynolds shear stress profiles, $\overline{v'w'/U_w^2}$ at five spanwise locations across one serration for the 1.27 cm serration: **(a)** $y/c_a = 0.83$, **(b)** $y/c_a = 0.87$, **(c)** $y/c_a = 0.91$, **(d)** $y/c_a = 0.95$, **(e)** $y/c_a = 0.97$

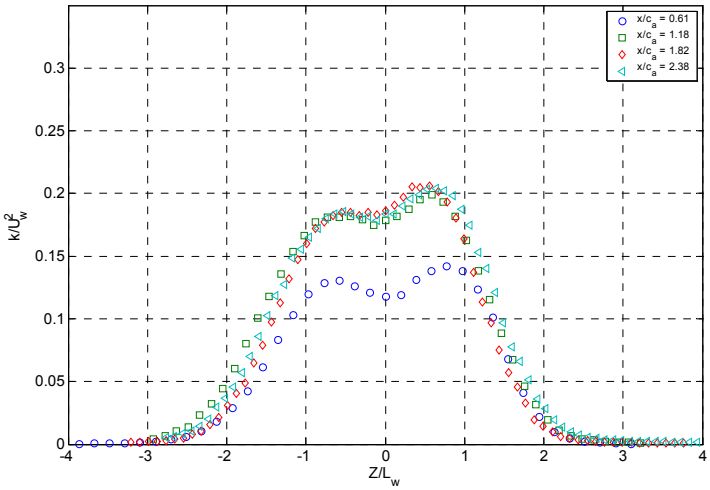

(a)

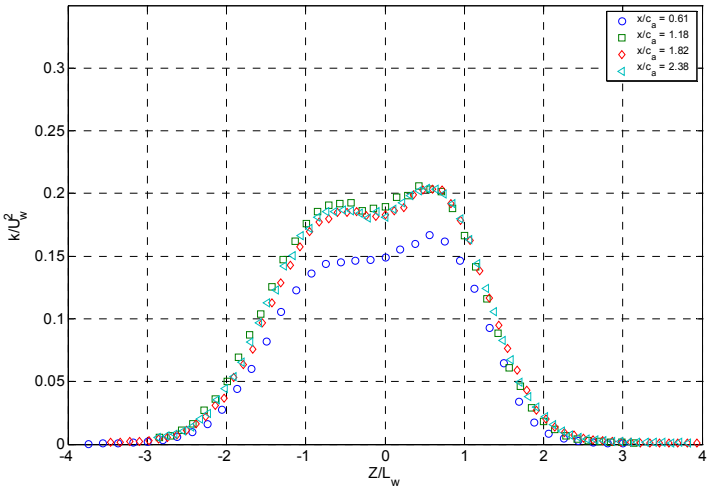

(b)

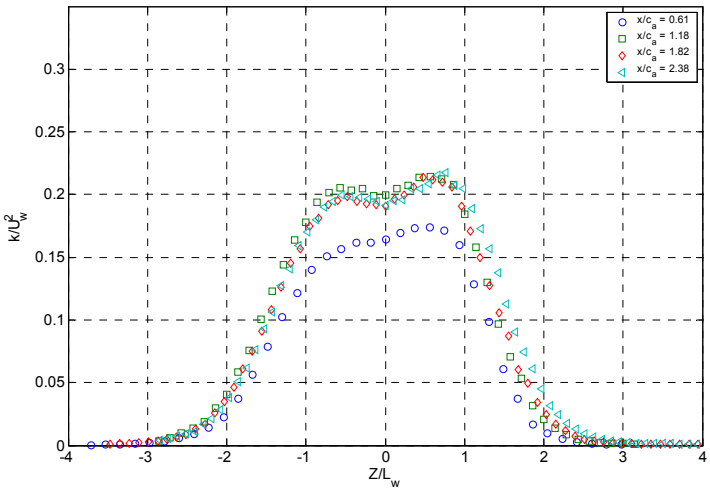

(c)

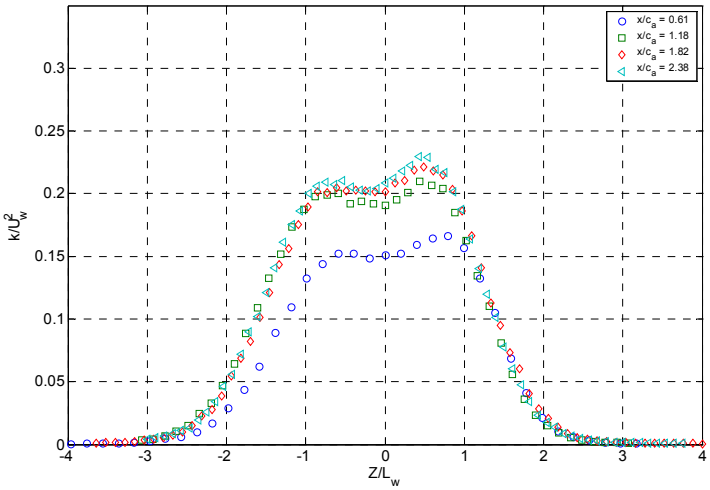

(d)

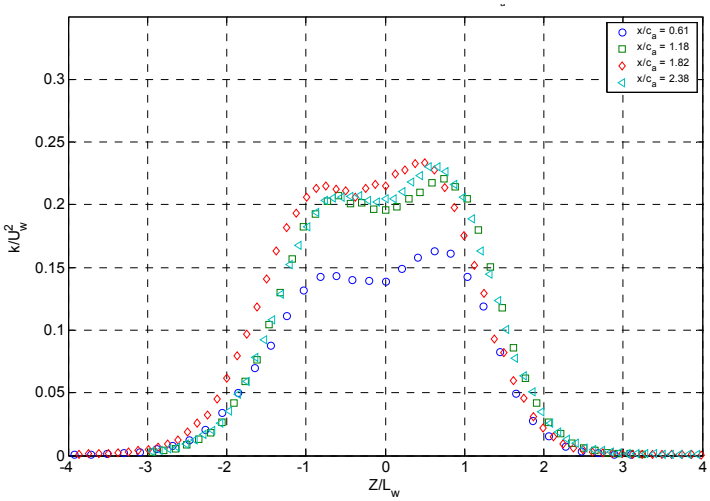

(e)

Figure 5-57: Turbulence kinetic energy profiles, k/U_w^2 at five locations spanwise locations across one serration for the 1.27 cm serration: **(a)** $y/c_a = 0.83$, **(b)** $y/c_a = 0.87$, **(c)** $y/c_a = 0.91$, **(d)** $y/c_a = 0.95$, **(e)** $y/c_a = 0.97$

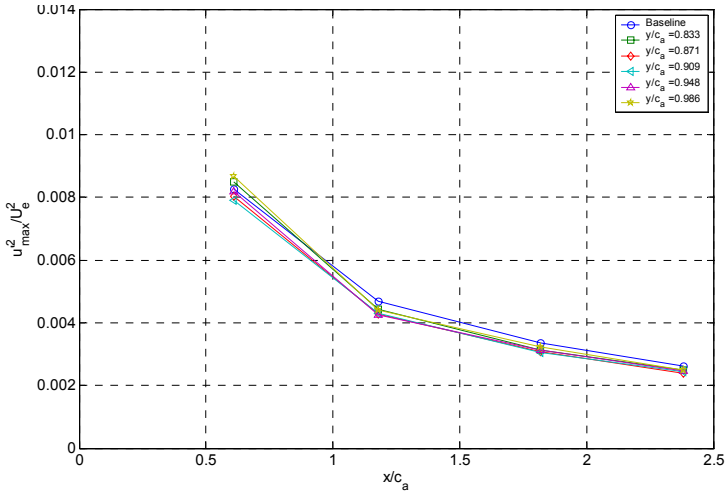

(a)

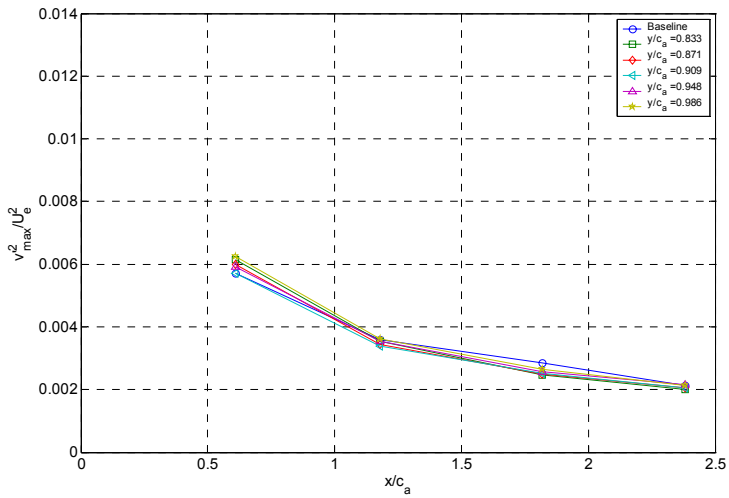

(b)

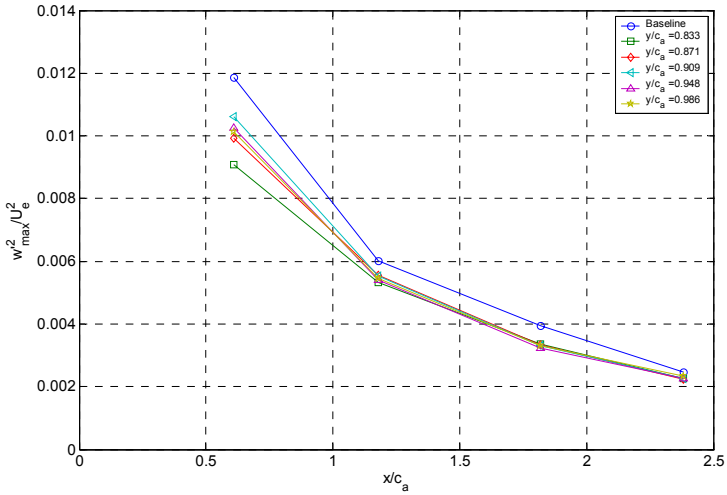

(c)

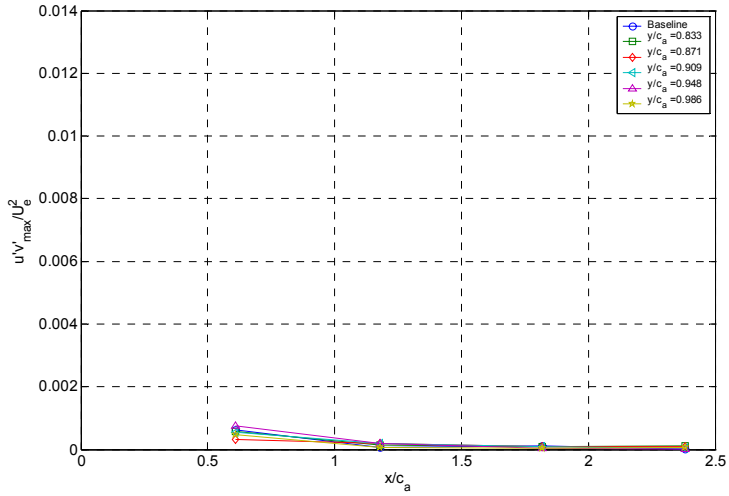

(d)

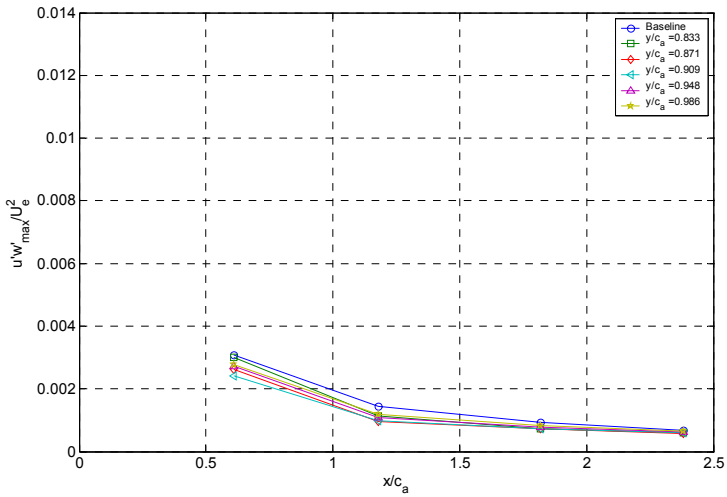

(e)

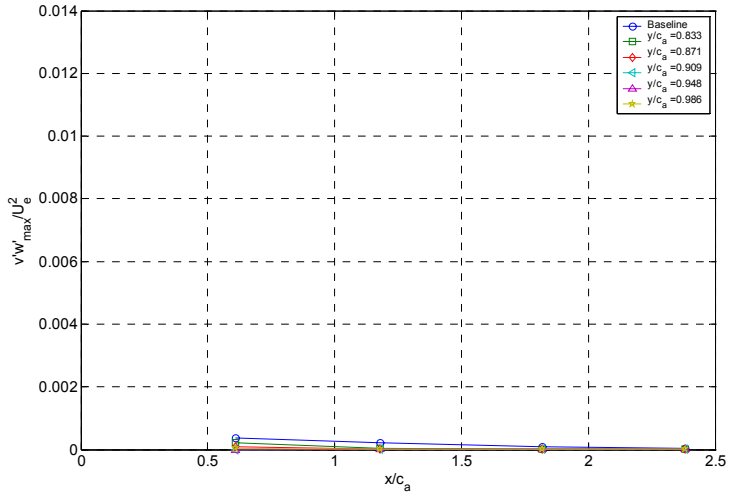

(f)

Figure 5-58: Maximum normalized Reynolds stress levels at five spanwise locations across one serration for the 1.27 cm serration compared to the baseline: **(a)** $\overline{|u'^2/U_\infty^2|}_{max}$, **(b)** $\overline{|v'^2/U_\infty^2|}_{max}$, **(c)** $\overline{|w'^2/U_\infty^2|}_{max}$, **(d)** $\overline{|u'v'/U_\infty^2|}_{max}$, **(e)** $\overline{|u'w'/U_\infty^2|}_{max}$, **(f)** $\overline{|v'w'/U_\infty^2|}_{max}$

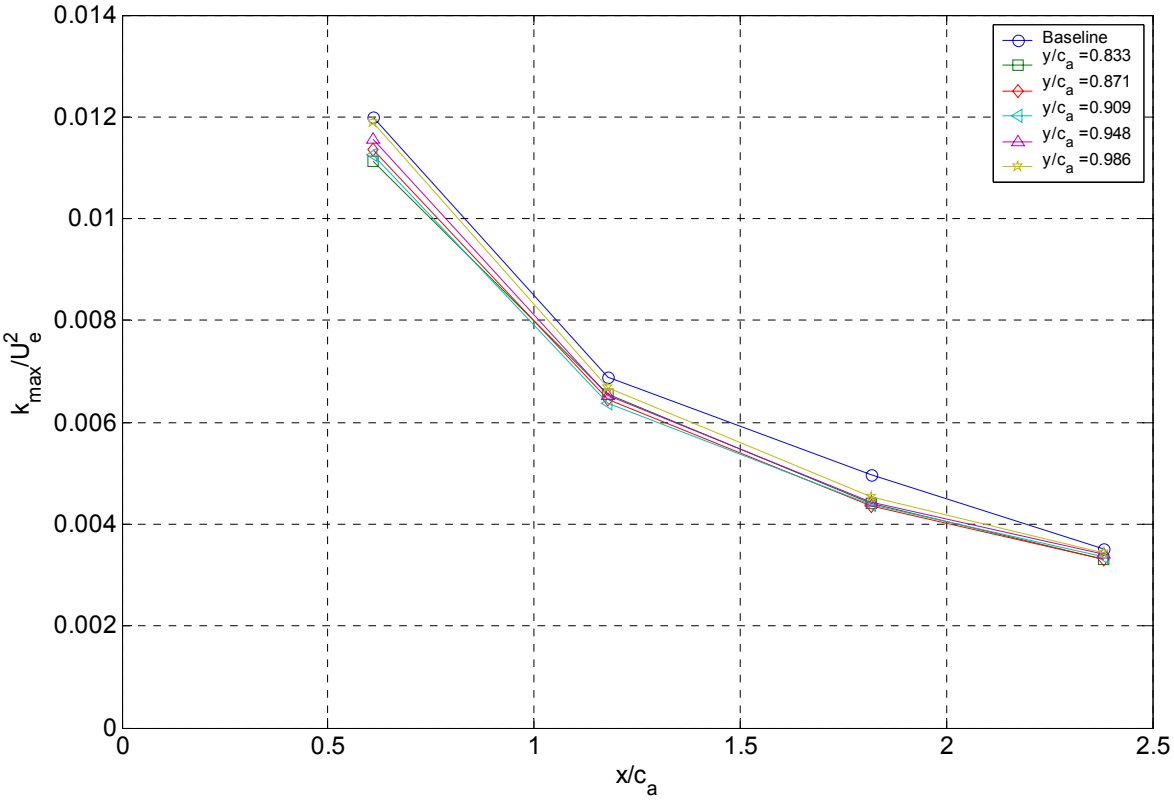

Figure 5-59: Maximum normalized turbulence kinetic energy, $|k/U_w^2|_{max}$, at five spanwise locations across one serration for the 1.27 cm serration compared to the baseline.

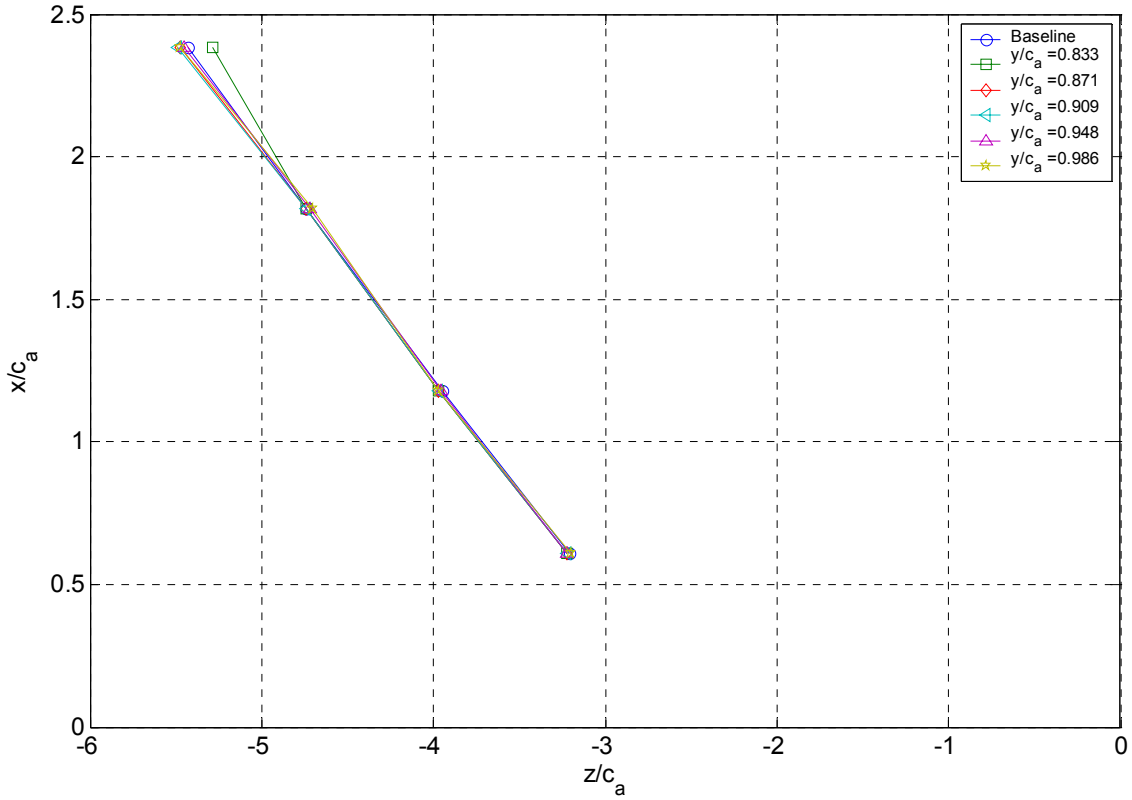

Figure 5-60: Propagation of the minimum velocity point in the wake for the 1.27 cm serration compared to the baseline case

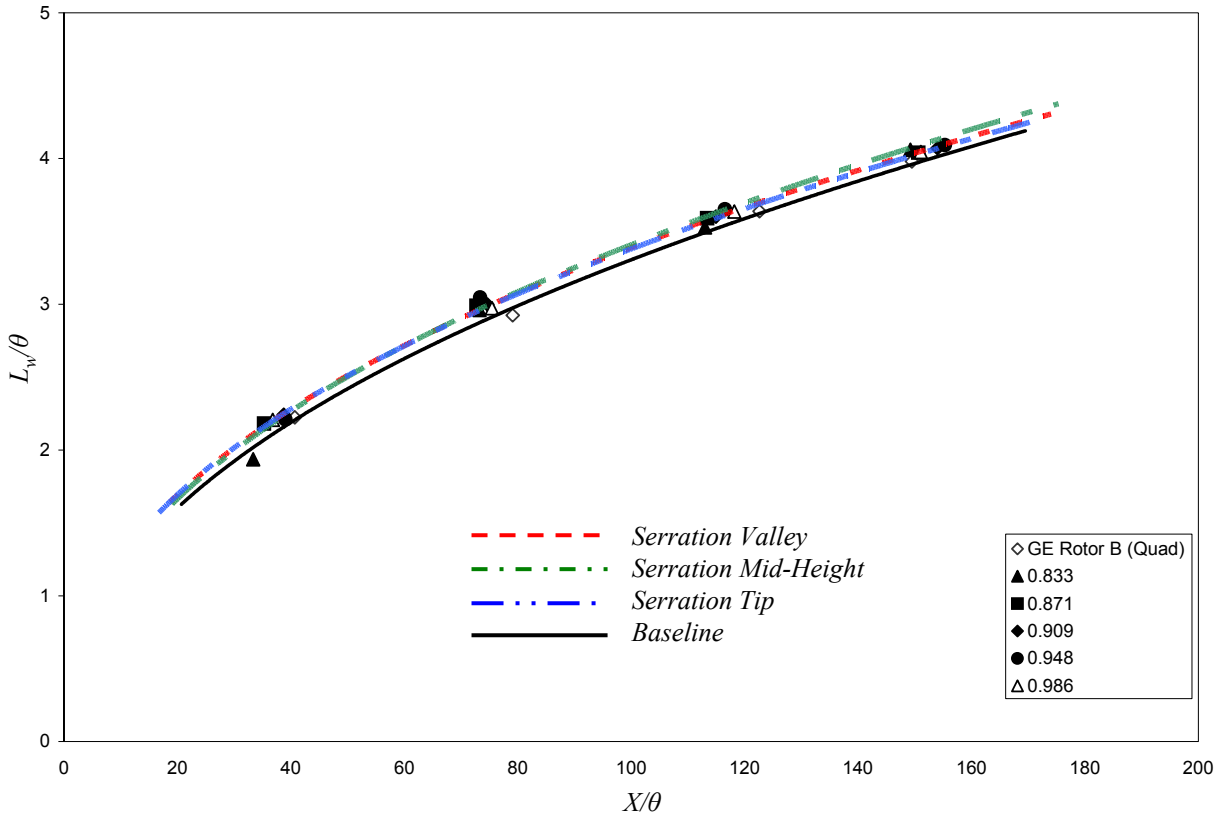

Figure 5-61: Normalized wake half-width of the wake, L_w/θ, as a function of normalized downstream distance, X/θ, for the 1.27 cm droop serration.

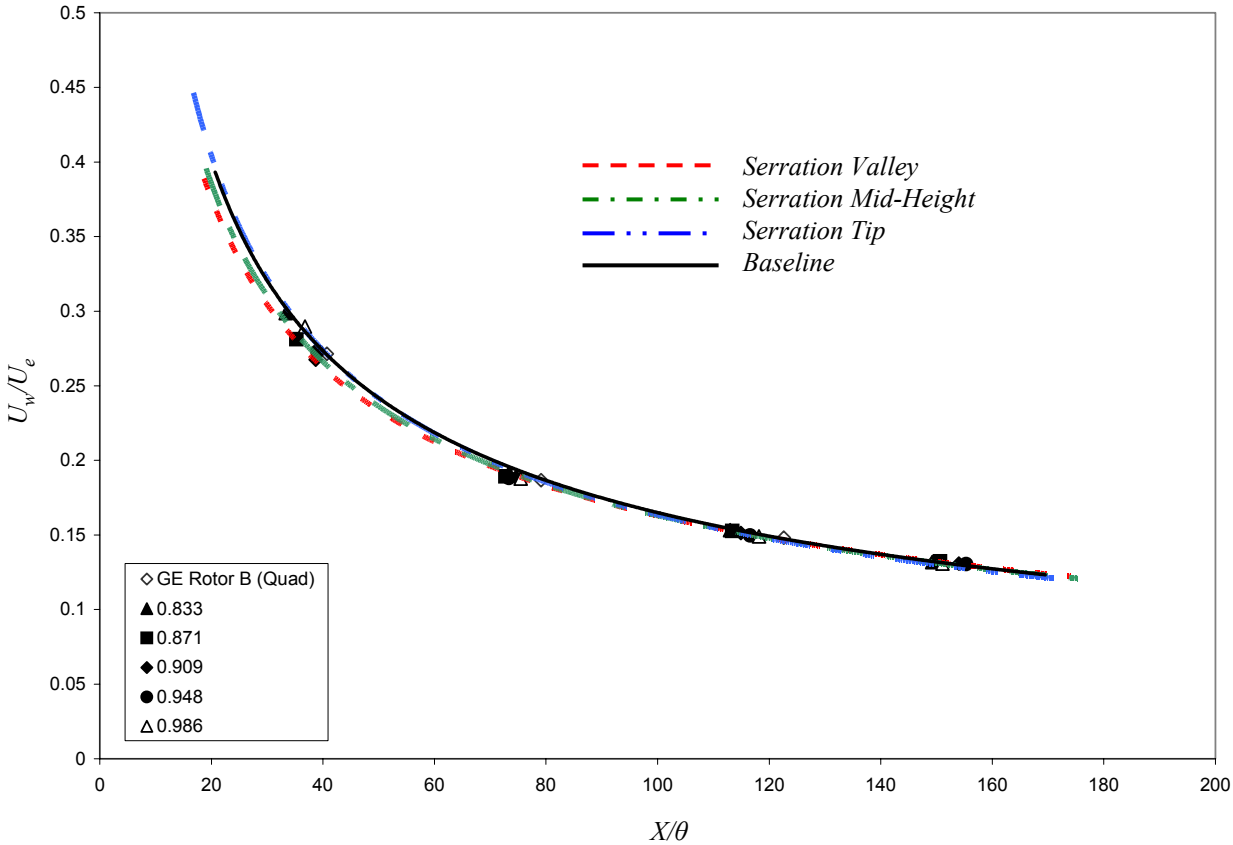

Figure 5-62: Normalized maximum velocity deficit in the wake, U_w/U_e, function of the normalized downstream distance, X/θ, for the 1.27 cm droop serration.

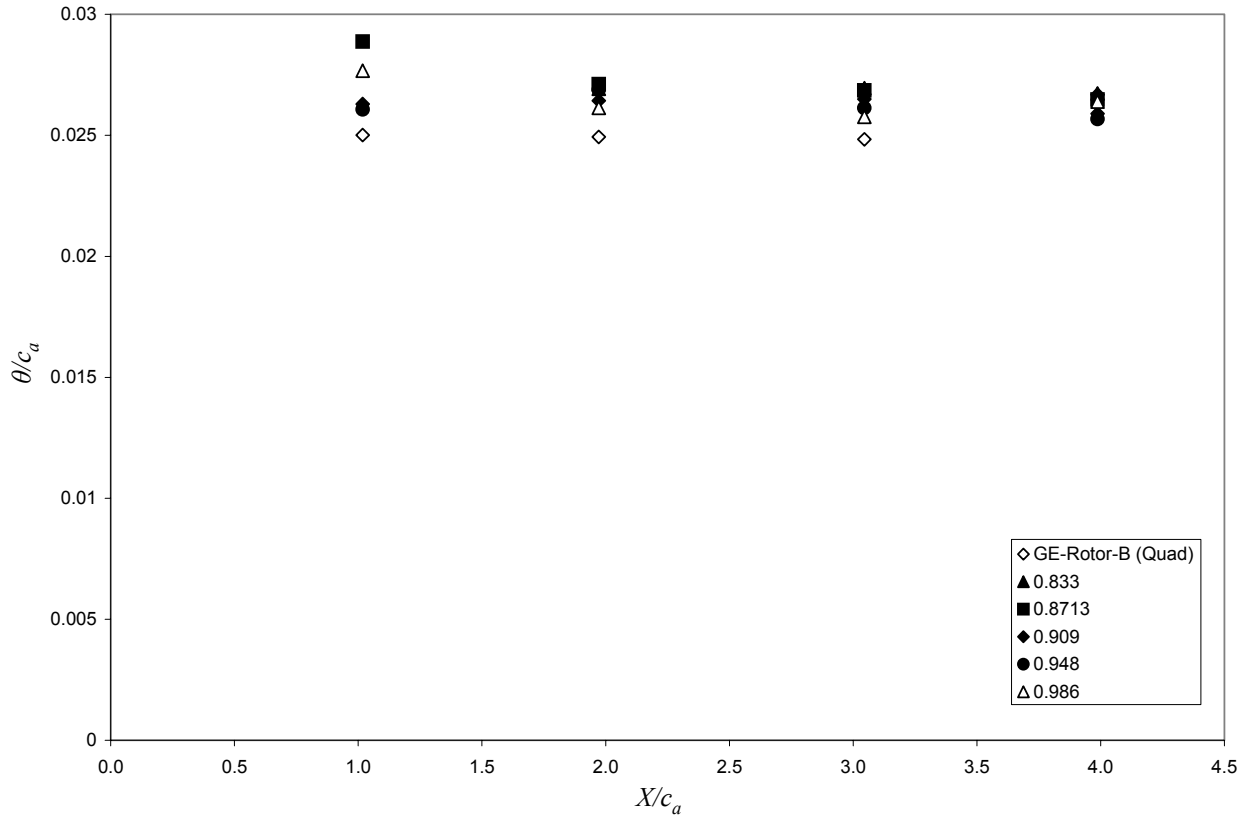

Figure 5-63: Normalized momentum thickness, θ/c_a, as a function of normalized distance downstream, X/c_a, for the 1.27 cm droop serration.

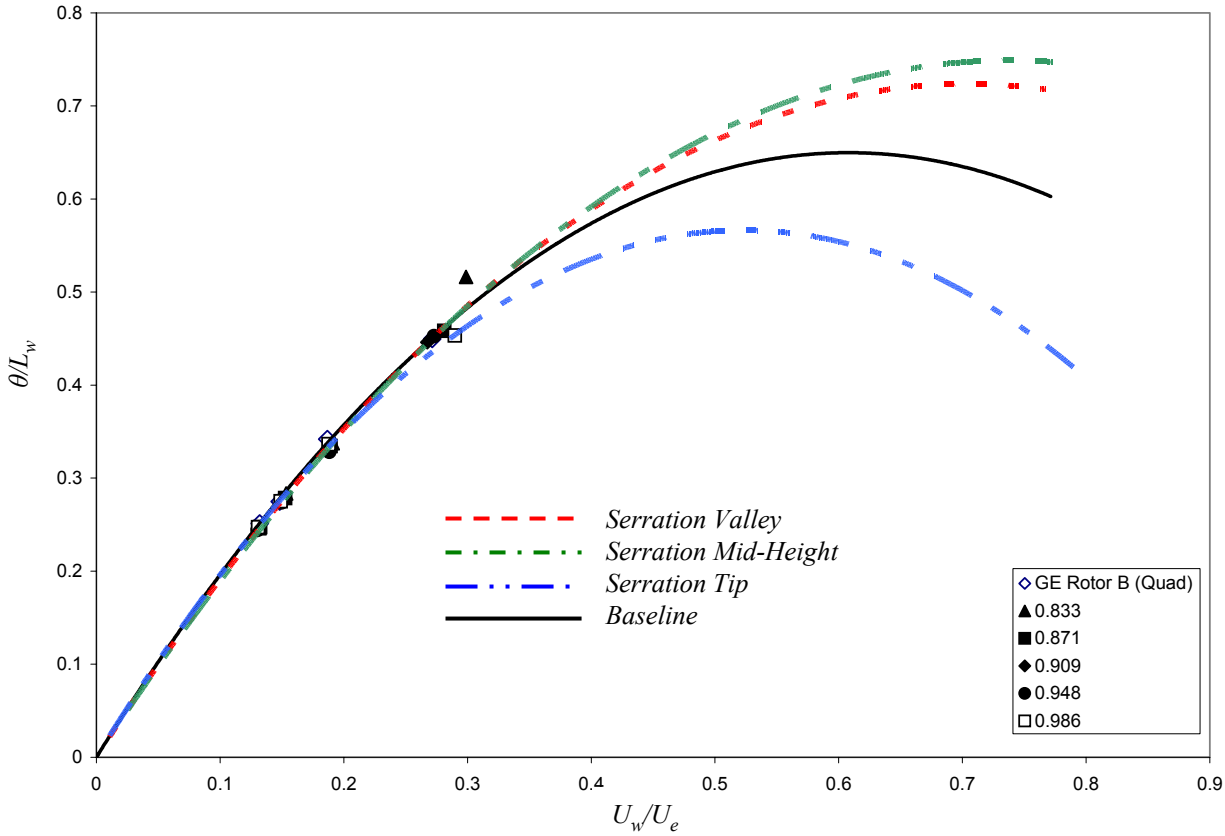

Figure 5-64: Normalized momentum thickness, θ/L_w as a function of normalized velocity deficit of wake, U_w/U_e, for the 1.27 cm droop serration.

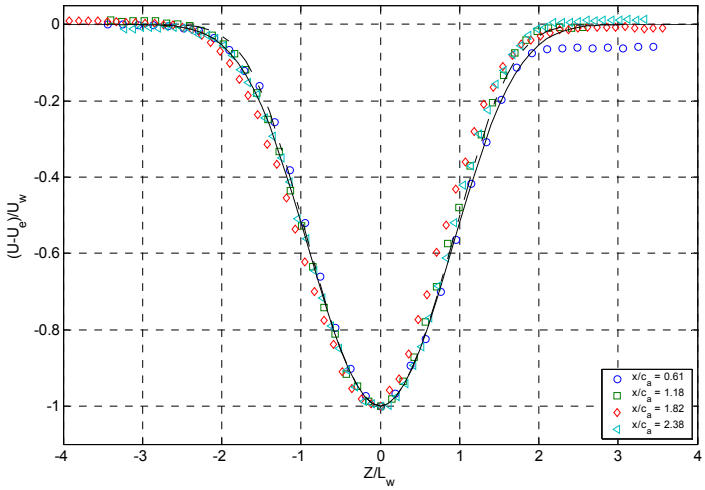

(a)

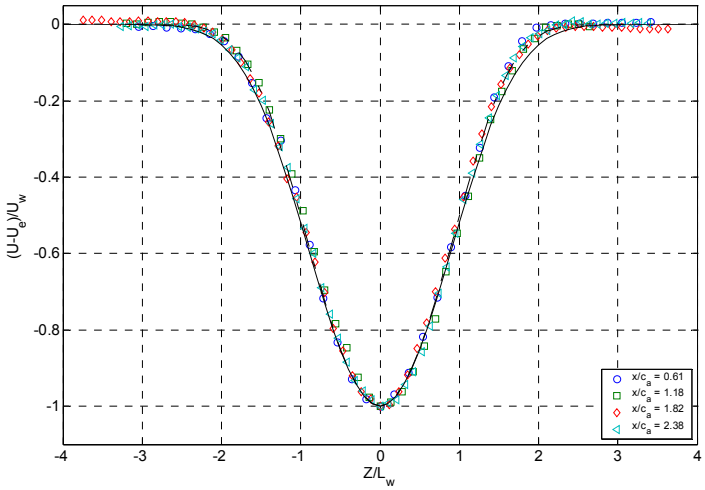

(b)

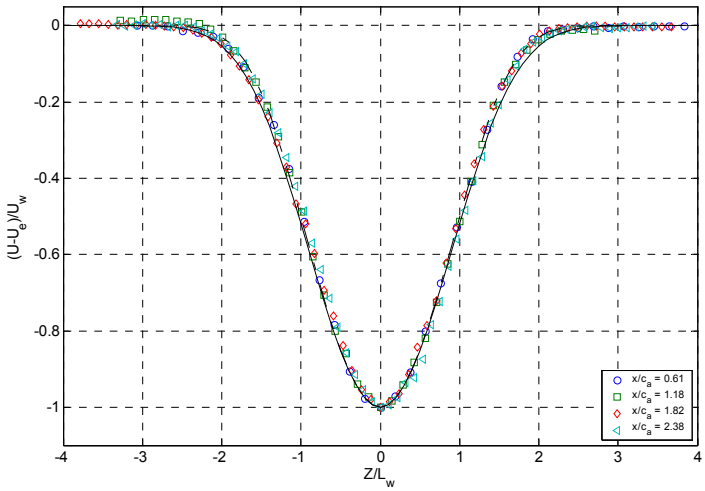

(c)

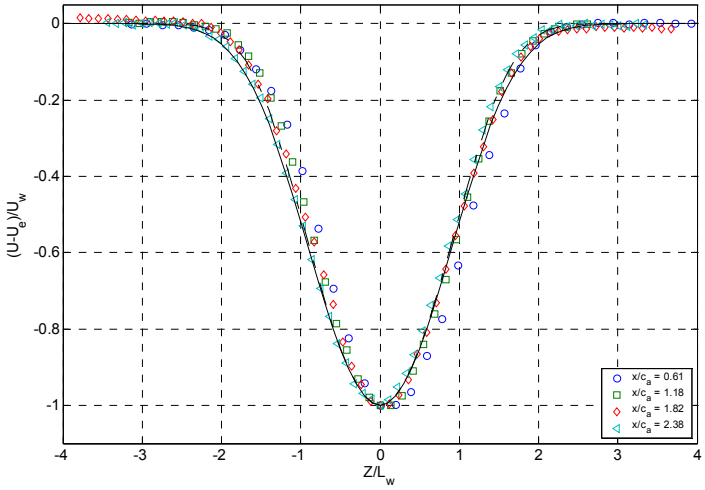

(d)

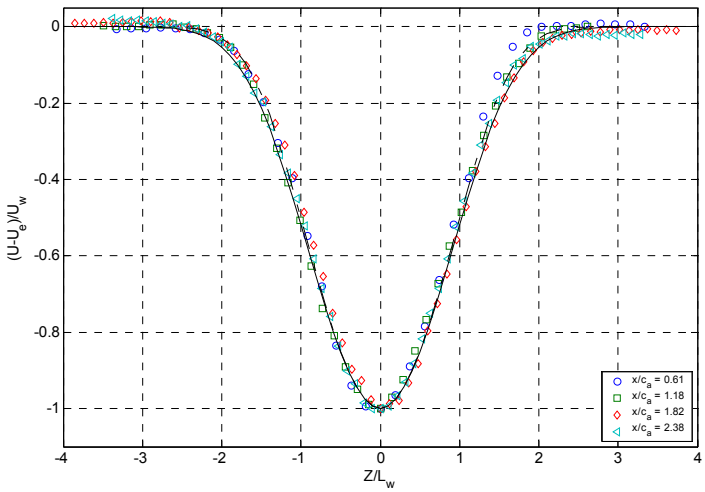

(e)

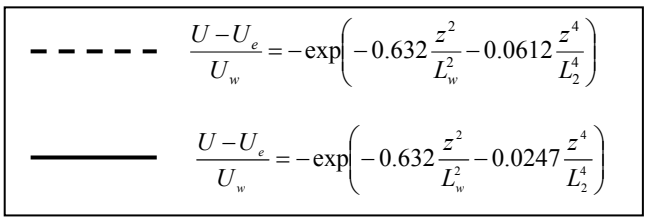

Figure 5-65: Streamwise mean velocity profile, $(U\text{-}U_e)/U_w$ at five spanwise locations across one serration for the 1.27 cm droop serration: **(a)** $y/c_a = 0.83$, **(b)** $y/c_a = 0.87$, **(c)** $y/c_a = 0.91$, **(d)** $y/c_a = 0.95$, **(e)** $y/c_a = 0.97$

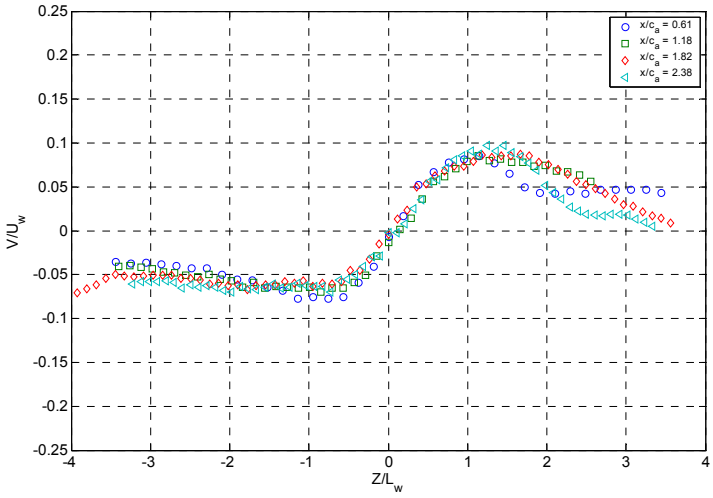

(a)

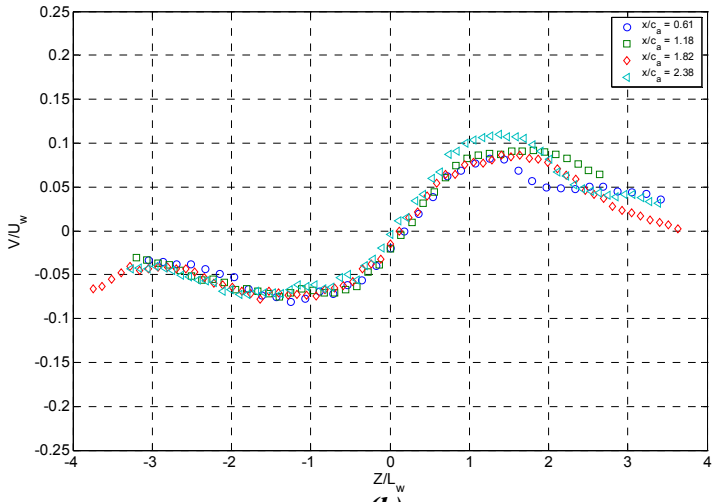

(b)

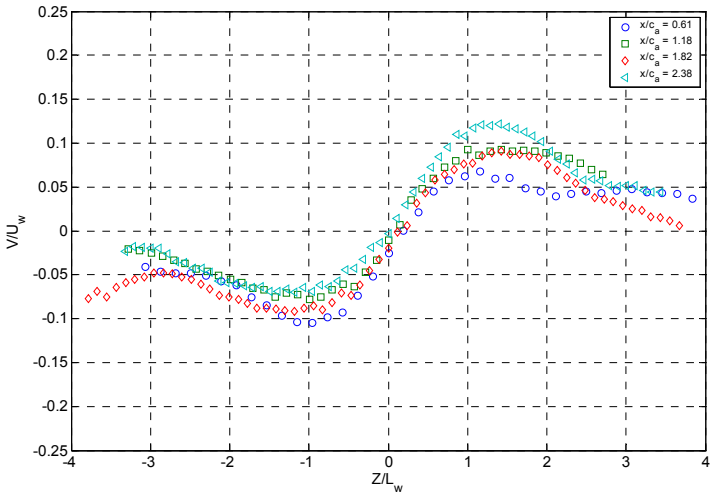

(c)

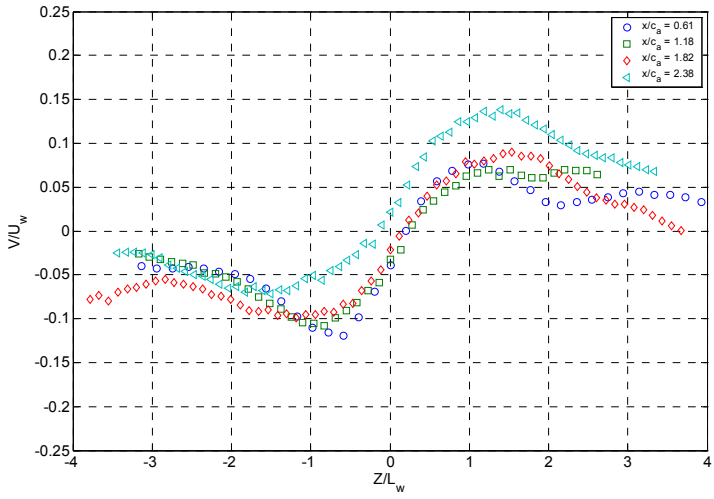

(d)

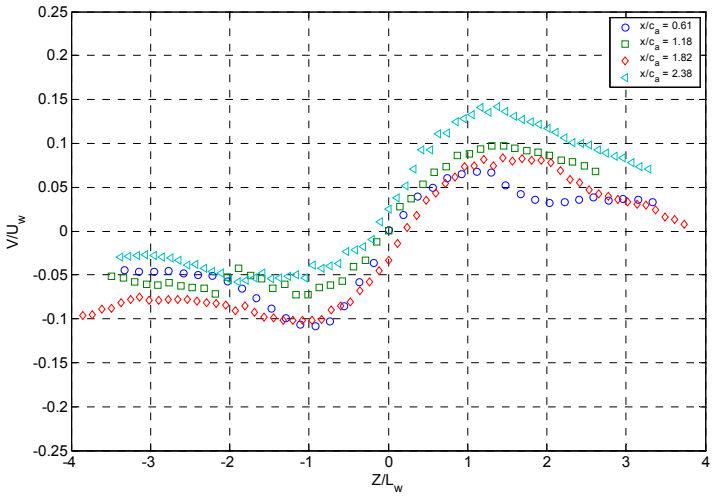

(e)

Figure 5-66: Spanwise mean velocity profiles, $V/U_{w.}$ at five spanwise locations across one serration for the 1.27 cm droop serration: **(a)** $y/c_a = 0.83$, **(b)** $y/c_a = 0.87$, **(c)** $y/c_a = 0.91$, **(d)** $y/c_a = 0.95$, **(e)** $y/c_a = 0.97$

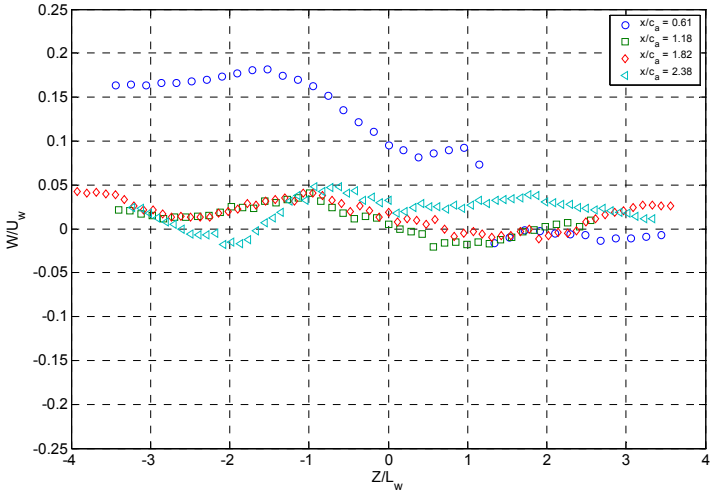

(a)

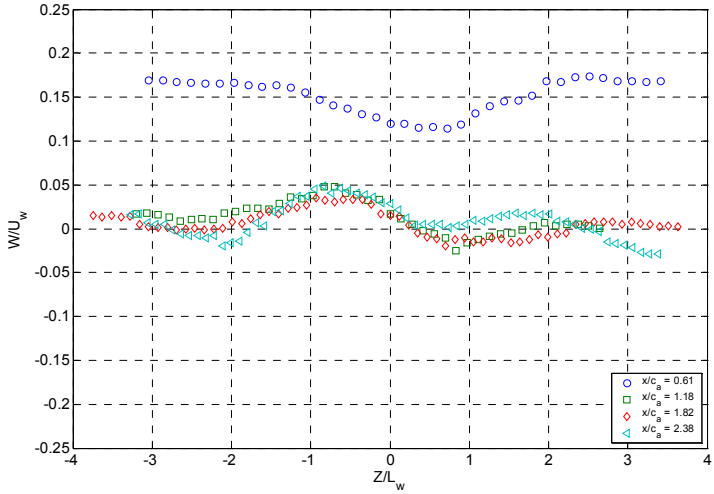

(b)

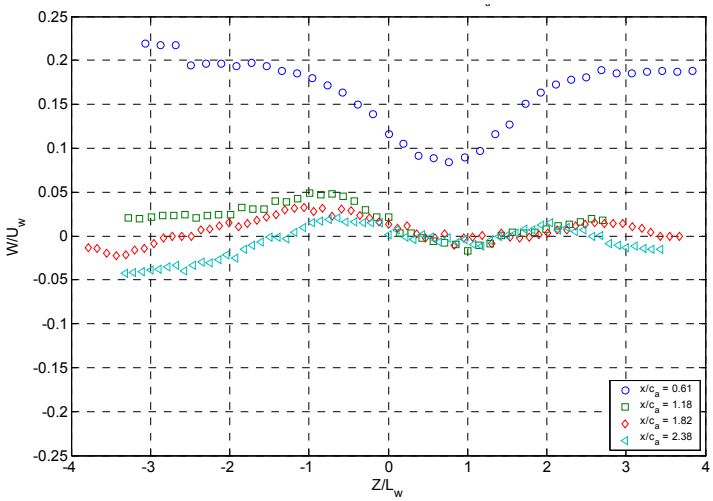

(c)

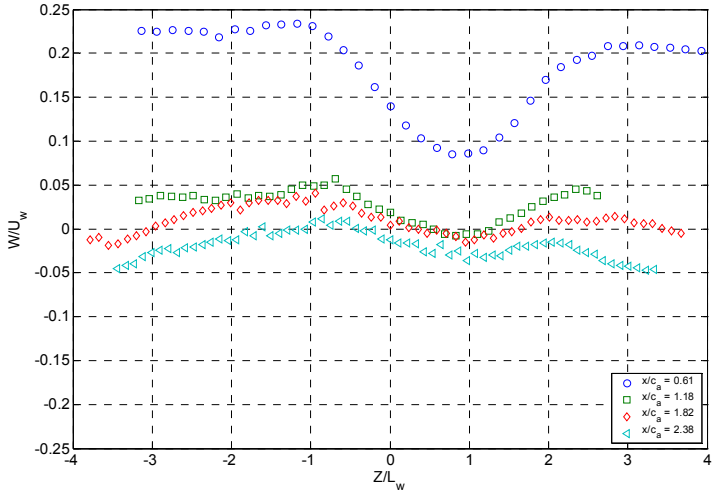

(d)

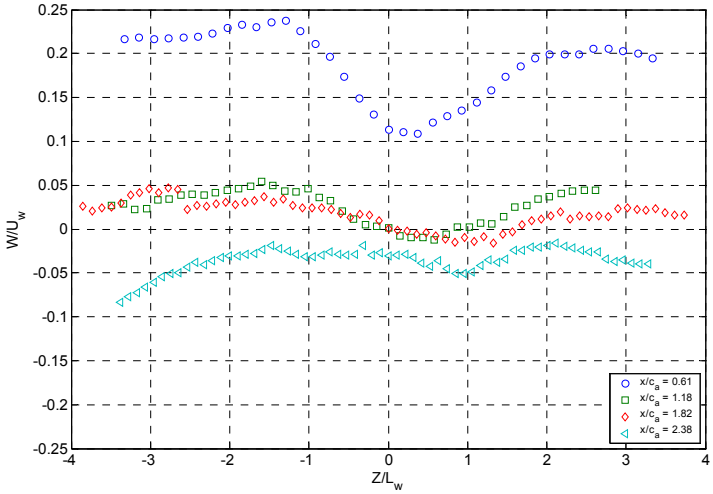

(e)

Figure 5-67: Cross-wake mean velocity profiles, $W/U_{w.}$ at five spanwise locations across one serration for the 1.27 cm droop serration: **(a)** $y/c_a = 0.83$, **(b)** $y/c_a = 0.87$, **(c)** $y/c_a = 0.91$, **(d)** $y/c_a = 0.95$, **(e)** $y/c_a = 0.97$

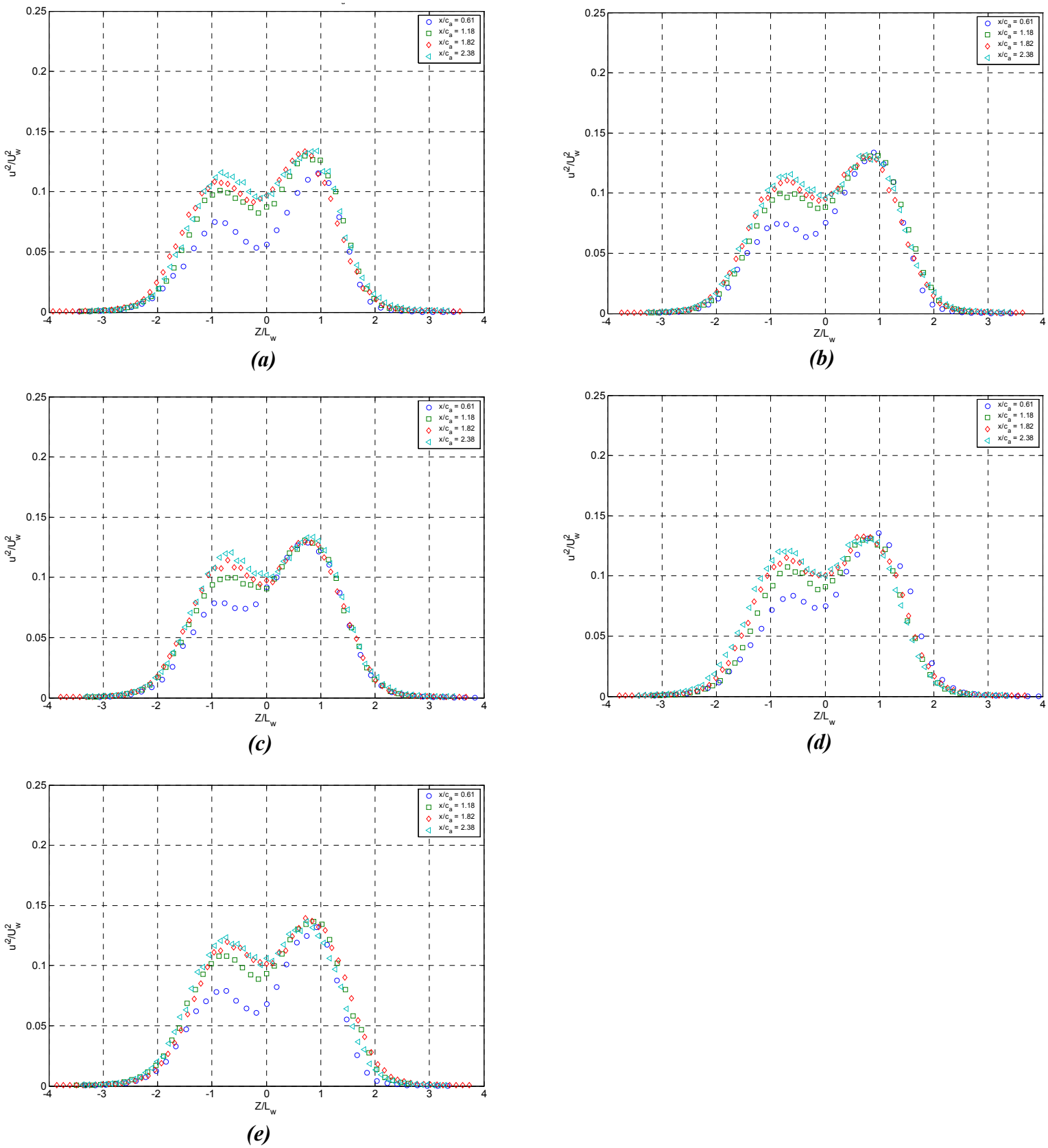

Figure 5-68: Streamwise Reynolds stress profiles, $\overline{u'^2/U_w^2}$ at five spanwise locations across one serration for the 1.27 cm droop serration: **(a)** $y/c_a = 0.83$, **(b)** $y/c_a = 0.87$, **(c)** $y/c_a = 0.91$, **(d)** $y/c_a = 0.95$, **(e)** $y/c_a = 0.97$

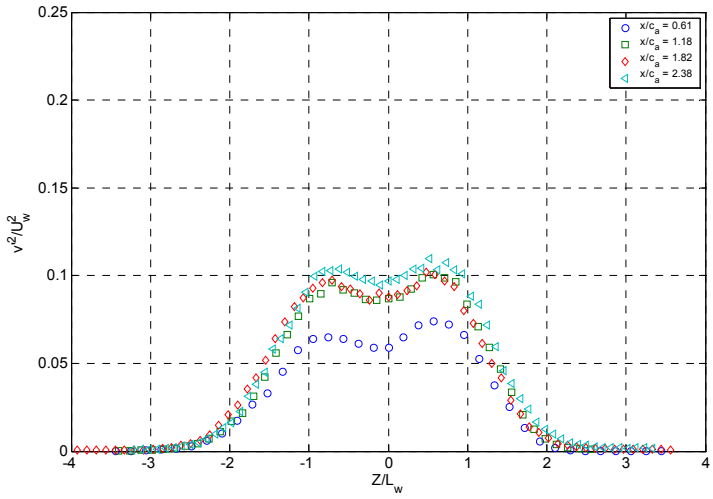

(a)

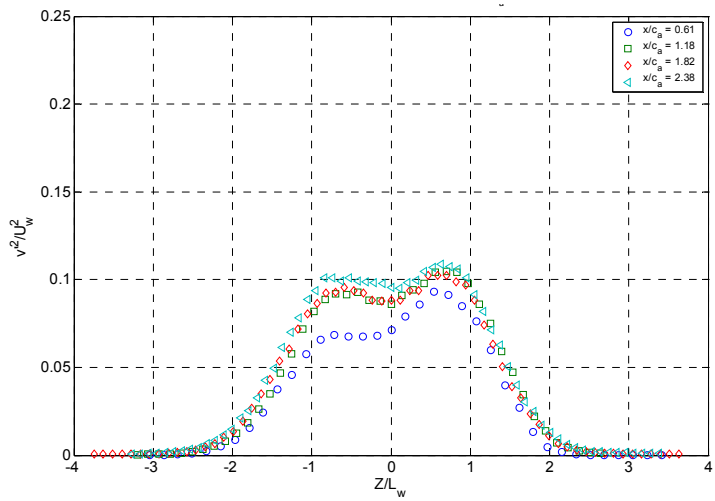

(b)

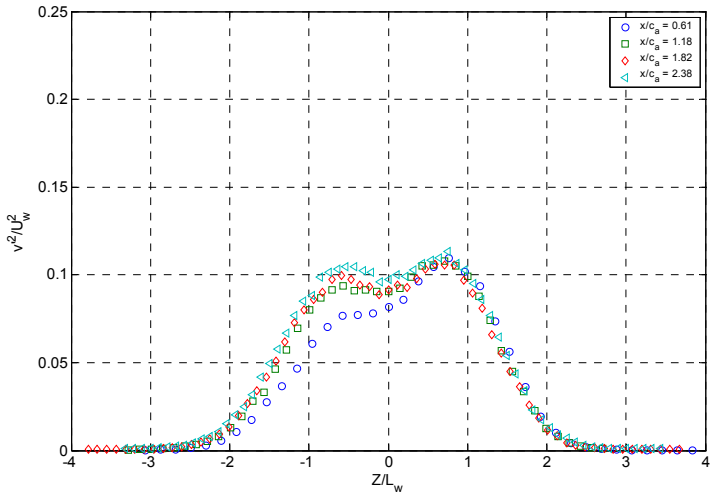

(c)

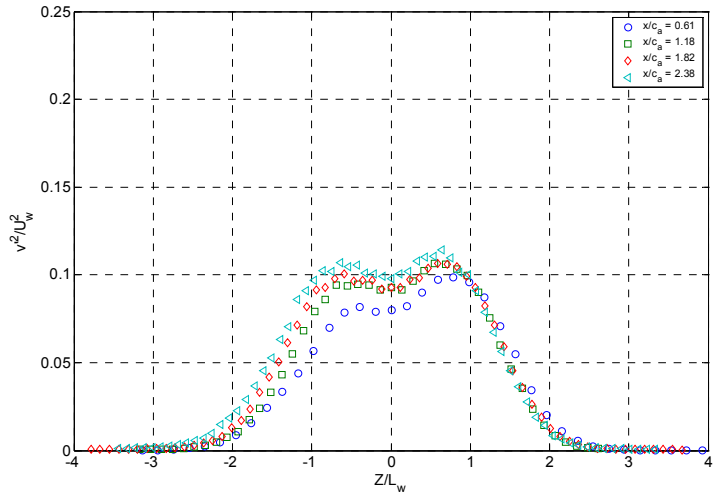

(d)

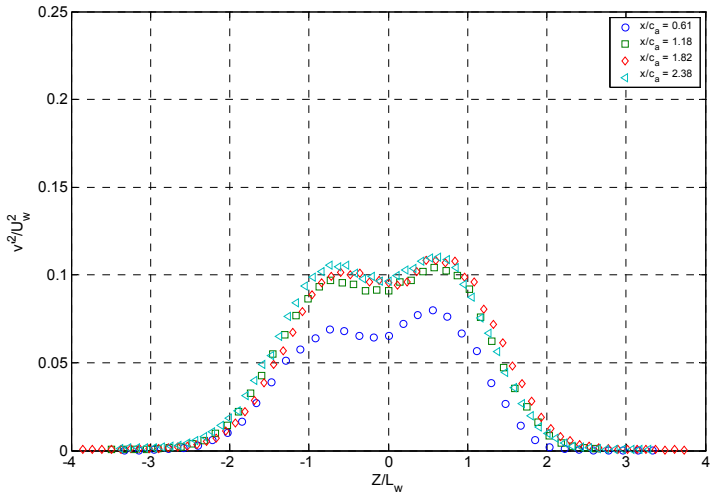

(e)

Figure 5-69: Spanwise Reynolds stress profiles, $\overline{v'^2/U_w^2}$ at five spanwise locations across one serration for the 1.27 cm droop serration: **(a)** $y/c_a = 0.83$, **(b)** $y/c_a = 0.87$, **(c)** $y/c_a = 0.91$, **(d)** $y/c_a = 0.95$, **(e)** $y/c_a = 0.97$

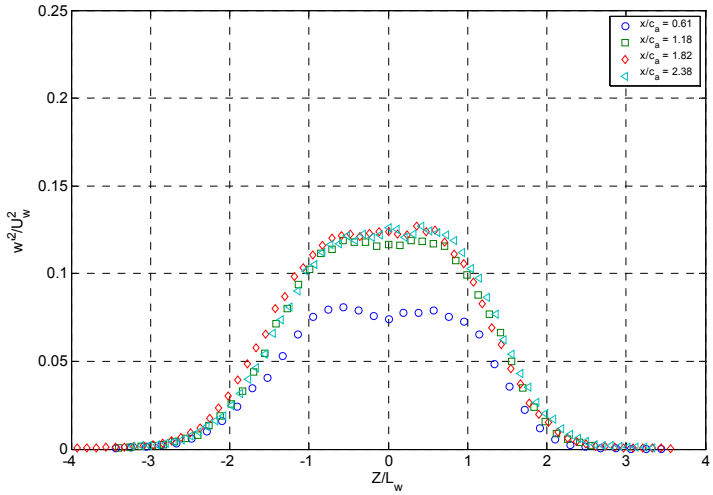

(a)

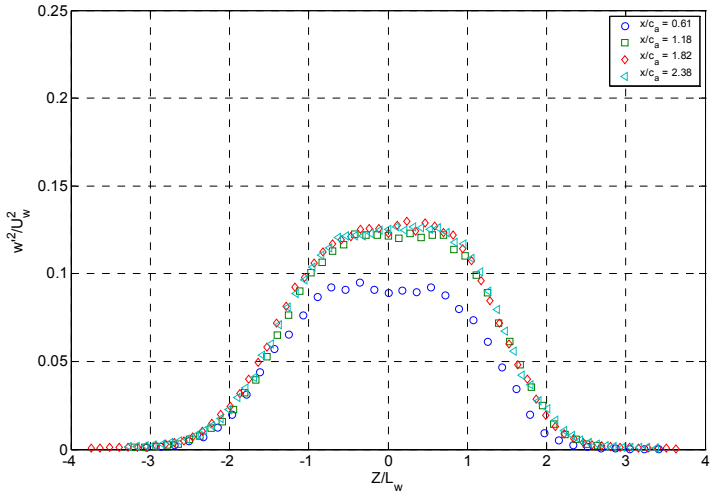

(b)

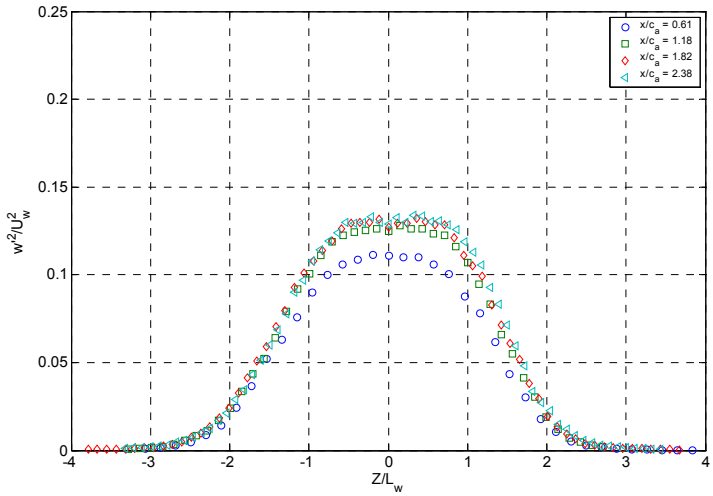

(c)

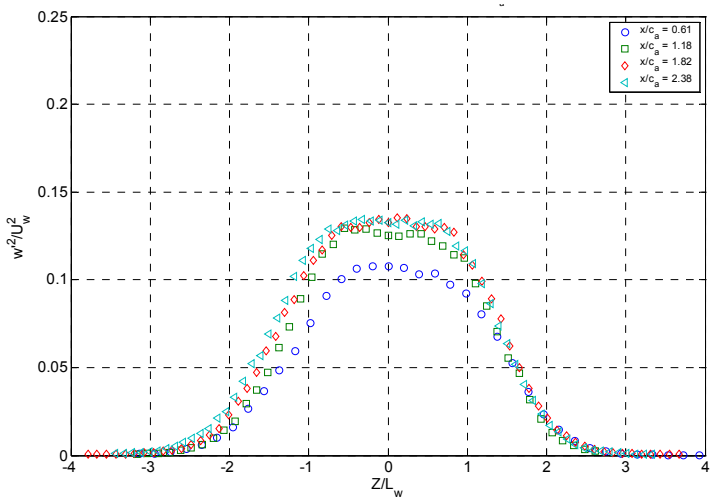

(d)

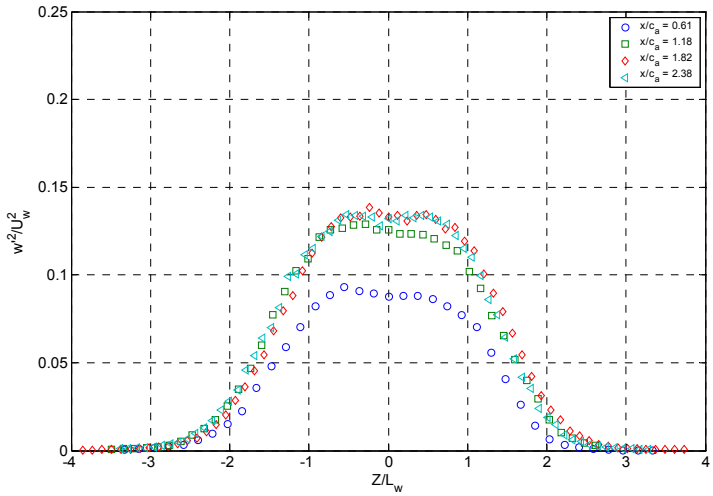

(e)

Figure 5-70: Cross-wake Reynolds stress profiles, $\overline{w'^2/U_w^2}$ at five spanwise locations across one serration for the 1.27 cm droop serration: **(a)** $y/c_a = 0.83$, **(b)** $y/c_a = 0.87$, **(c)** $y/c_a = 0.91$, **(d)** $y/c_a = 0.95$, **(e)** $y/c_a = 0.97$

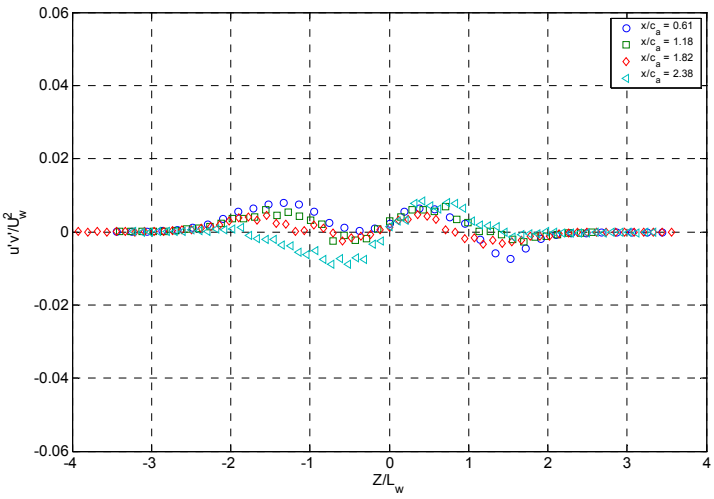

(a)

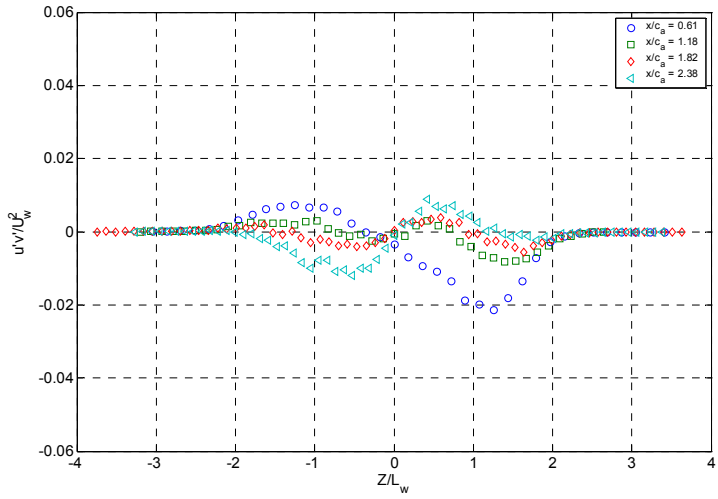

(b)

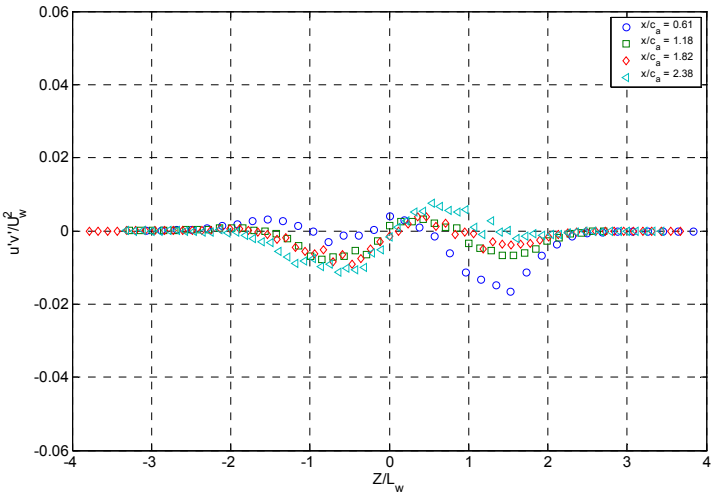

(c)

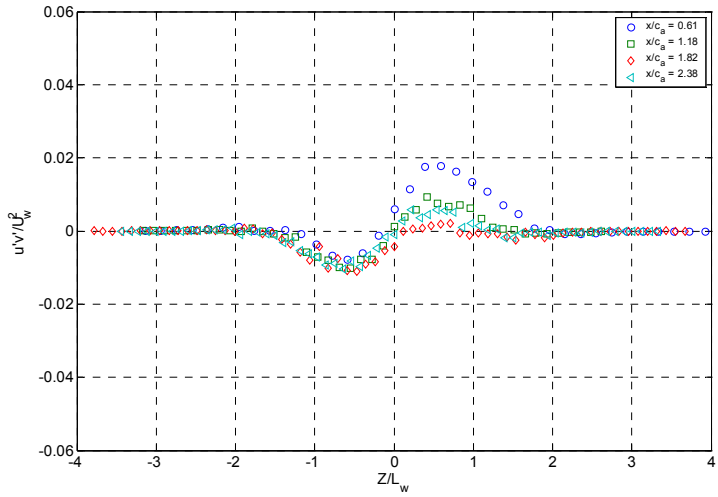

(d)

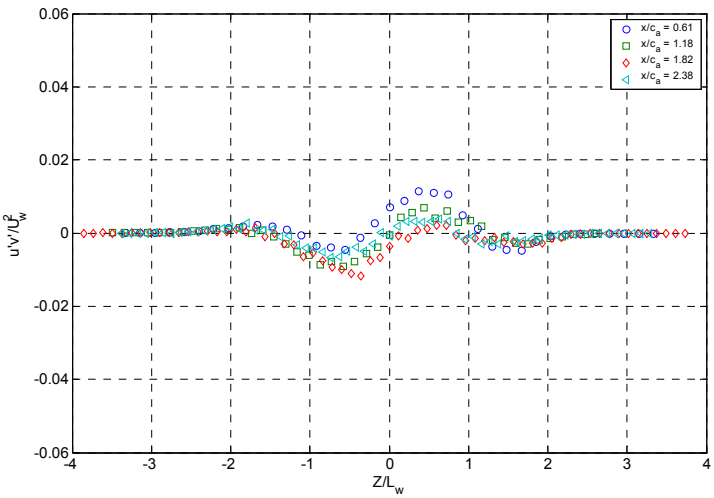

(e)

Figure 5-71: Reynolds shear stress profiles, $\overline{u'v'/U_w^2}$ at five spanwise locations across one serration for the 1.27 cm droop serration: **(a)** $y/c_a = 0.83$, **(b)** $y/c_a = 0.87$, **(c)** $y/c_a = 0.91$, **(d)** $y/c_a = 0.95$, **(e)** $y/c_a = 0.97$

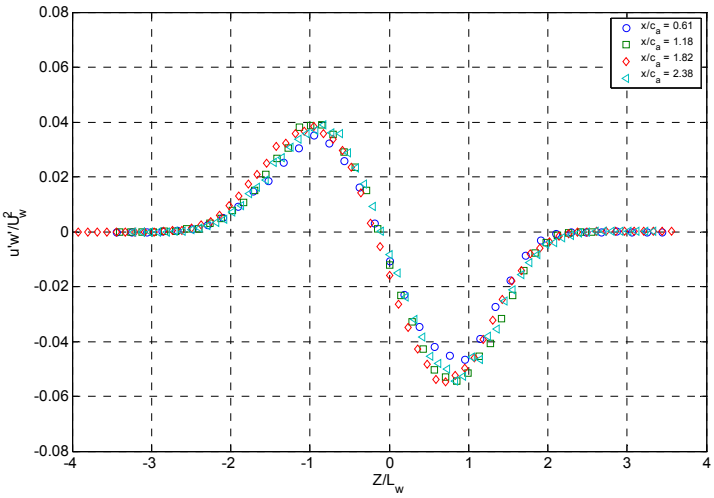

(a)

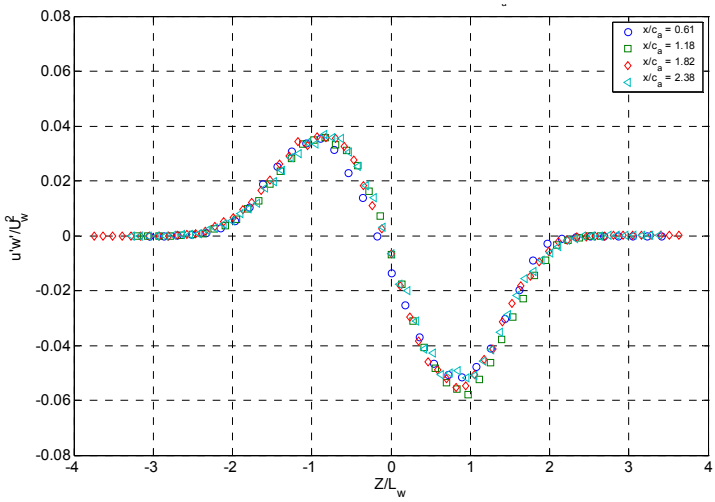

(b)

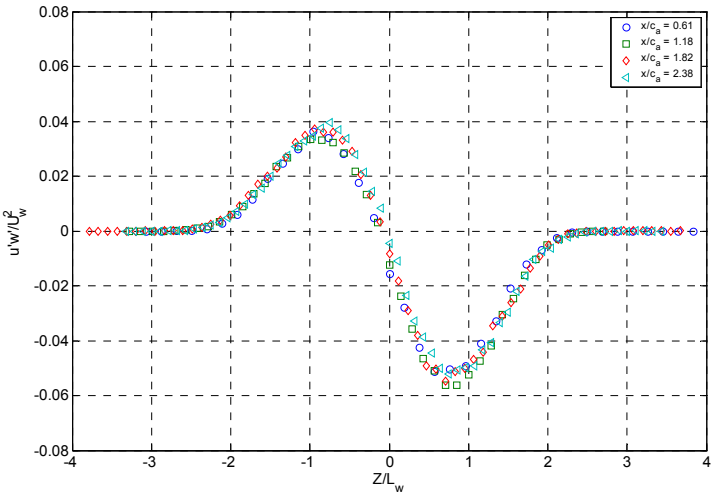

(c)

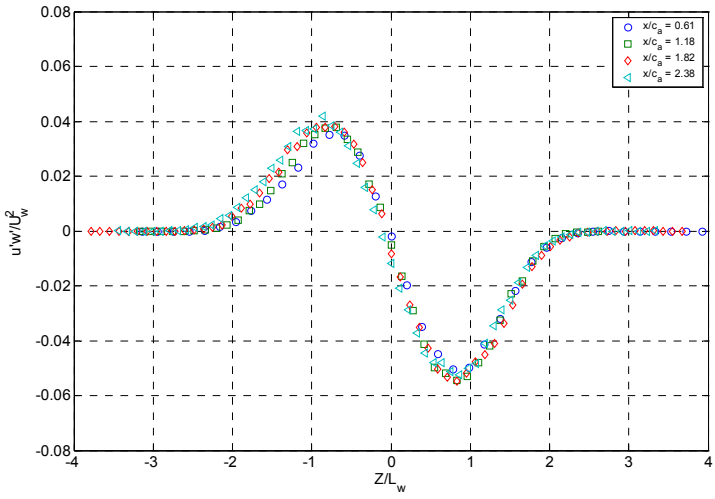

(d)

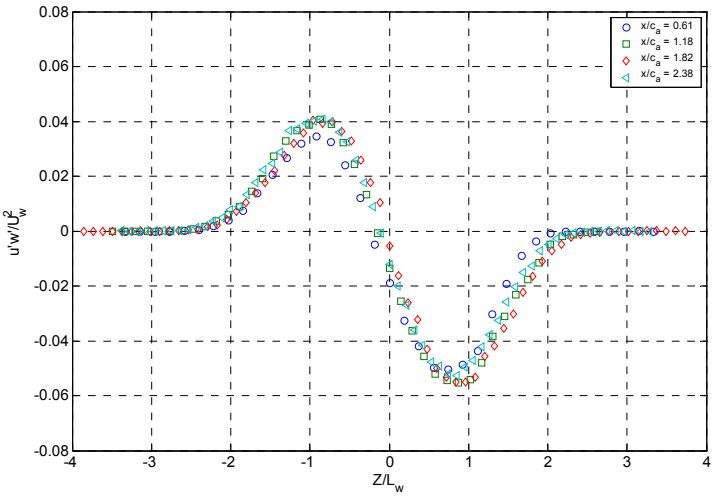

(e)

Figure 5-72: Reynolds shear stress profiles, $\overline{u'w'/U_w^2}$ at five spanwise locations across one serration for the 1.27 cm droop serration: **(a)** $y/c_a = 0.83$, **(b)** $y/c_a = 0.87$, **(c)** $y/c_a = 0.91$, **(d)** $y/c_a = 0.95$, **(e)** $y/c_a = 0.97$

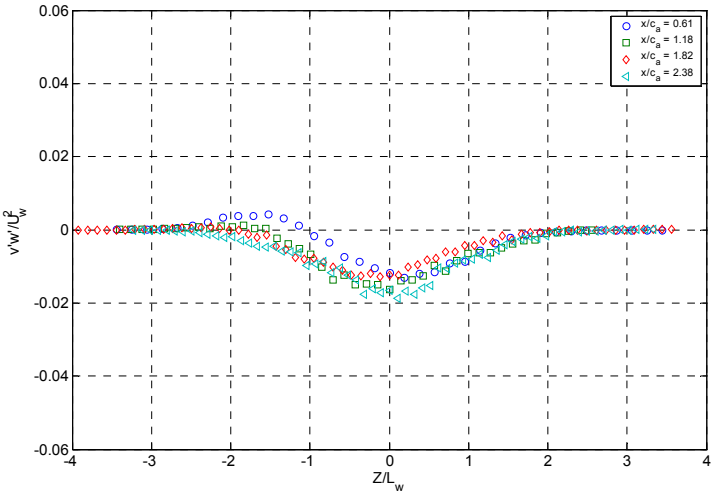

(a)

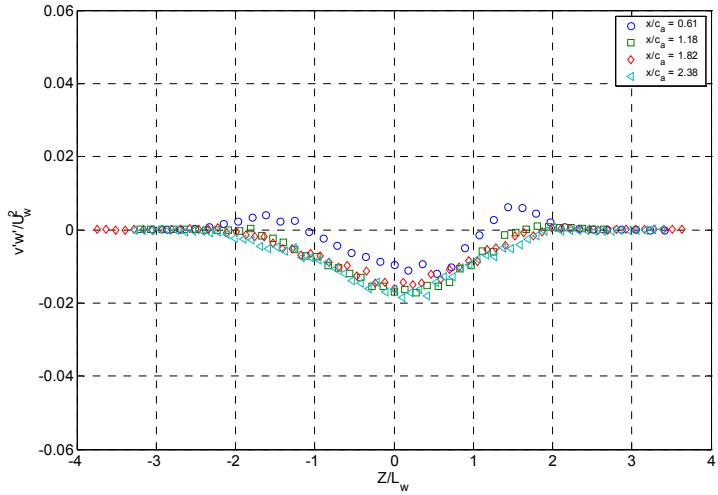

(b)

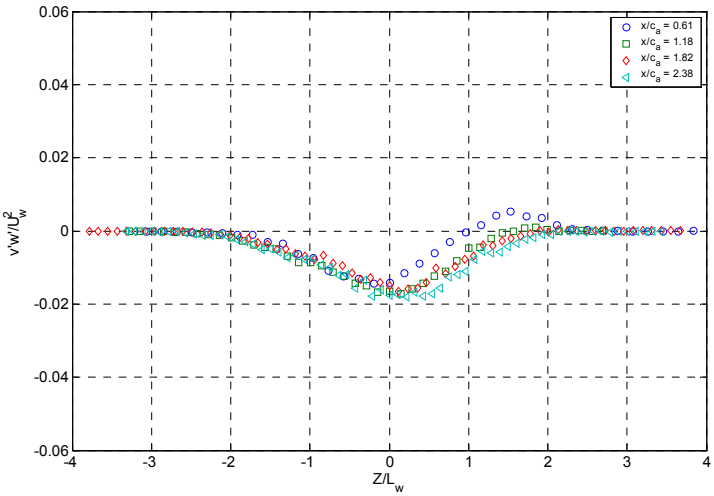

(c)

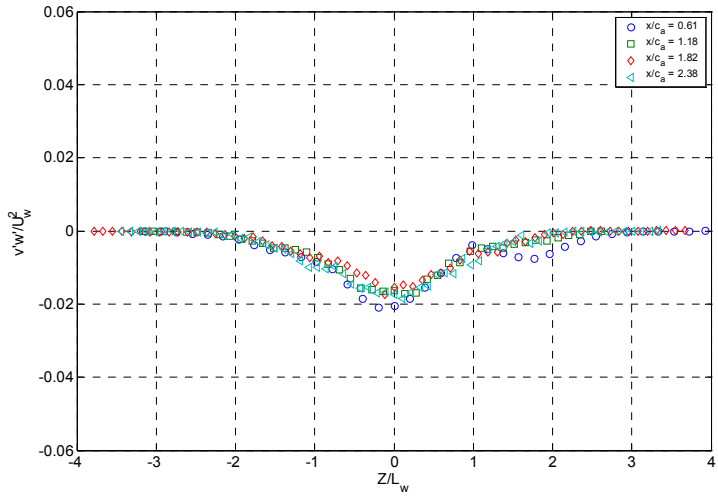

(d)

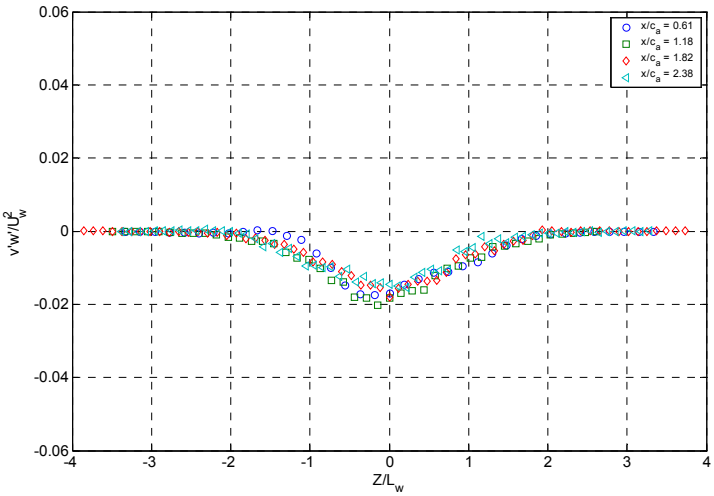

(e)

Figure 5-73: Reynolds shear stress profiles, $\overline{v'w'/U_w^2}$ at five spanwise locations across one serration for the 1.27 cm droop serration: **(a)** $y/c_a = 0.83$, **(b)** $y/c_a = 0.87$, **(c)** $y/c_a = 0.91$, **(d)** $y/c_a = 0.95$, **(e)** $y/c_a = 0.97$

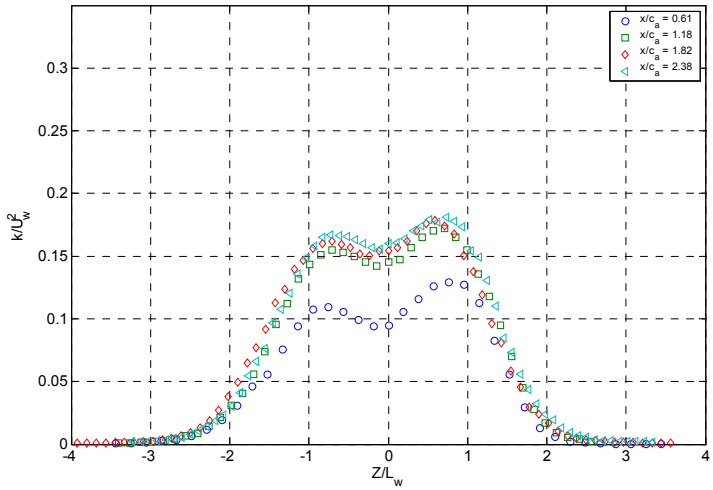

(a)

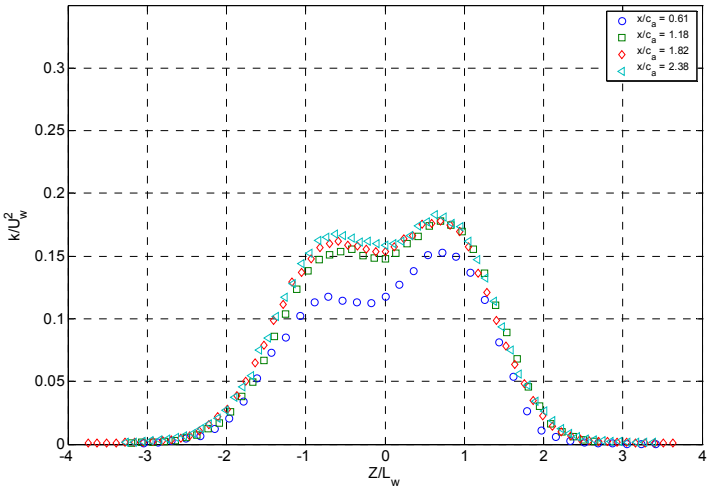

(b)

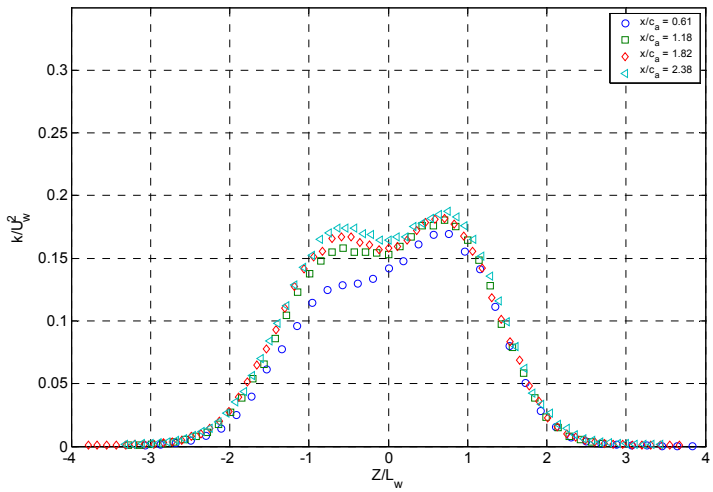

(c)

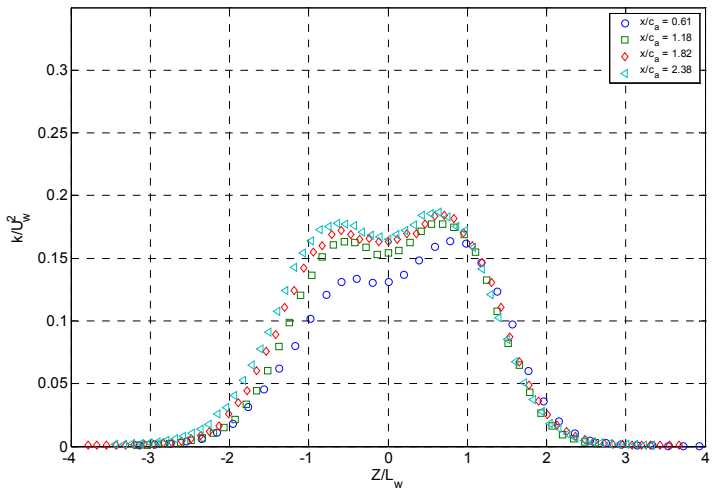

(d)

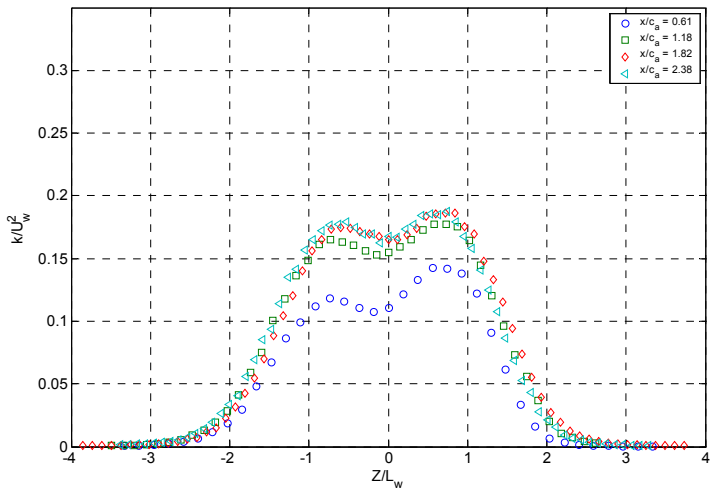

(e)

Figure 5-74: Turbulence kinetic energy profiles, k/U_w^2 at five locations spanwise locations across one serration for the 1.27 droop cm serration: **(a)** $y/c_a = 0.83$, **(b)** $y/c_a = 0.87$, **(c)** $y/c_a = 0.91$, **(d)** $y/c_a = 0.95$, **(e)** $y/c_a = 0.97$

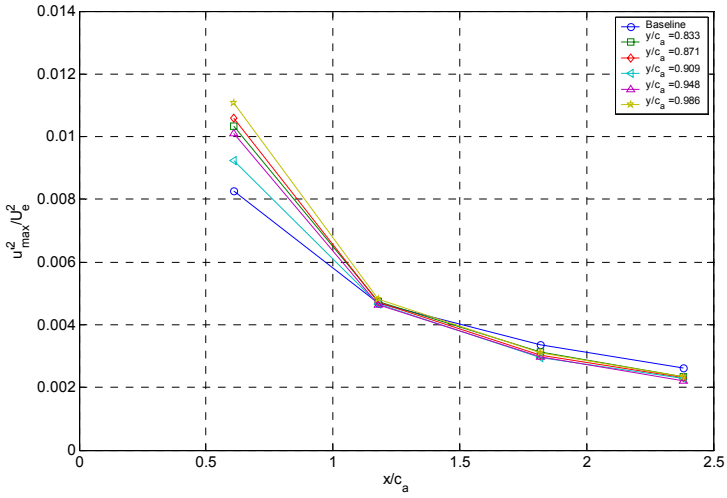

(a)

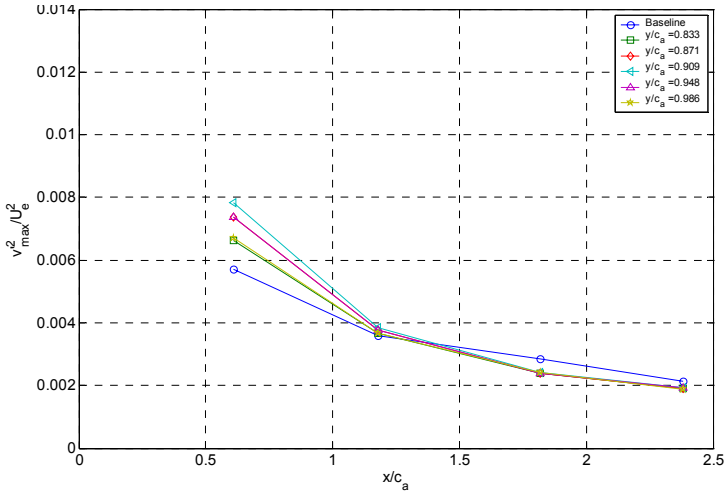

(b)

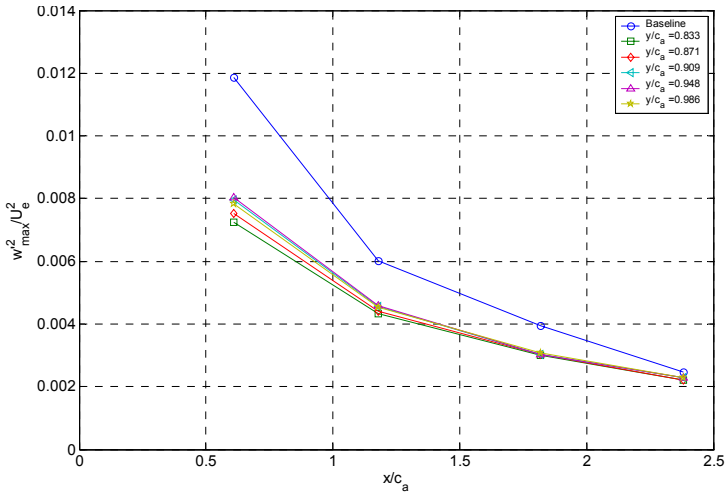

(c)

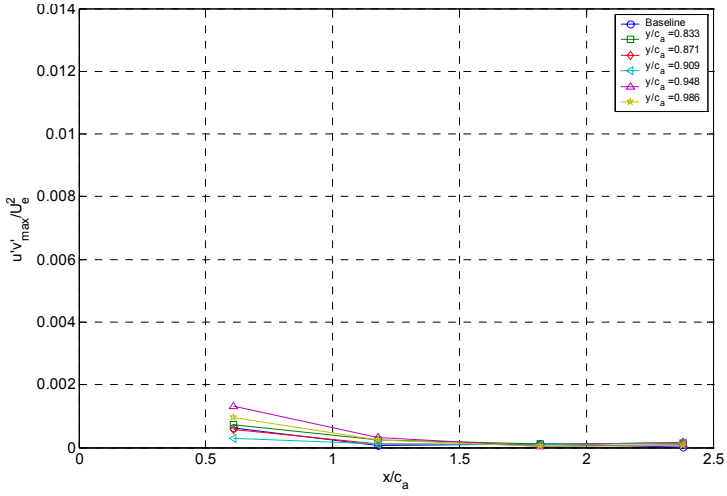

(d)

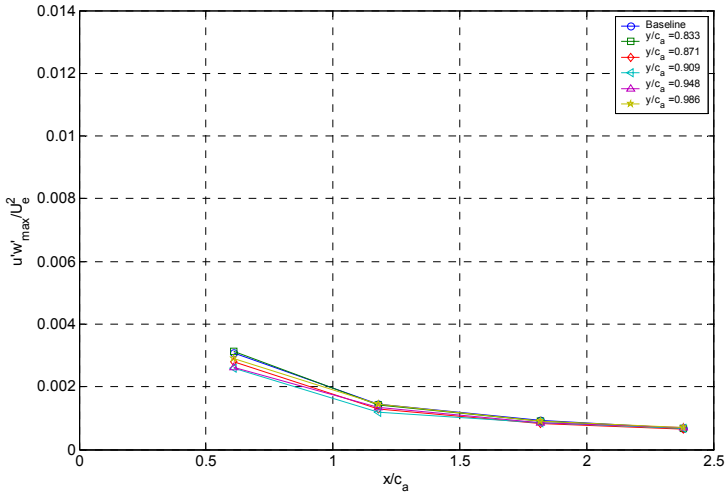

(e)

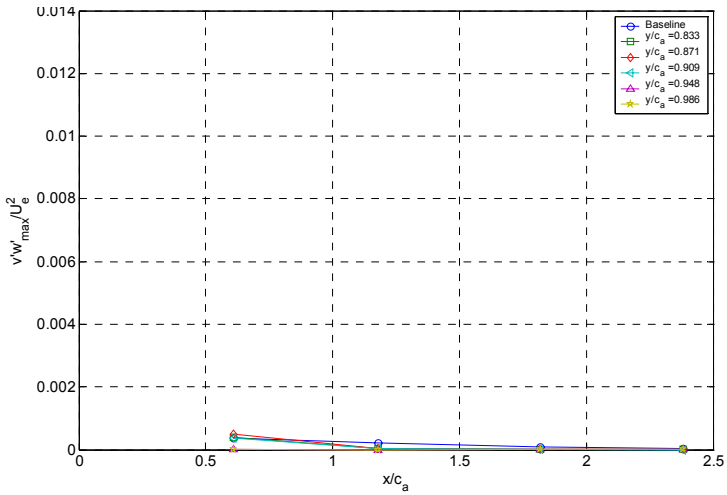

(f)

Figure 5-75: Maximum normalized Reynolds stress levels at five spanwise locations across one serration for the 1.27 cm droop serration compared to the baseline: **(a)** $\overline{|u'^2/U_\infty^2|}_{max}$, **(b)** $\overline{|v'^2/U_\infty^2|}_{max}$, **(c)** $\overline{|w'^2/U_\infty^2|}_{max}$, **(d)** $\overline{|u'v'/U_\infty^2|}_{max}$, **(e)** $\overline{|u'w'/U_\infty^2|}_{max}$, **(f)** $\overline{|v'w'/U_\infty^2|}_{max}$

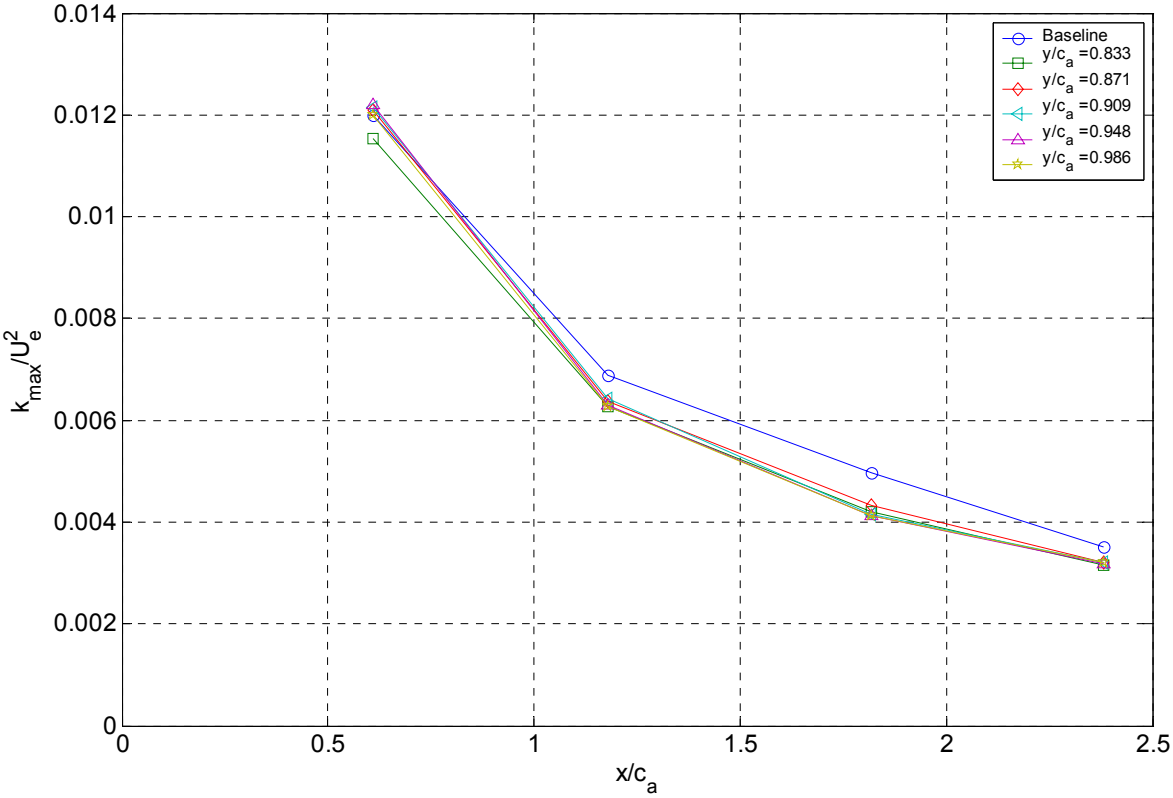

Figure 5-76: Maximum normalized turbulence kinetic energy, $|k/U_w^2|_{max}$, at five spanwise locations across one serration for the 1.27 cm droop serration compared to the baseline,

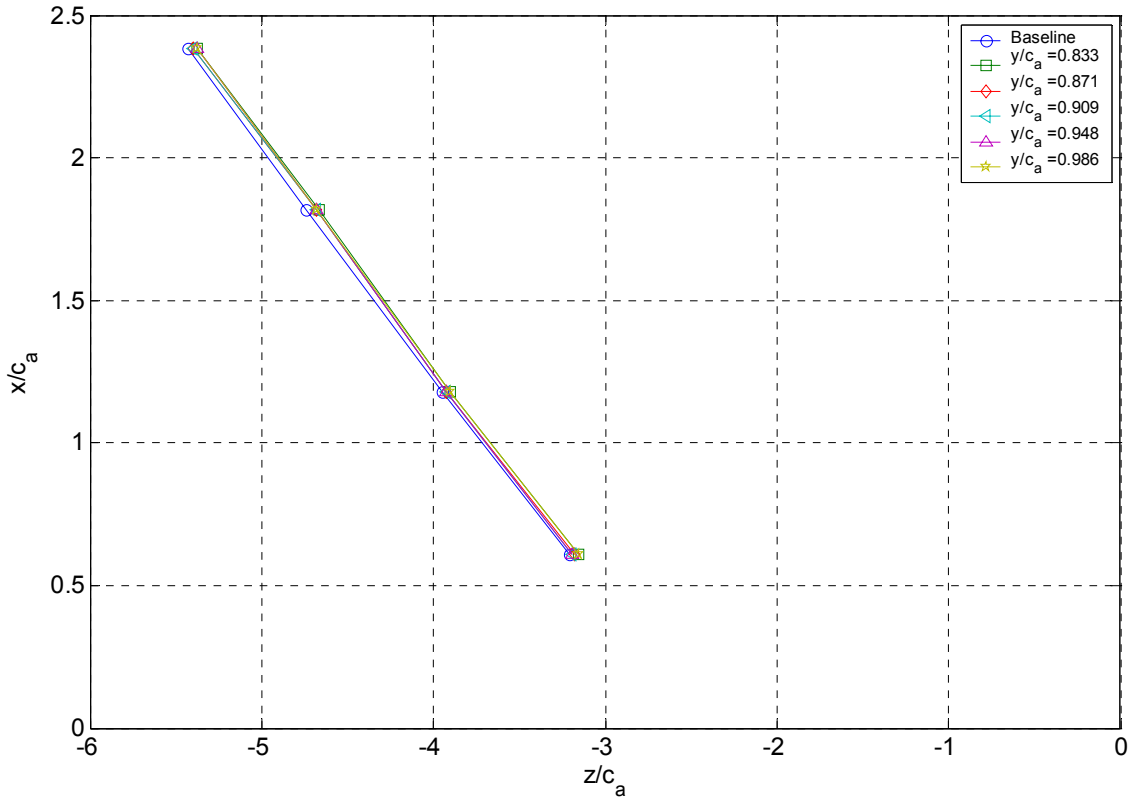

Figure 5-77: Propagation of the minimum velocity point in the wake for the 1.27 cm droop serration compared to the baseline case

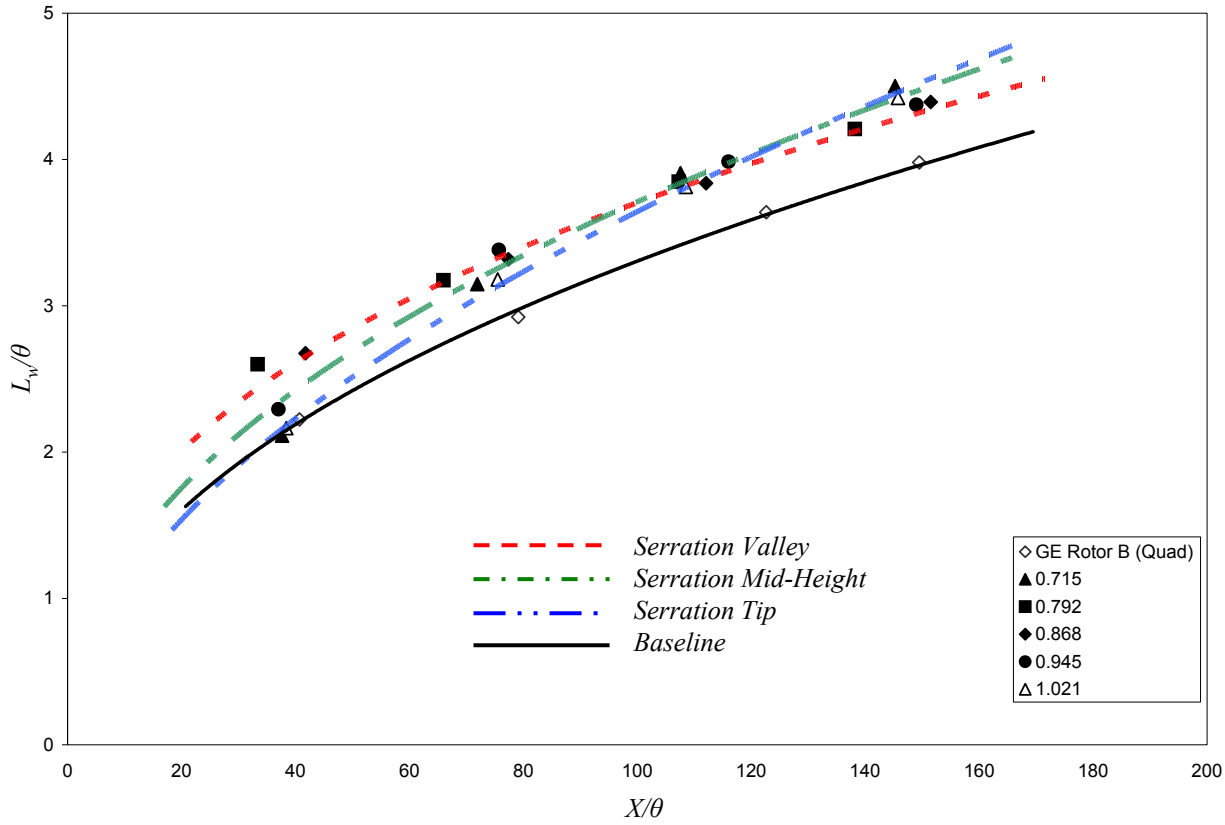

Figure 5-78: Normalized wake half-width of the wake, L_w/θ, as a function of normalized downstream distance, X/θ, for the 2.54 cm droop serration.

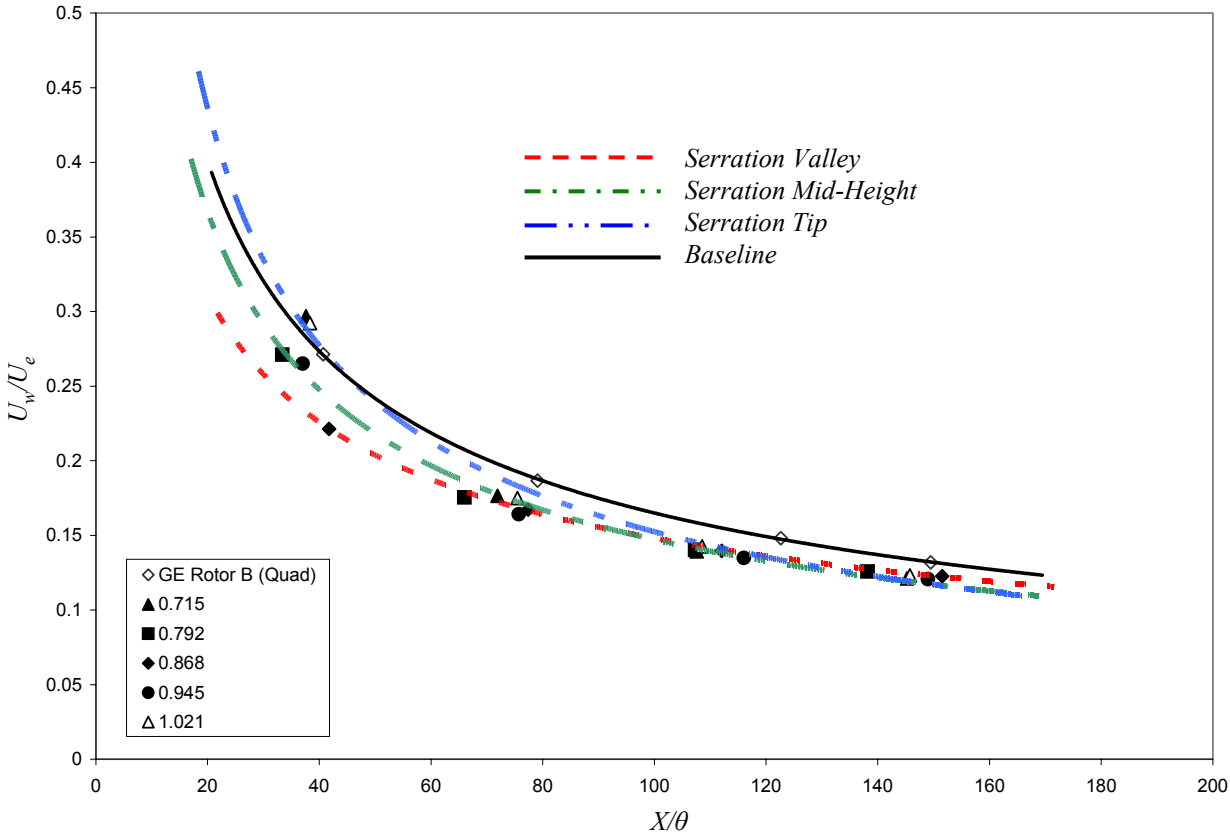

Figure 5-79: Normalized maximum velocity deficit in the wake, U_w/U_e, function of the normalized downstream distance, X/θ, for the 2.54 cm droop serration.

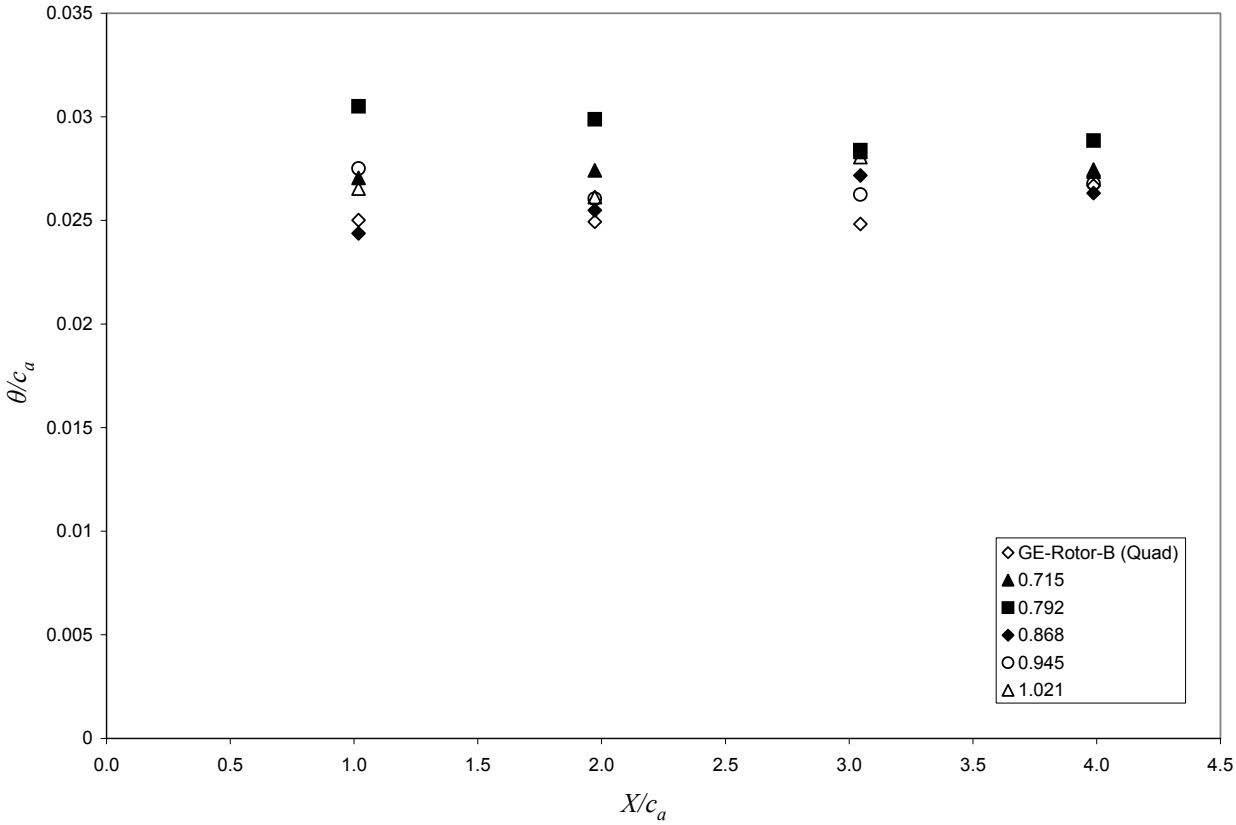

Figure 5-80: Normalized momentum thickness, θ/c_a, as a function of normalized distance downstream, X/c_a, for the 2.54 cm droop serration.

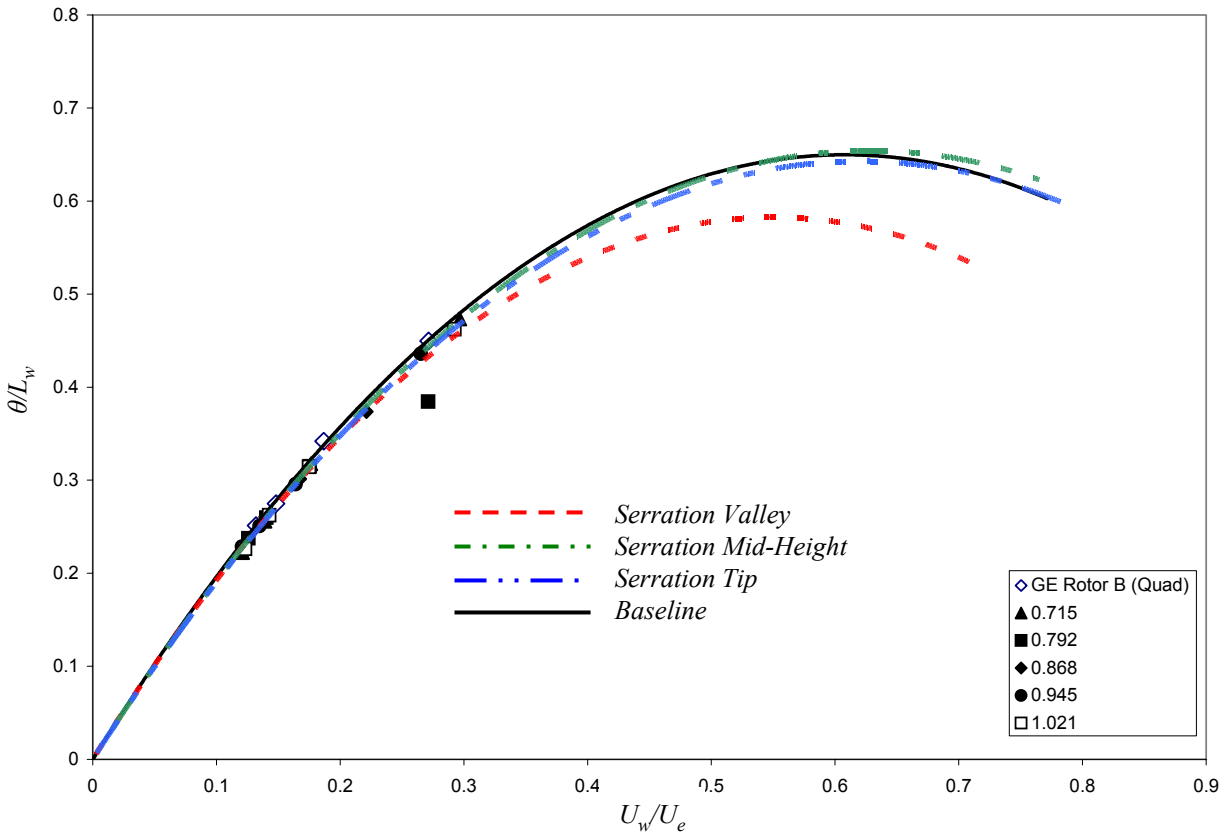

Figure 5-81: Normalized momentum thickness, θ/L_w as a function of normalized velocity deficit of wake, U_w/U_e, for the 2.54 cm droop serration.

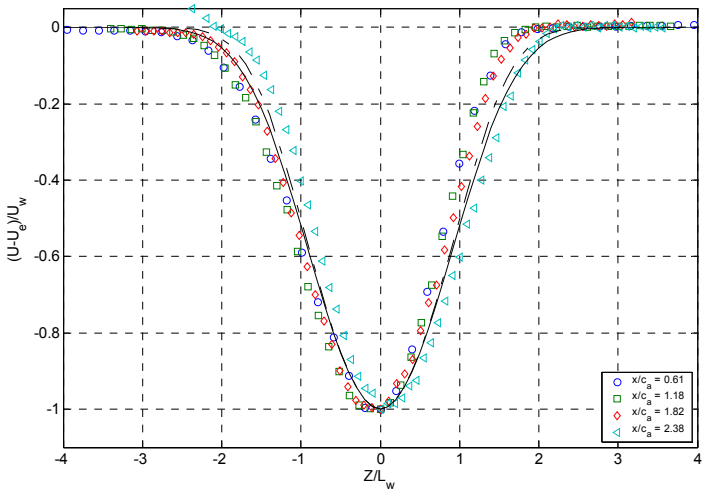

(a)

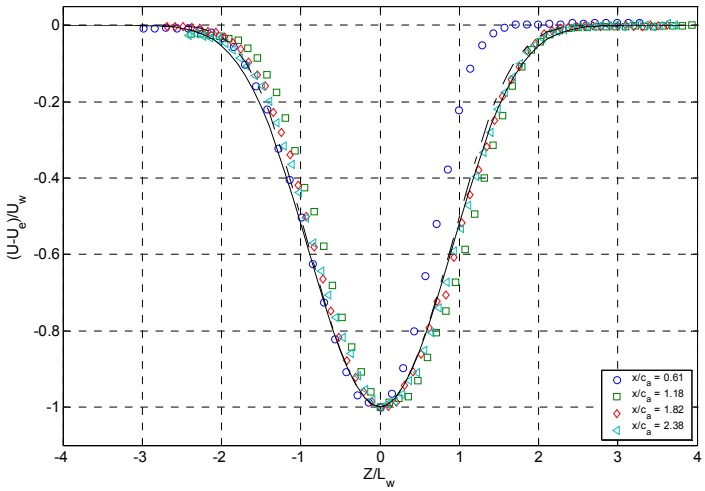

(b)

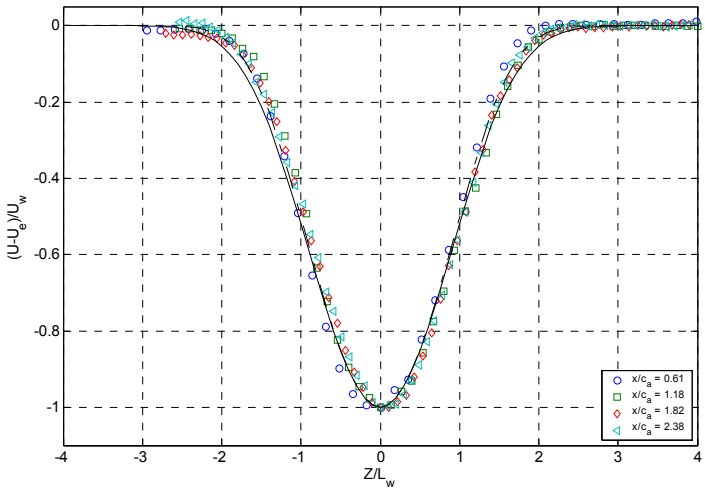

(c)

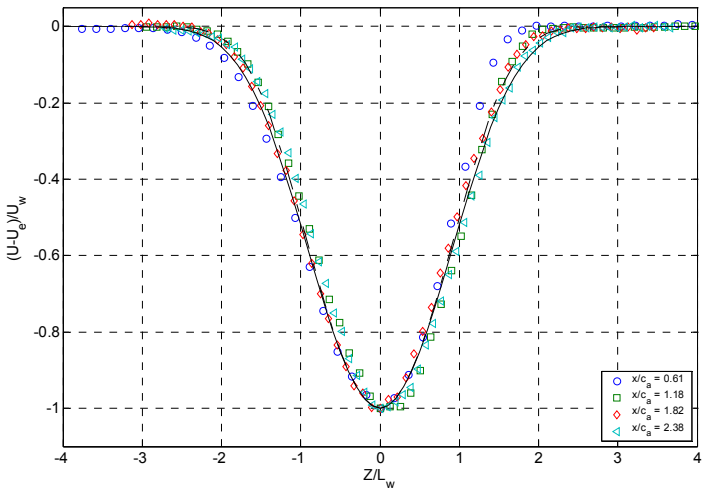

(d)

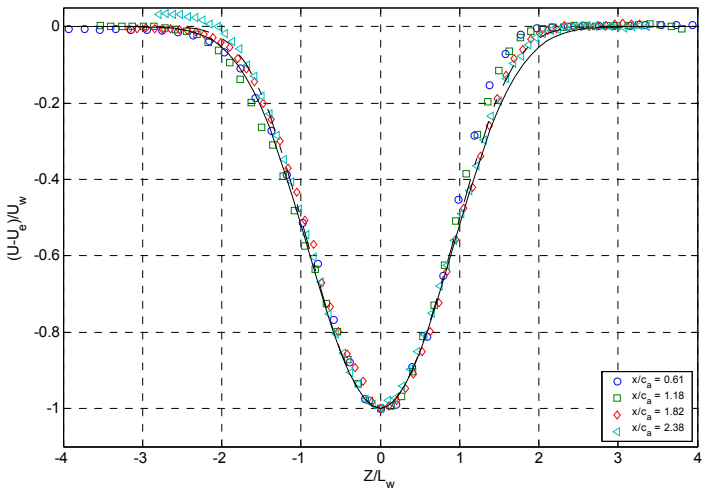

(e)

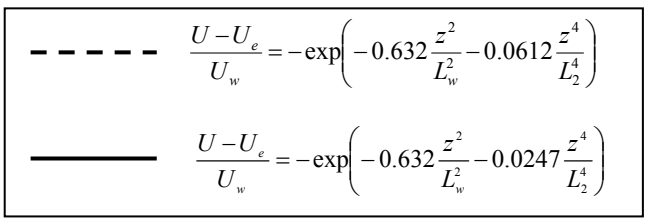

Figure 5-82: Streamwise mean velocity profile, $(U\text{-}U_e)/U_w$ at five spanwise locations across one serration for the 2.54 cm serration: **(a)** $y/c_a = 0.72$, **(b)** $y/c_a = 0.79$, **(c)** $y/c_a = 0.87$, **(d)** $y/c_a = 0.95$, **(e)** $y/c_a = 1.021$

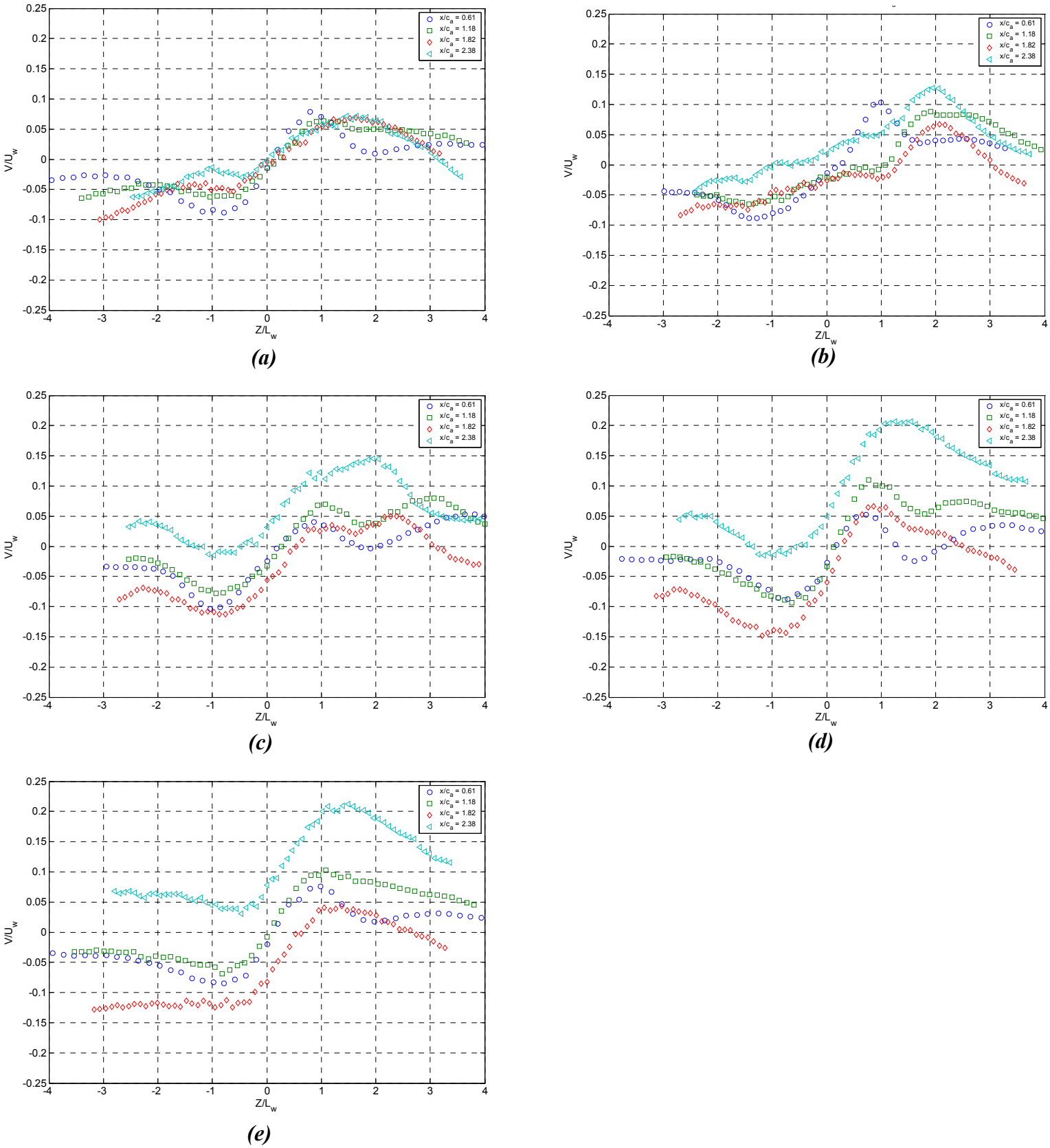

Figure 5-83: Spanwise mean velocity profiles, $V/U_{w.}$ at five spanwise locations across one serration for the 2.54 cm serration: **(a)** $y/c_a = 0.72$, **(b)** $y/c_a = 0.79$, **(c)** $y/c_a = 0.87$, **(d)** $y/c_a = 0.95$, **(e)** $y/c_a = 1.021$

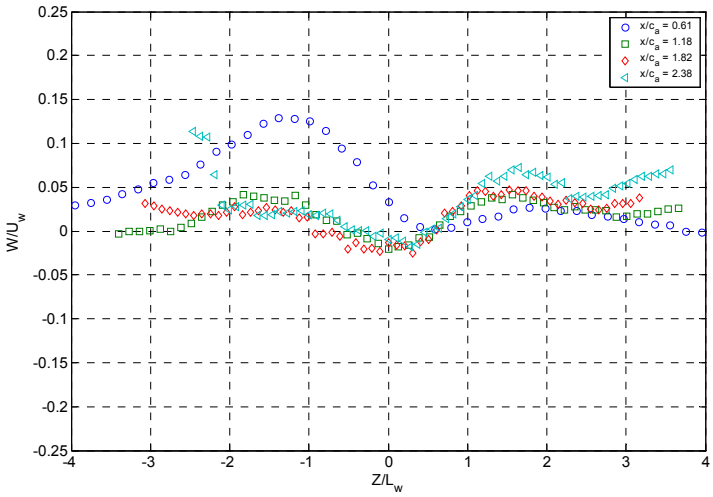

(a)

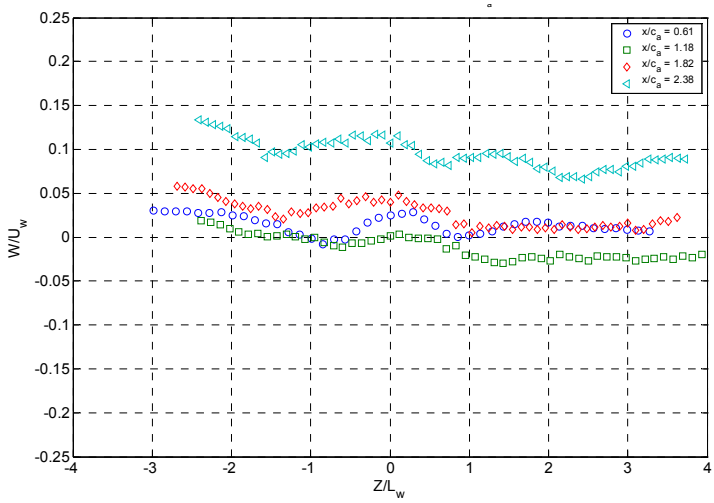

(b)

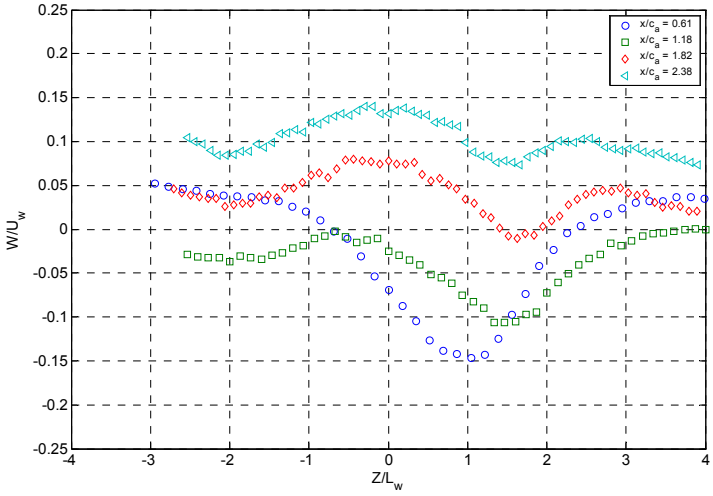

(c)

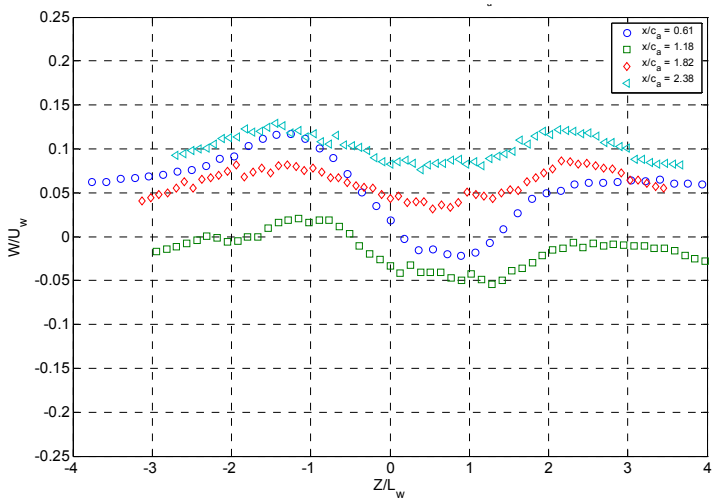

(d)

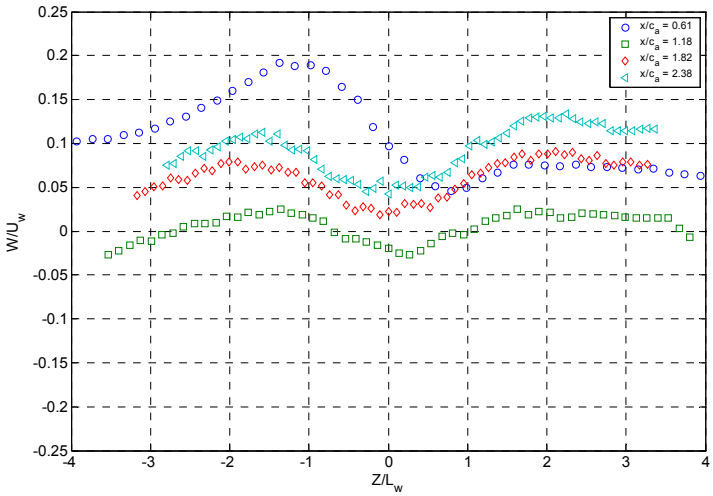

(e)

Figure 5-84: Cross-wake mean velocity profiles, $W/U_{w.}$ at five spanwise locations across one serration for the 2.54 cm serration: **(a)** $y/c_a = 0.72$, **(b)** $y/c_a = 0.79$, **(c)** $y/c_a = 0.87$, **(d)** $y/c_a = 0.95$, **(e)** $y/c_a = 1.021$

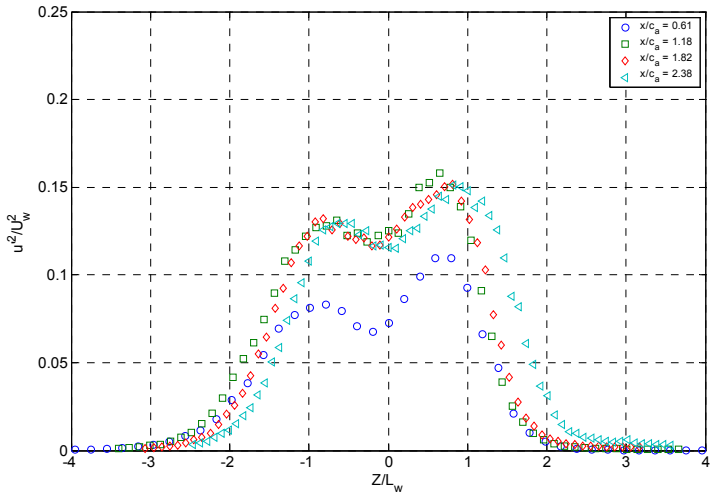

(a)

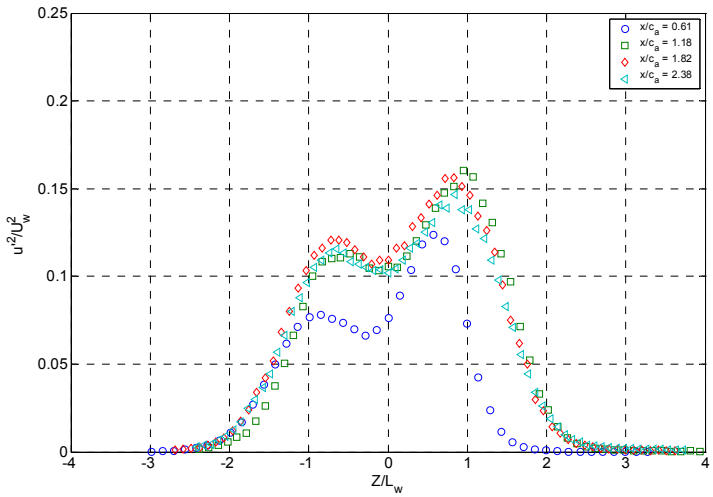

(b)

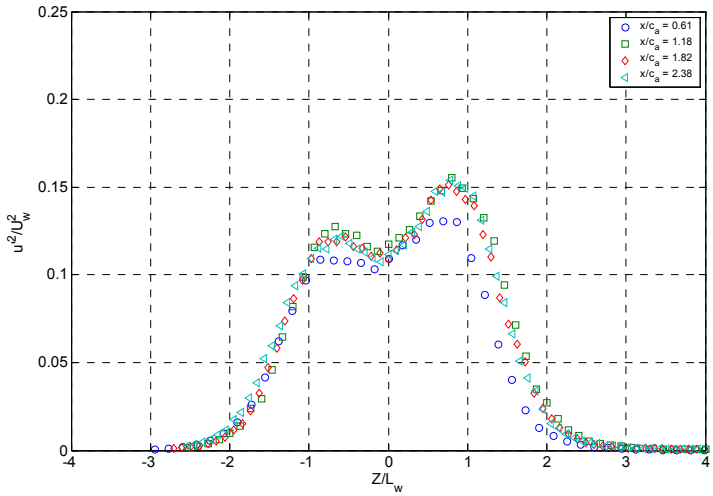

(c)

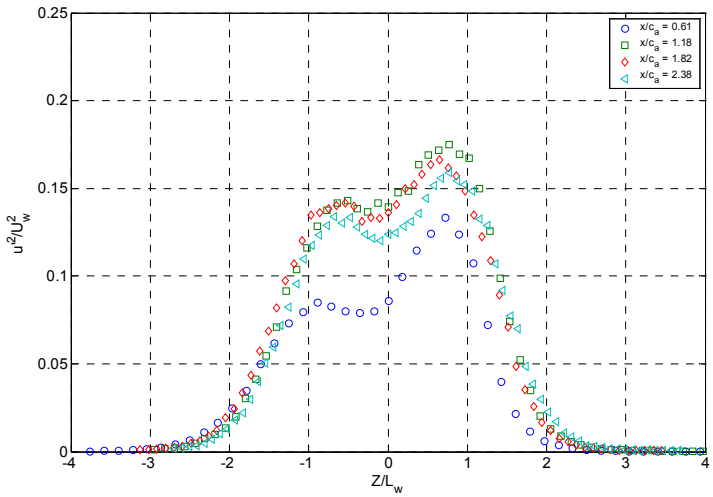

(d)

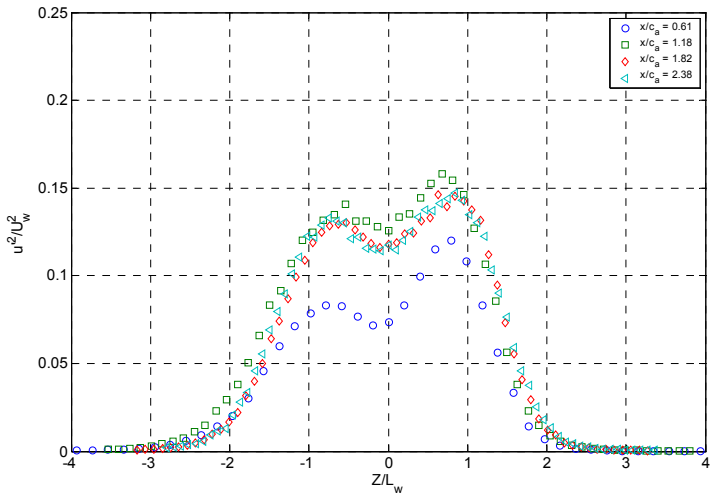

(e)

Figure 5-85: Streamwise Reynolds stress profiles, $\overline{u'^2/U_w^2}$ at five spanwise locations across one serration for the 2.54 cm serration: **(a)** $y/c_a = 0.72$, **(b)** $y/c_a = 0.79$, **(c)** $y/c_a = 0.87$, **(d)** $y/c_a = 0.95$, **(e)** $y/c_a = 1.021$

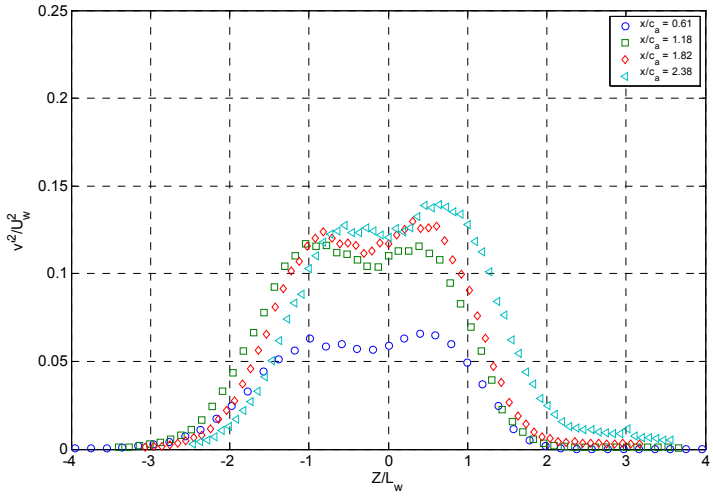

(a)

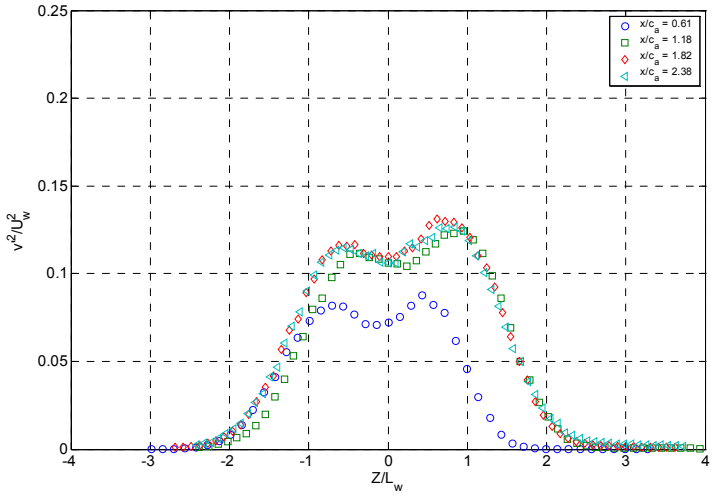

(b)

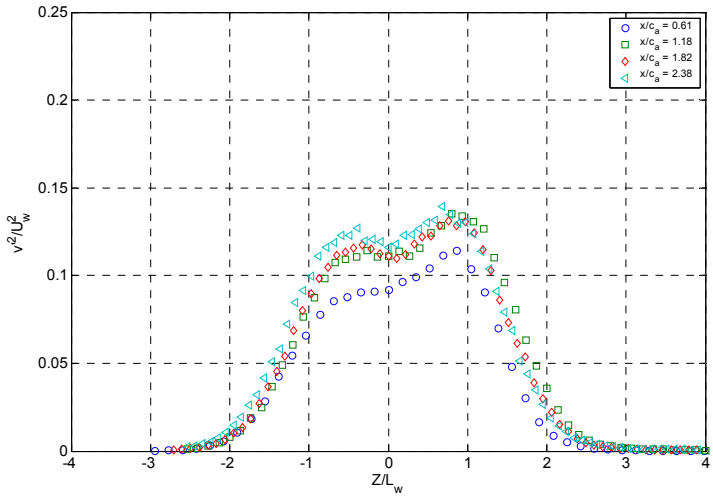

(c)

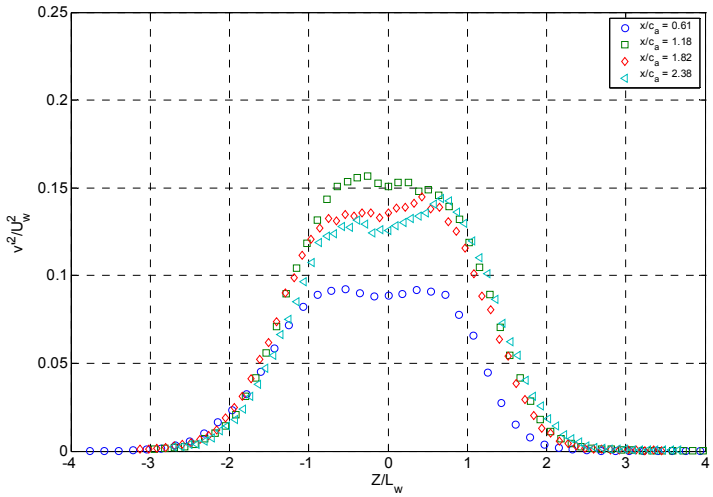

(d)

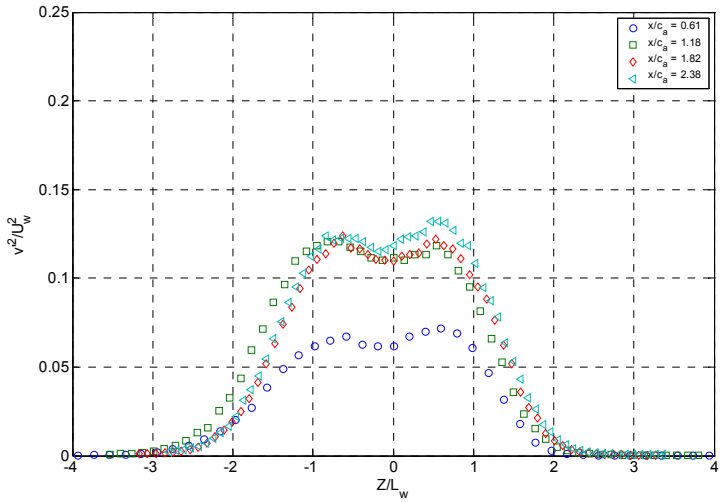

(e)

Figure 5-86: Spamwise Reynolds stress profiles, $\overline{v'^2/U_w^2}$ at five spanwise locations across one serration for the 2.54 cm serration: **(a)** $y/c_a = 0.72$, **(b)** $y/c_a = 0.79$, **(c)** $y/c_a = 0.87$, **(d)** $y/c_a = 0.95$, **(e)** $y/c_a = 1.021$

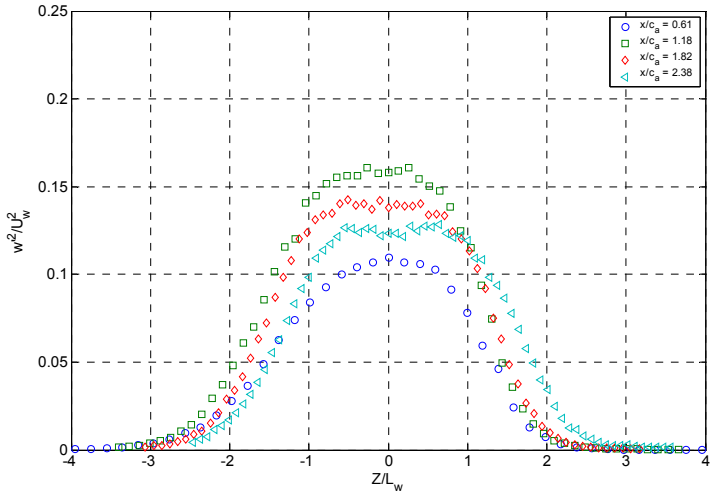

(a)

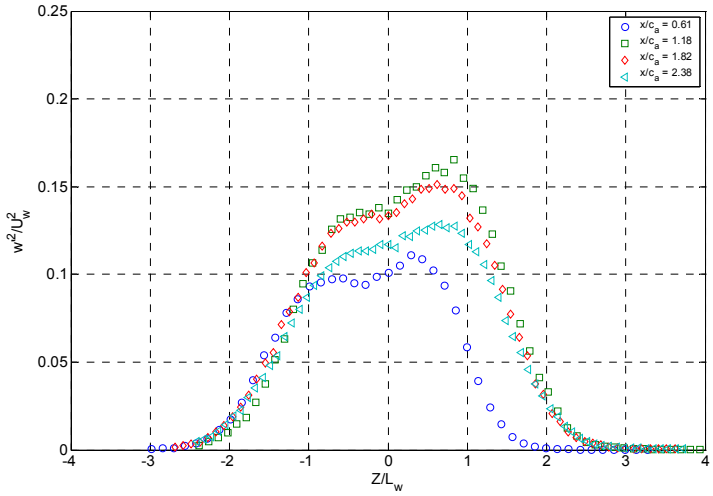

(b)

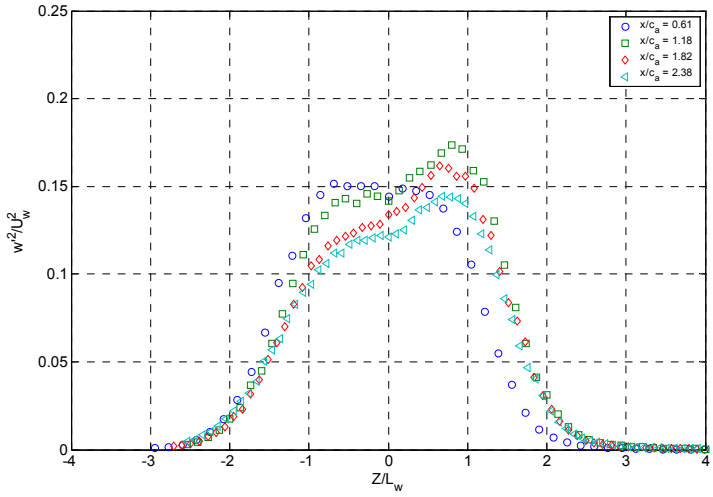

(c)

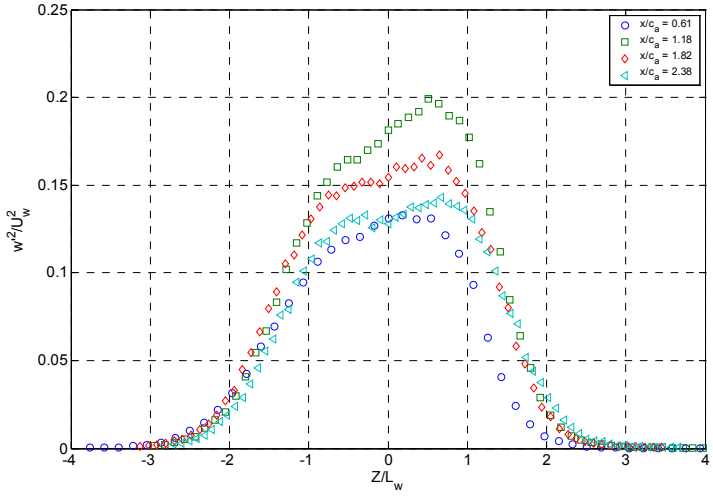

(d)

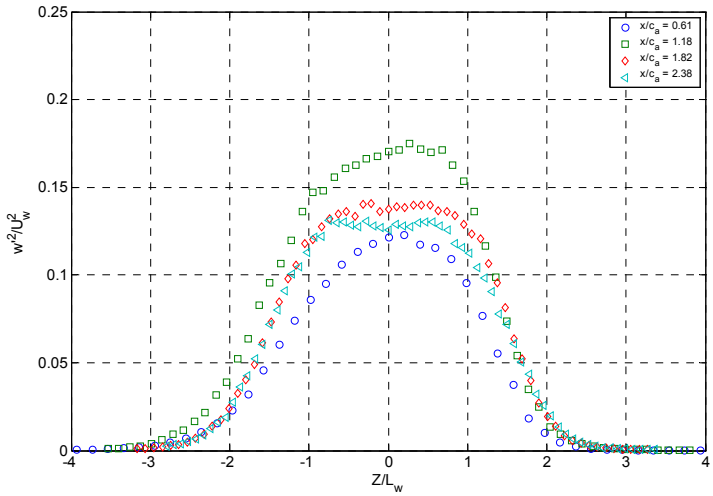

(e)

Figure 5-87: Cross-wake Reynolds stress profiles, $\overline{w'^2/U_w^2}$ at five spanwise locations across one serration for the 2.54 cm serration: **(a)** $y/c_a = 0.72$, **(b)** $y/c_a = 0.79$, **(c)** $y/c_a = 0.87$, **(d)** $y/c_a = 0.95$, **(e)** $y/c_a = 1.021$

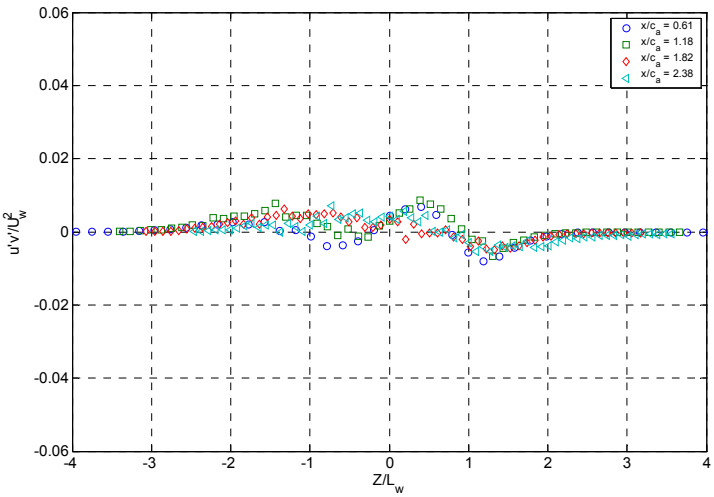

(a)

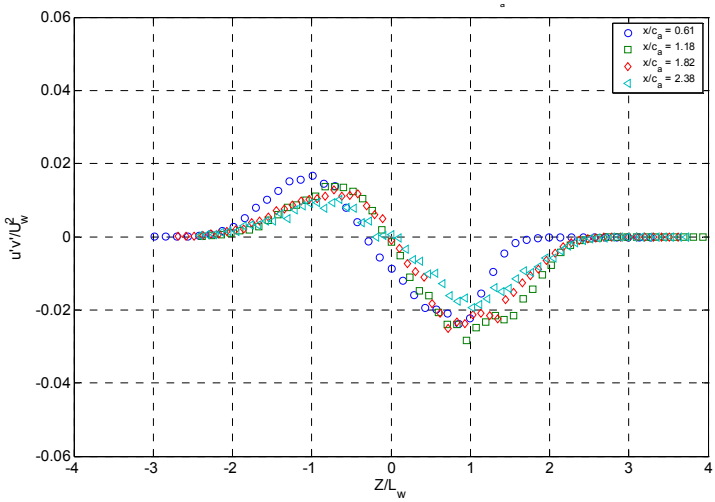

(b)

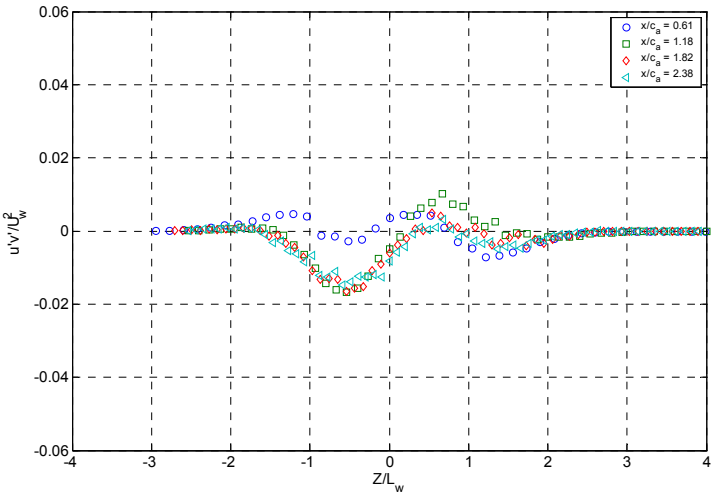

(c)

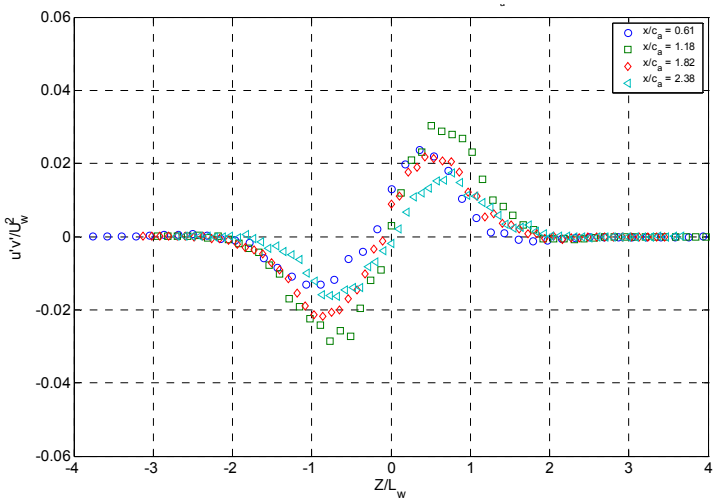

(d)

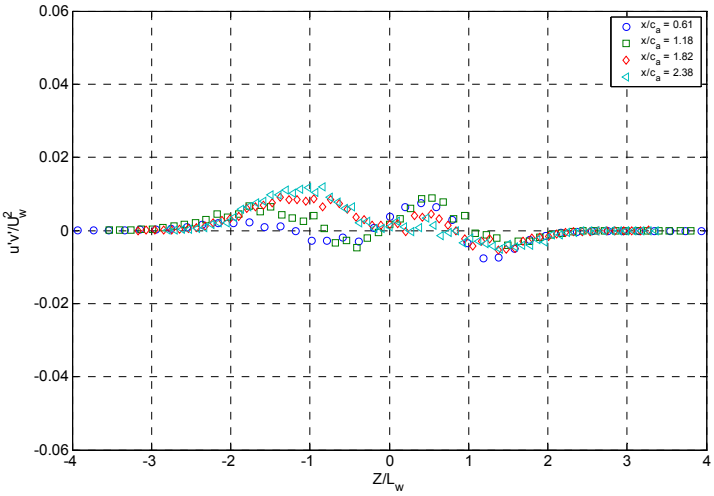

(e)

Figure 5-88: Reynolds shear stress profiles, $\overline{u'v'/U_w^2}$ at five spanwise locations across one serration for the 2.54 cm serration: **(a)** $y/c_a = 0.72$, **(b)** $y/c_a = 0.79$, **(c)** $y/c_a = 0.87$, **(d)** $y/c_a = 0.95$, **(e)** $y/c_a = 1.021$

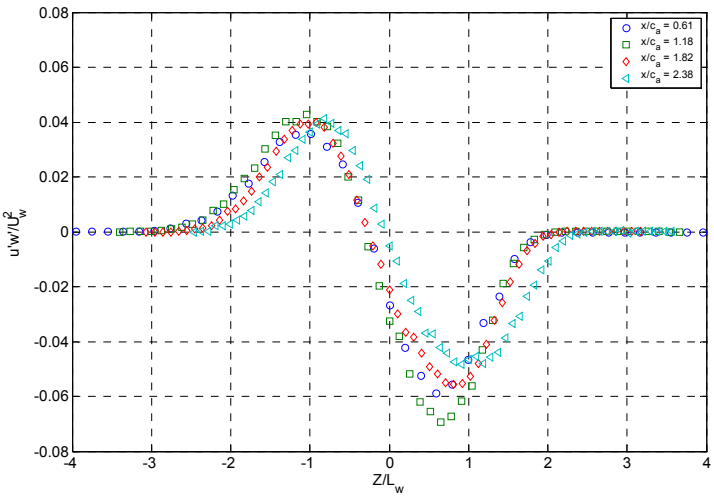

(a)

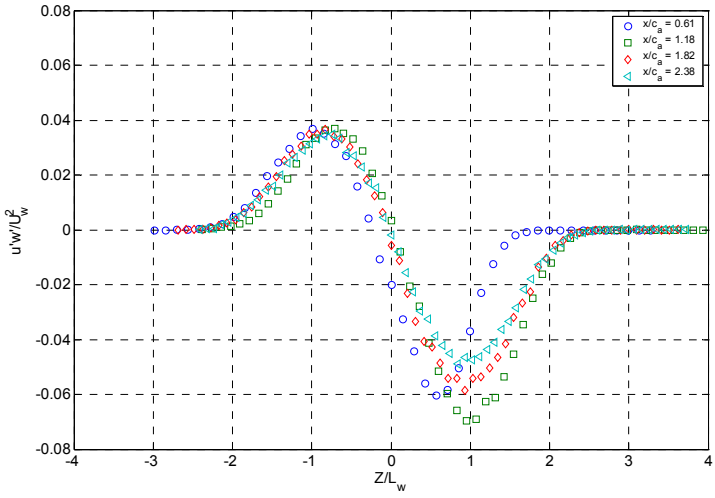

(b)

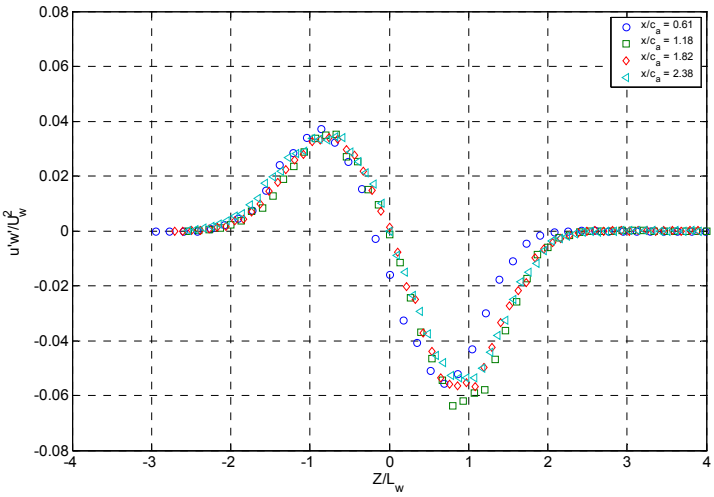

(c)

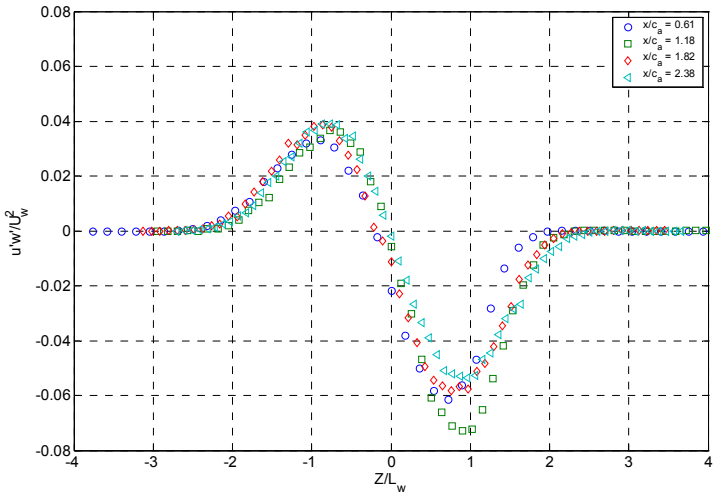

(d)

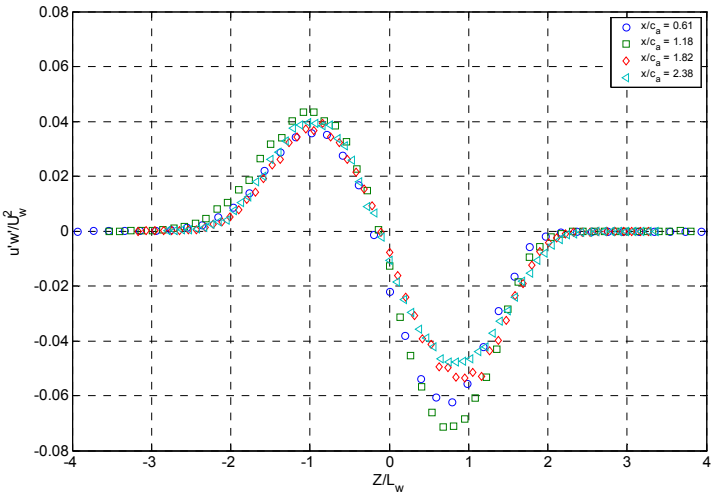

(e)

Figure 5-89: Reynolds shear stress profiles, $\overline{u'w'/U_w^2}$ at five spanwise locations across one serration for the 2.54 cm serration: **(a)** $y/c_a = 0.72$, **(b)** $y/c_a = 0.79$, **(c)** $y/c_a = 0.87$, **(d)** $y/c_a = 0.95$, **(e)** $y/c_a = 1.021$

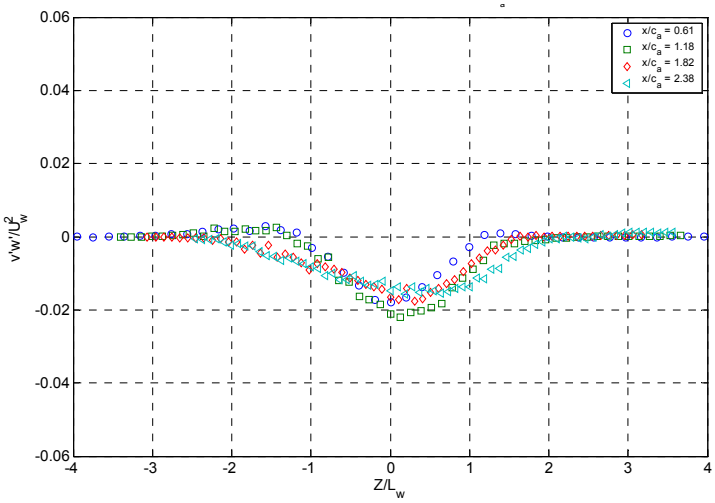

(a)

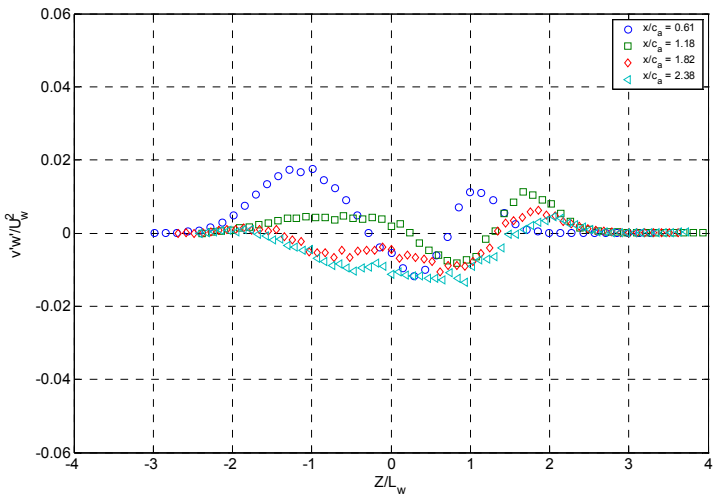

(b)

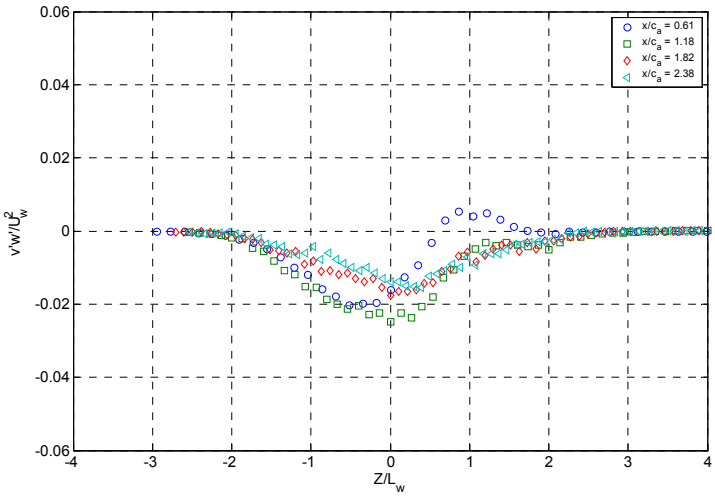

(c)

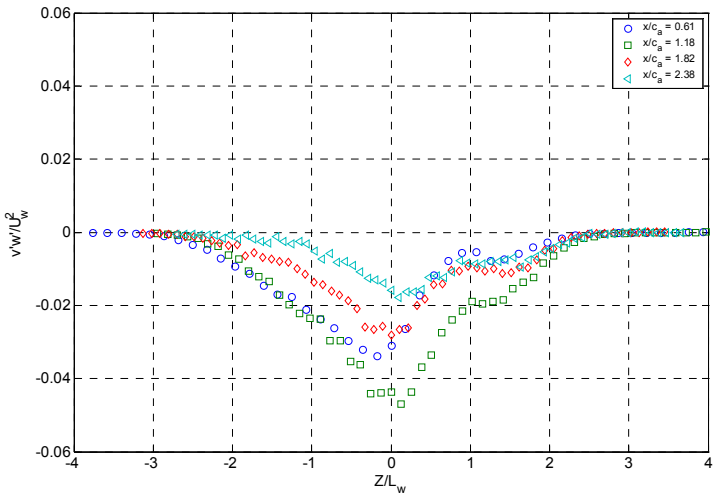

(d)

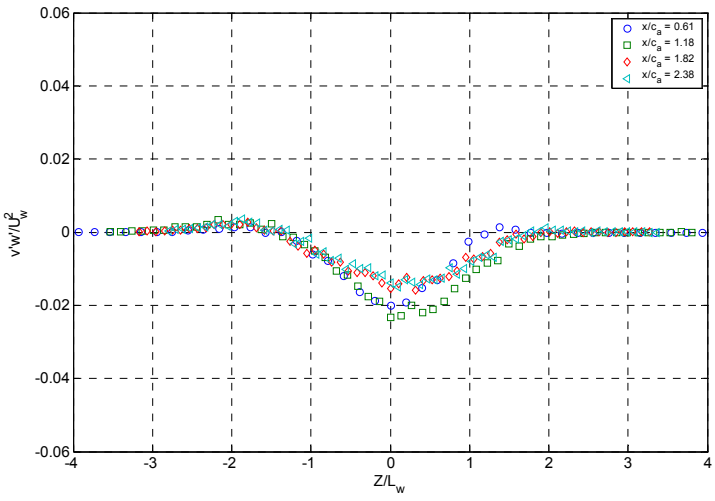

(e)

Figure 5-90: Reynolds shear stress profiles, $\overline{v'w'/U_w^2}$ at five spanwise locations across one serration for the 2.54 cm serration: **(a)** $y/c_a = 0.72$, **(b)** $y/c_a = 0.79$, **(c)** $y/c_a = 0.87$, **(d)** $y/c_a = 0.95$, **(e)** $y/c_a = 1.021$

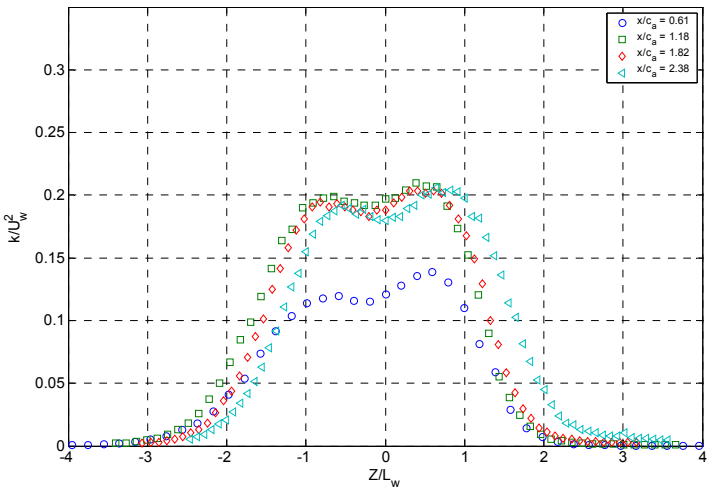

(a)

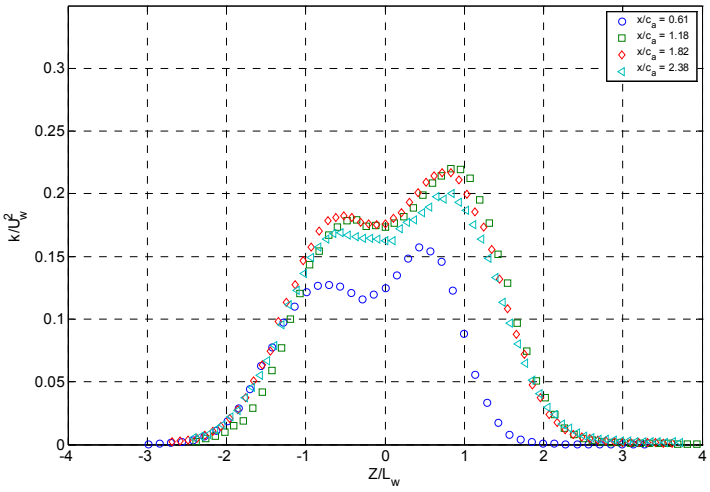

(b)

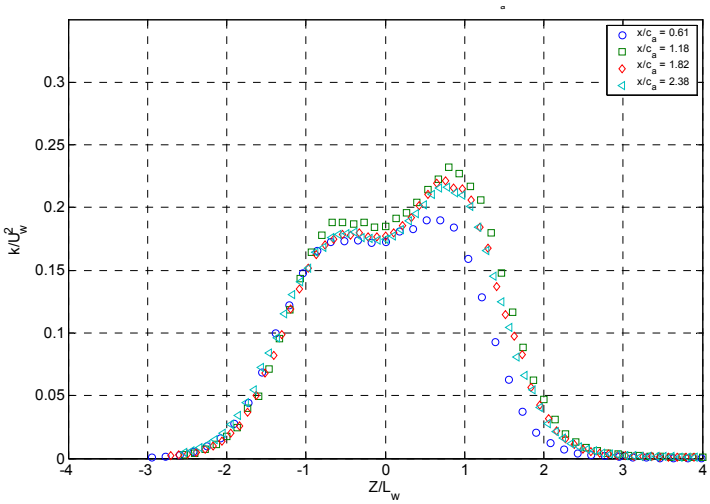

(c)

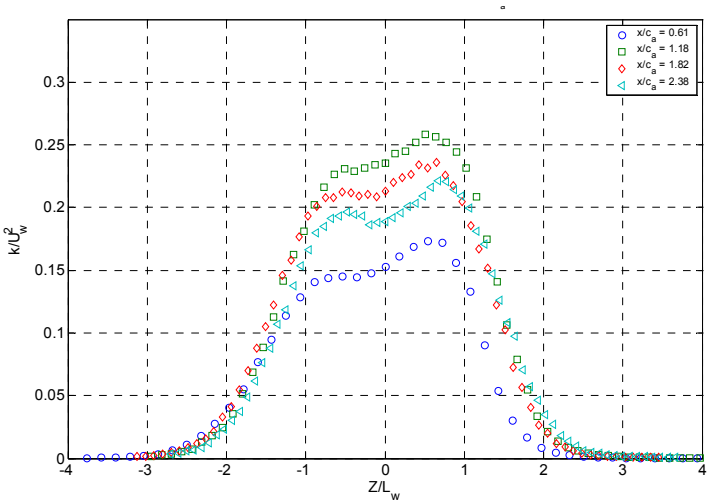

(d)

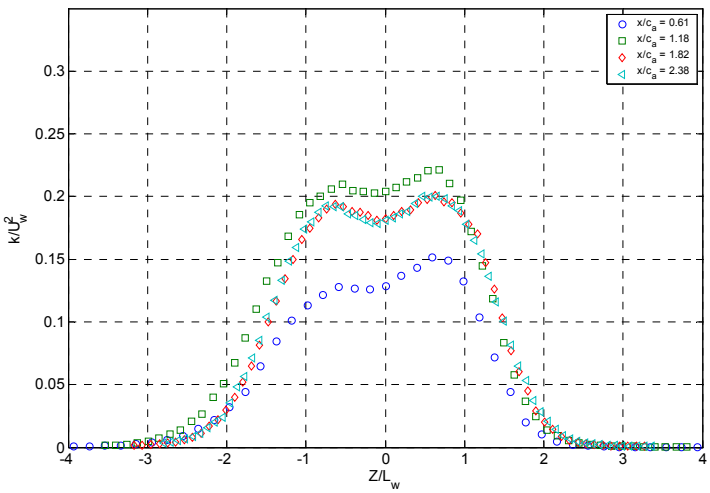

(e)

Figure 5-91: Turbulence kinetic energy profiles, k/U_w^2 at five locations spanwise locations across one serration for the 2.54 cm serration: **(a)** $y/c_a = 0.72$, **(b)** $y/c_a = 0.79$, **(c)** $y/c_a = 0.87$, **(d)** $y/c_a = 0.95$, **(e)** $y/c_a = 1.021$

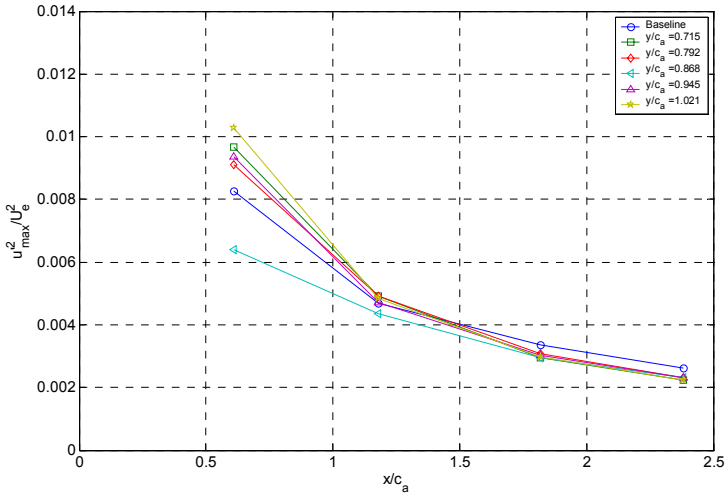

(a)

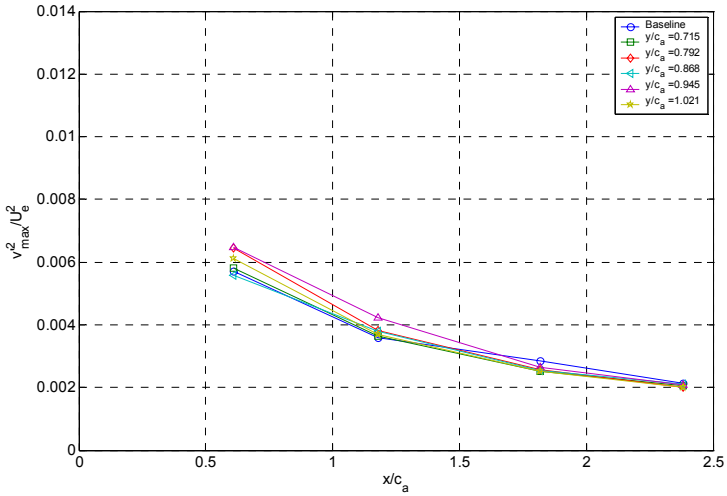

(b)

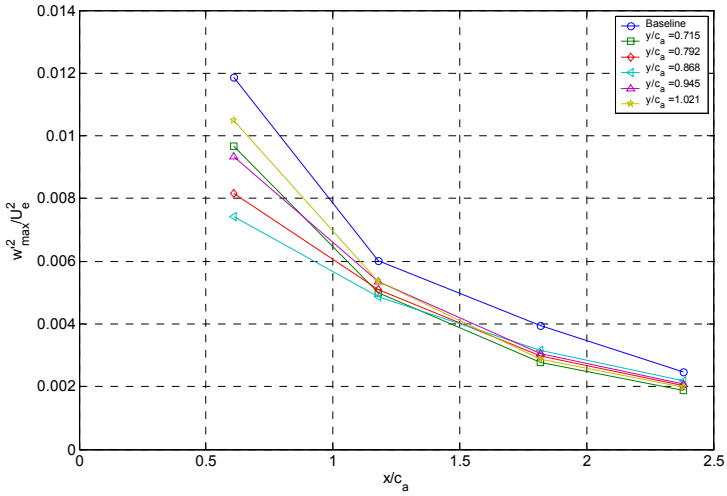

(c)

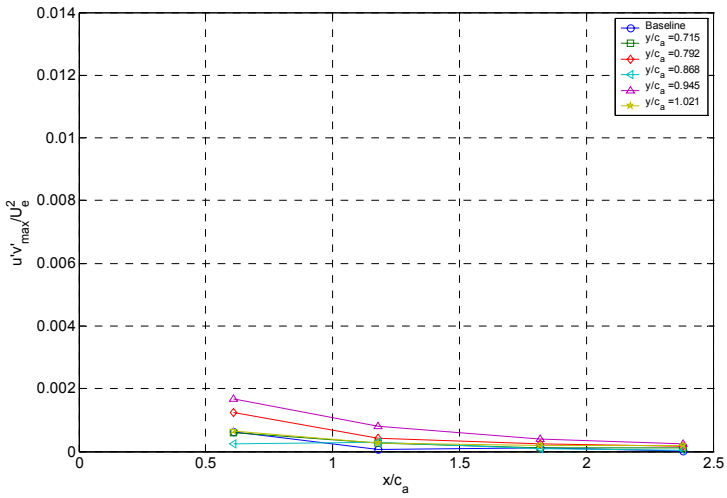

(d)

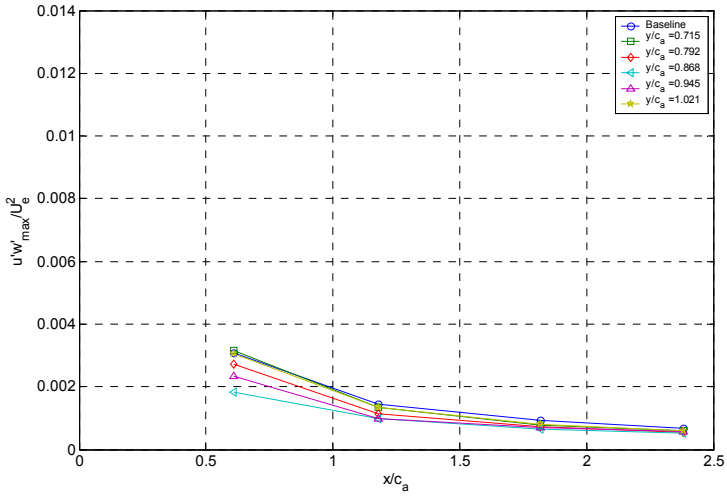

(e)

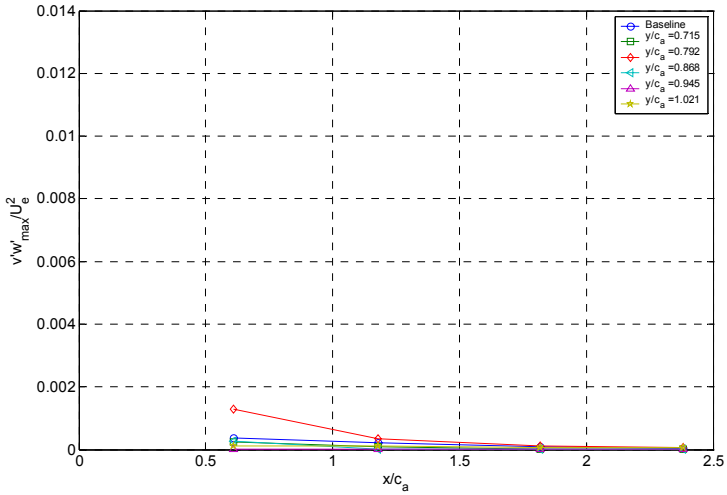

(f)

Figure 5-92: Maximum normalized Reynolds stress levels at five spanwise locations across one serration for the 2.54 cm serration compared to the baseline: **(a)** $\overline{|u'^2/U_\infty^2|}_{max}$, **(b)** $\overline{|v'^2/U_\infty^2|}_{max}$, **(c)** $\overline{|w'^2/U_\infty^2|}_{max}$, **(d)** $\overline{|u'v'/U_\infty^2|}_{max}$, **(e)** $\overline{|u'w'/U_\infty^2|}_{max}$, **(f)** $\overline{|v'w'/U_\infty^2|}_{max}$

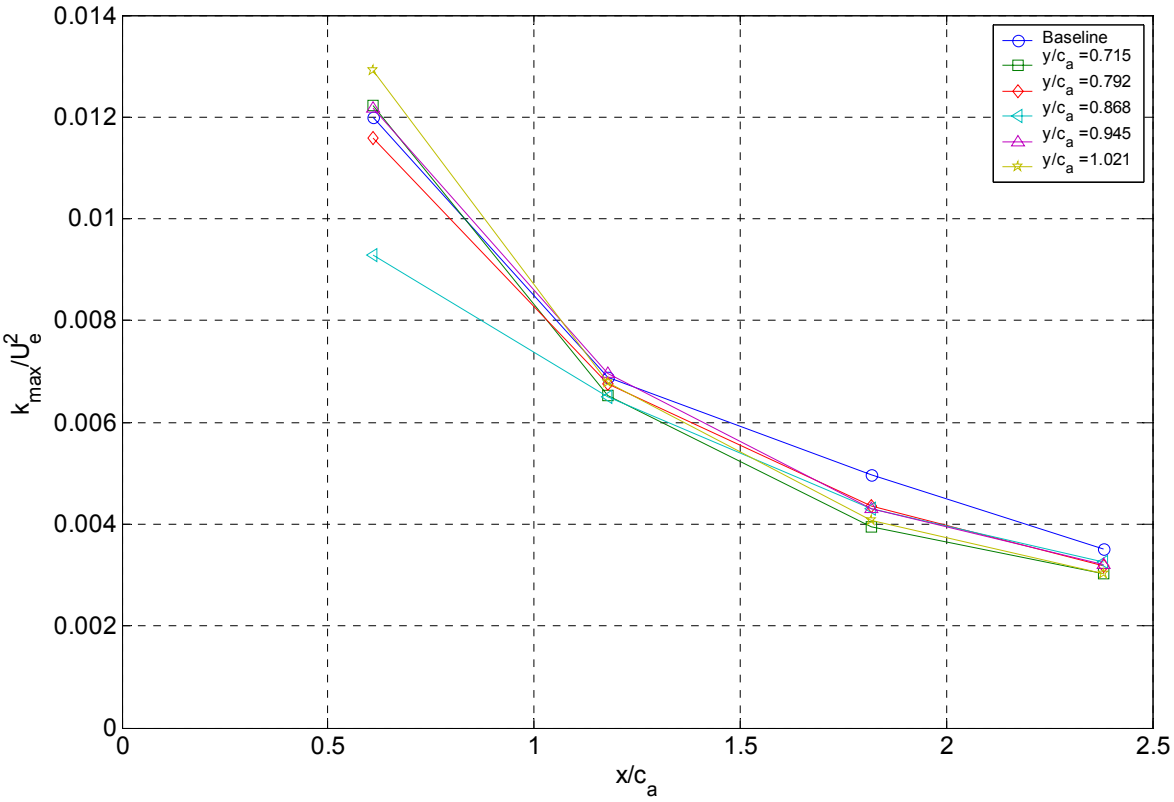

Figure 5-93: Maximum normalized turbulence kinetic energy, $|k/U_w^2|_{max}$, at five spanwise locations across one serration for the 2.54 cm serration compared to the baseline,

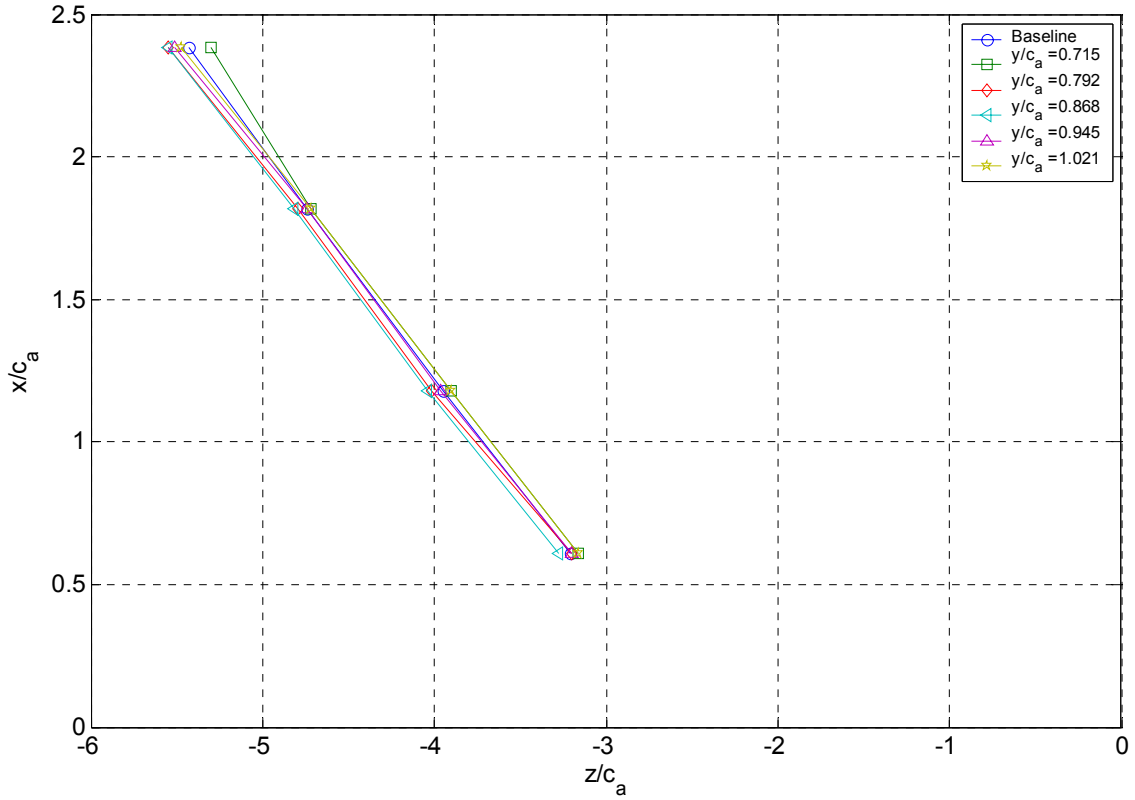

Figure 5-94: Propagation of the minimum velocity point in the wake for the 2.54 cm serration compared to the baseline case

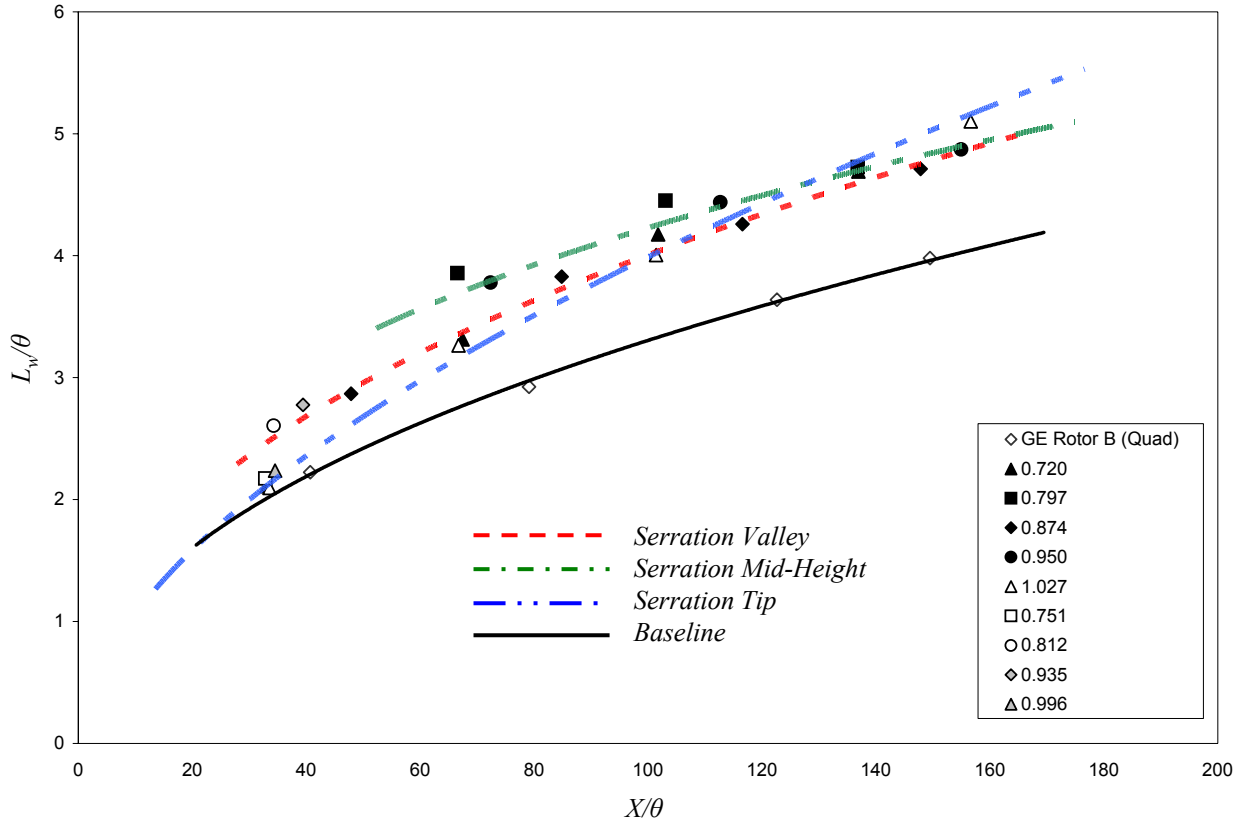

Figure 5-95: Normalized wake half-width of the wake, L_w/θ, as a function of normalized downstream distance, X/θ, for the 2.54 cm droop serration.

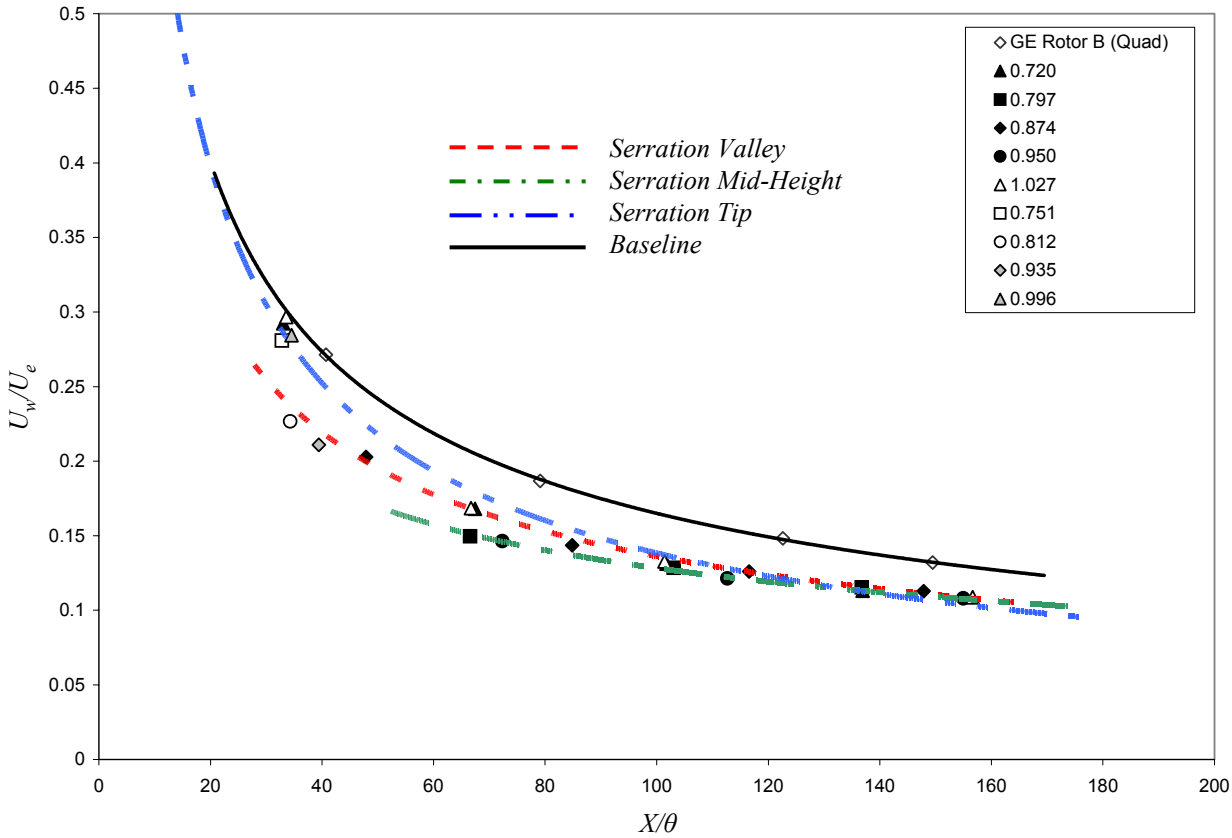

Figure 5-96: Normalized maximum velocity deficit in the wake, U_w/U_e, function of the normalized downstream distance, X/θ, for the 2.54 cm droop serration.

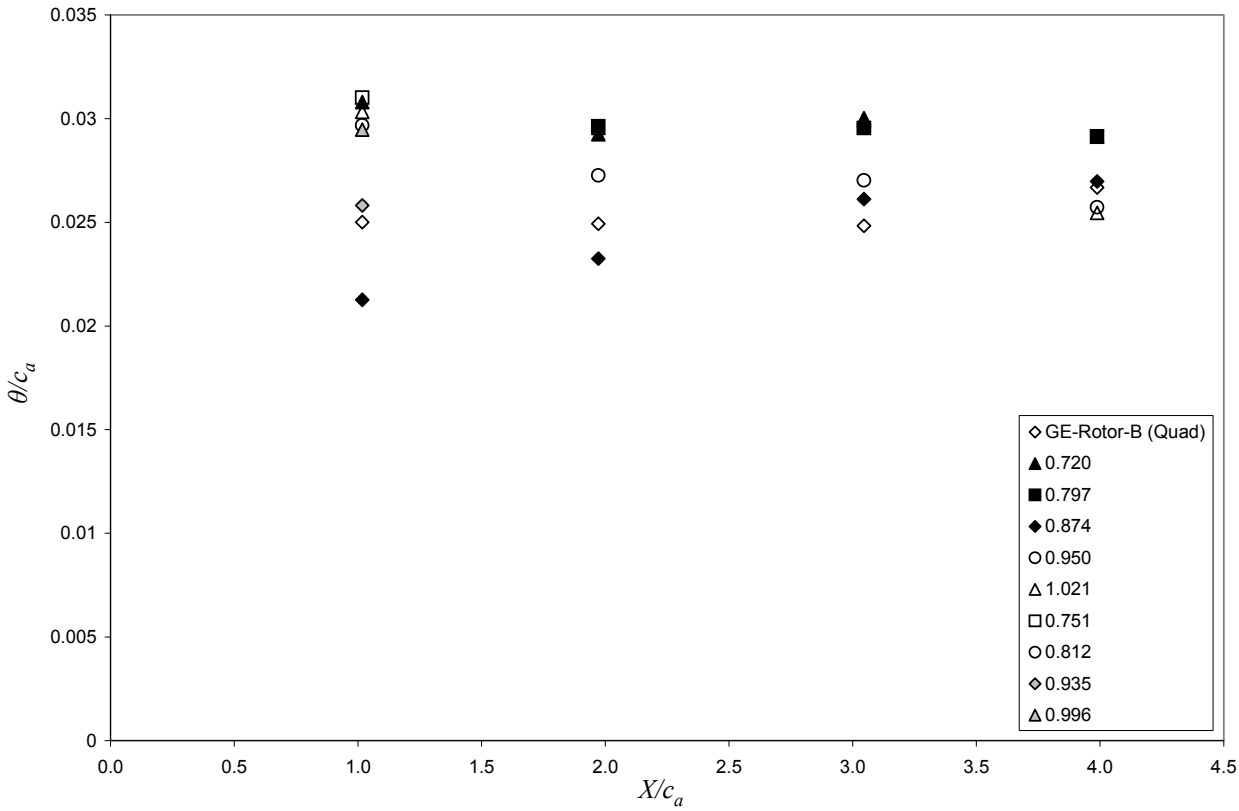

Figure 5-97: Normalized momentum thickness, θ/c_a, as a function of normalized distance downstream, X/c_a, for the 2.54 cm droop serration.

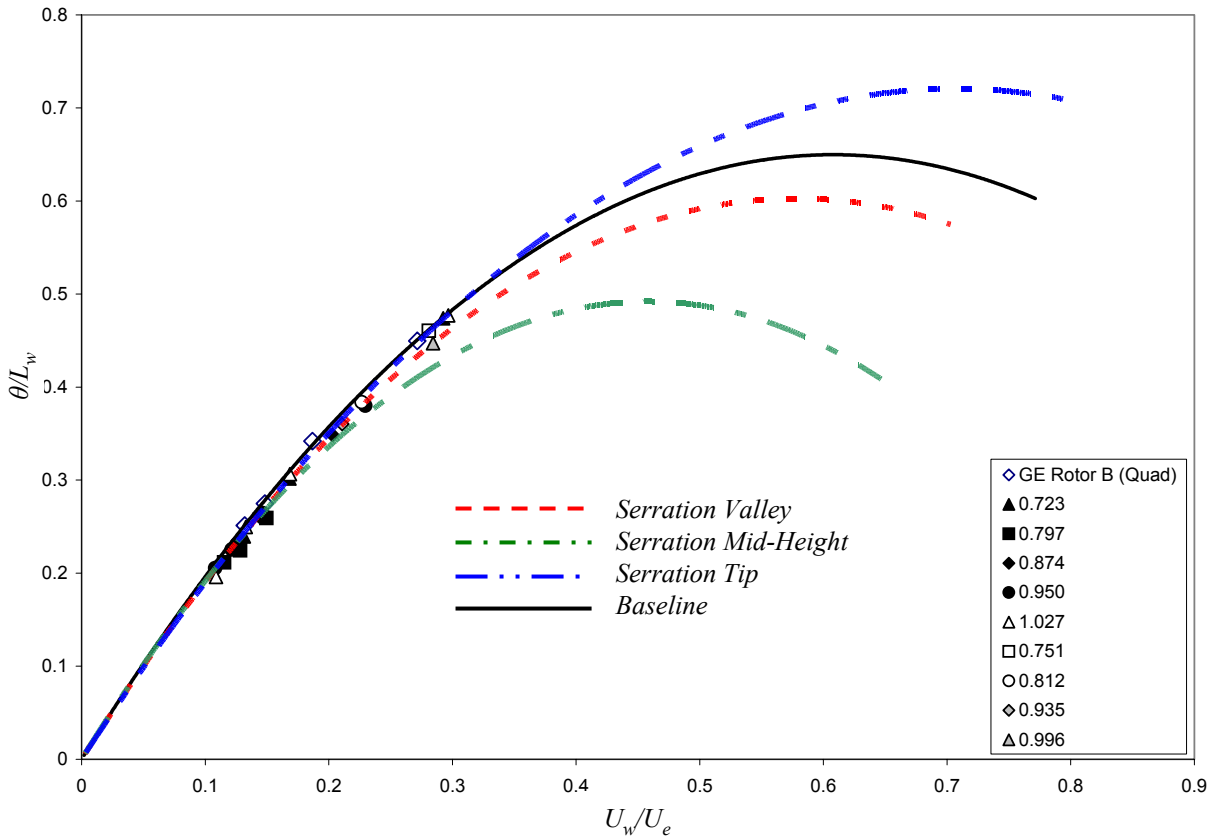

Figure 5-98: Normalized momentum thickness, θ/L_w as a function of normalized velocity deficit of wake, U_w/U_e, for the 1.27 cm droop serration.

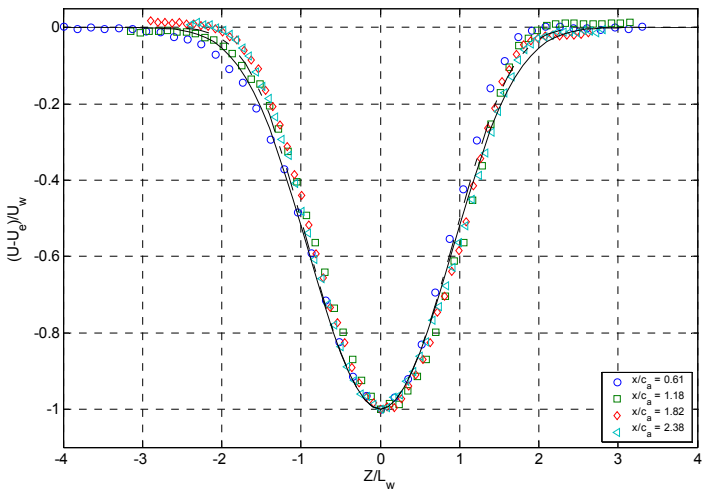

(a)

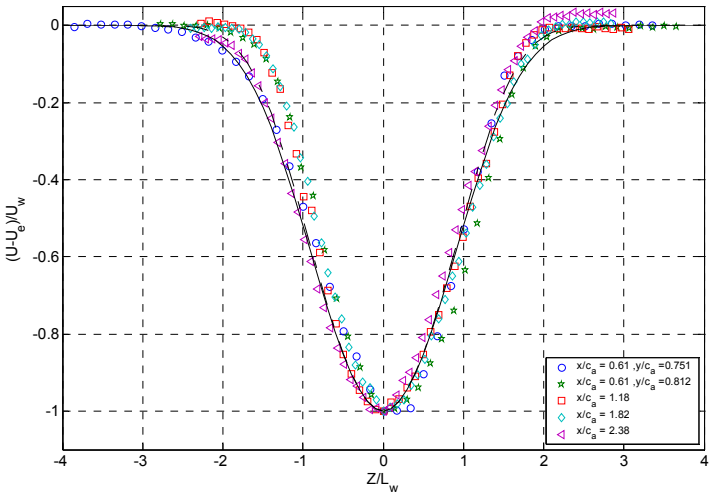

(b)

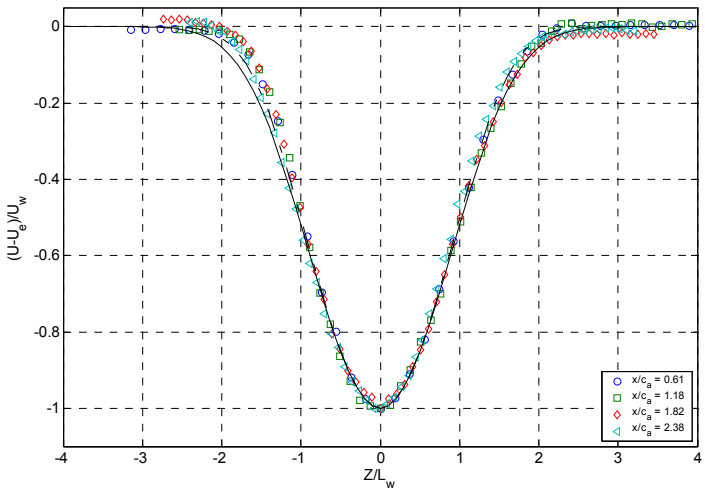

(c)

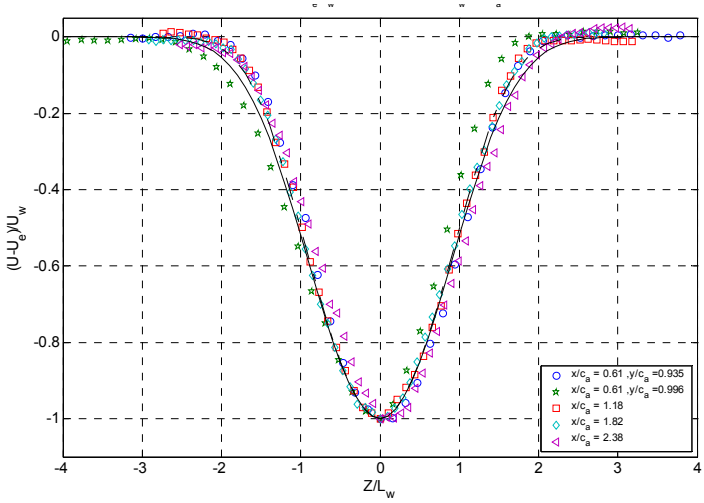

(d)

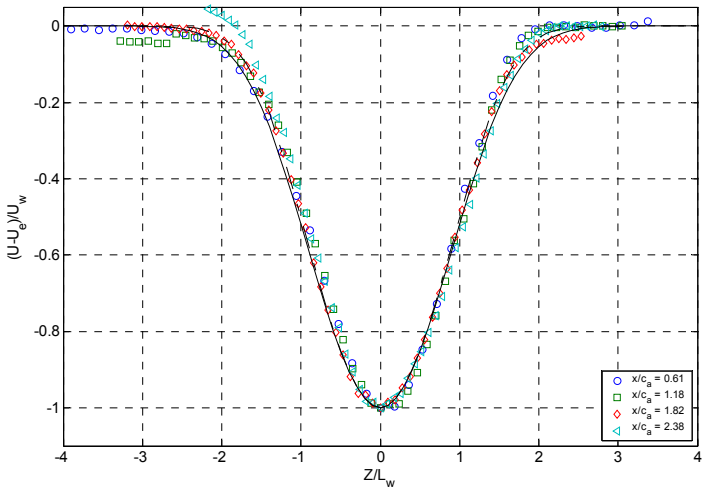

(e)

$$\frac{U-U_e}{U_w} = -\exp\left(-0.632\frac{z^2}{L_w^2} - 0.0612\frac{z^4}{L_2^4}\right)$$

$$\frac{U-U_e}{U_w} = -\exp\left(-0.632\frac{z^2}{L_w^2} - 0.0247\frac{z^4}{L_2^4}\right)$$

Figure 5-99: Streamwise mean velocity profile, $(U\text{-}U_e)/U_w$ at five spanwise locations across one serration for the 2.54 cm droop serration: **(a)** $y/c_a = 0.72$, **(b)** $y/c_a = 0.80$, **(c)** $y/c_a = 0.87$, **(d)** $y/c_a = 0.95$, **(e)** $y/c_a = 1.021$

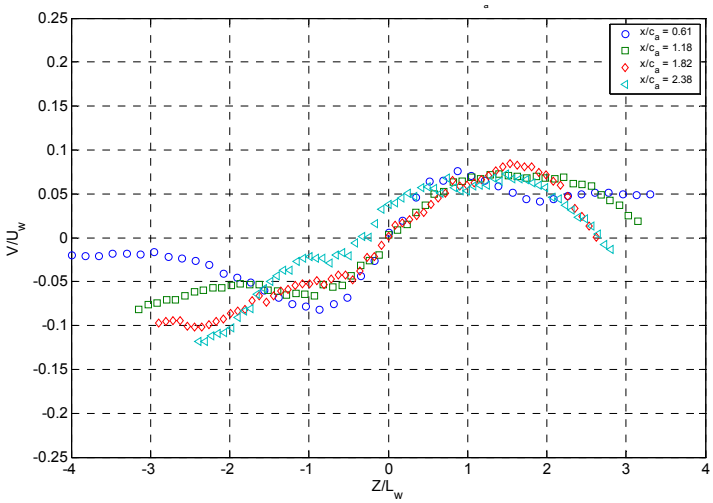

(a)

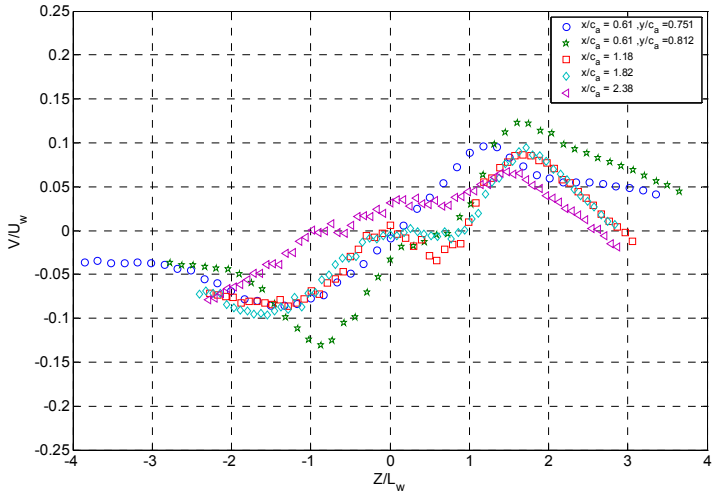

(b)

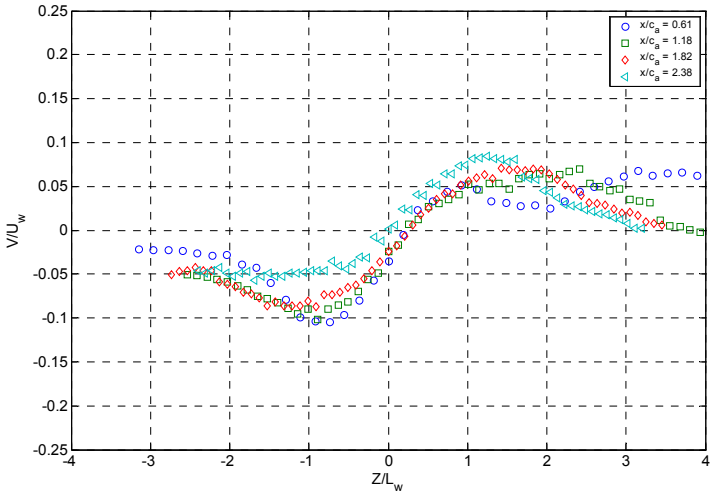

(c)

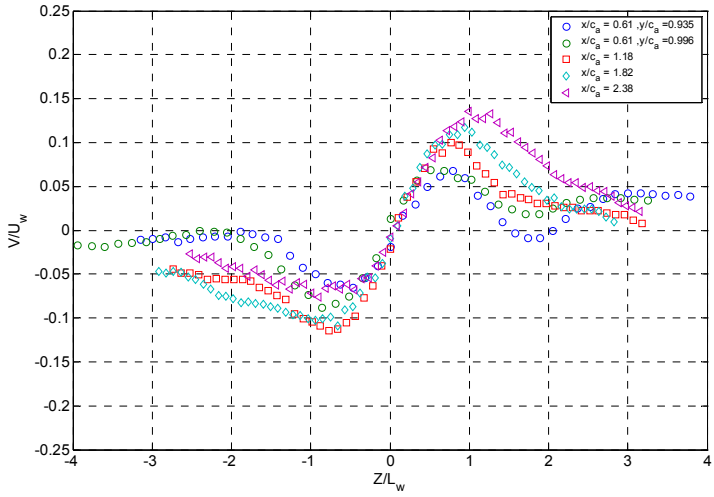

(d)

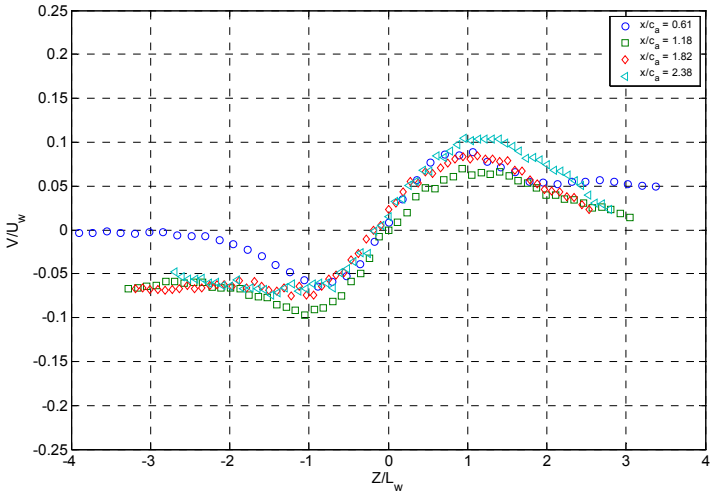

(e)

Figure 5-100: Spanwise mean velocity profiles, $V/U_{w.}$ at five spanwise locations across one serration for the 2.54 cm droop serration: **(a)** $y/c_a = 0.72$, **(b)** $y/c_a = 0.80$, **(c)** $y/c_a = 0.87$, **(d)** $y/c_a = 0.95$, **(e)** $y/c_a = 1.021$

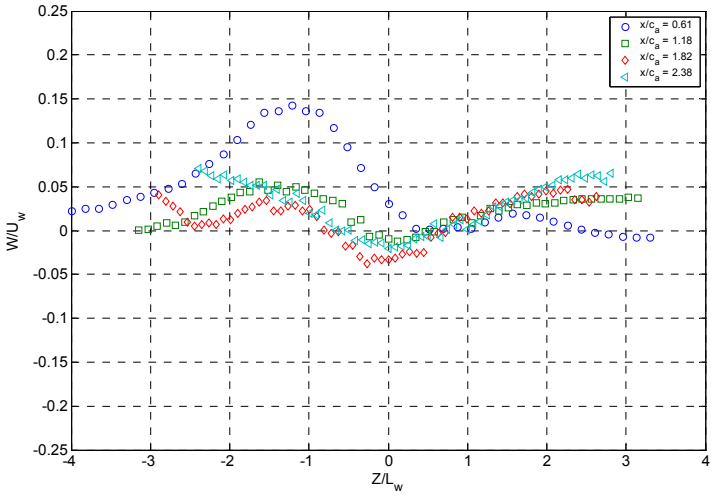

(a)

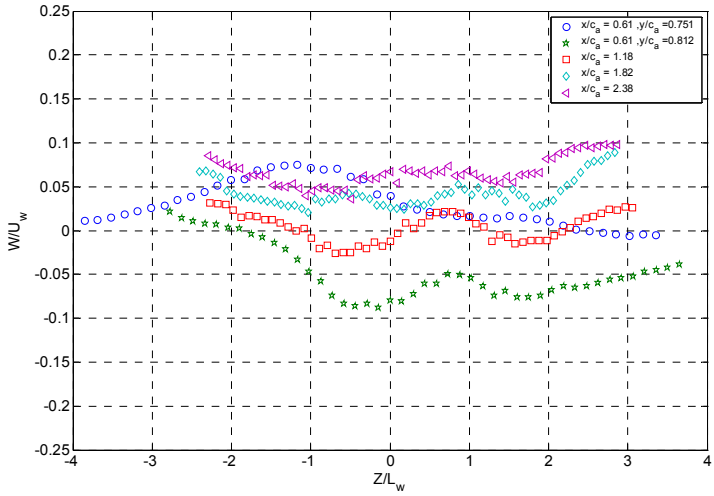

(b)

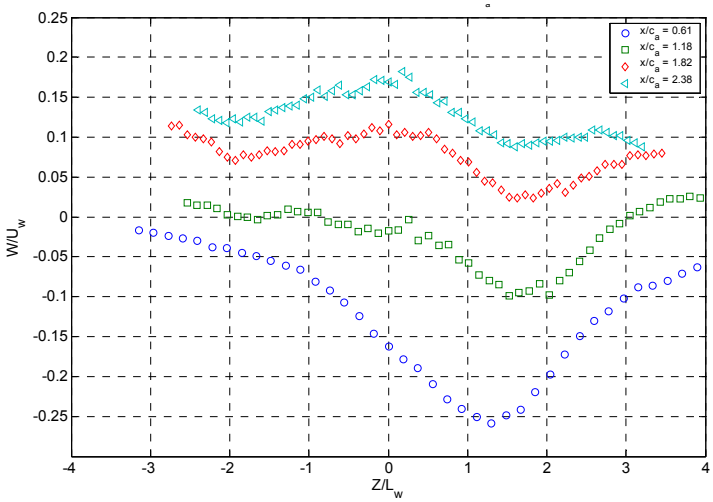

(c)

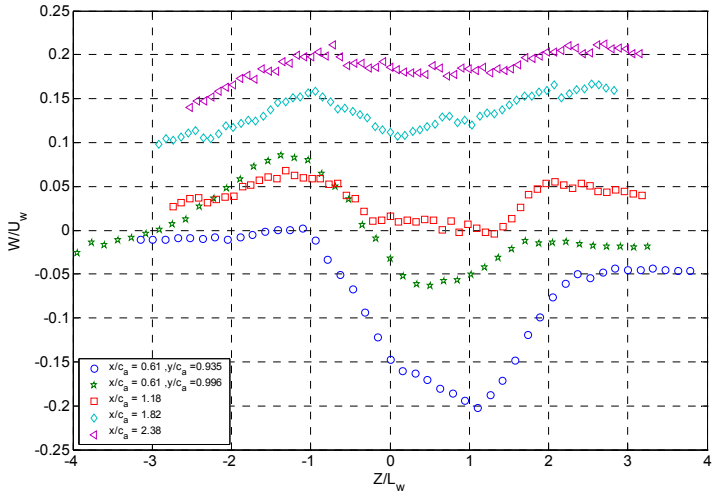

(d)

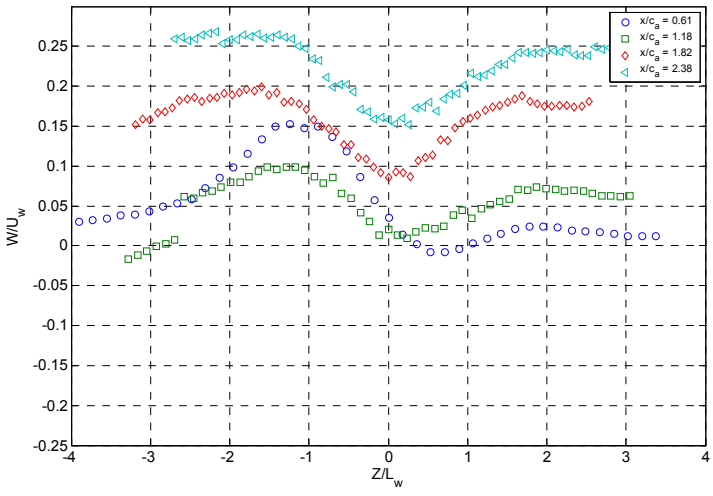

(e)

Figure 5-101: Cross-wake mean velocity profiles, $W/U_{w.}$ at five spanwise locations across one serration for the 2.54 cm droop serration: **(a)** $y/c_a = 0.72$, **(b)** $y/c_a = 0.80$, **(c)** $y/c_a = 0.87$, **(d)** $y/c_a = 0.95$, **(e)** $y/c_a = 1.021$

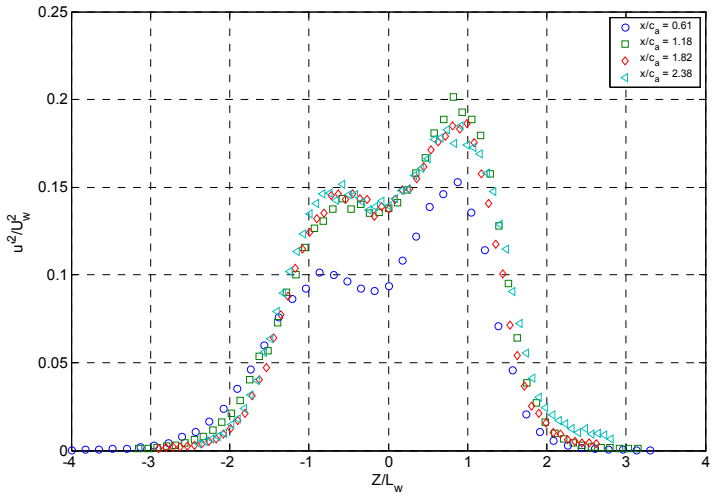

(a)

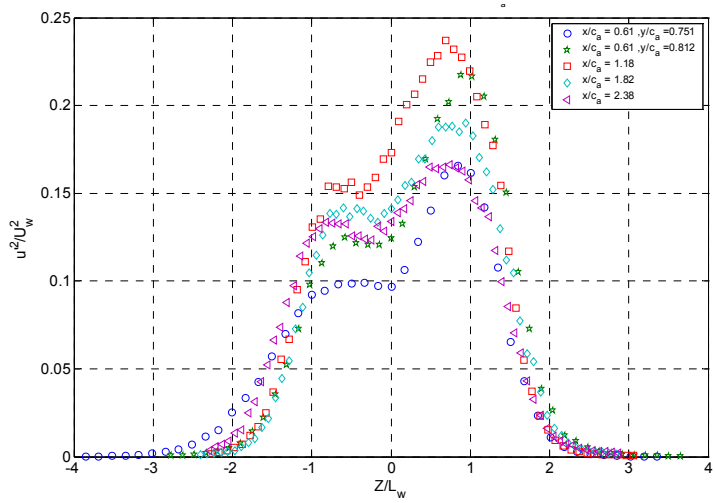

(b)

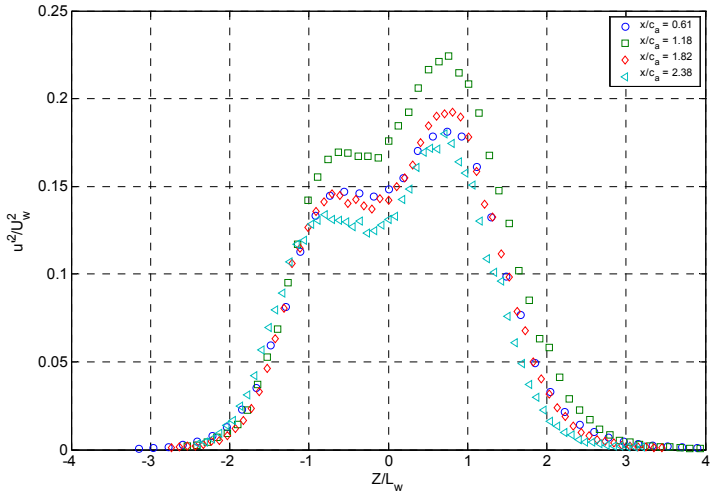

(c)

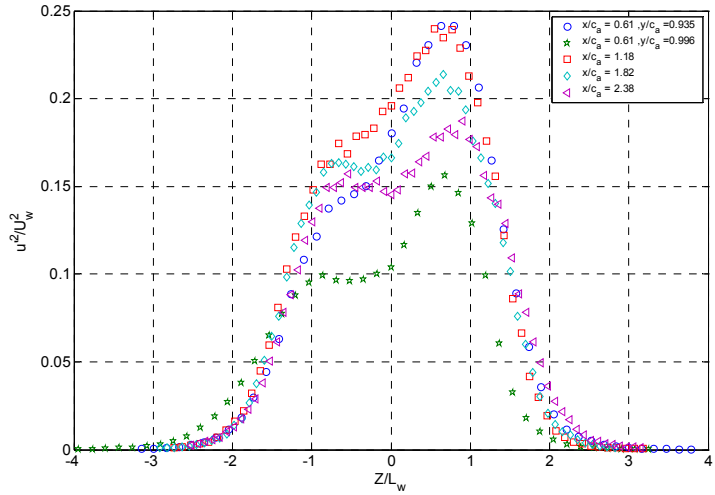

(d)

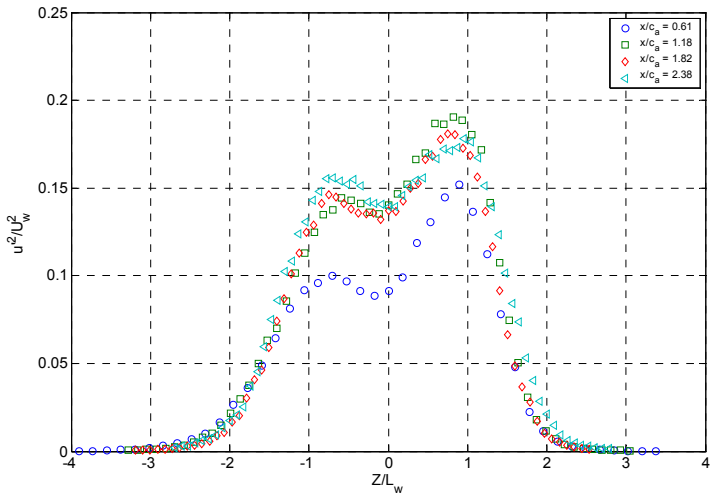

(e)

Figure 5-102: Streamwise Reynolds stress profiles, $\overline{u'^2/U_w^2}$ at five spanwise locations across one serration for the 2.54 cm droop serration: **(a)** $y/c_a = 0.72$, **(b)** $y/c_a = 0.80$, **(c)** $y/c_a = 0.87$, **(d)** $y/c_a = 0.95$, **(e)** $y/c_a = 1.021$

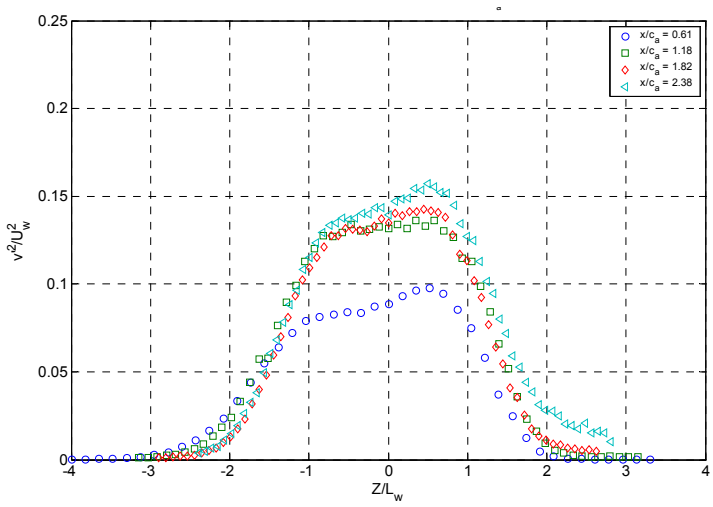

(a)

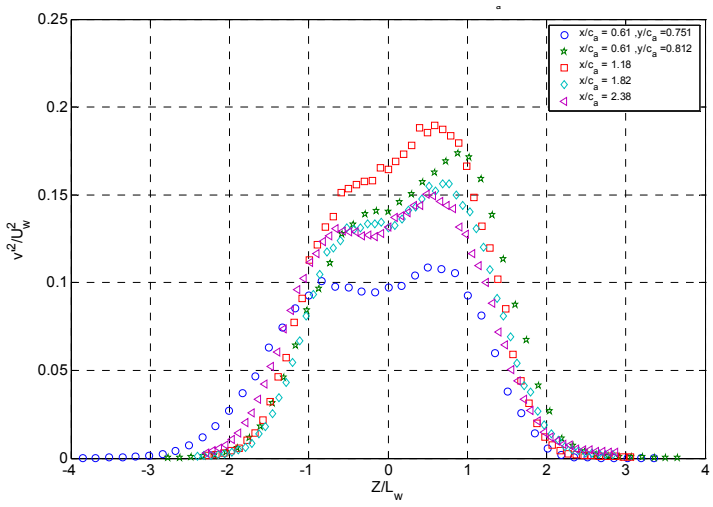

(b)

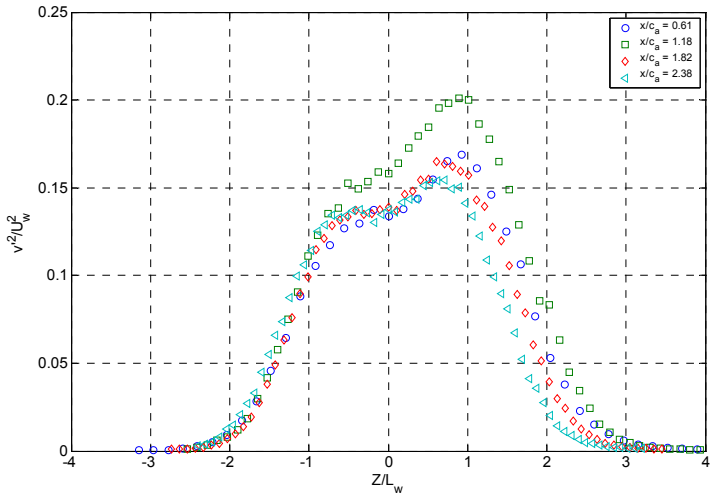

(c)

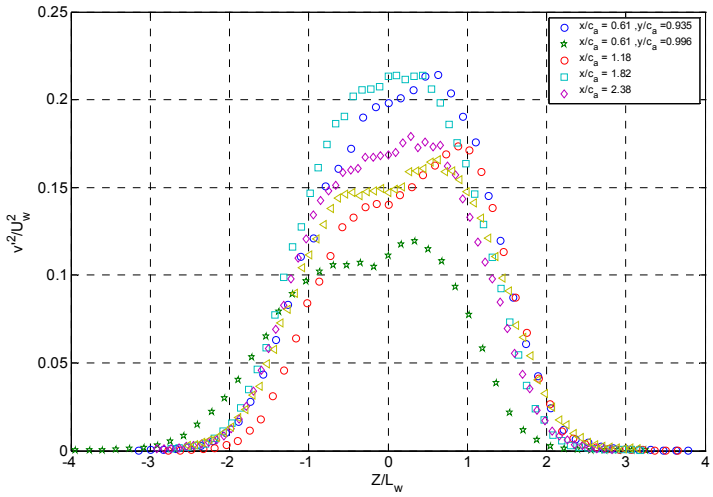

(d)

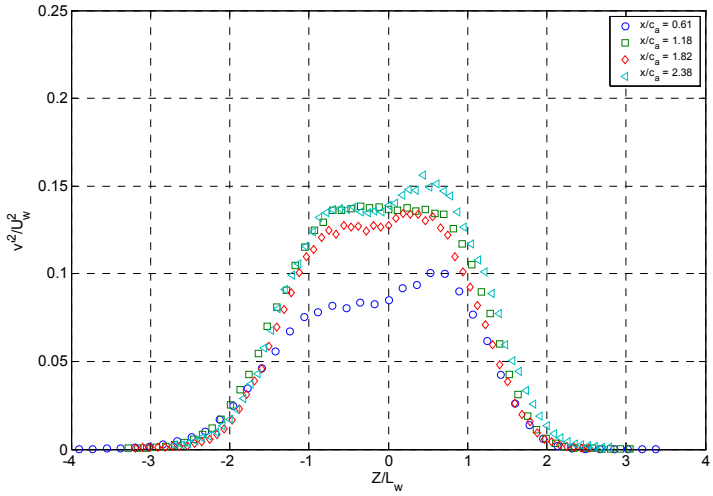

(e)

Figure 5-103: Spanwise Reynolds stress profiles, $\overline{v'^2/U_w^2}$ at five spanwise locations across one serration for the 2.54 cm droop serration: **(a)** $y/c_a = 0.72$, **(b)** $y/c_a = 0.80$, **(c)** $y/c_a = 0.87$, **(d)** $y/c_a = 0.95$, **(e)** $y/c_a = 1.021$

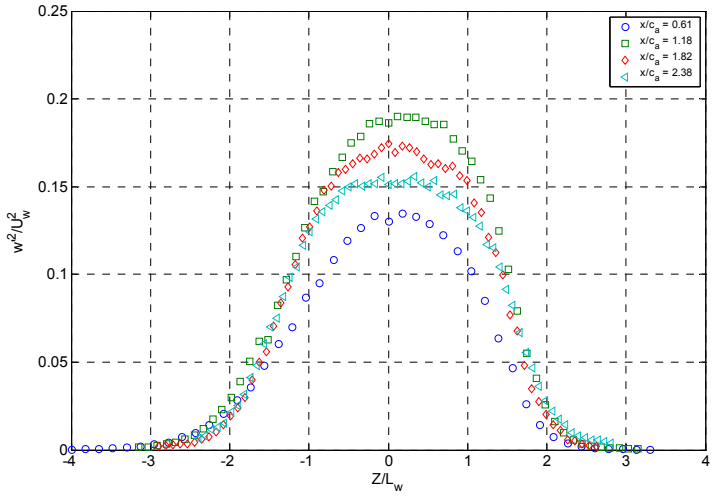

(a)

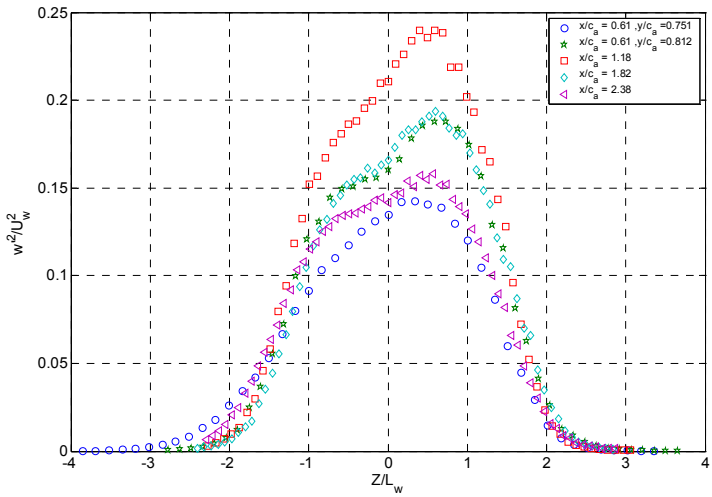

(b)

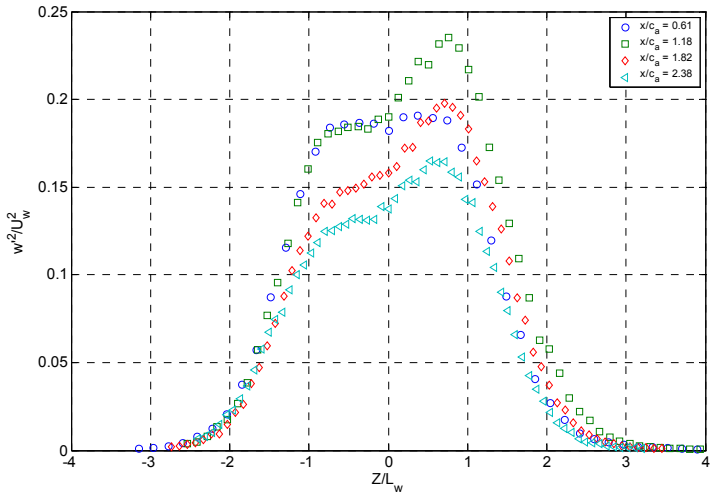

(c)

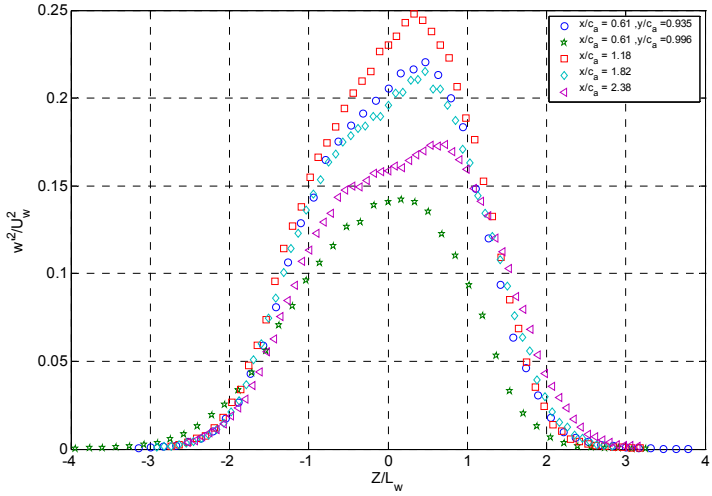

(d)

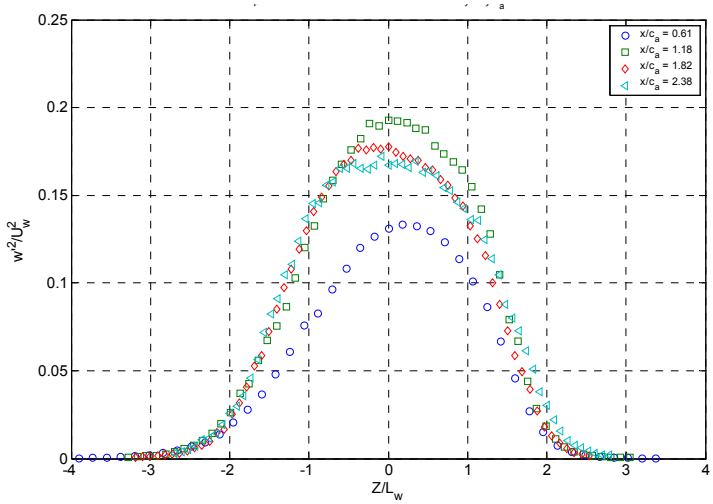

(e)

Figure 5-104: Cross-wake Reynolds stress profiles, $\overline{w'^2/U_w^2}$ at five spanwise locations across one serration for the 2.54 cm droop serration: **(a)** $y/c_a = 0.72$, **(b)** $y/c_a = 0.80$, **(c)** $y/c_a = 0.87$, **(d)** $y/c_a = 0.95$, **(e)** $y/c_a = 1.021$

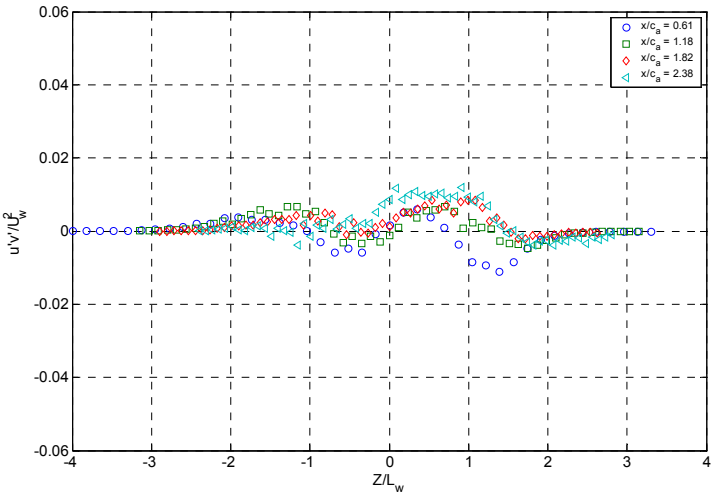

(a)

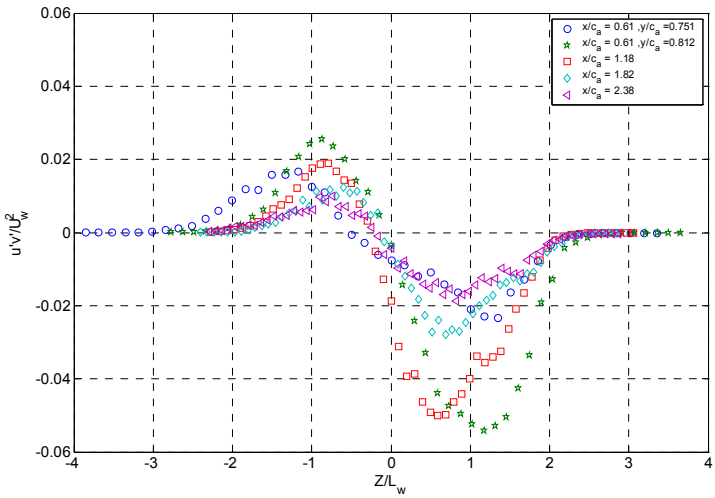

(b)

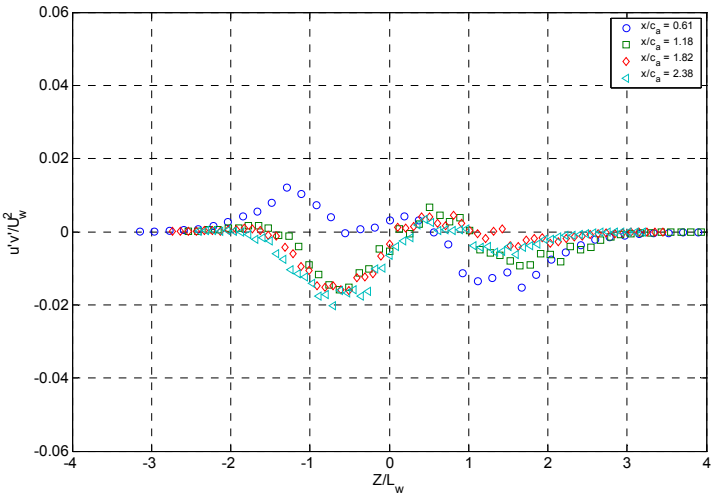

(c)

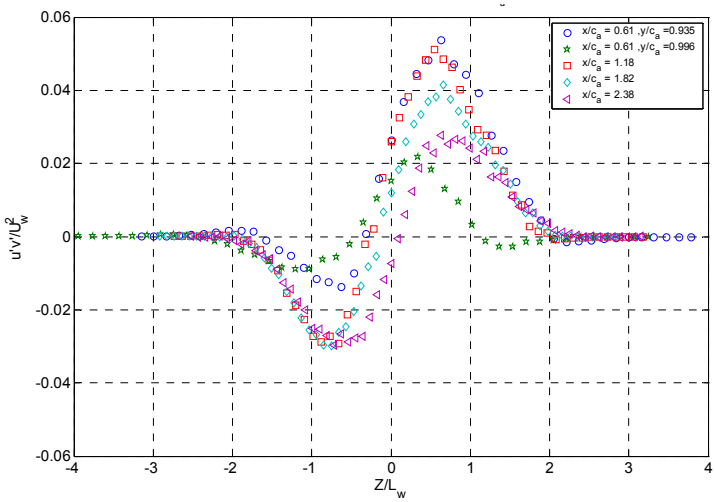

(d)

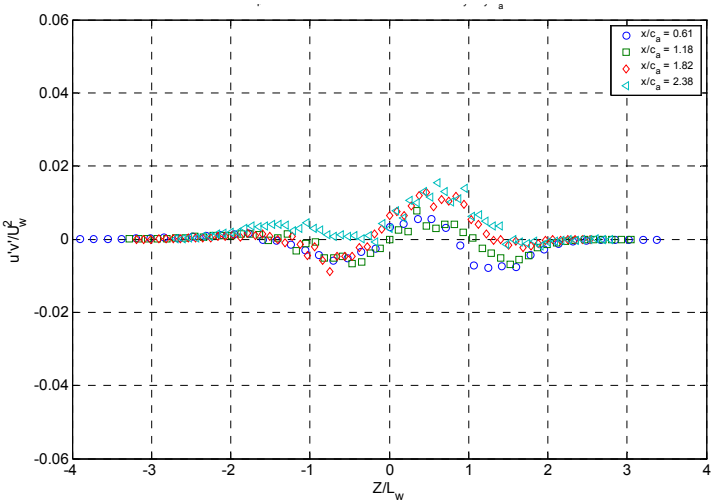

(e)

Figure 5-105: Reynolds shear stress profiles, $\overline{u'v'/U_w^2}$ at five spanwise locations across one serration for the 2.54 cm droop serration: **(a)** $y/c_a = 0.72$, **(b)** $y/c_a = 0.80$, **(c)** $y/c_a = 0.87$, **(d)** $y/c_a = 0.95$, **(e)** $y/c_a = 1.021$

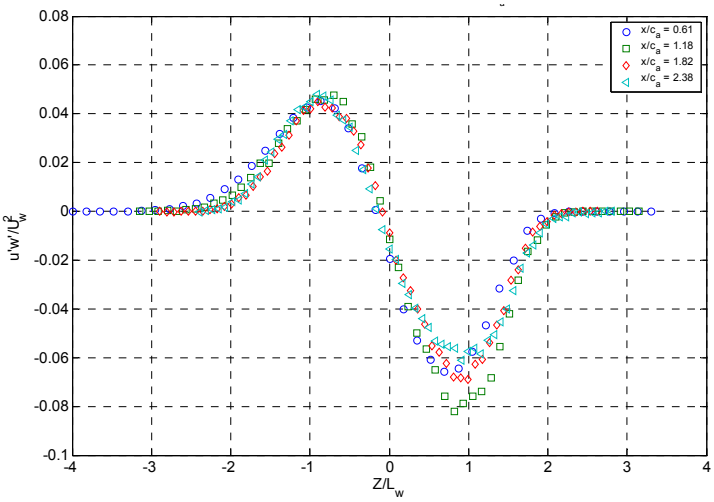

(a)

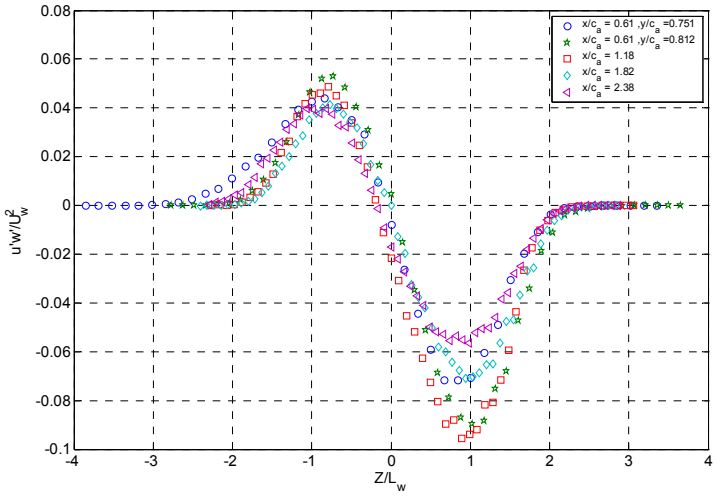

(b)

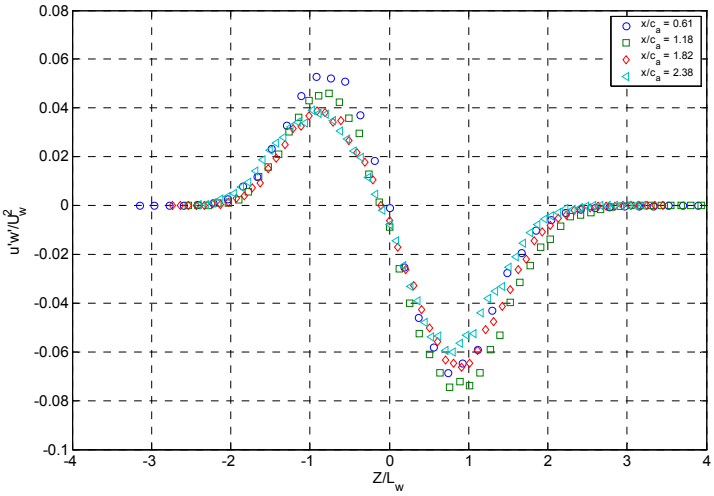

(c)

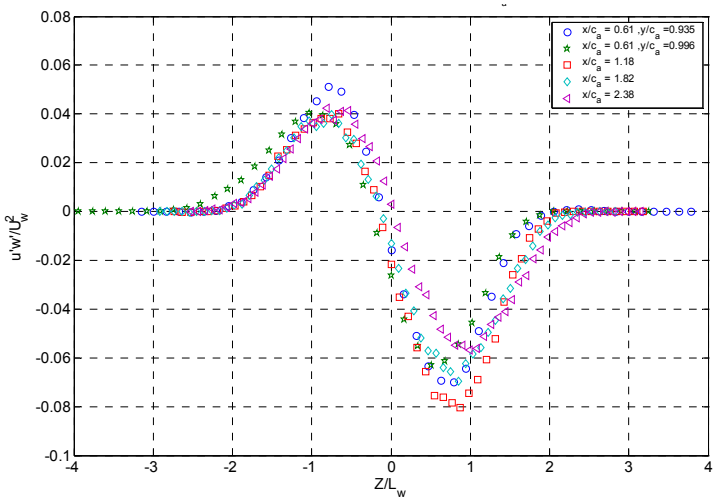

(d)

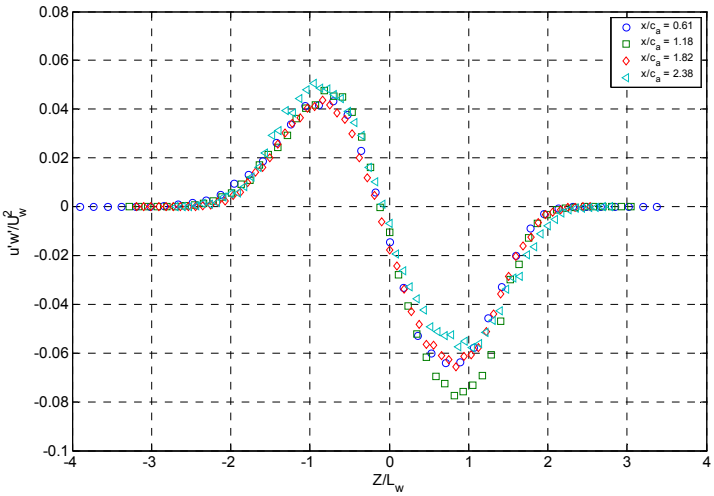

(e)

Figure 5-106: Reynolds shear stress profiles, $\overline{u'w'/U_w^2}$ at five spanwise locations across one serration for the 2.54 cm droop serration: **(a)** $y/c_a = 0.72$, **(b)** $y/c_a = 0.80$, **(c)** $y/c_a = 0.87$, **(d)** $y/c_a = 0.95$, **(e)** $y/c_a = 1.021$

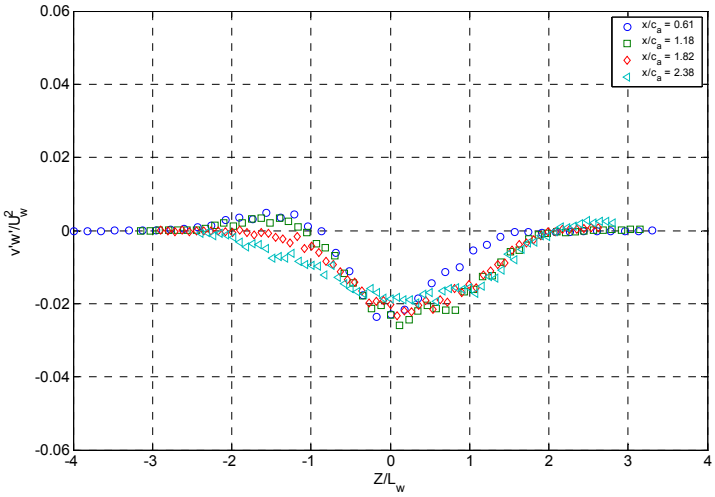

(a)

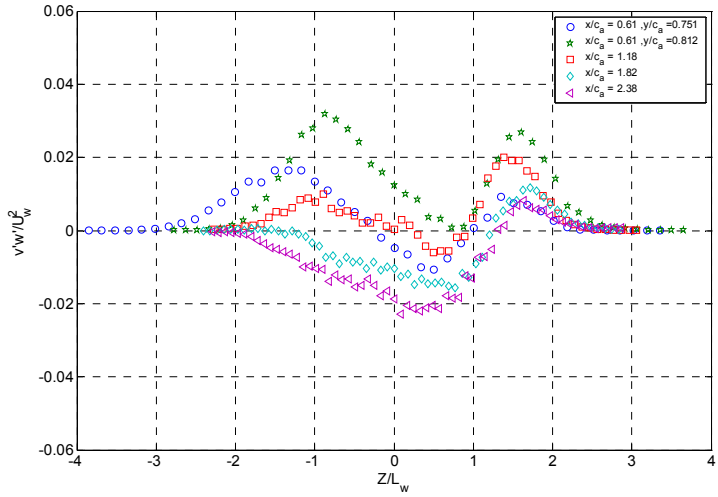

(b)

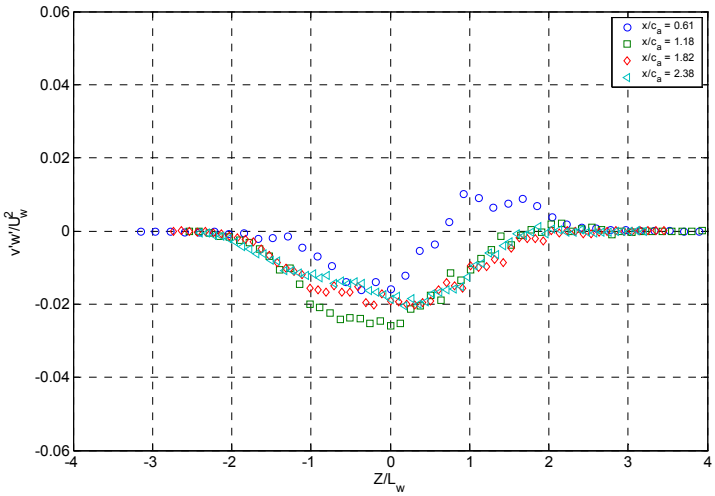

(c)

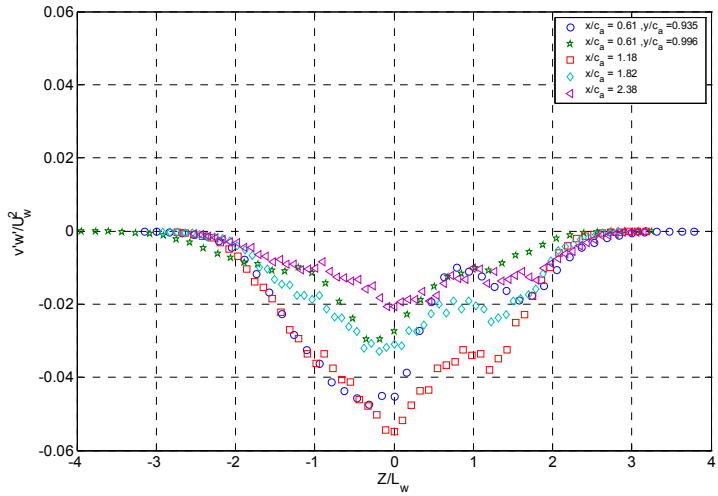

(d)

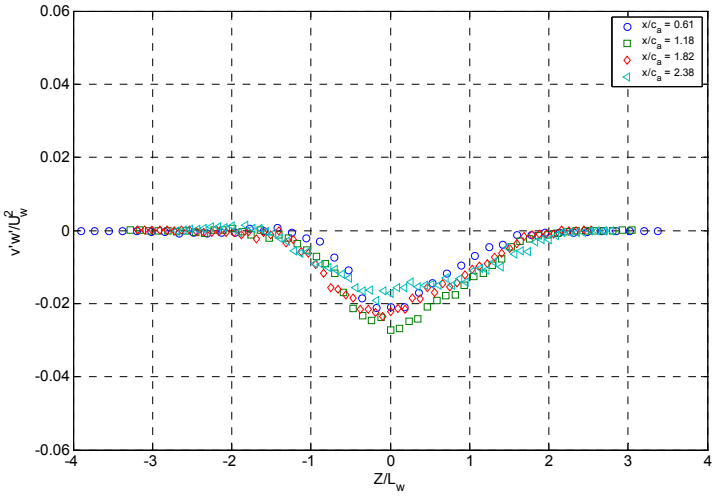

(e)

Figure 5-107: Reynolds shear stress profiles, $\overline{v'w'/U_w^2}$ at five spanwise locations across one serration for the 2.54 cm droop serration: **(a)** $y/c_a = 0.72$, **(b)** $y/c_a = 0.80$, **(c)** $y/c_a = 0.87$, **(d)** $y/c_a = 0.95$, **(e)** $y/c_a = 1.021$

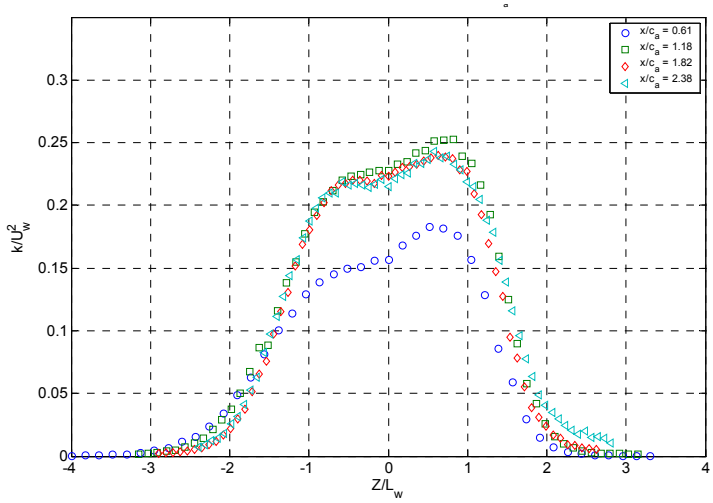

(a)

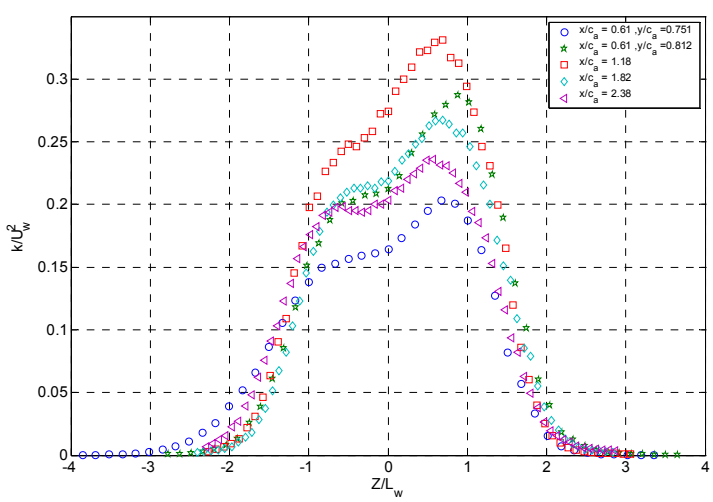

(b)

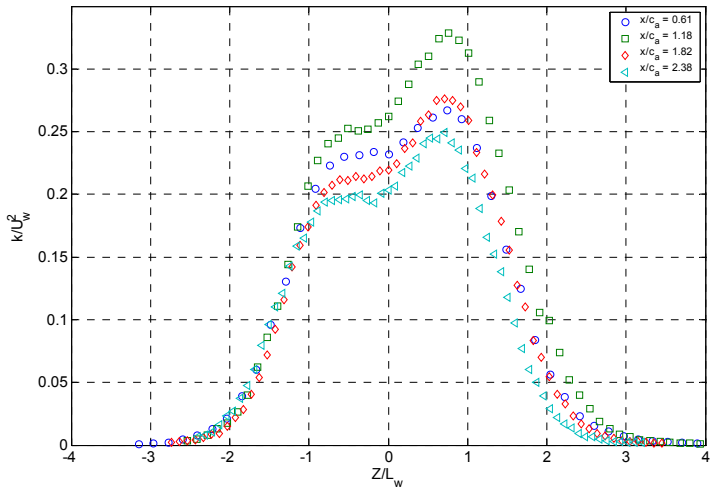

(c)

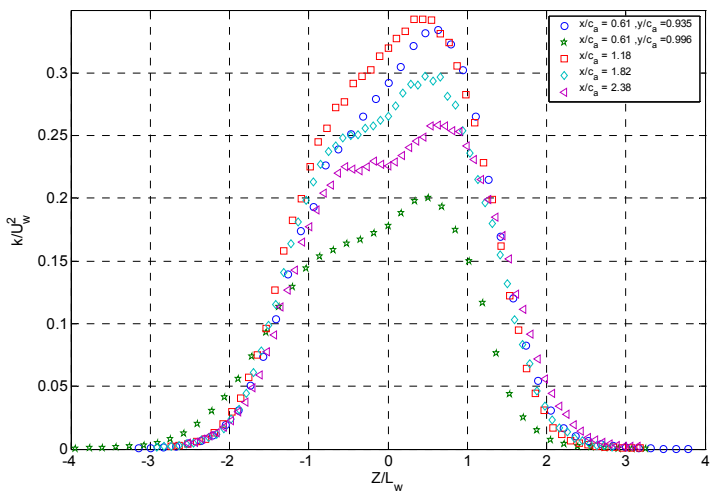

(d)

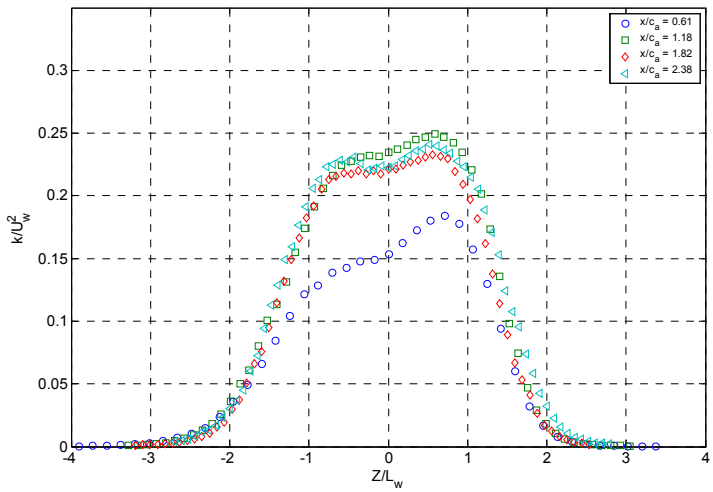

(e)

Figure 5-108: Turbulence kinetic energy profiles, k/U_w^2 at five locations spanwise locations across one serration for the 2.54 cm droop serration: **(a)** $y/c_a = 0.72$, **(b)** $y/c_a = 0.80$, **(c)** $y/c_a = 0.87$, **(d)** $y/c_a = 0.95$, **(e)** $y/c_a = 1.021$

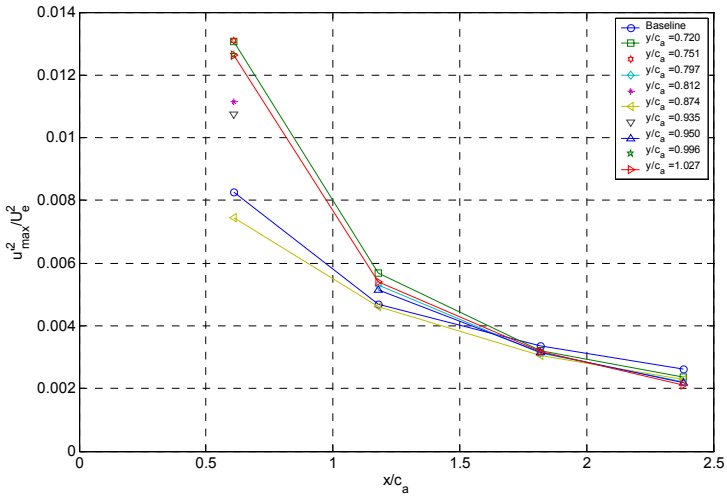

(a)

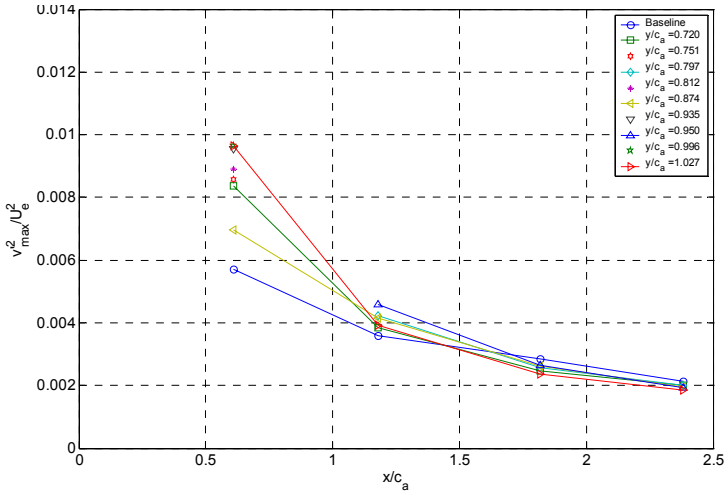

(b)

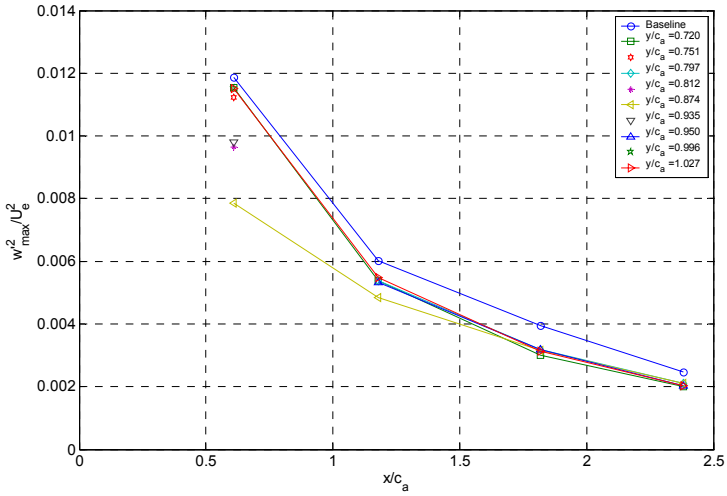

(c)

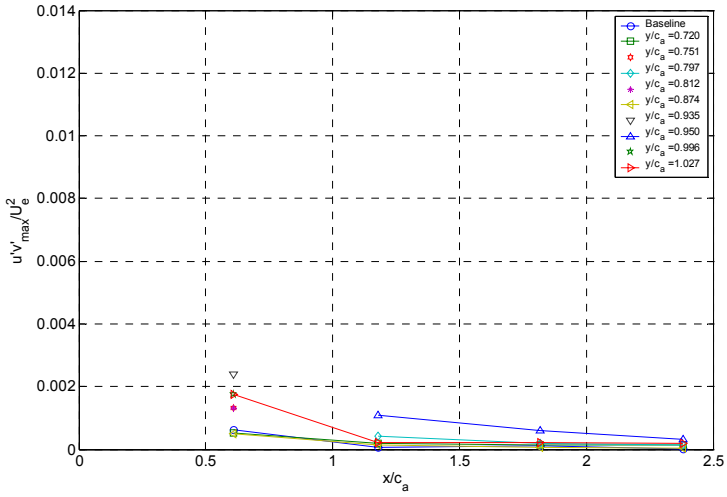

(d)

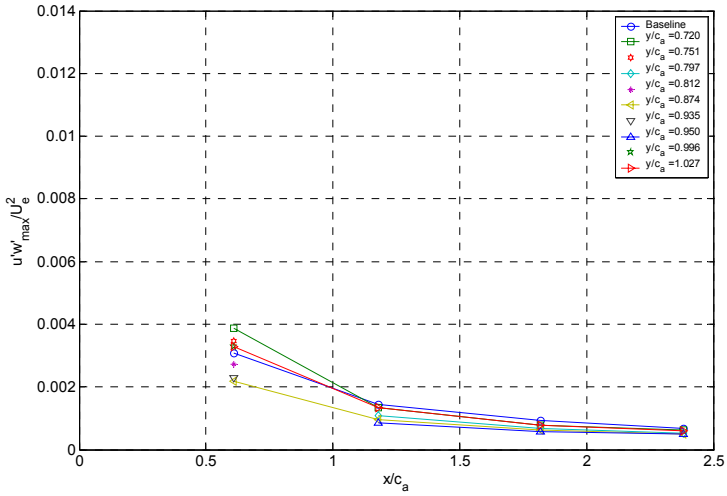

(e)

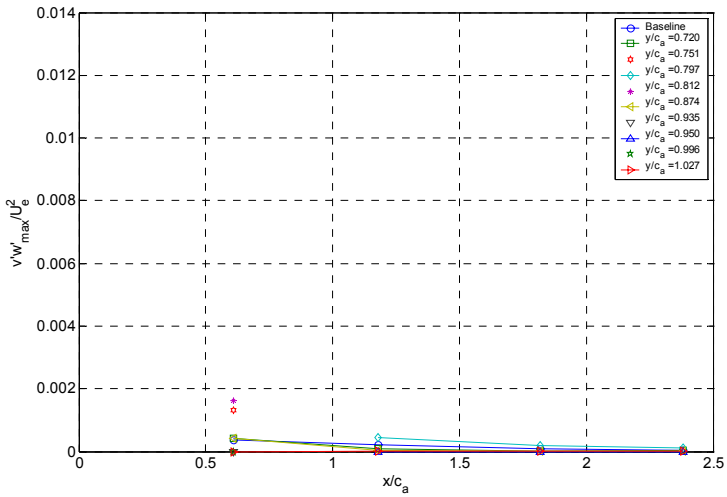

(f)

Figure 5-109: Maximum normalized Reynolds stress levels at five spanwise locations across one serration for the 2.54 cm droop serration compared to the baseline: **(a)** $\overline{|u'^2/U_\infty^2|}_{max}$, **(b)** $\overline{|v'^2/U_\infty^2|}_{max}$, **(c)** $\overline{|w'^2/U_\infty^2|}_{max}$, **(d)** $\overline{|u'v'/U_\infty^2|}_{max}$, **(e)** $\overline{|u'w'/U_\infty^2|}_{max}$, **(f)** $\overline{|v'w'/U_\infty^2|}_{max}$

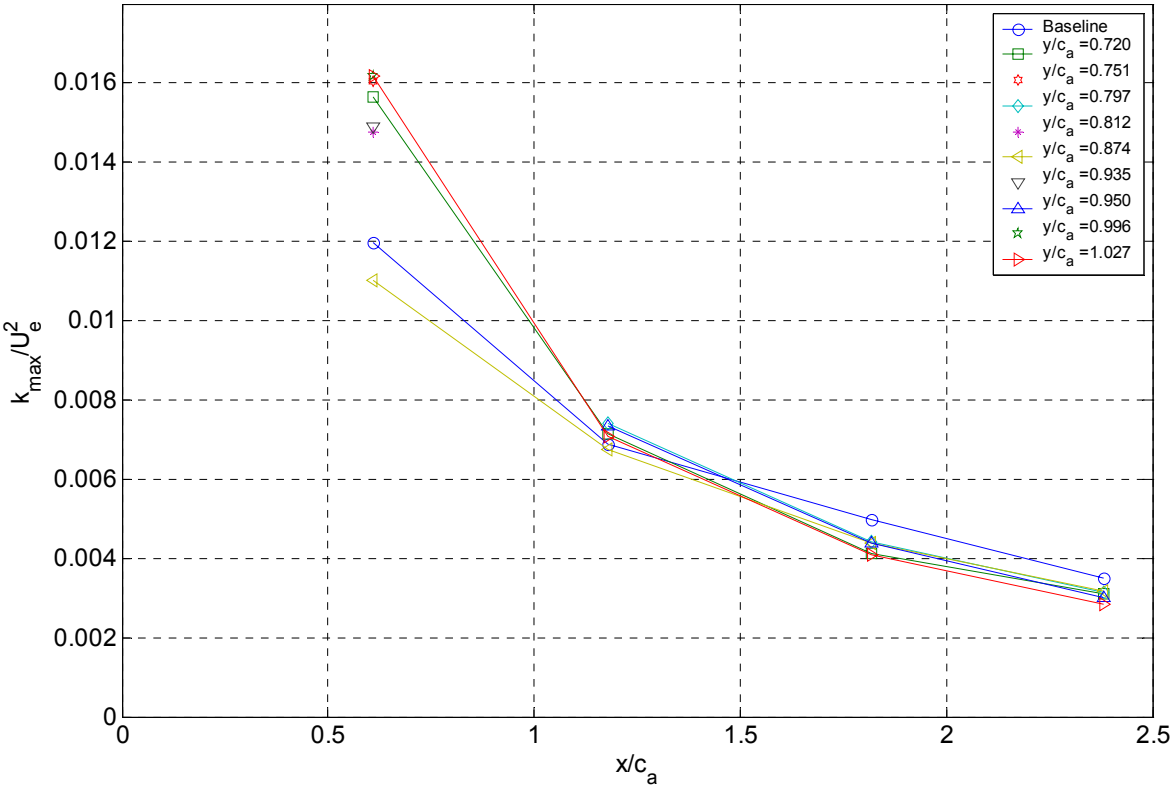

Figure 5-110: Maximum normalized turbulence kinetic energy, $|k/U_w^2|_{max}$, at five spanwise locations across one serration for the 2.54 cm droop serration compared to the baseline,

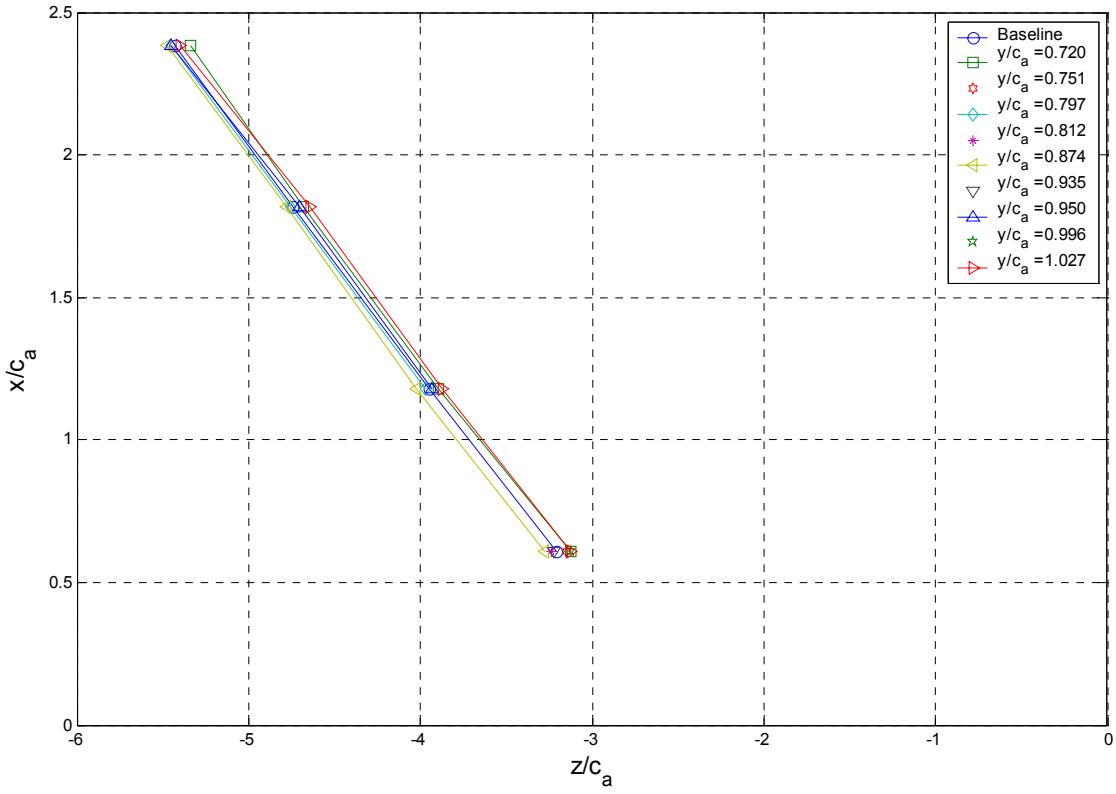

Figure 5-111: Propagation of the minimum velocity point in the wake for the 2.54 cm droop serration compared to the baseline case

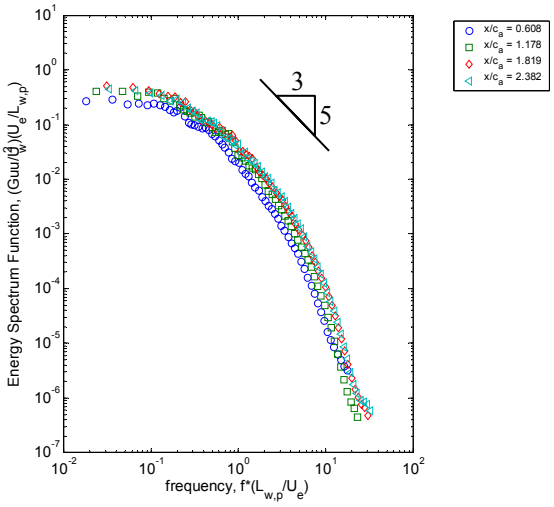

(a)

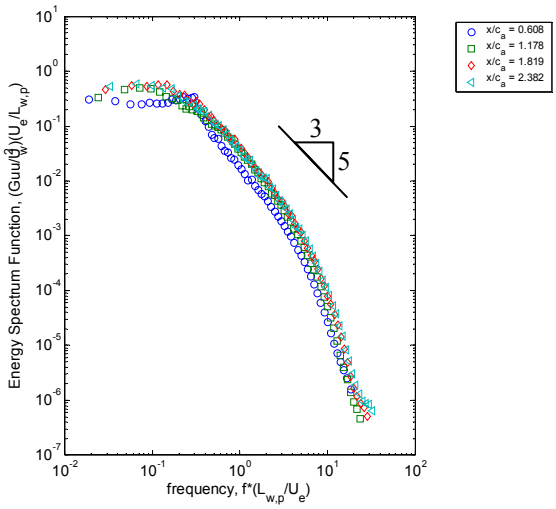

(b)

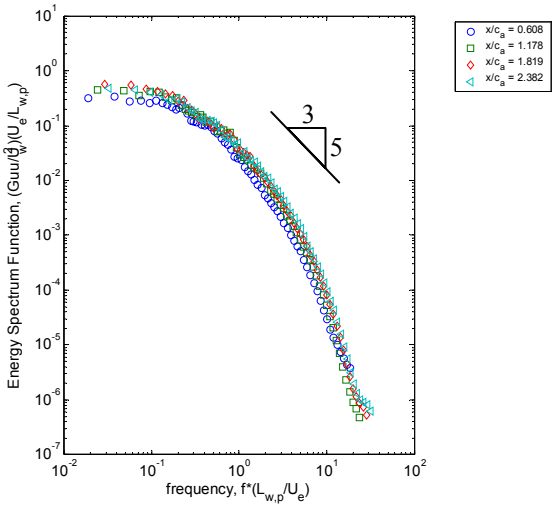

(c)

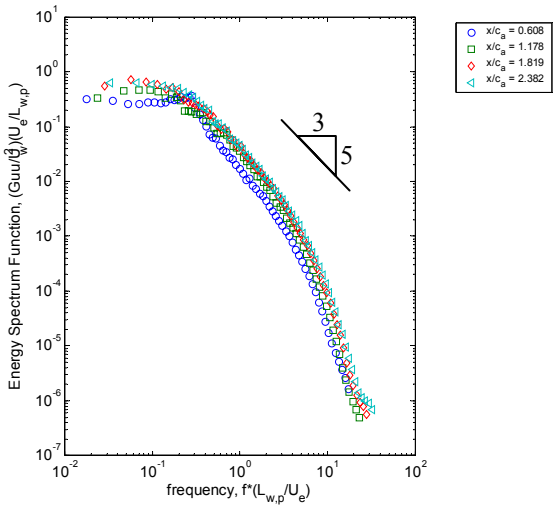

(d)

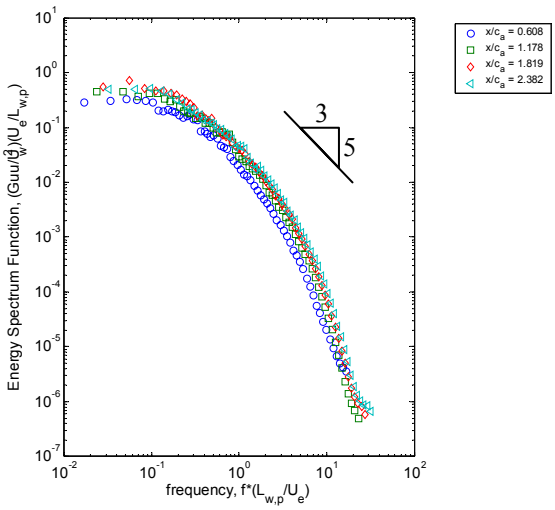

(e)

Figure 5-112: Streamwise ***s***pectral profiles, $(G_{uu}/U_w^2)(U_e/L_{w,p})$, at the wake center at five spanwise locations across one wake serration for the 1.27 cm serration: **(a)** $y/c_a = 0.83$, **(b)** $y/c_a = 0.87$, **(c)** $y/c_a = 0.91$, **(d)** $y/c_a = 0.95$, **(e)** $y/c_a = 0.97$

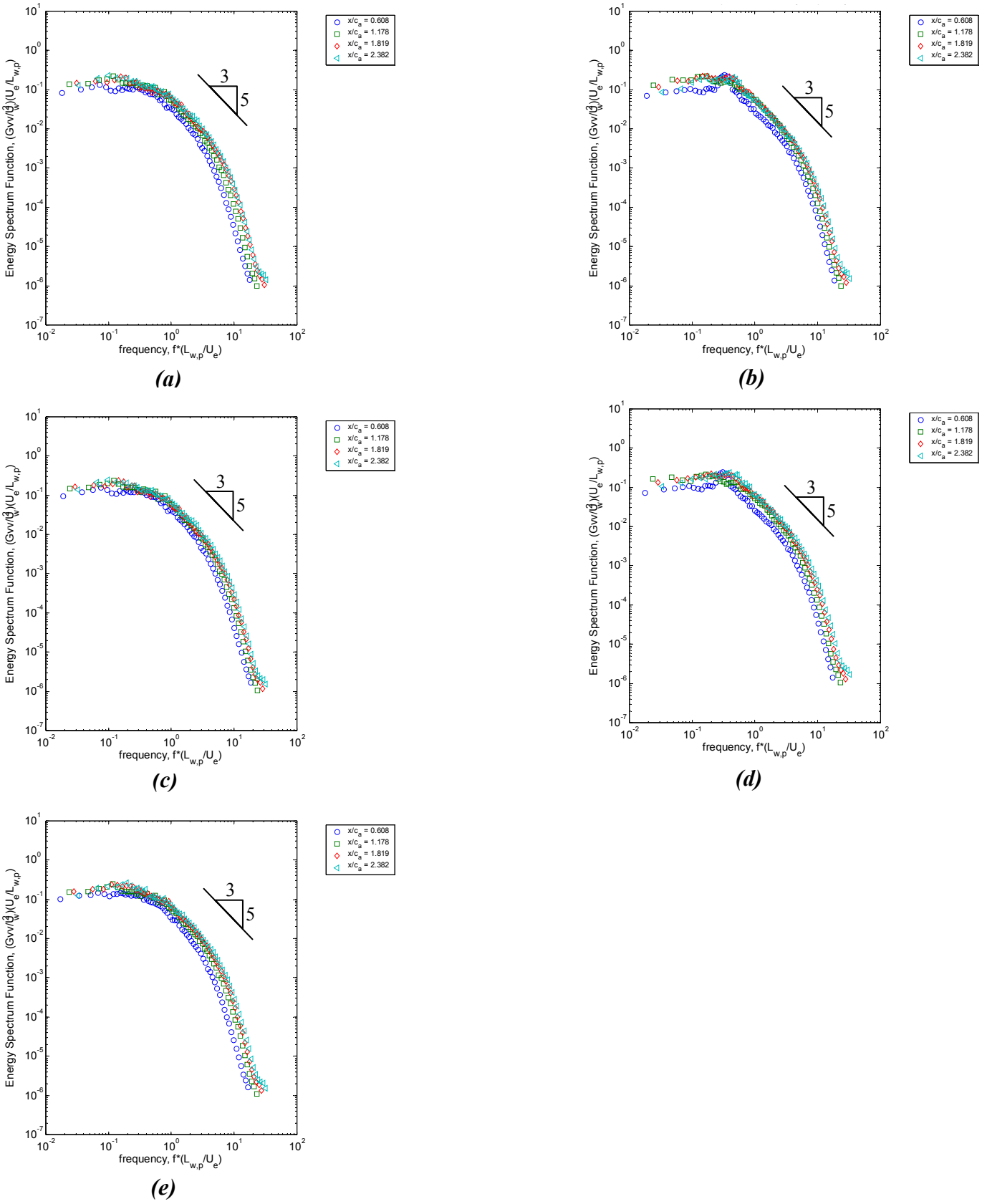

Figure 5-113: Spanwise ***s***pectral profiles, $(G_{vv}/U_w^2)(U_e/L_{w,p})$, at the wake center at five spanwise locations across one wake serration for the 1.27 cm serration: **(a)** $y/c_a = 0.83$, **(b)** $y/c_a = 0.87$, **(c)** $y/c_a = 0.91$, **(d)** $y/c_a = 0.95$, **(e)** $y/c_a = 0.97$

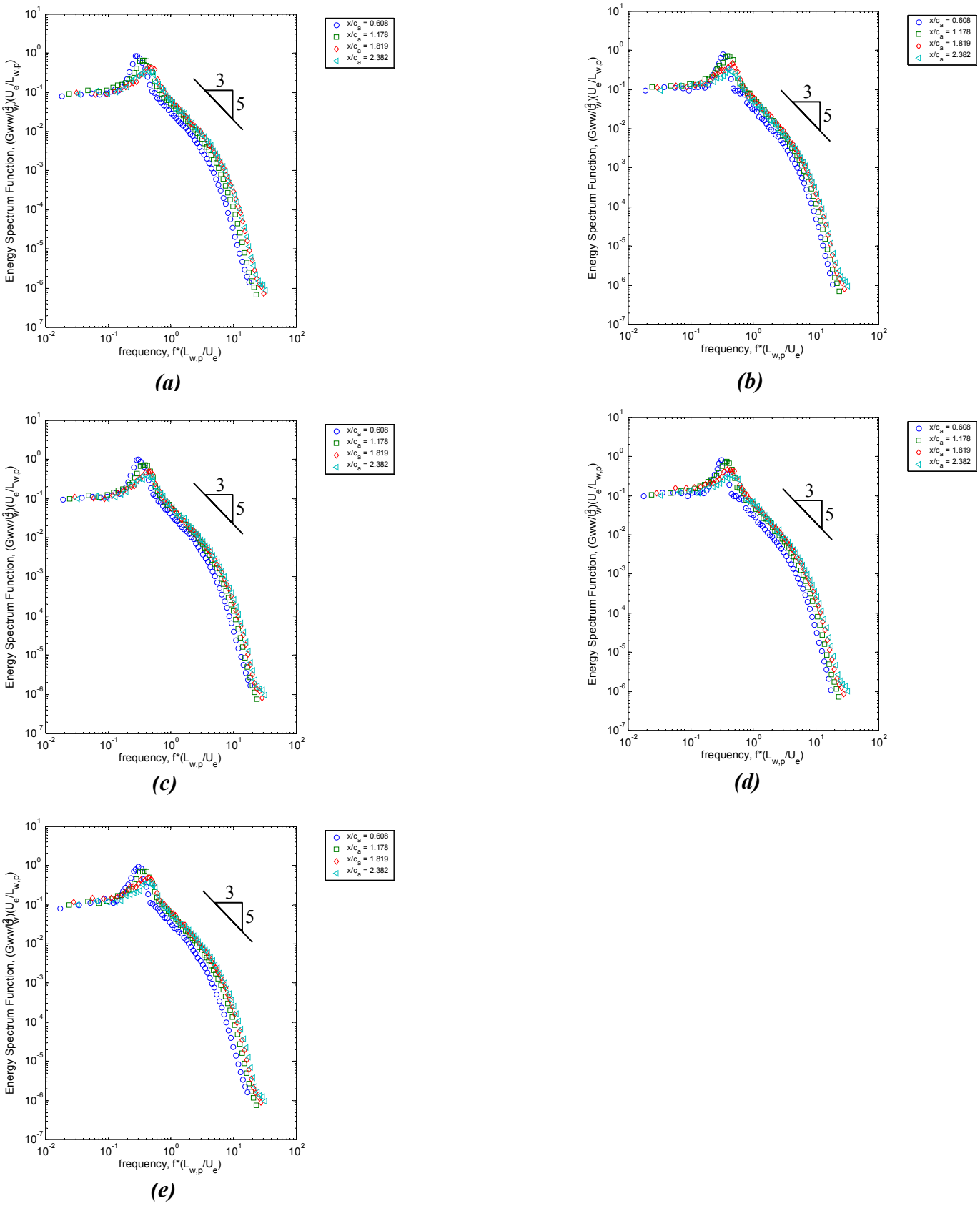

Figure 5-114: Cross-wake **s**pectral profiles, $(G_{ww}/U_w^2)(U_e/L_{w,p})$, at the wake center at five spanwise locations across one wake serration for the 1.27 cm serration: **(a)** $y/c_a = 0.83$, **(b)** $y/c_a = 0.87$, **(c)** $y/c_a = 0.91$, **(d)** $y/c_a = 0.95$, **(e)** $y/c_a = 0.97$

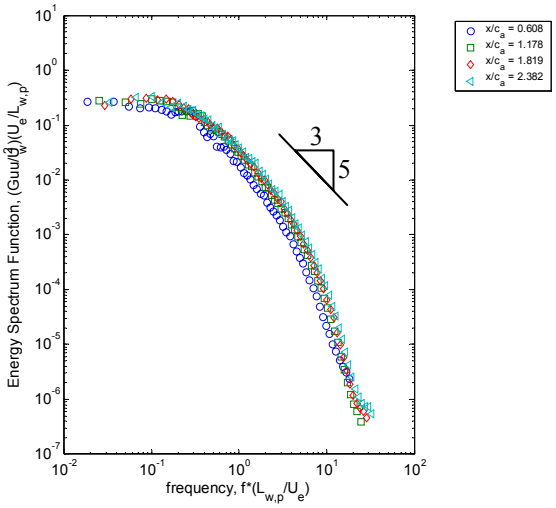

(a)

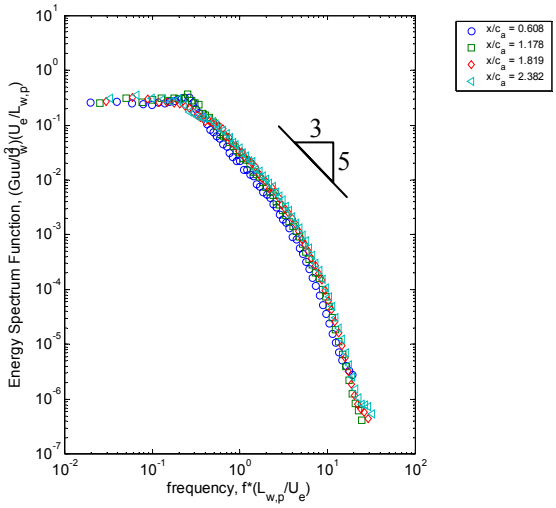

(b)

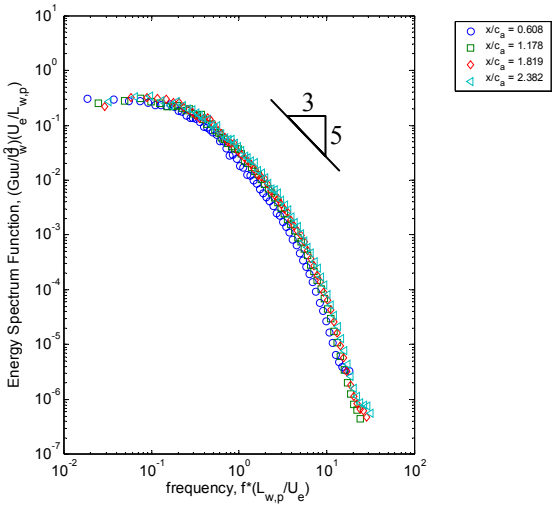

(c)

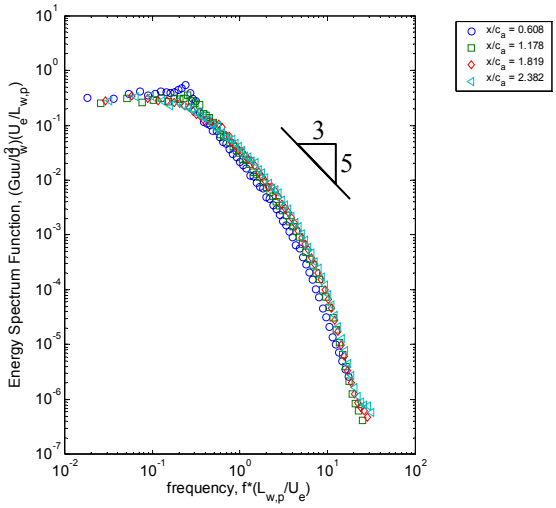

(d)

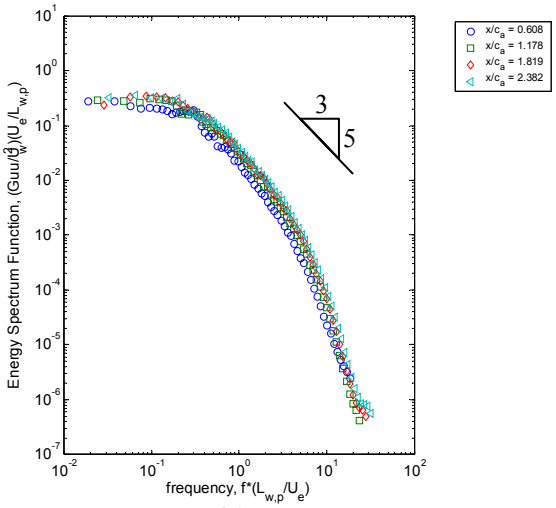

(e)

Figure 5-115: Streamwise spectral profiles, $(G_{uu}/U_w^2)(U_e/L_{w,p})$, at the wake center at five spanwise locations across one wake serration for the 1.27 cm droop serration: **(a)** $y/c_a = 0.83$, **(b)** $y/c_a = 0.87$, **(c)** $y/c_a = 0.91$, **(d)** $y/c_a = 0.95$, **(e)** $y/c_a = 0.97$

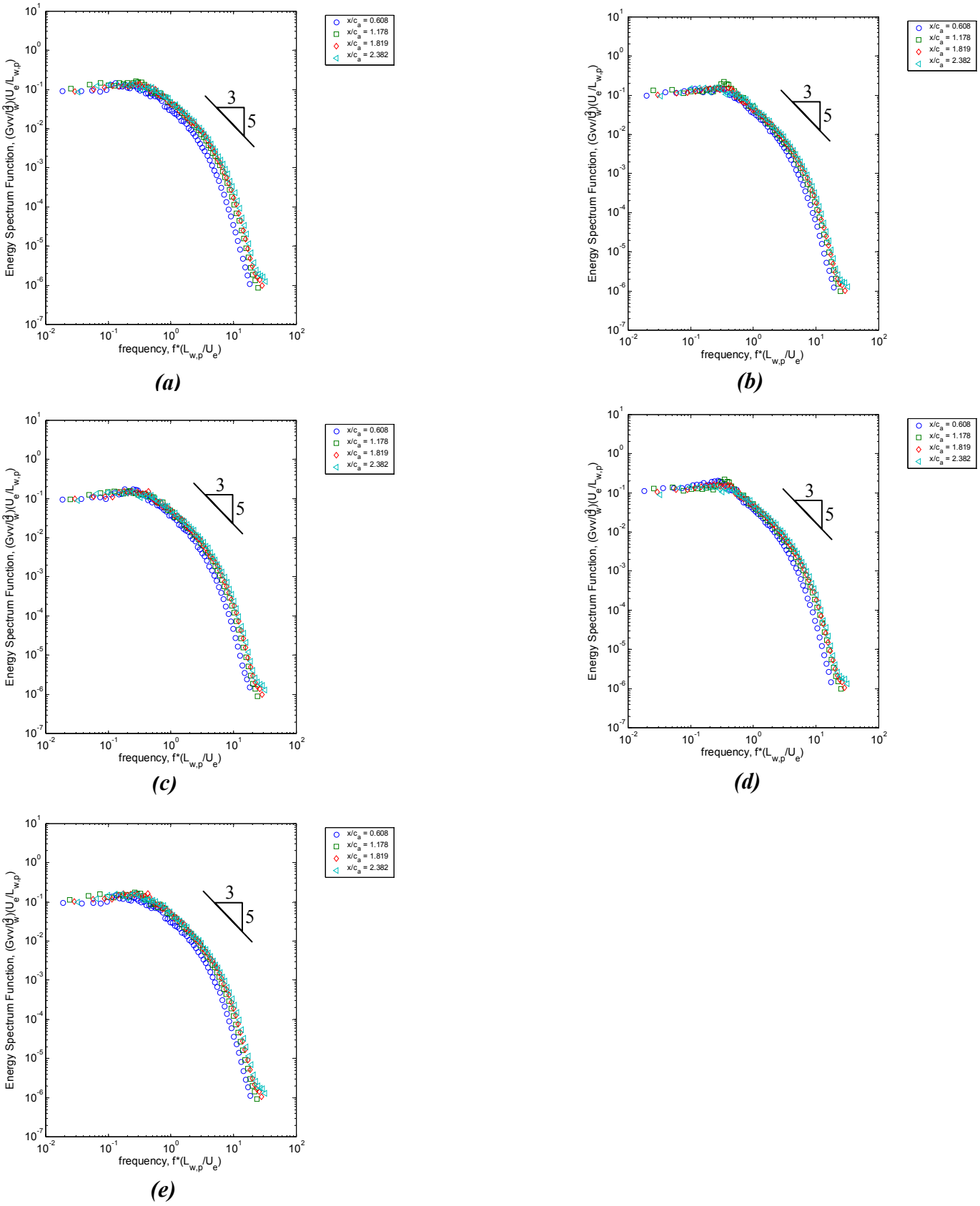

Figure 5-116: Spanwise **s**pectral profiles, $(G_{vv}/U_w^2)(U_e/L_{w,p})$, at the wake center at five spanwise locations across one wake serration for the 1.27 cm droop serration: **(a)** $y/c_a = 0.83$, **(b)** $y/c_a = 0.87$, **(c)** $y/c_a = 0.91$, **(d)** $y/c_a = 0.95$, **(e)** $y/c_a = 0.97$

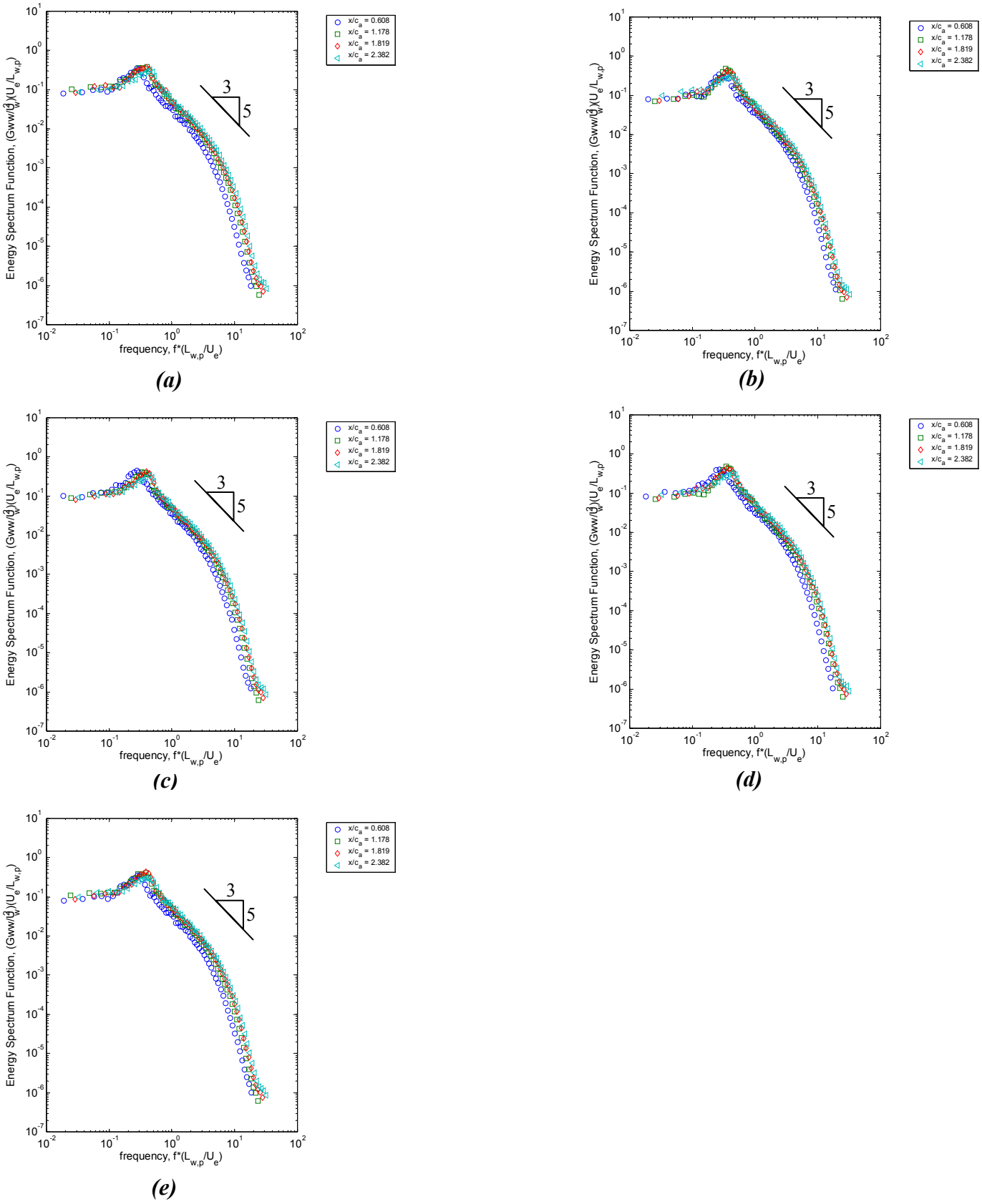

Figure 5-117: Cross-wake **s**pectral profiles, $(G_{ww}/U_w^2)(U_e/L_{w,p})$, at the wake center at five spanwise locations across one wake serration for the 1.27 droop cm serration: **(a)** $y/c_a = 0.83$, **(b)** $y/c_a = 0.87$, **(c)** $y/c_a = 0.91$, **(d)** $y/c_a = 0.95$, **(e)** $y/c_a = 0.97$

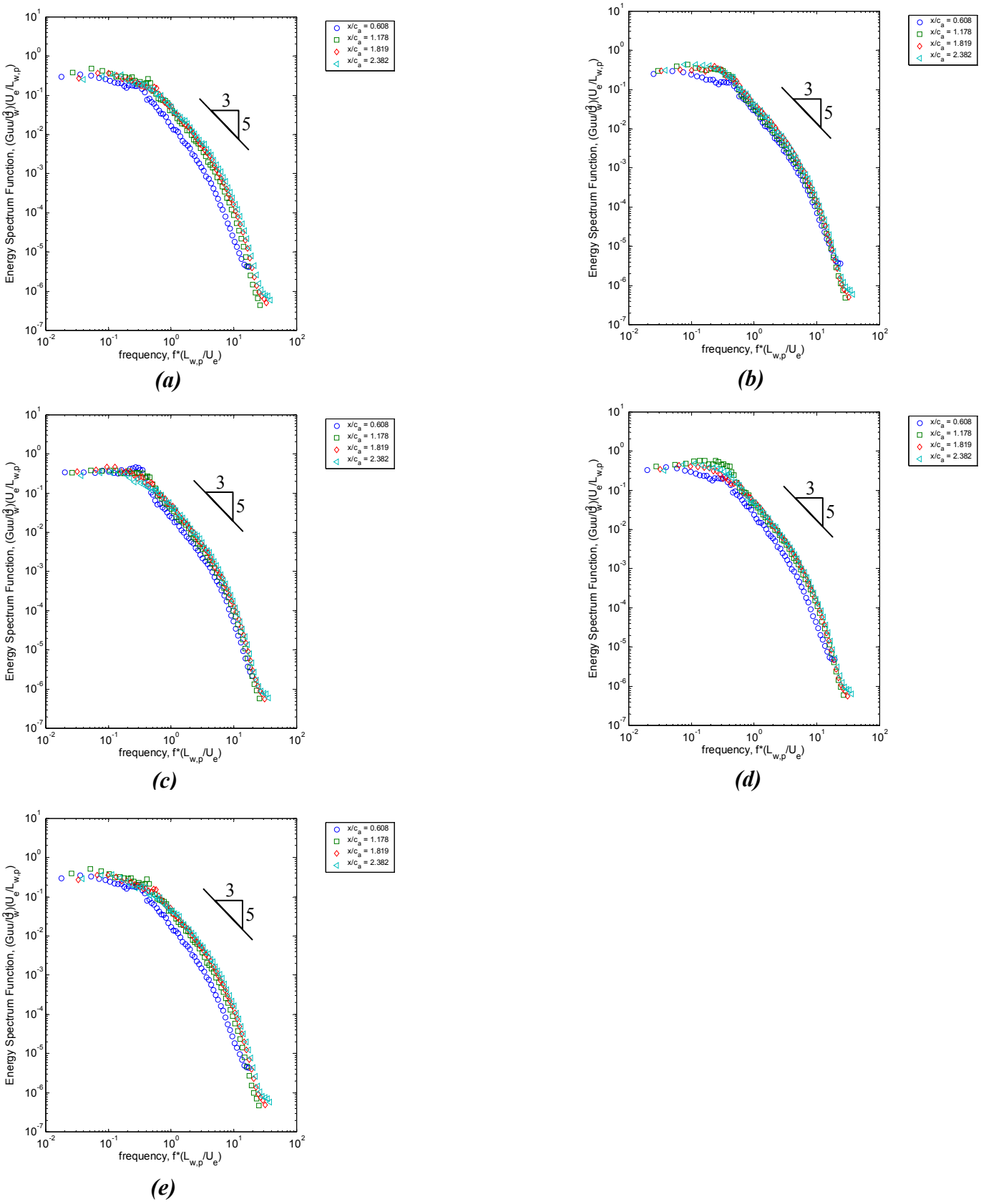

Figure 5-118: Streamwise **s**pectral profiles, $(G_{uu}/U_w^2)(U_e/L_{w,p})$, at the wake center at five spanwise locations across one wake serration for the 2.54 cm serration: **(a)** $y/c_a = 0.72$, **(b)** $y/c_a = 0.79$, **(c)** $y/c_a = 0.87$, **(d)** $y/c_a = 0.95$, **(e)** $y/c_a = 1.021$

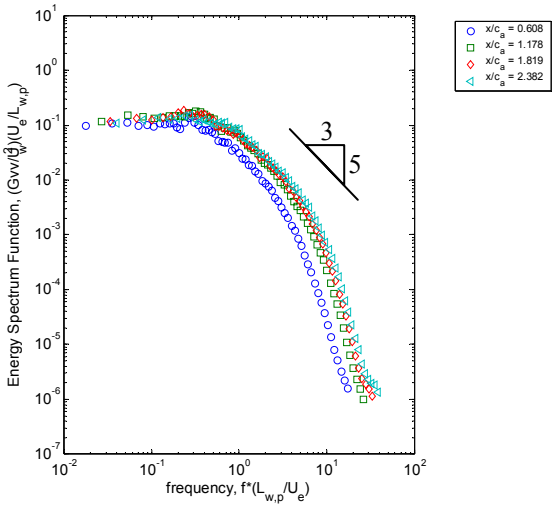

(a)

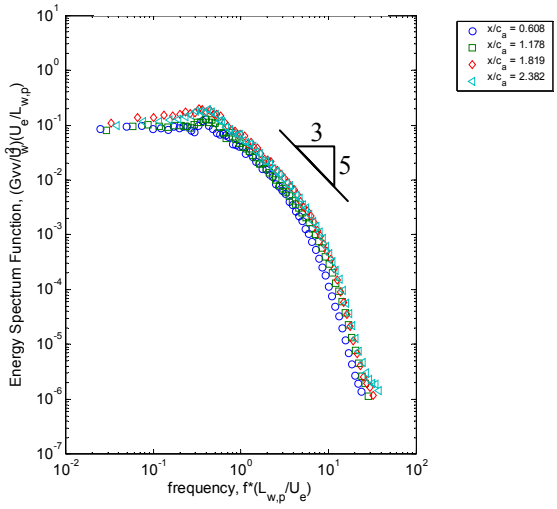

(b)

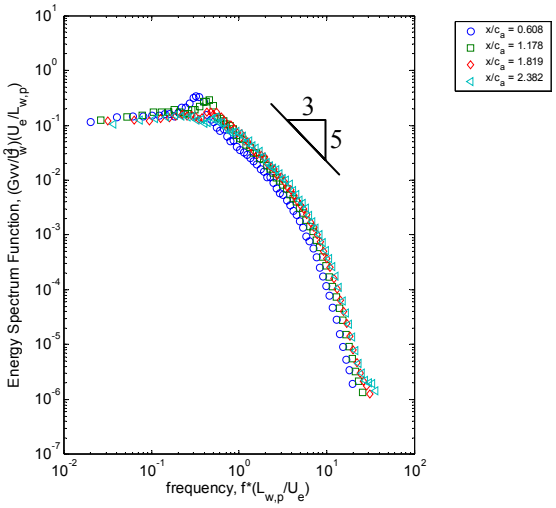

(c)

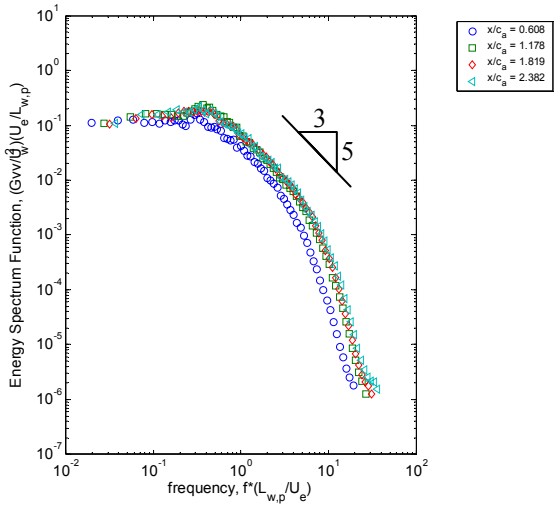

(d)

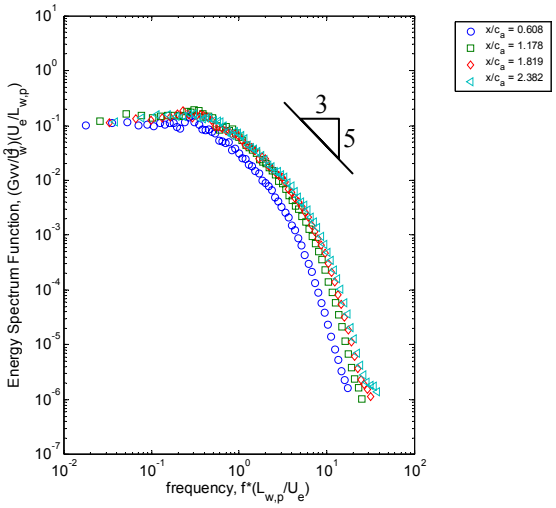

(e)

Figure 5-119: Spanwise spectral profiles, $(G_{vv}/U_w^2)(U_e/L_{w,p})$, at the wake center at five spanwise locations across one wake serration for the 2.54 cm serration: **(a)** $y/c_a = 0.72$, **(b)** $y/c_a = 0.79$, **(c)** $y/c_a = 0.87$, **(d)** $y/c_a = 0.95$, **(e)** $y/c_a = 1.021$

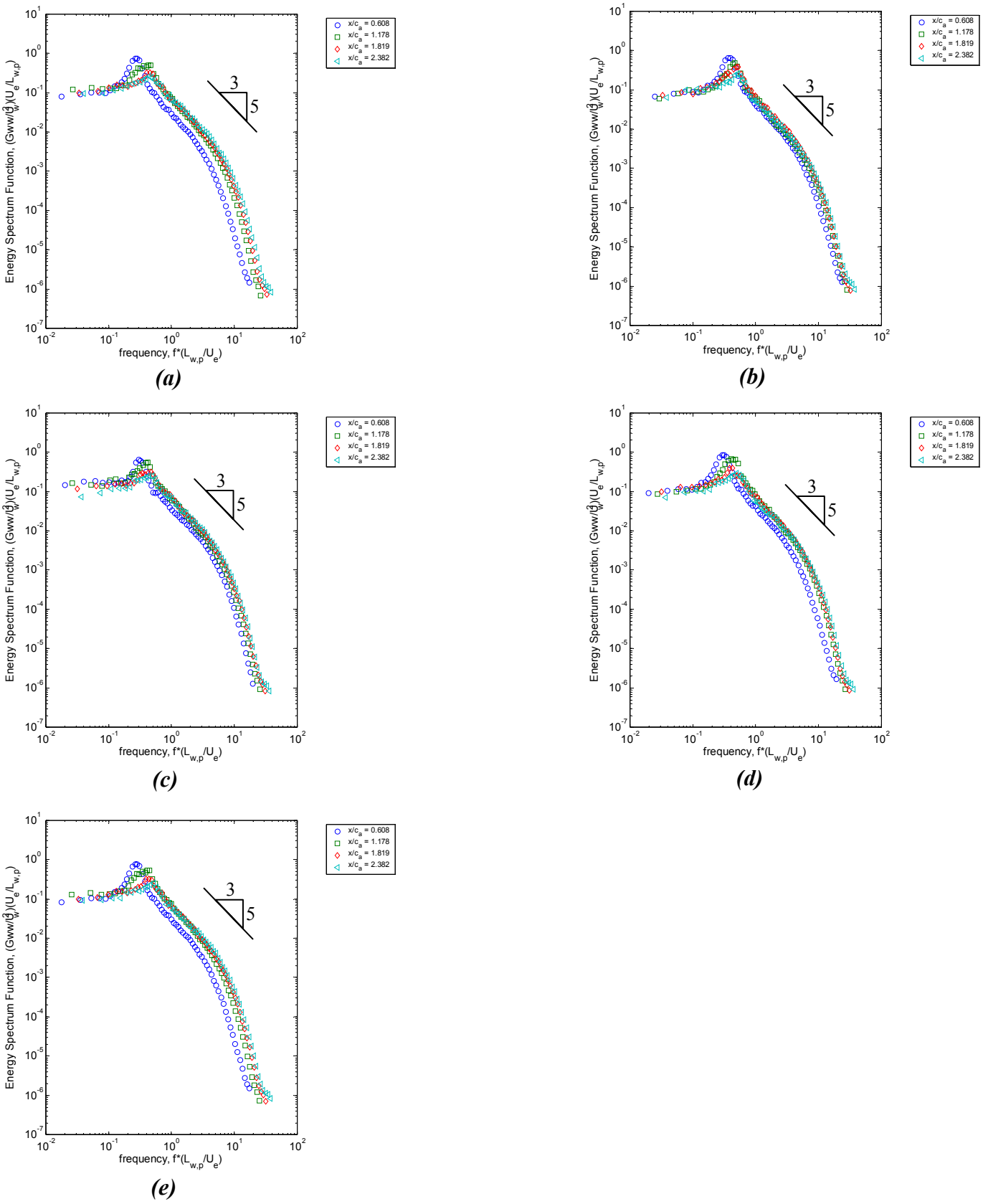

Figure 5-120: Cross-wake **s**pectral profiles, $(G_{ww}/U_w^2)(U_e/L_{w,p})$, at the wake center at five spanwise locations across one wake serration for the 2.54 cm serration: **(a)** y/c_a = 0.72, **(b)** y/c_a = 0.79, **(c)** y/c_a = 0.87, **(d)** y/c_a = 0.95, **(e)** y/c_a = 1.021

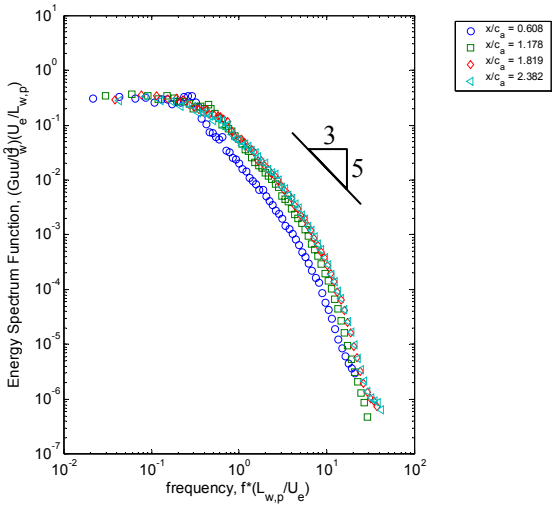

(a)

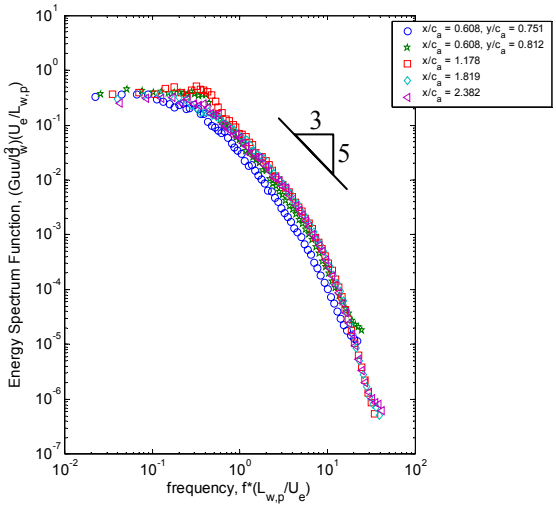

(b)

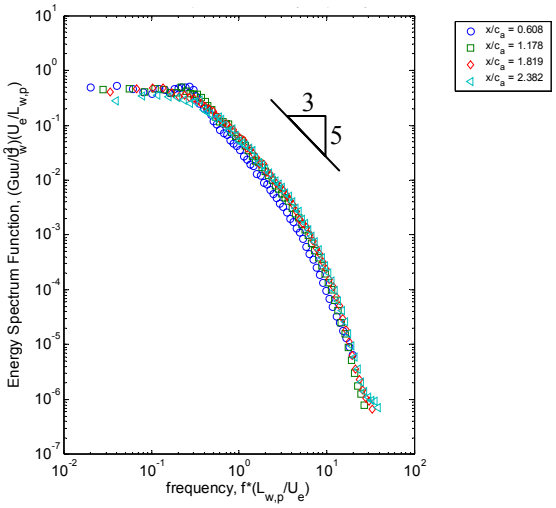

(c)

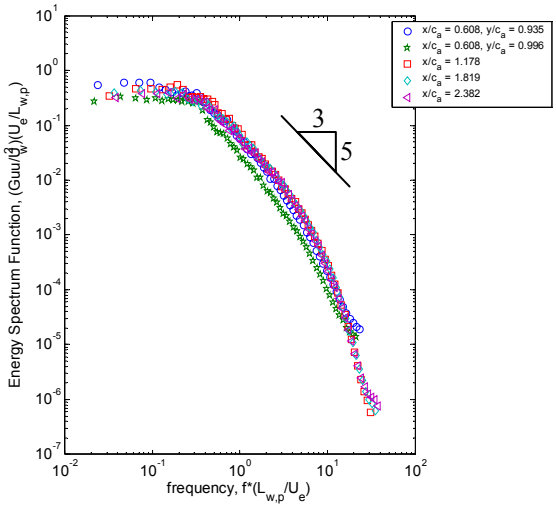

(d)

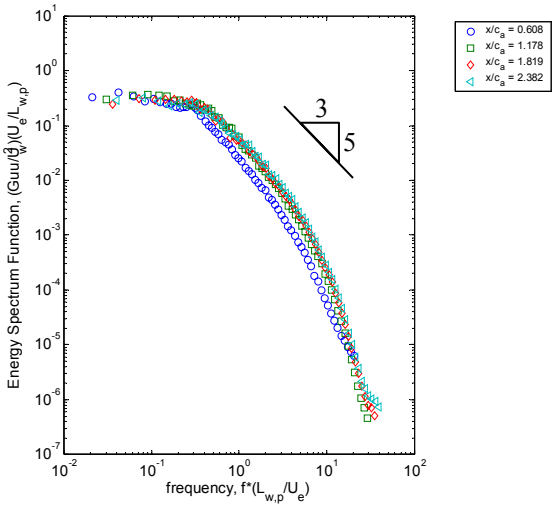

(e)

Figure 5-121: Streamwise ***s***pectral profiles, $(G_{uu}/U_w^2)(U_e/L_{w,p})$, at the wake center at five spanwise locations across one wake serration for the 2.54 cm droop serration: **(a)** $y/c_a = 0.72$, **(b)** $y/c_a = 0.80$, **(c)** $y/c_a = 0.87$, **(d)** $y/c_a = 0.95$, **(e)** $y/c_a = 1.021$

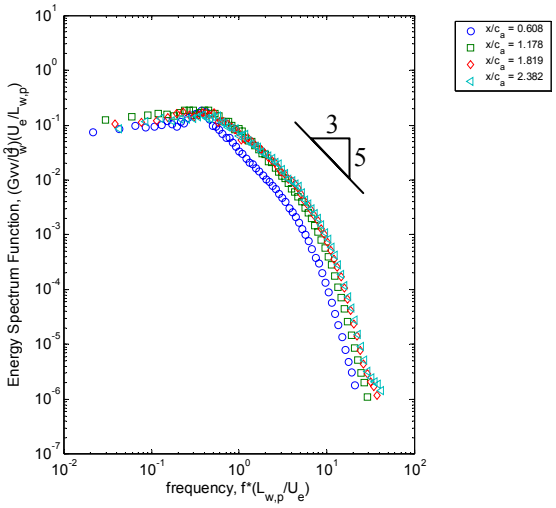

(a)

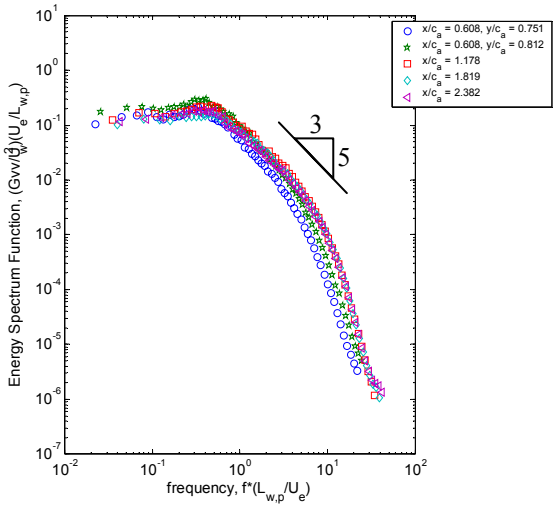

(b)

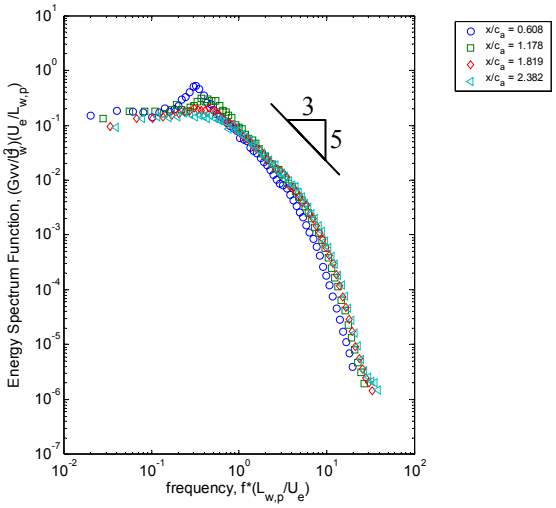

(c)

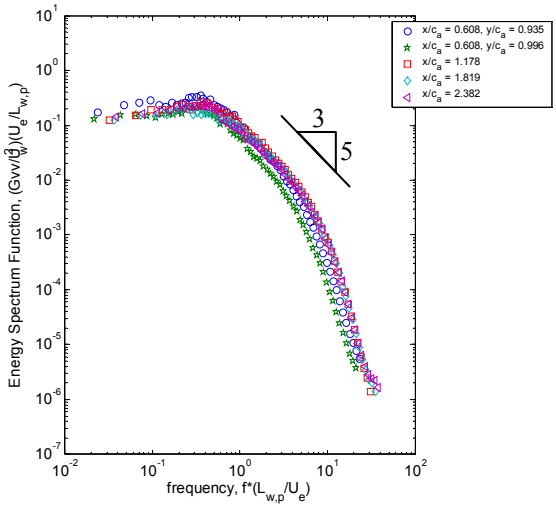

(d)

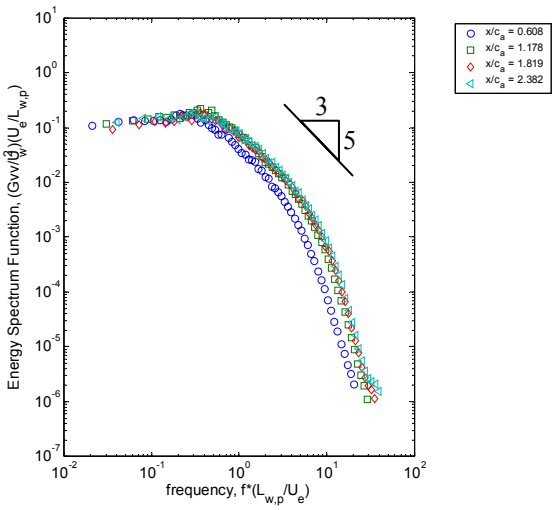

(e)

Figure 5-122: Spanwise spectral profiles, $(G_{vv}/U_w^2)(U_e/L_{w,p})$, at the wake center at five spanwise locations across one wake serration for the 2.54 cm droop serration: **(a)** $y/c_a = 0.72$, **(b)** $y/c_a = 0.80$, **(c)** $y/c_a = 0.87$, **(d)** $y/c_a = 0.95$, **(e)** $y/c_a = 1.021$

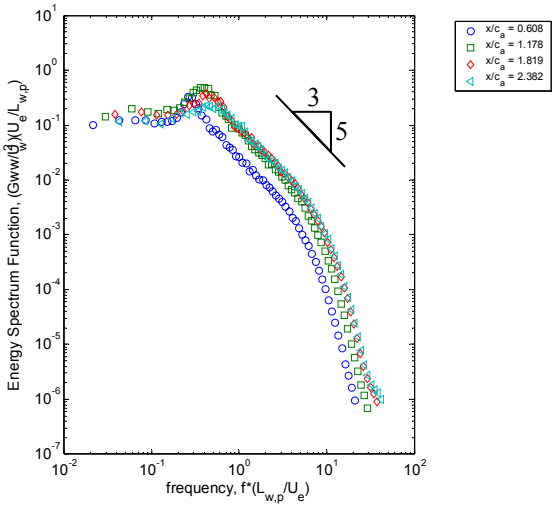

(a)

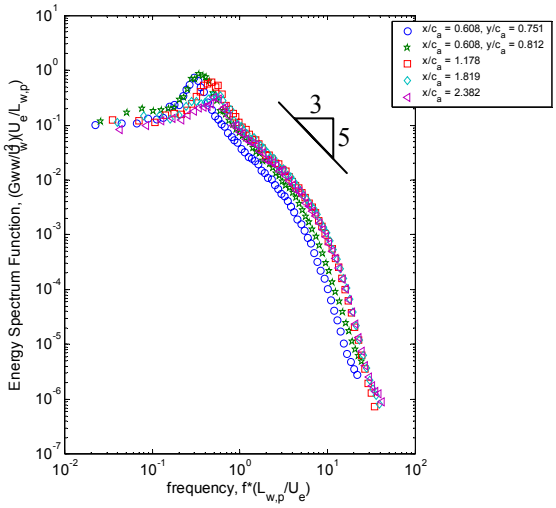

(b)

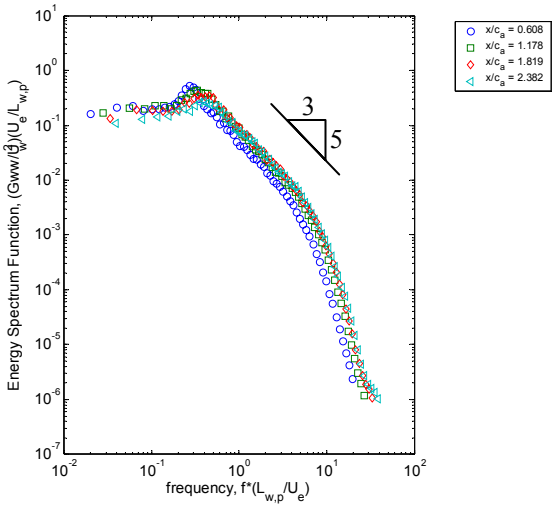

(c)

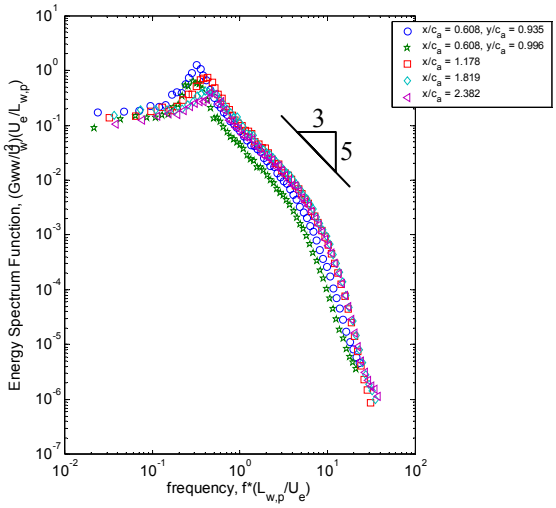

(d)

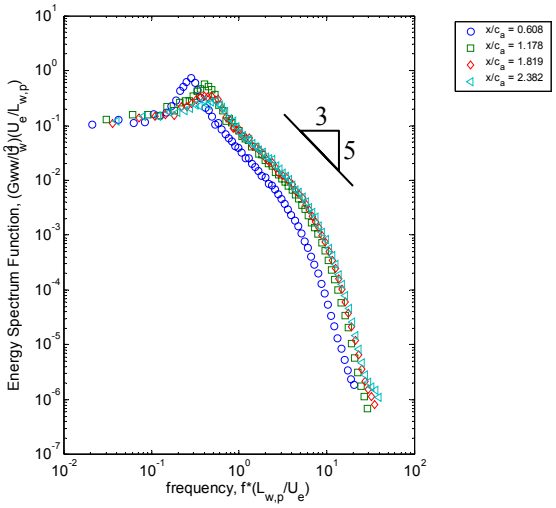

(e)

Figure 5-123: Cross-wake spectral profiles, $(G_{ww}/U_w^2)(U_e/L_{w,p})$, at the wake center at five spanwise locations across one wake serration for the 2.54 cm droop serration: **(a)** $y/c_a = 0.72$, **(b)** $y/c_a = 0.80$, **(c)** $y/c_a = 0.87$, **(d)** $y/c_a = 0.95$, **(e)** $y/c_a = 1.021$

CHAPTER SIX

6. Conclusions

The Virginia Tech low speed linear cascade tunnel was used to investigate the effect of the trailing edge serrations on the flow field downstream of the blade row. The cascade row consists of 8 GE-Rotor-B blades and 7-passages with adjustable tip gap settings. It has an inlet angle of 65.1º, stagger angle of 56.9º and a turning angle of 11.8º. The tunnel was operated with a tip gap setting of 1.65% chord, with a Reynolds number based on the chord of 390,000 and a free stream velocity of 24.7 m/s.

6.1 Conclusions Concerning the Baseline GE-Rotor-B Blades

Single-sensor hot-wire and four-sensor hot-wire measurements were performed at four locations downstream of the cascade blade row near the mid-span height of the blade. These measurements were performed to accurately define the wakes created by the baseline blades far from the effects of the both the upper and lower endwalls. Cross-sectional measurements were performed with the four-senor hot-wire at two downstream locations and additional cross-sectional measurements were performed with a telescoping Pitot-static at a further two locations. Through these measurements the mean velocity and turbulence structures of the tip leakage vortex were revealed.

The measurements performed on the baseline blades showed the following:

(1) The blade loading for the measurements performed on the blades with blade root covers that did not accurately control the opening at the blade root had a larger blade loading and circulation than those with the 1 mm controlled opening. Circulation was 4.9% lower for the controlled 1 mm blade root opening.

(2) The Pitot-static cross-sectional measurements reveal the tip leakage vortex of blade 4 in lower endwall region, the wake of blade 5 and the boundary layer

on the upper endwall. The tip leakage vortex dominates the lower end wall region. The boundary layer on the upper endwall is largest on the suction side of the blade and is half as thick on the pressure side. The growth of the wake, the tip leakage vortex region and the upper end wall boundary layer was seen between the two downstream locations.

(3) The maximum deficit in the streamwise velocity is found in the tip leakage vortex center and the deficit decays as the flow field travels downstream.

(4) The tip leakage vortex produced both negative and positive regions of streamwise vorticity that can be seen near the lower endwall. The positive vorticity is almost 3 times stronger than the negative vorticity.

(5) The turbulence kinetic energy is largest in the tip leakage vortex and it is found outside edge of the vortex, near the pressure side of blade 5 at x/c_a = 0.61. At x/c_a = 1.82, the TKE levels are largest near the center of the tip leakage vortex

(6) Small magnitudes of V and W velocities are seen near the mid-height of the tunnel but they are much smaller then what is seen in the vortex region.

(7) When normalized on the wake parameters, the wakes of the baseline blades near the mid-span height have similar characteristics to a plane wake in both the mean velocity and turbulence. The mean velocity deficit and the spreading rates of the wake are similar to the plane wake.

(8) Velocity spectral plots suggest the shedding of coherent motion in the wake as a result of vortex shedding.

6.2 Conclusions Concerning the Serrated Trailing Edge GE-Rotor-B Blades

The trailing edges of the baseline blades were modified by adding serrations. Serration lengths of 1.27 cm and 2.54 cm as well as the drooping of the two different serration sizes were investigated. Four sensor hot-wire at the four downstream axial locations were performed near the mid-height of the blade across one serration in the spanwise direction. These measurements were performed to determine to what extent the

wakes of the new blades differed from the baseline blades. Cross-sections measured at the two downstream locations were measured and compared to the baseline to determine if the tip leakage vortex had been changed by any of the serrated blades. Pitot-static cross-sectional measurements were performed to determine the flowfield prior to any hot-wire measurements were performed.

The measurements performed on the serrated blades showed the following:

(1) The Pitot-static measurements showed the tip leakage vortex structure and the boundary layer near the upper end wall were not affected by the trailing edge serrations. The wake shape was a function of the serration length and droop effects. Also, periodic behavior could be seen in the spanwise direction.

(2) The blade loading and circulation compared to the baseline blades varied with each set of serrations. The best agreement was seen with the 1.27 cm serration. The 1.27 cm drooped serration had a larger blade loading and circulation, while the 2.54 cm serration had the lower blade loading and circulation. The 2.54 cm drooped serration was comparable to the 1.27 cm serration and the baseline.

(3) The mean streamwise velocity cross-sections showed that the largest mean velocity deficit was found in the tip leakage vortex center for all serration cases. The mean velocity deficit was similar to the baseline for all serration cases.

(4) The maximum voriticity in the tip leakage vortex were higher for the serrated cases than the baseline. The vorticity is higher for the 2.54 cm cases than the 1.27 cm cases and the droop decreases the vorticity strength. Compared to the baseline at x/c_a = 0.61, the vorticity was between 24% and 33% stronger for the serrated cases. Similar results were seen at x/c_a = 1.82, with the vorticity 23% stronger for the serrated blades.

(5) The vorticity of the secondary vortex was larger in magnitude for the larger serration sizes and drooping increased the magnitude. The vorticity strength of the secondary vortex was slightly higher than the baseline.

(6) The turbulence kinetic energy in the tip leakage vortex is similar for the serrated cases compared to the baseline case.

(7) The turbulence kinetic energy production is highest in the vicinity of the highest levels of turbulence kinetic energy.

(8) Measurements near the mid-span height of the blades showed the decay rate of the centerline velocity deficit has increased over the baseline case. The decay rate increases with the serration size and drooping does not increase it further. The largest centerline velocity deficit decay rate is found downstream of the serration tips while the lowest at the serration valley. This is predicted to reduce the periodic fluctuations in the pitchwise direction of the mean velocity profile, and hence reduce the tonal noise at the leading edge of the downstream stator vane associated with this.

(9) The spreading rates of the wake are higher for the serrated trailing edge cases. The larger serration size increases the spreading rates of the wake further. The largest spreading rates are found downstream of the serration tips and the lowest are found downstream of the serration valley. The increased spreading rates will reduce the periodic fluctuations in the wake associated with the non-uniformity of the downstream mean velocity and hence reduce the tonal noise reduction at the leading edge of the downstream stator vanes.

(10) The 1.27 cm and the 2.54 cm cases downstream of the serration tips and valley have the best agreement with the unique relationship for the momentum thickness of a plane wake.

(11) The 1.27 cm case is the only trailing edge serrated case that follows the same pattern toward self-similiary that is seen in plane wakes and was seen in the baseline case. The other cases reach maximum values at $x/c_a = 1.18$ and then decay.

(12) The velocity spectra showed the some evidence of coherent motion in the wake as a result of vortex shedding. This was seen in all of the velocity directions.

BIBLIOGRAPHY

Ahn, W. J. and Sung, H. J., "Prediction of Two-Dimensional Momentumless Wake by k-ε-γ Model", AIAA Journal, Vol. 33, No. 4, 1995, pp. 611 – 617.

Braun, K.A., Gordner, A., van der Borg, N., Dassan, A.G.M, Doorenspeet, F. Parchen, R., "Serrated Trailing Edge Noise (STENO)", Proceedings of the European Wind Energy Conference, Nice, March 1999.

Braun, K.A., van der Borg, N., Dassan, A.G.M, Doorenspeet, F. Gordner, A., Parchen, R., "Geraueschreduktion mit Gezahnten Blattinterkannten", Proceedings of the German Wind Energy Conference, 1998.

Brookfield, J.M. and Waitz, I.A., "Trailing-Edge Blowing for Reduction of Turbomachinery Fan Noise", Journal of Propulsion and Power, Vol. 16, No. 1, 2000, pp. 57-64.

Chevepanov, P. Y., and Babenko, V.A., "Experimental and Numerical Studyof Flat Momentumless Wake", International Journal of Heat and Fluid Flow, 19, 1998, pp 608– 22.

Cimbala, J.M., and Park W.J., "An Experimental Investigation of the Turbulent Structure in a 2-D Momentumless Wake", Journal of Fluid Mechanics, Vol. 213, 1990, pp. 479–509.

Dassen, A.G., Parchen, R., Bruggemann, J., Hagg, F., 1996, "Results of Wind Tunnel Study on the Reduction of Airfoil Self-Noise by the Application of Serrated Blade Trailing Edges", Proceedings of the European Wind Energy Conference, Goeteborg, May 1996, pp 800-803.

Dassen, A.G., Parchen, R., Bruggemann, J., Hagg, F., "Wind Tunnel Measurements of the Aerodynamic Noise of Blade Sections", Proceedings of the European Wind Energy Conference, Thessaloniki, October 1994, vol. 1, pp 791-798

de la Riva D H, 2001, "Turbulence interaction in a highly staggered cascade-propulsor configuration", M.S. thesis, Aerospace and Ocean Engineering Dept., Virginia Polytechnic Institute and State University **http://scholar.lib.vt.edu/theses/available/etd-04272001-172809/**

Dmitrenko, Y. M., Kovalev, I. I., Luchko, N. N., Cherenpanov, P.Y., "Plane Turbulent Wake with Zero Excess Momentum", Journal of Engineering Physics, Vol. 52, No. 5, 1987, pp. 536-542.

Durham, W. C. "Aircraft Dynamics and Control", Virginia Tech, 2002, pg. 21-32.

Elliot, D.M. and J.M. Dittmar, "Some Acoustic Results from the NASA/Pratt and Whitney Advanced Ducted Propulsor Model", 38th Aerospace Sciences Meeting and Exhibit, 10-13 January 2000, Reno, NV, AIAA-2000-0351.

Envia, E., "Fan Noise Reduction: An Overview", 39th Aerospace Sciences Meeting and Exhibit, 8-11 January 2001, Reno, NV, AIAA-2001-0661.

Ffowcs –Williams J, E, and L. H. Hall, 1970, "Aerodynamic Sound Generation by Turbulent Flow in the Vicinity of a Scattered Half Plane", Journal of Fluid Mechanics, Vol. 40, No. 4, pp. 657-670

"Growth in Airport Noise Restrictions", Airport Noise Regulation Information Web Site, Boeing, http://www.boeing.com/commercial/noise/airport2004.pdf

Guidati, G., Ostertag, S., Wagner, S., "Prediction and Reduction of Wind Turbine Noise: An Overview of Research Activities in Europe", 2000 ASME Wind Energy Symposium, 19th, Aerospace Sciences Meeting and Exhibit, 38th, Reno, NV, January 10 – 13, 2000, pp 219 – 229.

Haag, F., van Kuik, G.A.M., Parchen, R., van der Bong, N.J.C.M, " Noise Reduction on a 1 MW Size Wind Turbine with a Serrated Trailing Edge", Proceedings of the European Wind Energy Conference, Dublin, October 1997, pp 165-168.

Howe, M.S. 1991, "Noise Produced by a Sawtooth Trailing Edge", Journal of Acoustical Society of America, Vol. 90, No. 1, 1991, pp. 482 – 487.

International Civil Aviation Organization (ICAO), "Growth in Air Traffic Projected to Continue: ICAO Releases Long-Term Forecasts", 13 June 2001, http://www.icao.int/icao/en/nr/2001/pio200106.htm.

Juve, D., "Aeroacoustic Research in Europe: The CEAS-ASC Report on 1998 Highlights", AIAA-99-1916.

Kline S J and McClintock F A, 1953, "Describing uncertainties in single sample experiments", Mechanical Engineering, vol. 75, pp3

Krammer, P., Rued, K., Truebenbach, J., "Technology Preparation for Green Aero Engines", AIAA/ICAS International Air and Space Symposium and Exhibition: The Next 100 Years, 14-17 July 2003, Dayton, OH, AIAA-2003-2790.

Leitch, T.A., Sanders, C.A., Ng, W.F., "Reduction of Unsteady Stator-Rotor Interaction Using Trailing Edge Blowing", Journal of Sound and Vibration, Vol. 235, No. 2, 2000, pp. 235-245.

Lord, W. K., "Aircraft Noise Source Reduction Technology", Aircraft Noise Symposium, 2 March 2004, Palm Springs, CA.

Ma R., 2003, "Unsteady turbulence interaction in a tip leakage flow downstream a simulated axial compressor rotor", Ph.D. dissertation, VPI&SU.

Ma R., Saha N., Devenport W.J. and Wang Y., 2000, "Unsteady Behavior of a Tip-Leakage Vortex Produced by Simulated Stator/Rotor Interaction", AIAA Fluids 2000, 19-22 June, Denver CO, AIAA-2000-2217.

Myose, R.W. and Iwata, J., "Flow Visualization of an Oscillating Airfoil with Sawtooth Trailing Edge", AIAA Journal, Vol. 34, No. 8, 1995, pp. 1748-1750.

"Making Future Commercial Aircraft Quieter", NASA Facts, FS-1997-07-003-LeRC, www.lerc.nasa.gov/WWW/AST/noise.htm.

Muthanna C, 1998, "Flowfield downstream of a compressor cascade with tip leakage", M.S. thesis, Aerospace and Ocean Engineering Dept., Virginia Polytechnic Institute and State University
http://scholar.lib.vt.edu/theses/available/etd-110798-235327/

Muthanna C., Wittmer K. S. and Devenport W. J., 1998, "Turbulence structure of the flow downstream of a compressor cascade with tip leakage", AIAA 36th Aerospace Sciences Meeting, Reno, Nevada, AIAA 98-0420.

Muthanna C, 2002, "The effects of free stream turbulence on the flow field through a compressor cascade", Ph.D. dissertation, Aerospace and Ocean Engineering Dept., Virginia Polytechnic Institute and State University
http://scholar.lib.vt.edu/theses/available/etd-08222002-194441/

Moore J, Moore J G, and Liu B, 1996, "CFD computation to aid noise research, progress report, 2/96-10/96", Department of Mechanical Engineering, Virginia Tech, Blacksburg, VA.

Owens, R. E., "Energy Efficient Engine Performance System – Aircraft Integration Evaluation", NASA/CR 159488, 1979.

Park, W.J., and Cimbala, J.M., "The Effect of Jet Injection Geometry on 2-D Momentumless Wakes", Journal of Fluid Mechanics, Vol. 224, 1991, pp. 29 – 47.

Pope S. B., 2001, "Turbulent Flows", Cambridge University Press, New York.

Rao, N.M., Feng, J., Burdisso, R.A., Ng, W.F., "Experimental Demonstration of Active Flow Control to Reduce Stator-Rotor Interaction", AIAA Journal, Vol. 39, No.3, 2001, pp. 458-464.

Shin S, Ragab S A and Devenport W J, 1999, "Numerical simulation of highly staggered cascade flow using an unstructured grid", 30th AIAA Fluid Dynamics Conference, Norfolk, VA, June 28-July 1, 1999, AIAA 99-3713.

Shin S, 2001, "Reynolds-averaged Navier-Stokes computation of tip clearance flow in a compressor cascade using an unstructured grid", Ph.D. dissertation, Aerospace and Ocean Engineering Dept., Virginia Polytechnic Institute and State University **http://scholar.lib.vt.edu/theses/available/etd-09122001-174121/**

Sutliff, D.L., Tweedt, D.L., Fite, E.B., Envia, E., "Low-Speed Fan Noise Reduction with Trailing Edge Blowing", 8th AIAA/CEAS Aeroacoustic Conference Exhibit, 17-19 June 2002, Breckenridge, Colorado, AIAA 2002-2992.

Takami, H. and Maekawa, H., "Experimental Investigation of Turbulent Structures in a Two-Dimensional Momentumless Wake", JSME International Journal, B63, No. 608, 1997, pp. 1145-1153.

Wang Y, 2000, "Tip leakage flow downstream a compressor cascade with moving end wall", MS Thesis, Aerospace and Ocean Engineering Dept., Virginia Polytechnic Institute and State University **http://scholar.lib.vt.edu/theses/available/etd-04052000-14200057/**

Wang Y and Devenport W J, 2003, "The wake of a compressor cascade with tip gap. Part 2. Effects of endwall motion ", Under consideration for publication in AIAA journal

Wisler, D C, 1977, "Core compressor exit stage design study, Volume I – Blading design", NASA CR-135391

Wisler, D C, 1981, "Core compressor exit stage study, Volume IV - Data and performance report for the best stage configuration", NASA CR-165357

Wittmer K S, Devenport W J, Zsoldos J S, 1998, "A four-sensor hot-wire probe system for three-component velocity measurement", Experiments in Fluids, vol. 24, pp. 416-423.

Wygnanski I., Champagne F. and Marasli B., 1986, "On the Large Scale Structures in Two-Dimensional Small Deficit Turbulent Wakes", Journal of Fluid Mechanics, vol. 168, pp. 31-71.

Wo, A.M., Lo. A.C., Chang. W.C., "Flow Control via Rotor Trailing Edge Blowing in Rotor/Stator Axial Compressor", Journal of Propulsion and Power, Vol. 18, No. 1, 2002, pp. 93-99.

VITA

The author, Derek H. Geiger, was born in Englewood, New Jersey, USA, on September 5, 1979. He received his Bachelor of Science degree in Aerospace Engineering from Virginia Polytechnic Institute and State University (Virginia Tech) in May 2002. While attending Virginia Tech as an undergraduate, he participated in the Co-op program which landing him in Munich, Germany working for MTU Aero Engines GmbH for a period of 18 months. Upon completing his undergraduate requirements, he immediately began work on his Master of Science in Aerospace Engineering at Virginia Tech and completed his work in December 2004. He is currently employed by Sikorsky Aircraft Corporation in Stratford, CT.